CHARACTERISATION OF PLACENTAL AND PLATELET EXOSOME-BOUND CARDIOTROPHIN-1 IN CARDIOMYOCYTE AND ENDOTHELIAL CELL FUNCTION



Dr. Vuyane Mhlomi

New College

Thesis submitted for the Degree of Doctor of Philosophy

Trinity Term 2017

This thesis is submitted to the University of Oxford, in partial fulfillment of the requirements for the degree of Doctor of Philosophy.

This thesis is entirely my own work, and except where otherwise stated, describes my own research.

Copyright © Vuyane Mhlomi
All rights reserved.

ABSTRACT

TITLE: Characterisation of placental and platelet exosome-bound cardiotrophin-1 in cardiomyocyte and endothelial cell function
NAME AND COLLEGE: Dr Vuyane Mhlomi, New College
DEGREE: DPhil in Obstetrics and Gynaecology
TERM AND YEAR OF SUBMISSION: Trinity 2016

Maternal cardiovascular adaptions during pregnancy have been well described and include characteristic changes in cardiac morphology and function. The mechanisms behind these changes remain largely unknown but are tied to the developing feto-placental unit. Extracellular vesicles are membrane-encapsulated particles carrying cargo originating from their parental cells and are critical mediators of intercellular communication. Syncytiotrophoblast extracellular vesicles (STB-EV), comprising of microvesicles and exosomes, are released by the placenta into the maternal circulation throughout pregnancy. We hypothesized that there might be molecules on the STB-EV that had cardiac effects. In this thesis, we characterised the expression of Cardiotrophin 1 (CT-1), a known potent inducer of cardiac hypertrophy and regulator of cardiac physiology, as being present on the human placenta. Importantly, we demonstrated that CT-1 is present on both microvesicles and exosomes, with a greater expression on exosomes. Furthermore, we show that CT-1 is biologically active and can phosphorylate its cognate receptor gp130/LIFR. Moreover, we demonstrate downstream signaling pathways that are mediated by STB-EV, most notably STAT 3 and ERK 1/2. We subsequently conducted a transcriptomic analysis using microarrays to investigate the effects of CT-1 positive STB-EV on cardiomyocytes derived from human induced pluripotent stem cells. This analysis showed significantly upregulated and downregulated genes involved in cardiovascular function. Furthermore, gene networking using Ingenuity Pathway Analysis (IPA) revealed STAT 3 as the most likely mediator of these gene changes. Intriguingly, real-time quantitative PCR validation confirmed the vesicular changes seen in the array but revealed that while some of the gene changes are directly due to CT-1, some are almost certainly due to the cargo within the vesicles. As a corollary to our experimental investigations we also identified, for the first time that CT-1 was present in platelets and platelet extracellular vesicles (PEV). We found in vitro evidence that PEV-bound CT-1 phosphorylated gp130 signaling leading to the activation of STAT 3 and ERK 1/2. Furthermore, we demonstrated that CT-1 positive vesicles protect against cytotoxicity in endothelial cells raising the possibility that this cytokine performs a cellular protective role.

This thesis thus reports the first observation of active CT-1 expressed in STB-EV from normal placentae and points to a novel finding that the placenta may well play a role in the orchestration of cardiovascular adaptation in pregnancy. Moreover, our results suggest that the placenta can communicate with the maternal heart. Additionally, it places CT-1 in vesicles as playing a significant role in both cardiomyocyte and vascular biology. Finally, the finding that platelets contain Cardiotrophin-1 positive vesicles suggests that this cytokine may well have a role in cellular protection outside pregnancy.

ACKNOWLEDGEMENTS

A race run alone can be lonely, making the prize a lot less sweet. Mine was not such a path, but a journey I shall cherish for many years to come. That said, it has not come without its challenges; however, it was not a lonely journey- the presence of community made all the difference. I stood and leaned on the shoulders of a community of champions whose care, counsel and companionship helped me overcome the many detours and hurdles along the way. You were champions who served as a source of strength, encouragement, support, and counsel. You offered me shoulders on which I stood to reach great heights and leaned on when I was tired and weary.

To my friend, sparring partner, confidant and supervisor, Dr Manu Vatish. You have been the sword upon which I sharpened my finesse for research. Thank you for your generosity of spirit, support and counsel. Watching you serve and support our lab team, giving us your time and investing resources into our development as researchers, and as individuals, taught me a lot about excellence and servant leadership. *Enkosi mhlekazi.* We have walked an incredible journey together that will continue as it takes a different form.

To my second supervisor, Professor Ian Sargent, thank you for the essential part you played in my development. Your patience and expertise have been highly appreciated.

To Professor Christopher Redman, Professor Furqan Bari, and Yale Michaels, for your assistance and support, I am forever grateful.

To my awesome lab team, for love, support, fun, and all those great experiments that always went according to plan, to you: Dr Wei Zhang, Neva Kadzinja, Carolina Motta Meijia, Dr Sofia Cerdeira, Alexandra Burdrujuna, Jenny McGowan-Downey, and Dr Gavin Collet. Thank you for the companionship on this journey, I wouldn't change a single thing about our time together. Special thanks to our research midwife, Linda Holden, Dr Rebecca Dragovic, and Ms Janet Carver who were always willing to lend a helping hand.

To my friends, I am deeply appreciative of your contributions to my studies. I consider myself to be one of the most fortunate DPhil students, as I was availed the opportunity to set upon unchartered terrain, leaving home but never leaving your hearts. Nobulali Dangazele, Victor Motsa, Sisa Njongwe, Nkosiyedwa Jingose, Razaq Doherty, Ndumiso Mngomezulu, Skhathisomusa Mthembu and Jonathan Macauley. To Thabang Makgalemele who started this journey with me, I am grateful for your support. Friends, you know that the start of this journey was not an easy one, and its end has been filled with its difficult moments too. Words cannot encapsulate the magnitude of love I have for you, so in sum, I shall say, to each of you, *nithandwa ndim*!

To you, the many doctors and friends who are not only witnesses to this journey, but comrades who fought alongside me: Dr Boyboy Ntanjana, Dr Annette Afari-Twumasi, Dr Sicelo Mkhize, Dr Thula Siluma, Dr Lindikhaya Nabela, Dr Kitso Mrubata, Dr Akwaowo Akpabio, Dr Kopano Mabaso, Dr Chrystelle Wedi, Dr David Favara, Professor Reno Morar and Professor Bongani Mayosi. It was your courage and bravery that kept me going, kept me fighting for what often seemed an impossible dream, thank you.

To Reinette Vermaak, Nonkosi Malala, and Professor Marian Jacobs, I have never doubted the unyielding power and strength of women, thank you for sharing yours with me. I am a better man and a better doctor because of you.

It is through my time in Oxford that I truly discovered who I was. While cold and grey, the community in Oxford helped me recover and uncover my destiny, bringing light and warmth into my heart. To Nhlakanipho Mkhize, Nomfundo Ramalekana, Karen Mumba, Ntokozo Qwabe, Sehaam Areff, Sarah Yerima, Sam Peter and Dylan Smith. Oxford would have been a cold, dark and lonely place without your constant care and support. Thank you for the many drinks at old English pubs, the many nights spent cooking in your kitchens, laughing, crying, dancing and building a community far from home.

To Dr Tsepo Moseme, Sizwe Mpofu-Walsh, Paballo Chauke and Dr Ismail Cassimjee, for providing me with unfailing support, continuous encouragement and brotherhood.

To my remarkable friends, Zikho Pali and Lebo Kwela. Thank you for showing up for me, time and time again; for walking with me (and sometimes carrying me). Thank you for keeping me accountable and helping me see this DPhil through.

To the Rhodes Scholarship and South African Medical Research Council, thank you for supporting my dream, for being generous in your funding and enabling me to focus only on the dream; for securing my well-being by surrounding me with people invested in my success. Special thanks to Mary Eaton, I am forever grateful for your generosity and kindness.

And to my family - my mother, Nomsa Mhlomi, and brothers, Vuyile, Siviwe and Vukile – for your enduring and unchanging love, this belongs to you.

Ndiyabulela ngothando lwenu, INkosi inisikelele ngendlela emangalisayo!

To God be the glory.

For my mom, Nomsa Mhlomi.

LIST OF ABBREVIATIONS

ADP	Adenosine diphosphate
ALIX	ALG-2-interacting protein X
ANP	Atrial natriuretic peptide
APC	Allophycocyanin
ATP	Adenosine triphosphate
ATP2A2	ATPase Sarcoplasmic/Endoplasmic Reticulum Calcium Transporting 2
BCA	Bicinchoninic acid
bFGF	Basic fibroblast growth factor
BNP	Brain natriuretic peptide
BrdU	5-bromo-2'-deoxyuridine
CD	Cluster of differentiation
cDNA	complementary DNA
CO	Cardiac output
CO_2	Carbon dioxide
CT-1	Cardiotrophin 1
DMSO	Dimethyl sulfoxide
DNA	Deoxyribonucleic acid
ECL	Enhanced chemiluminescence
EDTA	Ethylenediaminetetraacetic acid
EGF	Epidermal Growth Factor
EGM	Endothelial cell growth media
ELISA	Enzyme-linked immunosorbent assay
EM	Electron Microscopy
ERK	Extracellular receptor kinase
ESCRT	Endosomal sorting complexes required for transport
ET-1	Endothelin 1
EV	Extracellular vesicles
FBS	Fetal bovine serum
FcR	Fc Receptor
FCS	Fetal calf serum
FMO	Fluorescence minus one
FSC	Forward scatter
GP130	Glycoprotein 130
HCAEC	Human coronary artery endothelial cells
hFGF-b	Human fibroblast growth factor beta
HLA	Human Leukocyte Antigen
HMEC	Human microvascular endothelial cells
HRP	Horseradish peroxidase
HSP	Heat Shock Protein
HUVEC	Human umbilica endotheliall vein cells
ICC	Immunocytochemistry

IGF-1	Insulin-like growth factor-1
IHC	Immunohistochemistry
IL-6	Interleukin 6
JAK	Janus Kinase
JNK	c-Jun N-terminal kinase
LAMP	Lysosomal-associated membrane proteins
LIF	Leukemia inhibitory Factor
LPS	Lipopolysaccharide
LV	Left ventricle
MAPK	Mitogen-activated protein kinase
MFI	Mean fluorescence intensity
MH7B	Myosin heavy chain 7 beta
mRNA	Messenger ribonucleic acid
MV	Microvesicle
MVB	Multivesicular bodies
NTA	Nanoparticle Tracking Analysis
OSM	Oncostatin M
PBS	Phosphate Buffered Saline
PBS-T	Phosphate Buffered Saline-Tween
PE-CY5	Phycoerythrin Cyanine 5
PE-CY7	Phycoerythrin Cyanine 7
PEV	Platelet extracellular vesicles
Phycoerythin	PE
PI3K	Phosphatidylinositol 3-OH kinase
PLAP	Placental alkaline phosphatase
PMV	Platelet microvesicles
PS	Phosphatidylserine
PVDF	Polyvinylidene difluoride
RT-qPCR	Real Time Quantitative Polymerase Chain Reaction
RBC	Red Blood Cells
RNA	Ribonucleic acid
RT	Room temperature
SCC	Side scatter
SERCA	Sarcoplasmic reticulum calcium pump
STAT	Signal transducer and activator of transcription
STB-EV	Syncytiotrophoblast extracellular vesicles
STB-EX	Syncytiotrophoblast exosomes
STB-MV	Syncytiotrophoblast microvesicles
TBS	Tris-buffered saline
TEM	Transmission electron Microscopy
TRAP	Thrombin receptor-activating peptide
VEGF	Vascular endothelial growth factor

TABLE OF CONTENTS

CHAPTER 1

1.1. Cardiovascular adaptations in pregnancy 1
1.1.1. Changes in blood volume, plasma volume and red cell mass 1
1.1.2. Changes in cardiac output, heart rate and stroke volume 2
1.1.3. Changes in myocardial contractility 3
1.1.4. Changes in systemic vascular resistance and blood pressure 3
1.1.5. Haemodynamic and structural cardiac changes 4
1.2. Extracellular vesicles 8
1.2.1. Properties and biogenesis of extracellular vesicles 8
1.2.2. Syncytiotrophoblast Extracellular Vesicles (STB-EV) 15
1.2.3. Background to CT-1 18
1.2.4. Discovery and molecular biology of CT-1 19
1.2.5. Distribution of CT-1 21
1.2.6. Synthesis and secretion of CT-1 21
1.2.7. CT-1 Receptor 22
1.2.8. CT-1 Signaling pathways 24
1.2.9. Biological actions of CT-1 26
1.2.9.1. Cardiac hypertrophy 27
1.2.9.2. Cardioprotection 28
1.2.9.3. CT-1 effect on cardiac fibroblast, myofibroblasts and endothelial cells 30
1.2.10. Systemic actions of CT-1 30

CHAPTER 2

2.1. INTRODUCTION 36
2.1.1. Aims 39
2.2. MATERIALS AND METHODS 40
2.2.1. Patient information 40
2.2.2. Immunohistochemistry 40
2.2.3. Isolation of STB-EV by Ex-vivo Dual Placental Lobe Perfusion 41
2.2.4. Assessment of STB-EV size and concentration by Nanoparticle Tracking Analysis (NTA) 44
2.2.5. Characterisation of STB-MV by Flow Cytometry 46
2.2.6. Assessment of CT-1 expression on STB-MV by Flow Cytometry 49
2.2.7. Western Blotting 50
2.2.8. Immunoprecipitation of PLAP and CT-1 STB-EX determined by Western blotting and Flow Cytometry 52
2.2.9. Cell Cultures 53
2.2.9.1. HepG2 cells – Human Hepatocellular liver carcinoma cell line used as a positive control for APC-conjugated CT-1 antibody 53
2.2.9.2. HUVEC – Human umbilical endothelial vein cells used for the study of changes in gp130 in response to treatment with STB-EX 54
2.2.9.3. HCAEC – Human coronary artery endothelial cells used for the study of gene changes in response to treatment with STB-EX 56

2.2.9.4. Rat cardiomyocytes –used for the study of genes associated with cardiac myocytes hypertrophy in response to treatment with STB-EX 57
2.2.10. Determining the non-toxic concentration of STB-EX for functional studies 58
2.2.11. Cell treatment with STB-EX 59
2.2.11.1. For the study of changes in in gp130, ERK 1/2 and Akt in HUVEC 59
2.2.11.2. To demonstrate internalisation of STB-EX by HUVEC and rat cardiomyocytes 60
2.2.11.3. The study of gene changes caused by STB-EX in HCAEC 61
2.2.11.4. The study of gene changes caused by STB-EX in rat cardiomyocytes 62
2.2.12. Quantitative Real-Time Polymerase Chain Reaction (RT-qPCR) 62
2.2.12.1. RNA isolation 62
2.2.12.2. Taqman® Gene expression assay 63
2.2.13. Statistical analysis 66

2.3. RESULTS 67
2.3.1. Cardiotrophin 1 is expressed on the syncytiotrophoblast layer of the human placenta 67
2.3.2. Isolation and characterisation of STB-EV 68
2.3.3. Characterisation of STB-MV by Flow Cytometry 71
2.3.4. Determination of level of CT-1 expression on STB-MV and STB-EX by Western blotting 74
2.3.5. Validation of in-house conjugation of anti - CT-1 antibody for use on flow cytometry 76
2.3.6. Determination of levels of CT-1 expression on STB-MV by Flow Cytometry 77
2.3.7. Determination of CT-1 expression on PLAP positive STB-EX 81
2.3.8. Determining the non-toxic concentration of STB-EX for function studies 83
2.3.9. STB-EX-bound CT-1 phophorylates gp130, ERK 1/2 and STAT 3 but not Akt. 85
2.3.10. Internalisation of STB-EX by endothelial cells and cardiomyocytes 89
2.3.11. Gene changes associated with treatment of cardiomyocytes with STB-EX 91

2.4. DISCUSSION 95

2.5. SUMMARY 103

CHAPTER 3

3.1. INTRODUCTION 105
3.2. MATERIALS AND METHODS 106
3.2.1. Cell culture 106
3.2.2. The study of gene changes caused by STB-EX in hiPSC-CM. 107
3.2.3. RNA isolation 108
3.2.4. Microarray gene expression profiling and data analysis 109
3.2.5. Taqman® Gene expression assay for gene validation by RT-qPCR 113
3.2.6. Statistical Analysis 114
3.3. RESULTS 115

3.3.1. Total RNA quality assessment 115
3.3.2. Hierarchical Clustering 117
3.3.3. Gene array and IPA analysis 118
3.3.4. Gene validation by RT-qPCR 133
3.4. DISCUSSION 136
3.5. SUMMARY 143

CHAPTER 4

4.1. INTRODUCTION 145
4.1.1. Aims 151
4.2. MATERIALS AND METHODS 152
4.2.1. Subject Information 152
4.2.2. Platelet isolation and activation 152
4.2.3. Immunocytochemistry 154
4.2.4. Isolation of Platelet extracellular vesicles 155
4.2.5. Isolation of Red blood cells (RBC) and RBC extracellular vesicles 157
4.2.6. Assessment of extracellular vesicles by Nanoparticle Tracking Analysis 158
4.2.7. Assessment of CT-1 by flow cytometry 158
4.2.8. Western blotting 160
4.2.9. HUVEC treatment with platelet extracellular vesicles for the study of changes in GP130, STAT 3, ERK and AKT 161
4.2.10. Cytotoxicity/ Survival Assay – to determine whether PEV bound CT-1 has protective effects on endothelial cell *in vitro* 162
4.2.11. Statistical Analysis 163
4.3. RESULTS 164
4.3.1. Determination of CT-1 expression on human platelets by immunocytochemistry and Western blotting 164
4.3.2. Determination of CT-1 expression on human platelets by flow cytometry 166
4.3.3. Isolation and characterisation of platelet extracellular vesicles 168
4.3.4. Determining the expression on CT-1 on PMV and PEV by Western blotting 171
4.3.5. Determining the expression on CT-1 on PMV by flow cytometry 173
4.3.6. PEV-bound CT-1 phosphorylates gp130 and STAT 3 but not ERK and Akt 175
4.3.7. Determining the cytoprotective effects of PEV-bound CT-1 on endothelial cells *in vitro*. 177
4.4. DISCUSSION 180
4.5. SUMMARY 188

CHAPTER 5

5.1. GENERAL DISCUSSION 190
5.1.1. Characterisation of STB-EV- bound CT-1 190
5.1.2. Characterisation of PEV- bound CT-1 193
5.1.3. Future work 194
REFERENCES 196

CHAPTER 1

GENERAL INTRODUCTION

GENERAL INTRODUCTION

The maternal cardiovascular system undergoes profound anatomic and physiological changes in pregnancy to support the increased metabolic demands of the enlarging uterus, placenta and the developing fetus within [1]. It responds to physiological, molecular and metabolic stimuli with both acute and chronic changes [1].

1.1. Cardiovascular adaptations in pregnancy

1.1.1. Changes in blood volume, plasma volume and red cell mass

Normal pregnancy is characterized by an increase in circulating blood volume and red blood cell mass from as early as 5 weeks of gestation thus ensuring adequate oxygenation of the feto-placental unit [2-4]. The total blood volume increases by approximately 1.5 litres (50% above non-pregnant values), most which of which occurs by the second trimester, and is maintained until the end of gestation [2, 3]. The change in plasma volume parallels that in blood volume and in fact contributes to a third of increase in blood volume [5, 6]. The increases in plasma volume are mediated by slightly elevated plasma renin activity and reduced atrial natriuretic peptide levels [7]. This suggests that, in normal pregnancy, the elevation in plasma volume is likely to be triggered by an under-filled vascular system resulting from the fall in systemic vascular tone in pregnancy, rather than actual blood volume expansion, which would produce the opposite hormonal profile (i.e. low plasma renin and elevated atrial natriuretic peptide levels [7].

The red cell mass increases by 15 to 20 percent and is largely driven by an increase plasma erythropoietin [8]. However, the increase is relatively less compared with the increase in plasma volume, the net result being a reduction in hemoglobin concentration, termed “anemia of pregnancy” [9, 10].

1.1.2. Changes in cardiac output, heart rate and stroke volume

Of particular relevance to this thesis are the structural and functional cardiac changes that occur in pregnancy. Cardiac output (CO), a product of the stroke volume and heart rate, is defined as the volume of blood pumped by the heart per minute, and considered to be a measure of the functional capacity of the heart [11]. In the first trimester, CO progressively increases (Figure 1.1.). By weeks 25-35, resting CO is at or near its peak, approximately 50% above non-pregnant values, a level that is maintained until late in pregnancy when it declines [12]. This increase in CO is initially driven by an increase in stroke volume (SV), which increases gradually until the end of the second trimester and then remains constant (Figure 1.1.) [12, 13]. As pregnancy advances, the maternal heart rate rises progressively and reaches a peak of about 15 beats per minute above non-pregnant levels. This maternal tachycardia becomes a more dominant factor in increasing the CO [14].

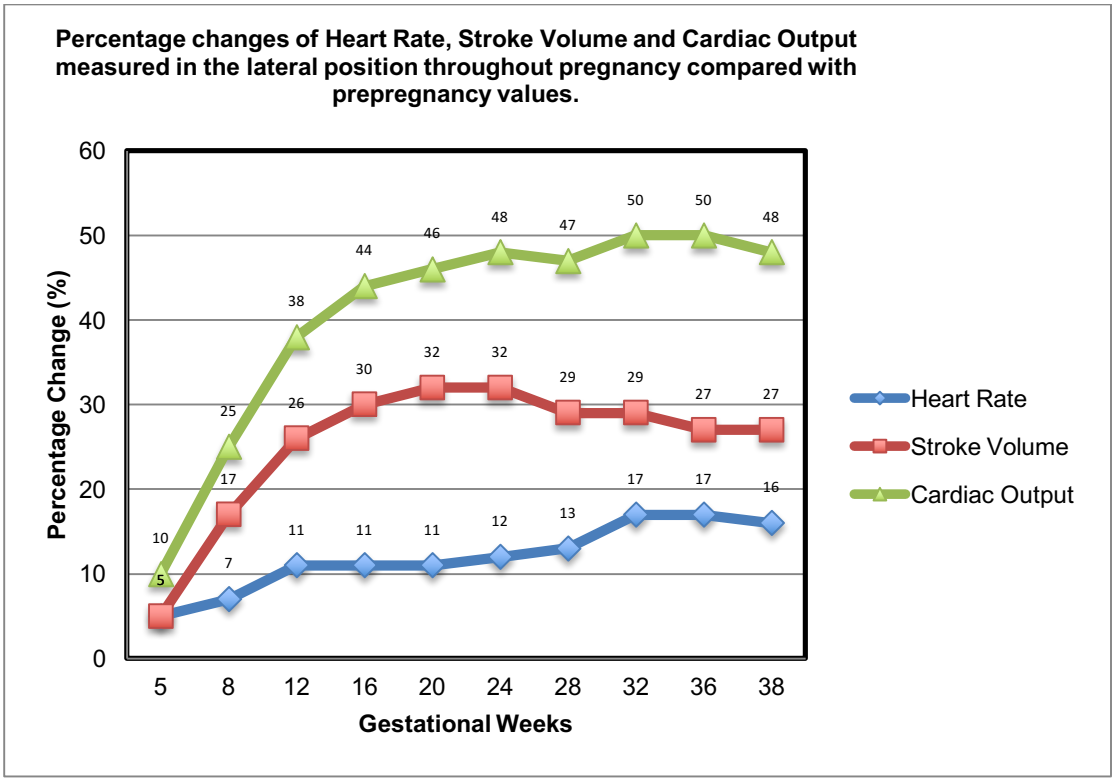


Figure 1.1. Physiological changes during normal pregnancy and delivery. Adapted from Ouzounian and Elkayam, 2012

1.1.3. Changes in myocardial contractility

There is not complete agreement amongst the various groups on how pregnancy influences myocardial contractility. Some authors have reported an increase in left ventricle (LV) contractility during pregnancy [15-18] while others have found no change [19] or decrease in contractile function of the maternal heart in healthy pregnancies [18].

1.1.4. Changes in systemic vascular resistance and blood pressure

In the first trimester, normal pregnancy is characterised by active vasodilatation and increased blood flow in the uteroplacental circulation resulting in a decrease in systemic vascular resistance [15, 18-22]. This is through action of local mediators such as nitric oxide and prostacyclin as well

as increased progesterone, relaxin and prostaglandins [21-23]. Furthermore, there is a decrease in arterial blood pressure - the lowest diastolic value averaging 10 mmHg below non-pregnant values in the second trimester, and increasing to basal values as term approaches [24].

1.1.5. Haemodynamic and structural cardiac changes

In addition to the hemodynamic changes described above, the maternal heart also undergoes physiological remodeling. This results in molecular, cellular and interstitial changes affecting the heart that manifest clinically as changes in shape and size [25].

From as early as 12 weeks of gestation, the left ventricular wall progressively increases in thickness by about 15 -25% [26]. Furthermore, the Left Ventricular Mass (LVM) increases by about 50%, mainly during the third trimester [26]. This increase in LVM indicates a true hypertrophic response because the Left Ventricular Mass Index (LVMI), designed to correct for increases in pregnant body size, is also elevated [26]. This enlargement of the left ventricle maintains left ventricular performance and myocardial oxygenation in pregnancy [27]. Of note, the physiological hypertrophy in pregnancy is characterized by a proportional enlargement of chamber size and wall thickness, eccentric hypertrophy, which is in contrast to concentric hypertrophy (e.g. occurring in essential hypertension and aortic stenosis), where there is an increase in wall thickness without concomitant chamber enlargement (Figure 1.2.) [28].

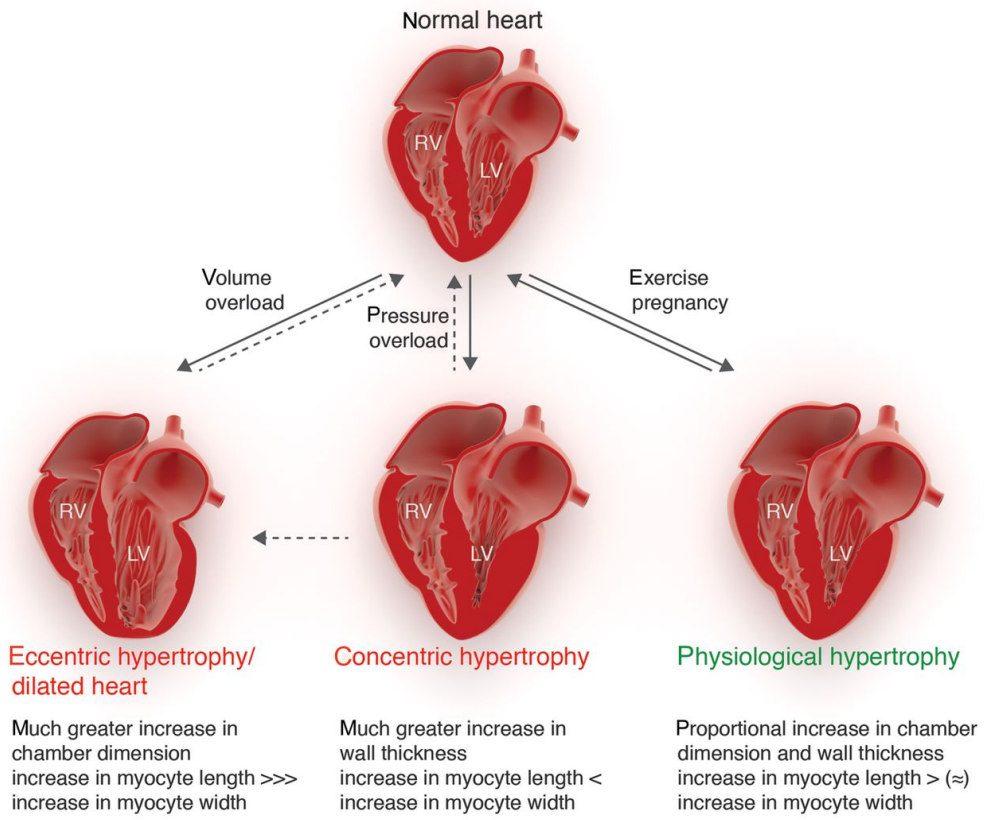


Figure 1.2. Morphometric alterations in response to various stimuli. Adapted from Chung and Leinwand, 2014

Given these startling changes, one would expect to see consistent changes in cardiac performance and yet, according to Melchiorre et al., there is a lack of standardized measurements for cardiac performance during pregnancy [26]. Some studies report enhanced left ventricular systolic function whilst others note no change [26]. Studies of diastolic function are more difficult to interpret due to the inconsistency in the parameters used to measure it [26]. Very little is known about the mechanisms that mediate these changes, but recent reports suggest that haemodynamic load, neurohormonal activation and other factors may play a role [25, 29].

It seems likely that the extent and type of these changes will have significance for both mother and fetus. For example, cardiac physiology is altered in

preeclampsia, a multisystem disorder of pregnancy characterized by *de novo* hypertension and proteinuria after 20 weeks of gestation [30]. Preeclampsia complicates 3% - 5% of all pregnancies and remains a leading cause of maternal morbidity & mortality [30]. Women with preeclampsia also show a more pronounced increase in LVM [31] and structurally, the heart undergoes concentric hypertrophy. This concentric cardiac remodeling is accompanied by impaired myocardial relaxation and a decline in diastolic function [32]. Systolic function is preserved in women with preeclampsia [32].

At a cellular level, the heart is composed of cardiomyocytes, non-myocytes such as fibroblasts, endothelial cells, mast cells, vascular smooth muscle cells and the surrounding extracellular matrix [33, 34]. Ventricular cardiac myocytes make up only one-third of the total cell number, but account for 70–80% of the heart's mass [33-35]. At birth or soon after, most cardiomyocytes lose the ability to proliferate, thus heart growth occurs primarily via an increase in myocyte size [36]. Cardiomyocyte growth is dependent on the initiation of several events in response to an increase in functional load. These responses include the activation of signaling pathways, changes in gene expression, increases in the rate of protein synthesis, and the organization of contractile proteins into sarcomeric units [37-40]. Furthermore, in response to hemodynamic overload, cardiomyocytes are subjected to mechanical stretch, and release humoral factors such as angiotensin II and endothelin 1 (ET-1) that, in an autocrine or paracrine fashion, bind to receptors on cardiac cells and activate intracellular signaling pathways that leads to cell growth [41-46].

The signaling cascades and proteins responsible for cardiac growth and hypertrophy are complex and extensive crosstalk has been identified. In general, signaling cascades responsible for mediating physiological and pathological cardiac hypertrophy are the IGF1-phosphoinositide 3-kinase [PI3K, (p110α)]-Akt pathway and Gαq signaling (downstream of G protein-coupled receptors (GPCR) activated by angiotensin II, ET-1 and catecholamines, respectively [41-51]. Other signaling pathways associated with physiological cardiac hypertrophy and/or protection include the JAK/STAT pathway, thyroid hormone signaling, and heat shock transcription factor 1 (HSF1) [52-55]. In contrast, pathological hypertrophy has also been associated with with activation of PI3K(p110γ), mitogen activated protein kinases (MAPKs), protein kinase C (PKC) and D (PKD), and calcineurin signaling [56].

In pregnancy, hypertrophic stimuli, including volume overload, mechanical stretch, and variations in sex hormones lead to changes in morphology, signaling pathways and gene expression. Gonzalez *et al.* characterized several of the signaling pathways involved in pregnancy induced cardiac hypertrophy; however, much remains to be elucidated [57]. They found decreased phospho-Akt/Akt, phospho-JNK/JNK and phospho-P38 expression during pregnancy but no change in ERK1/2 expression [57]. Furthermore, Hilfiker-Kleiner *et al*. observed that STAT 3 signaling in the heart was increased during pregnancy [58]. Additionally, research conducted in late pregnant mice and rats revealed modification in Kv4.3 channel messenger RNA (mRNA) which is altered in pathologic hypertrophy; increased c-Src phosphorylating activity, modulation in endothelial nitric oxide synthase

(eNOS) protein and brain natriuretic peptide (BNP) mRNA as well as reduction in estrogen receptor *α* (ER*α*) in relation to their corresponding mid-pregnancy levels [59, 60].

1.2. Extracellular vesicles

Over recent years there has been an increased interest in extracellular vesicles (EV) in both health and disease [61]. Different types of vesicles can engage in cell-cell communication by interacting with target cells in several ways: they can bind directly to receptors on the cell surface and induce intracellular signaling pathways [62]; they can also fuse with the target cell and release their cargo into the cytosol; lastly, they can be taken up by endocytosis and ultimately fuse with the endosome membrane to release their cargo into the cytosol that way [63]. Consequently, they have been shown to be involved in several physiological processes such as cell signaling, antigen presentation and inflammation, cancer and cardiovascular pathophysiology [61]. Furthermore, there is increased interest in the potential use of EV as biomarkers for disease but also as potential targets for disease therapy.

1.2.1. Properties and biogenesis of extracellular vesicles

Extracellular vesicles (EV) are membrane-encapsulated particles carrying cargo originating from their parental cells and are key mediators of intercellular communication. These spherical particles are enclosed by a phospholipid bilayer and have a diameter ranging from 30 nm up to 5 μm [64]. EV are

present in most biological fluids including breastmilk, blood and urine. In fact, in normal physiological conditions, the EV concentration in most human body fluids may be more than 10^{10} EV/ml [65, 66].

The term EV encompasses three main vesicle types: exosomes, microvesicles and apoptotic bodies. However, different terms have been used in the literature, often based on cells or tissues from which they originate, names that do not provide any information regarding the type of vesicles that are involved [67]. Figure 1.3 shows a list of common EV names to illustrate the plethora of terms used to describe EV.

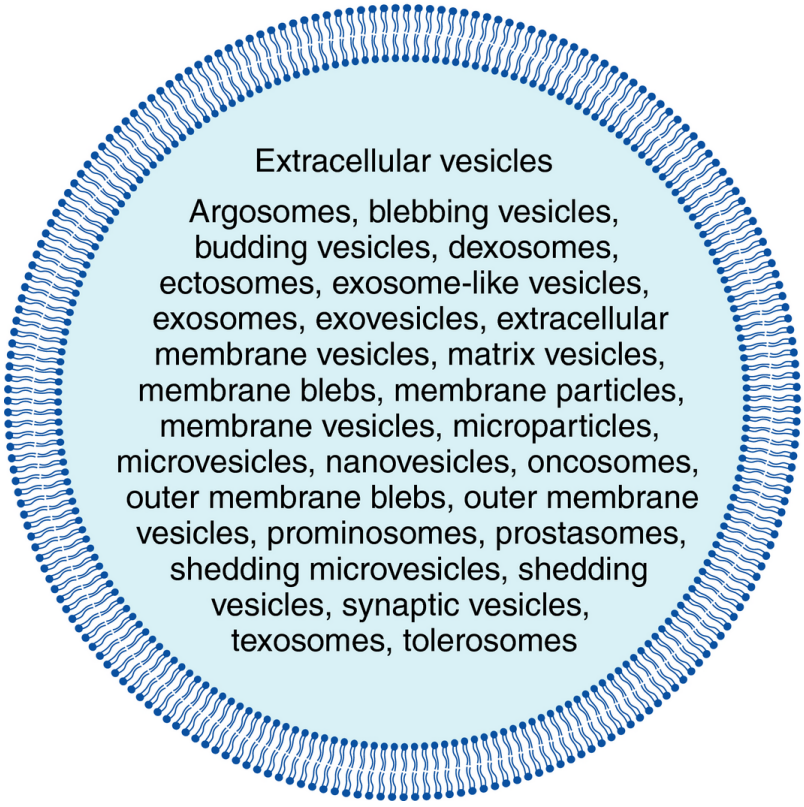


Figure 1.3. Nomenclature of extracellular vesicles. Adapted from van der Pol et al. 2015

The current understanding of EV suggests that they comprise a heterogeneous population of exosomes (40–200 nm diameter), microvesicles (50–1,000 nm) and apoptotic bodies (50–5,000 nm), which are formed through

distinct pathways and play different roles in physiological and pathological states (Figure 1.4.) [64].

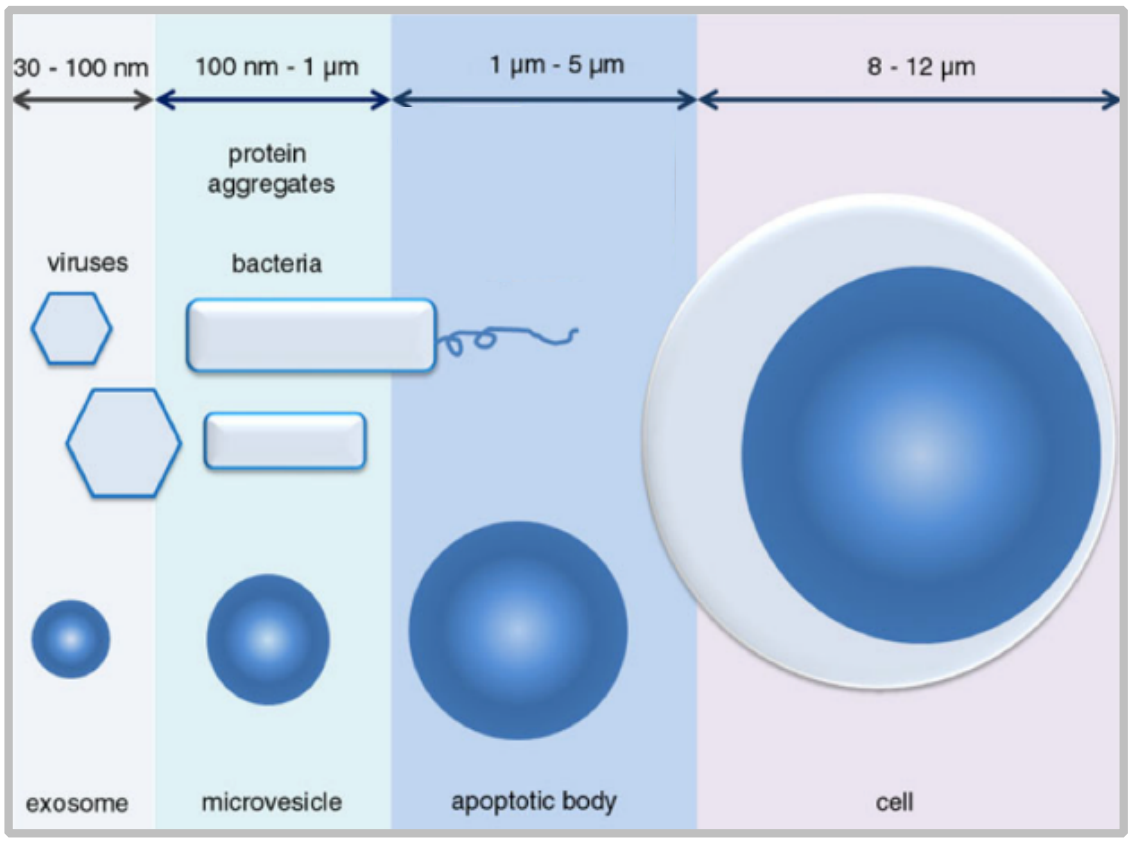


Figure 1.4. The size ranges of the major types of extracellular vesicles compared to the relative size distribution of viruses, bacteria and protein aggregates and eukaryotic cells. Adapted from György et al., 2011

Exosomes are the smallest vesicle type and have been described as having a "cup-shaped" morphology in electron microscopy [61]. It is thought that they are produced in a constitutive manner, using machinery of the endocytic pathway. One of the proposed molecular machineries implicated in the biogenesis and secretion of exosomes is the Endosomal Sorting Complex Required for Transport (ESCRT) [68]. It is thought that proteins and lipids are selectively recruited into recycling endosomes, or targeted for lysosomal degradation by ubiquitylation and ubiquitin-dependent interactions with ESCRT (Figure 1.5.) [69, 70]. Basically, exosomes are formed by inward budding of

endosomal membranes, resulting in the progressive accumulation of intraluminal vesicles within large multivesicular bodies (MVB) [69-71]. MVB (Figure 1.5.) can either be trafficked to lysosomes for degradation or alternatively, to the plasma membrane where, upon fusion with the plasma membrane, they release their contents into the extracellular space [69].

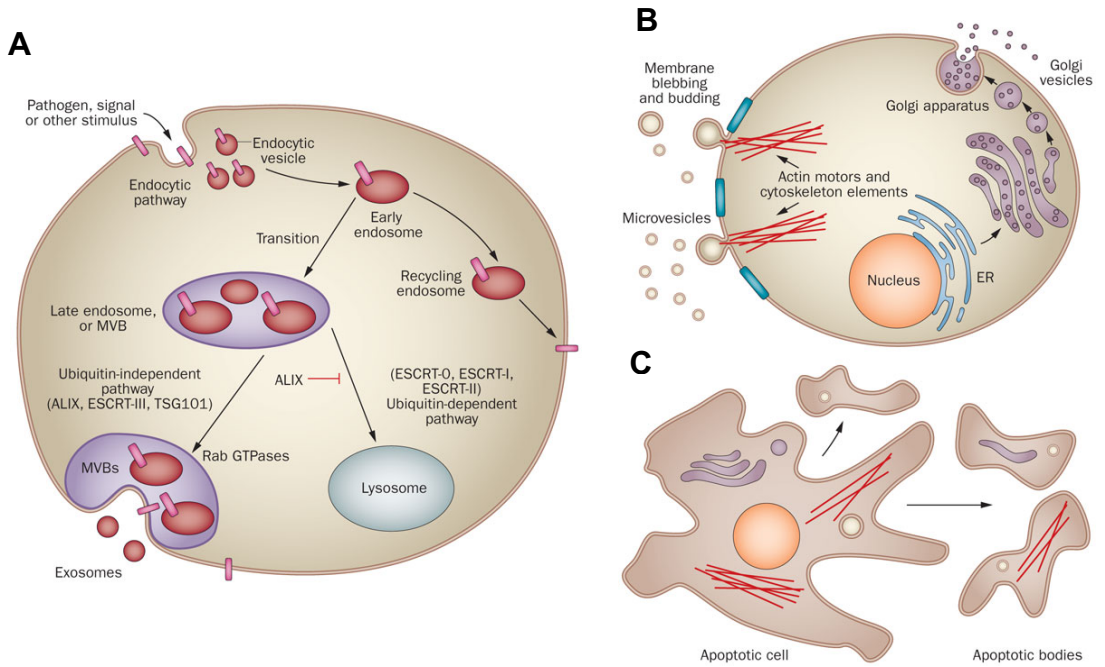


Figure 1.5. Extracellular vesicles originate through different mechanisms. A) Exosomes initiate as intraluminal vesicles that are formed by endocytosis in response to pathogens, ligands or other stimuli; these endocytic vesicles mature to early endosomes, and then into late endosomes, or MVBs. **B)** Microvesicles are formed by the outward budding and fission of plasma membrane lipid microdomains which is controlled by regulatory proteins and cytoskeletons. After synthesis in the ER, protein cargo is transported to the Golgi apparatus, modified and packaged into small vesicles secreted as transport Golgi vesicles. **C)** Cells undergoing apoptotic disaggregation produce large membrane blebs, known as apoptotic bodies. **Abbreviations:** ALIX, ALG-2-interacting protein X; ER, endoplasmic reticulum; ESCRT, endosomal sorting complexes required for transport; MVB, multivesicular body; TSG101, tumour susceptibility gene 101 protein. Adapted from Nawaz et al. (2014).

Exosome secretion is thought to be mediated by members of the Rab GTPase family of proteins, which are regulators of intracellular vesicle transport between different compartments. First, RAB4 and RAB5 were found to be enriched in exosomes [72]. It was later determined that inhibition of RAB11

resulted in decreased exosome production, thus implicating RAB11 in exosome secretion [73]. Recently, RAB2B, RAB5A, RAB9A, RAB27A/B and RAB35 have all been shown play role in in exosome secretion [74, 75]. In addition to Rab GTPases, other proteins involved in the ESCRT pathway such as ALG-2-interacting protein X (ALIX) and vacuolar protein sorting-associated protein 4(VPS4), syndecan and syntenin have also been found to mediate exomes secretion [76, 77].

Many molecules have emerged as potential markers of exosomes including CD63, CD81, CD9, TSG101, and externalized phosphatidylserine [78]. Nevertheless, these molecules are not unique to exosomes despite their enrichment in exosomes [78].

Microvesicles (MV) are a heterogeneous population of EV and form via direct budding from cell membrane [79]. Distinguishing between exosomes and microvesicles based on size can sometimes be difficult because the EV size range partially overlap, however, microvesicles have compositions that lack many of the endosomal features found in exosomes [64]. The mechanism behind MV formation is unclear, however, there is evidence from several reports that this budding process is regulated and induced by plasma membrane remodeling and a rise in intracellular calcium (Figure 1.5.) [80, 81]. This results in the cellular trafficking of biomolecules towards the cell surface resulting in membrane protrusion, budding and, finally, the detachment of spherical bodies from specific regions of the plasma membrane enriched in lipid rafts [82].

MV formation is closely connected to the formation of an anionic phospholipid called phosphatidylserine (PS) [83]. PS is normally located on the inner leaflet of the cellular membrane compared to outer leaflet of the plasma membrane which is enriched in phosphatidylcholine and sphingomyelin [84]. PS is externalized through the action of aminophospholipid translocases also called flippases and floppases which ensure the inward “flip” and outward “flop” traffic of phospholipids at the membrane bilayer [83]. Furthermore, this process is believed to be mediated by molecules such as the transmembrane proteins 16 (TMEM16) family and the proteasome [85-87]. More recent reports also show that in addition to plasma membrane remodeling, changes in the cell cytoskeleton outwards can also induce MV release either following small GTPase ADP-ribosylation factor 6 (ARF6) mediated actin depolymerization [88] [89] or loss of the actin-nucleating protein Diaphanous Related Formin 3 (DRF3/Dia2) [89]. Lastly, different lipid-metabolism enzymes such as phospholipase D2 and sphingomyelinases have also been involved in budding of MV [90].

Often included under the umbrella of extracellular vesicles are apopototic bodies (Figure 1.5.). As their name implies, these are released by cells undergoing apoptosis. Apoptotic bodies comprise the largest particles among the EV subpopulations which overlap in size with microvesicles (~200 nm–5 μm) [91-94]. It is thought they are formed from “blebbing” off the plasma membrane. Their buoyant density ranges between 1.16 g/mL and 1.28 g/mL, and their morphology is more heterogeneous than other cell-derived vesicles

[94]. There is evidence showing that there might be different subpopulations of apoptotic bodies depending on whether they are derived from the apoptotic cells' endoplasmic reticulum or plasma membrane. Some, but not all apoptotic bodies have DNA and histones [95].

Currently, there is no consensus in the field of EV research on protocols for the isolation of specific EV subtypes. Several methods have been described to isolate EV including differential centrifugation, density gradient ultracentrifugation, filtration, size exclusion chromatography and magnetic bead capture on beads or chips [96]. The choice of isolation technique is determined by sample complexity, sample volume, EV yield, enrichment of certain EV subtypes and purity of the resultant preparation [96]. The commonest technique used for EV purification is differential centrifugation. This technique has proven to be particularly useful to fractionate large and small EV from placental perfusate [97]. Differential ultracentrifugation involves an initial series of low-speed centrifugation steps which are used to remove cells and large debris [98]. This is then followed by increasing speed/centrifugal force to separate vesicles of different sizes/densities, and higher-speed centrifugal forces to pellet dense and large particles [98]. Regardless of the preparation, whether made up of exosomes or microvesicles, one thing is becoming increasingly evident: these circulating tiny vesicles have significant impact on both physiological and molecular signaling.

1.2.2. Syncytiotrophoblast Extracellular Vesicles (STB-EV)

Most recently, there has been a focus on the role of placental EV, termed syncytiotrophoblast extracellular vesicles (STB-EV), in pregnancy [99]. As previously discussed, EV are shed by many cell types both as a part of normal physiology and as part of disease; pregnancy is no exception. Using the *ex-vivo* placental perfusion model, our laboratory has demonstrated that the syncytiotrophoblast is the primary source of STB-EV [97]. The placental syncytiotrophoblast (STB) is a multinucleated, terminally differentiated, polarised epithelium that covers the entire surface of human placental villi [100-102]. It is the largest and most critical fetal-maternal interface, responsible for nutrient uptake, gas exchange, waste removal, protein and steroid hormone production and modulation of maternal physiology [100-102].

It is known that the STB releases extracellular vesicles, directly into the maternal circulation where they engage the maternal immune and vascular systems [61]. STB-EV are comprised of a mixture of vesicle types including exosomes, microvesicles and apoptotic bodies [61, 97, 103]. In our laboratory, the vesicles are also categorized according to the centrifugation force required to pellet them into the smaller exosomes (150 000 x *g*) and the larger microvesicles (10 000 x *g*). Not only do these vesicles differ in size, but there are also differences with regard to their formation, protein content and function [103].

STB-EV can be measured in maternal peripheral blood and are believed to be important for the maintenance of normal pregnancy, constituting a major

signaling mechanism between the feto-placental unit and the mother [61, 104-108]. Using a placental alkaline phosphatase (PLAP) based ELISA to distinguish STB-EV from other EV in the circulation, STB-EV have been found circulating at progressively higher levels with advancing pregnancy and labour, and returning to non-pregnant levels around 48 hours post-delivery [105, 108]. In 2014, Salomon et al. reported that they detected PLAP and CD63 double positive EV from as early as 6 weeks gestation and that the levels increased over the course of pregnancy [107].

Furthermore, excessive shedding of STB-EV has been demonstrated in preeclampsia and thought to be a consequence of placental oxidative and inflammatory stress [105]. Vesicles derived from preeclampsia placenta differ quantitatively and qualitatively from those derived from normal pregnancies. NTA analysis conducted in our laboratory showed a significant increase in the median size of STB-EV derived from preeclampsia placental perfusate, compared to normal pregnancy (201 nm vs 166 nm respectively); suggesting a shift towards release of more microvesicles and a potential impact on overall functional effects [109]. Additionally, mass spectrometry analysis of STB-EV from normal pregnancy and preeclampsia identified over 2500 proteins with over 500 unique to preeclampsia [99]. Seminal studies of STB-EV have shown that they contain key ligands, receptors and signaling molecules by which they may interact with various target cells [110].

Several studies have investigated the effects of STB-EV on endothelial cells *in vitro*. Our group has reported that endothelial cells readily bind and internalise STB-EV which in turn transfer functional placental miRNA [111]. Furthermore,

Smarason et al. demonstrated that STB-EV have antiangiogenic properties that might contribute to the endothelial dysfunction seen in abnormal pregnancy states like preeclampsia [112]. STB-EV have been shown to inhibit endothelial cell monolayer growth *in vitro* [112-114]. Additionally, there is *ex vivo* evidence that STB-EV inhibit the relaxation of pre-constricted blood vessels [115].

Placental vesicles have been shown to induce gene changes in endothelial cells [111, 116][51, 52]. Wei et al. demonstrated transcriptional and proteomic changes that occur in human microvascular endothelial cells -1 (HMEC-1) following exposure to placental vesicles from normal first-trimester placentas [116]. Moreover, they showed that vesicles alter the phenotype of endothelial cells in a manner that may help induce the cardiovascular changes necessary for healthy pregnancy [116].

In addition to their effects on endothelial cells, STB-EV have been shown to modulate the function of platelets and immune cells including the inhibition of T and natural killer (NK) cell cytotoxicity [106, 117, 118]. Von Dadelzen et al. reported that culture supernatants from human umbilical vein cells (HUVEC) treated with STB-EV activate neutrophils [119]. STB-EV have also been shown to interact with other immune cells such as monocytes and peripheral blood mononuclear cells (PBMCs) which release proinflammatory cytokines in response to treatment with STB-EV [105, 110, 120]. Additionally, Southcombe et al. have demonstrated that *in vitro*, B cells rapidly bind and internalise STB-

EV [110]. However, the functional consequences of these interactions are yet to be determined [110].

Whilst a significant body of research has focused on the role of these vesicles on causing endothelial dysfunction, **no** studies have examined their potential effects on cardiac function. To this end, we searched our mass spectrometry database for candidate molecules previously implicated in cardiovascular physiology and pathophysiology. Furthermore, a search of the literature found that Cardiotrophin 1 plays a major role in cardiac physiology and was deemed worthy of investigation.

1.3. Cardiotrophin 1 (CT-1)

1.3.1. Background to CT-1

Cardiotrophin 1 is a 21.5kDa member of the interleukin-6 family (Figure 1.6.) that is known to have pleiotropic functions on various tissues and cell types [121-124]. Most importantly, it induces cardiomyocyte hypertrophy *in vitro* and *in vivo*, and serves as a critical component for cardiomyocyte survival [123]. In cardiomyocytes, CT-1 signals through a specific combination of glycoprotein 130 (gp130)/Leukemia inhibitory factor receptor (LIFR,) activating mitogen-activated protein kinase (MAPK), extracellular signal regulated kinase (ERK) and Janus kinase (JAK) signal transducer and activator of transcription (STAT) pathways [121, 125]. CT-1 serum levels are modulated in patients with various types of cardiovascular disease, most notably hypertension [126]. Whilst studies have measured CT-1 levels in athletes [127], known to undergo

physiological cardiac hypertrophy, no one has studied CT-1 levels in pregnancy.

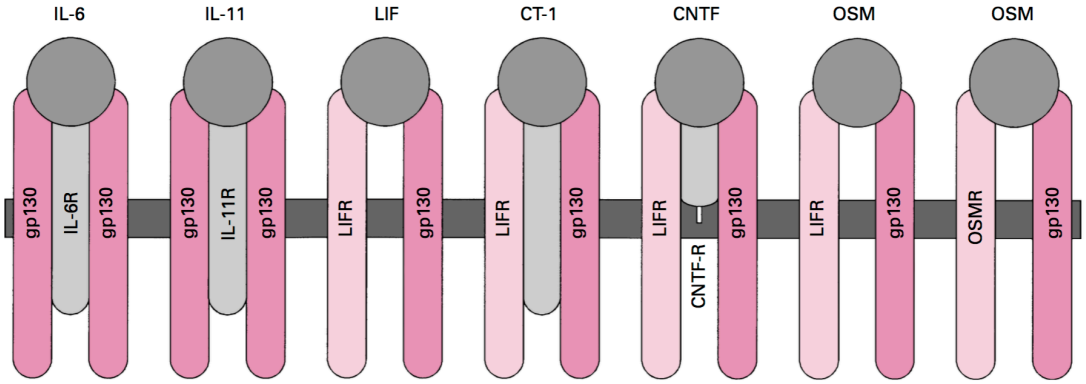


Figure 1.6. The IL-6 family of cytokine. The cytokines are schematically depicted as grey circles. Signal-transducing-receptor subunits are dark pink (gp130) or light pink (LIF-R). α-Recetor subunits are shown in light grey. **Abbreviations:** CT-1, Cardiotrophin 1; CNTF, ciliary neurotrophic factor (CNTF); gp130, glycoprotein 130; IL-6, Interleukin 6; IL-11, Interleukin 11, OSM, Oncostatin M; LIF, leukemia inhibitory factor; LIF-R, leukemia inhibitory factor receptor. Adapted from Heinrich et al., 1998.

1.3.2. Discovery and molecular biology of CT-1

Cardiotrophin 1 was isolated in 1995 by Diane Pennica and others, based on the initial observation that conditioned medium from differentiated embryoid bodies derived from mouse embryonic stem cells induced a hypertrophic response on neonatal cardiomyocytes [121]. Pools of clones from an expression cDNA library prepared from differentiated embryoid bodies were transfected into human embryonic kidney (HEK) cells 293 and a cardiomyocyte hypertrophy screen was conducted on neonatal rat ventricular cardiomyocytes [121]. This revealed that CT-1 induced cardiac hypertrophy as judged by cardiomyocyte enlargement, myosin light chain organisation, and atrial natriuretic peptide (ANP) induction [121]. The following screening of an expression cDNA library led to the discovery of a 203-amino acid protein with a DNA sequence that matched no other [121]. Furthermore, analysis of its amino

acid sequence revealed some homologies with leukotriene inhibitory factor (LIF) and ciliary neutrophic factor (CNTF), suggesting that CT-1 belongs to the IL-6 cytokine family [121].

A year later, Pennica et. al. screened a heart cDNA library with a mouse CT-1 probe. This work led to the isolation and characterisation of cDNA and genomic clones encoding human CT-1 [122]. The experiment revealed that the DNA sequence of these clones encodes a protein of 201 amino acids that was 80% identical with mouse CT-1 [122]. Human CT-1 had similar properties to mouse CT-1, in that they both lack the conventional hydrophobic N-terminal sequence indicative of a secretion signal [128, 129]. Furthermore, human CT-1 has one cysteine residue and no N-linked glycosylation, while the mouse protein has one cysteine residue and one potential glycosylation site [128, 129].

Fluorescence *in situ* hybridization (FISH) analysis demonstrated that CT-1 was found on the short arm of chromosome 16 in humans, and the mouse CT-1 gene was located on chromosome 7F3 [128, 129]. The coding regions in both the human and mouse CT-1 gene consists of three exons and two introns [128, 129]. Furthermore, when mouse nucleotide sequences of the coding regions of exons were compared with those of human, exon 1, 2 and 3 shared 96%, 84% and 81% homology, respectively [128, 129]. The 5'-flanking region of the mouse CT-1 gene contains a variety of transcription factor binding motif including CREB, MyoD, AP-1, NF-IL6, p53, Nkx2.5 and GATA-1 [128]. The 5'-

flanking region of the human CT-1 gene contains several *cis*-active DNA elements such AP-1, AP-2, CREB and GATA [122].

1.3.3. Distribution of CT-1

The CT-1 gene in the adult mouse was found predominantly expressed in the heart [121]. Sheng et. al. found that CT-1 is expressed in a relatively cardiac-restricted manner at the early stage of murine cardiogenesis [125]. However, CT-1 expression is not confined to the heart. It was also found expressed in mouse skeletal muscle, liver, lung, kidney, testis and brain [121]. Furthermore, Ishikawa et al. cloned rat CT-1 and found that CT-1 mRNA was expressed in the heart, lung, kidney, liver, skeletal muscle, stomach and bladder [124]. In humans, CT-1 mRNA was found to be expressed in the heart, skeletal muscle, ovary, colon, prostate and testis, and in fetal kidney and lung [122]. Additionally, CT-1 mRNA has been found to increase along with differentiation time from pre-adipocyte to mature adipocyte in 3T3-L1 cells [130]. In canines, CT-1 mRNA expression has also been demonstrated in the ventricle, atrium, skeletal muscle, adrenal gland, aorta and kidneys [131, 132]. Kuwahara et al. compared the expression of CT-1 in rat cardiomyocytes and cardiac non-myocytes and found that CT-1 mRNA in cardiac non-myocytes levels were 3.5 times higher than those in the cardiomyocytes [133].

1.3.4. Synthesis and secretion of CT-1

Above, we outlined CT-1 gene expression in different tissues. Following the synthesis of CT-1, it is possible that it is secreted from these tissues, and exerts its biological properties in autocrine, paracrine and endocrine fashion. To better understand the secretion of CT-1, Asai et al. collected blood from the

aorta and coronary sinus of 12 patients with angina pectoris undergoing diagnostic cardiac catheterization [134]. They found that CT-1 plasma levels were elevated in both the aorta and the coronary sinus, which suggests that the heart secretes CT-1 via the coronary sinus into the peripheral circulation [134]. No other sources of circulating CT-1 have been described.

The mechanisms regulating CT-1 synthesis are unclear, but mechanical and humoral factors ar believed to be involved. For example, mechanical stretch of cardiomyocytes stimulates CT-1 expression. Pressure overload induced by ligation of the abdominal aorta has been shown to increase cardiac CT-1 gene expression, a process mediated by the JAK/STAT pathway [135-137]. There is also evidence that hypoxia upregulates CT-1 expression, and hypoxia inducible factor (HIF)-1α has been shown to be involved [138, 139]. Furthermore, pro-oxidants like menadione, hydrogen peroxide and cobalt chloride have all been shown to augment protein and gene expression of CT-1 in embryoid bodies [139].

1.3.5. CT-1 Receptor

CT-1-induced effects are mediated through the molecular binding to a transmembrane receptor, composed of two subunits: the high-affinity gp130 and leukaemia inhibitory factor receptor (LIF-R) (Figure 1.7.) [140]. Gp130 is a glycosylated protein that consists of 918 amino acids with a single transmembrane domain [141]. It has a leader sequence of 22 amino acids, an extracellular domain of 597 amino acids, a membrane spanning domain of 22 amino acids and a cytoplasmic region of 277 amino acids [141]. The

extracellular region comprises six units of a fibronectin type III (FN III) module and the cytoplasmic domain is composed of an Ig-like, a haemotopoietin-like and FN III-like domain [141]. The predicted molecular weight of gp130 is 101 kDa [141]. However, due to glycosylation, the native weight of gp130 is 130 kDa. Gp130 is ubiquitously expressed in human and murine tissue cell lines where it has the potential to bind cytokines and inhibit their signaling via membrane bound gp130 [142].

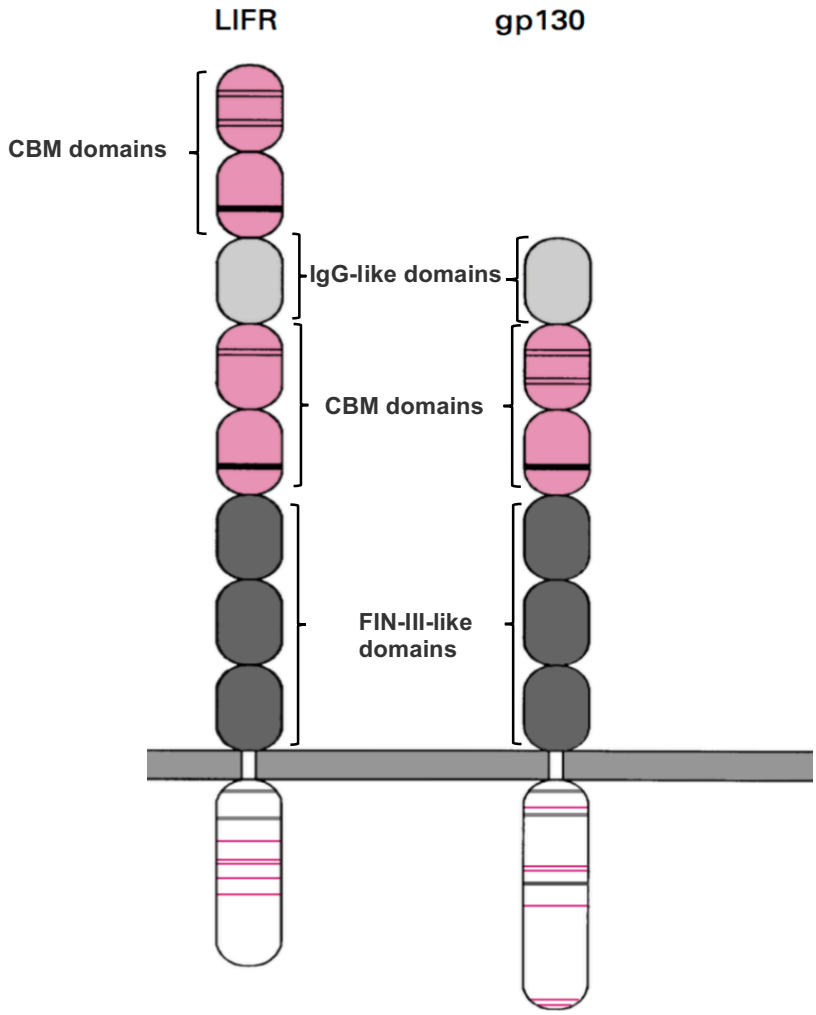


Figure 1.7. Domain composition of gp130 and LIF-R. Predicted IgG-like domains are shown light grey, fibronectin-type III-like domains dark grey and carbohydrate-binding module (CBM) in dark pink. The lengths of the cytoplasmic parts (white) correspond to the respective numbers of amino acids. Adapted from Heinrich et al., 1998.

The leukemia inhibitory factor receptor (LIF-R) subunit is a 190 kDa protein and a member of the haematopoietin receptor superfamily [143]. It most closely resembles gp130. LIF-R and gp130 subunits rapidly associate to form a high affinity receptor complex [144]. It is considered that CT-1 binds first to LIF-R with a lower affinity interaction, and then binds to gp130 with a higher affinity interaction to form a heterotrimeric complex on the cell membrane [145]. Wollert et al. demonstrated that both gp130 and LIF-R were tyrosine-phosphorylated upon stimulation with CT-1 [146]. Furthermore, in addition to the gp130 - LIF-R complex, Robledo et al. suggested a third component of the receptor (CT-1Rα) with an apparent molecular weight of 80 kDa [147]. Thus, CT-1 may form a tripartite receptor complex with LIF-R and gp130. However, this additional membrane component is apparently not required for CT-1 effects on other cells [148].

1.3.6. CT-1 Signaling pathways

Signal transduction via gp130 involves three major downstream pathways: the JAK (Janus-activated kinase)–STAT (signal transducer and activator of transcription) axis, mitogen-activated protein kinase (MAPK, MEK/ERK) signaling cascade, and the phosphatidylinositol 3-kinase-dependent (PI3K)/Akt (protein kinase B: PKB) pathway (Figure 1.8.). Downstream to gp130/LIF-R activation is the phosphorylation of JAK1, JAK2 and the tyrosine kinase associated with gp130, which in turn, phosphorylates tyrosine residues in the cytoplasmic domain of gp130 [149]. These phosphotyrosines subsequently serve as docking sites to recruit STAT proteins. The STAT proteins are then phosphorylated and translocated to the nucleus where they bind specific DNA

sequences to modulate gene expression [149]. Using a dominant-negative MEK 1 and protein inhibitor of activated STAT (PIAS) 3, Railson et al. reported that the hypertrophic action of CT-1 is dependent of STAT 3 and the cytoprotective action of CT-1 is MAPK dependent.

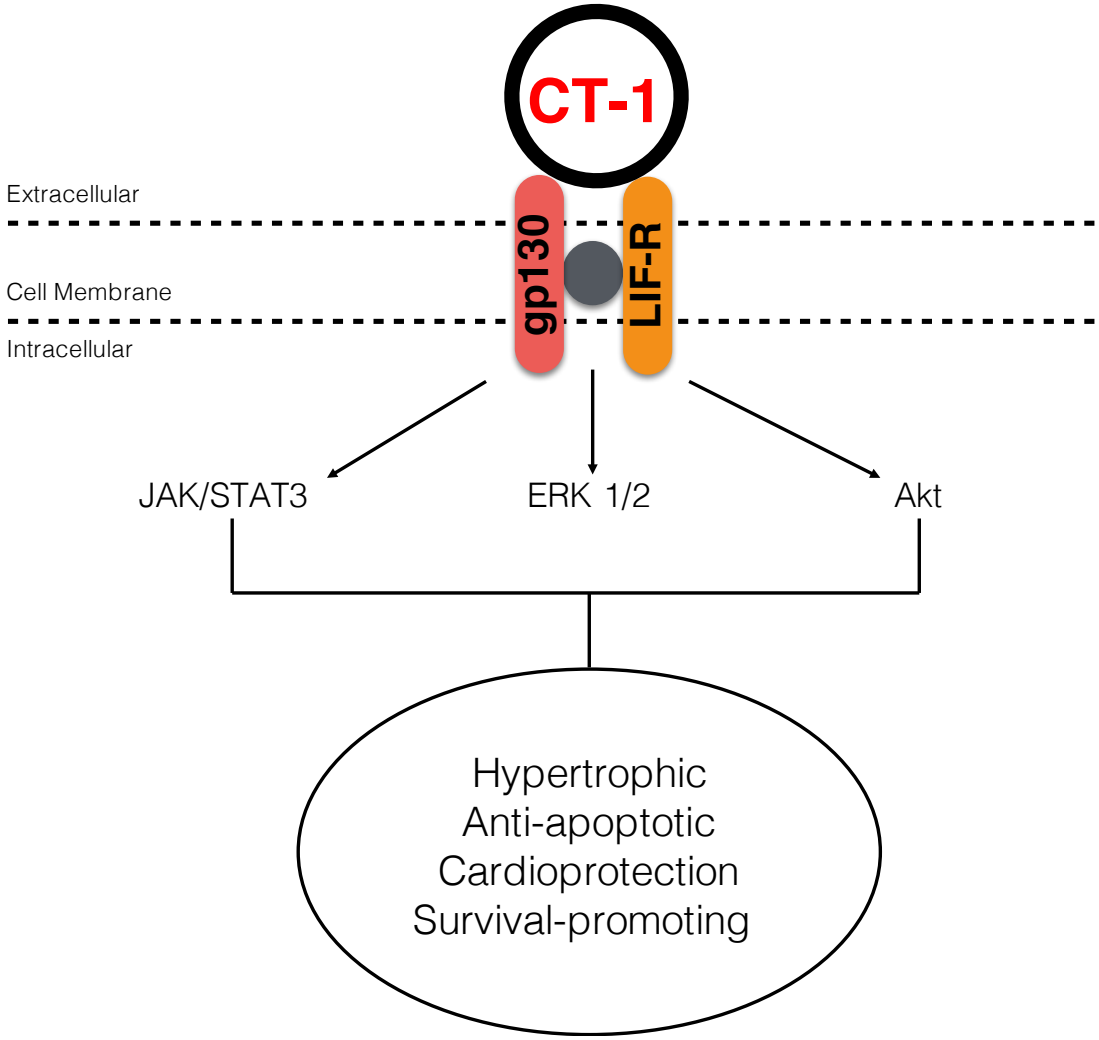


Figure 1.8. Schematic diagram of major pathways involved in Cardiotrophin 1 (CT-1) signaling

Gp130/LIF-R activation also leads to docking of other Src homology 2 (SH2) domain-containing proteins, such as PI3K, growth factor receptor-bound protein 2, adapter proteins (Shc), Ceacam1 (pp120) and the cytoplasmic SH2 domain containing protein tyrosine phosphatase (SHP2) [150, 151]. Recruitment of Shc to phosphorylated subunits of gp130 leads to complex

formation with Grb2 and SOS, which activates Ras-Raf MAPK (MEK/ERK) pathway [150, 151]. In studying the anti-apoptotic effects of CT-1, Sheng et al. transfected MAP kinase kinase (MEK) 1 dominant negative mutant cDNA into myocardial cells, and showed that MAP kinase was required for survival effect of CT-1 [152]. Takahashi et al. also demonstrated that CT-1 activates ERK5 in cardiomyocytes and mediates cardiac hypertrophy [153]. On the other hand, Li et al. reported that CT-1 simultaneously activated both ERK1/2 and STAT 3 in rat cardiomyocytes [154]. Similarly, Tian et al. reported that the hypertrophic effect of CT-1 was essentially mediated by STAT 3 [155].

He-nan et al. demonstrated that CT-1 stimulates gene expression of GATA4 and binding activity of cardiomyocytes [156]. GATA4 is a transcriptional regulator for cardiac hypertrophy and genes such as ANP and BNP [156]. Furthermore, in rat cardiomyocytes, the augmented expression of GATA4 mRNA by CT-1 was found to be mediated by STAT 3, and was negatively regulated by ERK 1/2 [156].

1.3.7. Biological actions of CT-1

CT-1 is a pleiotropic cytokine that has been shown to play an essential role in several organs systems including neural development [157-160] and neuroprotection [145, 161-163], energy homeostasis and hepato-protection [164-173], renal protection [174], photoreceptor protection and maintenance of extraocular muscle force [175], bone formation and resorption [176], regeneration and hypertrophy of skeletal muscle [177]. This thesis will, however, focus on the cardiovascular actions of CT-1.

1.3.7.1. Cardiac hypertrophy

CT-1 was first isolated as a factor capable of inducing cardiomyocyte hypertrophy in neonatal ventricular cardiomyocytes [145]. Subsequent *in vitro* studies demonstrated that CT-1 was capable of inducing hypertrophy in adult cardiomyocytes [178]. Furthermore, Wollert et al. showed that CT-1 cardiomyocyte hypertrophy that was distinct from hypertrophy induced by stimulation of G-protein-coupled receptors [146]. They also showed that, unlike cardiomyocyte hypertrophy that is induced by adrenergic agonists, endothelin 1 and angiotensin II, cardiomyocyte hypertrophy induced by CT-1 was characterised by the addition of sarcomeres in series rather than in parallel [146]. This results in an increase in cell length with minimal change in cell width [146].

In vivo, when CT-1 was administered to intact mice by intraperitoneal injection, a dose dependent increase in both overall cardiac weight and ventricular weight was observed in the mice treated with CT-1, although total body weight was unaffected [179].

The mechanisms mediating CT-1-induced cardiomyocyte hypertrophy have not been fully clarified. Initially, activation of the JAK/STAT 3 axis was responsible for this effect [155, 178]. However, a recent report has implicated the MEK5-ERK5 pathway in cardiomyocyte hypertrophy [153]. Furthermore, it has also been reported that the hypertrophic effects of CT-1 on cardiac cells are at least in part dependent on hsp56 induction downstream of JAK/STAT, MEK/ERK and PI3K/Akt [180]. Additionally, Tian et al. reported that ERK1/2

can inhibit STAT 3 phosphorylation, which negatively regulates CT-1-induced hypertrophic responses in cardiomyocytes [155]

1.3.7.2. Cardioprotection

The cardioprotective effects of CT-1 have been well described. In the heart, the gp130 receptor is essential in mediating protective effects against physiological and pathophysiological stress. For example, Lopez et al. demonstrated that CT-1 protects rat cardiomyocytes against angiotensin II via gp130 [181]. Furthermore, when Hirota et al. pressure overload in mice by aortic banding-induced, mice lacking gp130 had massive cardiac cell apoptosis and death from heart failure compared to control mice that underwent a hypertrophic response and survived [182].

In 1996, Sheng et al. first reported that treatment with CT-1 could enhance the survival of neonatal rat cardiac myocytes cultured in serum free medium [125]. Their findings were later corroborated by Stephano et al., when they demonstrated that CT-1 not only improved cell survival and resulted in less apoptotic cell death of neonatal rat cardiomyocytes, but that CT-1 also protects cardiomyocytes against subsequent exposure to heat shock or simulated ischaemia/hypoxia [183]. The resistance to hypoxic/ischaemic and heat shock induced injury was shown to be a result of the ability of CT-1 to induce enhanced levels of the hsp70 and hsp90 [183]. These heat shock proteins have been shown to protect cardiomyocytes against thermal and ischaemic stress [184, 185].

CT-1 has also been shown to phosphorylate Akt and BAD via a PI3 kinase dependent pathway by the action of selective PI3 kinase antagonist which inhibited the anti-apoptotic effects of CT-1 in rat neonatal cardiomyocytes [186]. Non-phosphorylated BAD has been shown to associate with Bcl-X_L, but phosphorylated BAD cannot bind Bcl-X_L, thus releasing Bcl-X_L to carry out anti-apoptotic effects [187]. Therefore, Akt phosphorylation mediates CT-1 induced cell survival signaling in cardiac myocytes by its ability to phosphorylate BAD [186, 188].

Cardioprotection by CT-1 has also been associated with other molecular mediators such as the activation of MEK 1/2 AND p44/42 MAP kinase [152, 178, 189, 190]. Furthermore, cardioprotection induced by CT-1 was shown to dependent on the downstream nuclear translocation of the nuclear factor kappa B (NFkB) [191]. Additionally, many of the signaling cascades described above inhibit pro-apoptotic proteins such as p53, Fas and Bax, and upregulate anti-apoptotic proteins such as Bcl2 [192]. Most notably, the JAK/STAT pathway has been shown to defend cardiomyocytes against ischemia/reperfusion injury by reducing ROS production and is also believed to be a mechanism behind the protective effects against ischaemic preconditioning [193].

1.3.7.3. CT-1 effect on cardiac fibroblast, myofibroblasts and endothelial cells

In addition to the effects of CT-1 of promoting cardiomyocyte survival and, cardiomyocyte hypertrophy, CT-1 has also been shown to stimulate the proliferation and migration of cardiac fibroblasts and myofibroblasts (phenotypic derivatives of interstitial fibroblasts) [194]. Furthermore, CT-1 increased synthesis of extracellular matrix proteins [195]. Cardiac fibroblast growth is mediated by activation of the gp130/LIF-R complex and endothelin 1 type A receptor phosphorylation resulting in the downstream activation of the JAK/STAT pathway, MAPK pathway and the PI3 kinase pathway [196].

With regards to endothelial cells, CT-1 has been shown to stimulate protein and gene expression of intercellular adhesion molecule (ICAM)-1 and monocyte chemoattractant protein (MCP)-1 in human aortic endothelial cells (HAEC) and human umbilical vein endothelial cells (HUVEC) [197, 198]. The upregulation of these two molecules was suppressed by PD98059, SB203580, LY294002, and parthenolide [197, 198]. Furthermore, the effects of ICAM and MCP-1 were mediated by ERK 1/2, p38 MAP kinase, PI3 kinase, and NF kB pathways [197, 198]. It is thought that these findings demonstrate a role played by CT-1 in the pathophysiology of vascular inflammation and atherosclerosis.

1.3.8. Systemic actions of CT-1

Hemodynamically, intravenous admiration of CT-1 resulted in a significant decrease in blood pressure with reflex tachycardia in rats [199-201]. This effect seems to be mediated by nitric oxide. Hamanaka et al. showed that pre-

treatment of cardiomyocytes with N^{ω}-Nitro-L-arginine methyl ester hydrochloride (L-NAME), a specific inhibitor of nitric oxide synthase (NOS), significantly attenuated depressor and tachycardia effects of CT-1 [200].

Although CT-1 is known for its cytoprotective and hypertrophy inducing properties, it also has a broad spectrum of biological activities *in vivo*. For example, Jin et al. showed that chronic administration of CT-1 in mice not only causes dose-depended cardiomyocyte hypertrophy, but also stimulated the growth of liver, kidney and spleen [199]. Furthermore, CT-1 administration also induced thrombocytosis and erythrocytosis [199].

Clinically, the plasma concentration of CT-1 is altered in various cardiovascular disorders, most notably, hypertensive heart disease (HHD) [126]. Lopez et al. reported that plasma CT-1 was increased in hypertensive patients as compared to normotensive controls [202], findings later corroborated by Pemberton et al. [137]. Additionally, CT-1 levels were higher in patients with left ventricular hypertrophy [202]. Plasma concentrations of CT-1 were directly correlated with the left ventricular mass index in all subjects, suggesting a true hypertrophic response [203]. Intriguingly, when subjects were treated with antihypertensive medication, the plasma CT-1 levels decreased in patients in which left ventricular mass regressed, whilst CT-1 levels remained elevated in those with persisted inappropriate left ventricular mass [203]. Similarly, Gonzalez et al. reported an association between the treatment-induced decreased of plasma CT-1 levels and regression of left ventricular hypertrophy in patients with essential hypertension [203].

Plasma concentration levels of CT-1 have also been associated with the progression of heart failure in patients with HHD. Lopez et al. reported that CT-1 plasma levels progressively increased along with the progression of congestive heart failure (CHF) stages in hypertensive patients [204]. Furthermore, they found that plasma CT-1 was directly and inversely correlated with left ventricular mass index and ejection fraction, respectively [204].

In contrast to elevated plasma levels seen in humans, CT-1 levels in untreated spontaneously hypertensive rats (SHR) were significantly lower than those in matched normotensive Wistar Kyoto rats (WKY) [137]. In a separate study, Dahl salt-sensitive (DS) rats with a high-salt diet showed a distinct transition from left ventricular hypertrophy to congestive heart failure [205]. The expression levels of CT-1 mRNA and protein were significantly increased at the CHF stage compared with the LVH stage and age-matched Dahl salt-resistant (DR) rats [205].

There have also been several reports describing the elevated plasma concentration levels of CT-1 in patients with other cardiac complications and associated conditions including congestive cardiac failure [206-208], dilated cardiomyopathy[209], valvular heart disease [210], and ischaemic heart disease [211, 212], and chronic kidney disease [213].

In contrast to pathological cardiac hypertrophy that occurs in cardiovascular diseases described above, physiological heart hypertrophy is associated with

normal or enhanced cardiac function, seen in athletes and normal pregnancy. Limongelli et al. measured plasma CT-1 levels during and after physical exercise in healthy individuals and elite athletes [127]. They found that most of the athletes and control group showed a rise in CT-1 levels at peak-exercise and a fall in CT-1 levels post-exercise, perhaps a reflection of the body's response to physical stress [127]. Surprisingly, no one has studied CT-1 levels in normal pregnancy, also known to undergo physiological cardiac hypertrophy.

Cardiotrophin 1 is pleiotropic cytokine that is expressed in the heart and several other tissues. It is considered to act in an autocrine and/or paracrine manner to affect its hypertrophic and cytoprotective properties both as a regulator of cardiac physiology and to maintain pathophysiological cardiovascular homeostasis. CT-1 is also circulating in the body, and its plasma concentration is modulated in many cardiovascular and associated diseases. What is not known is whether they are deported on extracellular vesicles.

This project was initially aimed at exploring:

1. The novel hypothesis that STB-EV have a role in cardiac specific adaptations in normal pregnancy thereby linking the placenta to the cardiac changes seen in pregnancy.
2. Genetic changes associated with CT-1 treatment of cardiomyocytes
3. When platelet extracellular vesicles were used as negative control for STB-EV, we found, incidentally, that CT-1 was also expressed on

platelet-derived EV, so this was also studied and novel findings of platelet-derived EV bound CT-1 cytoprotective effects on endothelial cells was reported

CHAPTER 2

CHARACTERISATION OF STB-EV BOUND CT-1 ON ENDOTHELIAL CELLS AND CARDIOMYOCYTES

2.1. INTRODUCTION

One of the key features of pregnancy that has been discussed in the Introduction to this thesis is maternal cardiac hypertrophy, a characteristic response of cardiomyocytes to mechanical and neuro-hormonal stimuli. Cardiac hypertrophy involves numerous molecular processes that include membrane receptors, second messengers, and transcription factors. A search of the literature found that Cardiotrophin 1, a member of the IL-6 cytokine family that consists of IL-6, IL-11, ciliary neurotrophic factor (CNTF), leukaemia inhibitory factor (LIF) and oncostatin M (OSM), plays a significant role in cardiac physiology, particularly, cardiac hypertrophy. This family of cytokines associates with glycoprotein 130 (gp130) and leads to tyrosine phosphorylation of gp130. [1, 2]. Downstream from gp130, three distinct pathways mediate CT-1 signaling. These pathways are: 1) the Janus kinase/signal transducer and activator of transcription (JAK/STAT) pathway and 2) the p42/44 mitogen-activated protein kinase (p42/44 MAPK) pathway also known as the extracellular receptor kinase-1/2 (ERK1/2) which are involved in the induction of cardiac myocyte hypertrophy and prevent myocyte apoptosis, and 3) the phosphatidylinositol 3-OH kinase (PI3K)/Akt pathway which is involved in the promotion of cardiomyocyte survival [3-5]. It is likely that CT-1 achieves its effects via a combination of these three signaling pathways.

However, CT-1 has effects not only on myocytes but also on the vasculature by decreasing systemic vascular resistance in animal models [6], hepato-protective effects in acute liver injury [7], and attenuation of endotoxin-induced

acute lung injury [8]. CT-1 has also been shown to be a potent survival factor for the survival of motor neurons during embryonic development [9]. CT-1 serum levels are modulated in patients with various types of cardiovascular disease, most notably hypertension [10]. While studies have measured CT-1 levels in athletes (who are known to undergo physiological cardiac hypertrophy) [11], CT-1 levels have not been considered in normal pregnancy.

During pregnancy, the heart develops a reversible physiological hypertrophic growth. Physiological heart hypertrophy is associated with normal or enhanced cardiac function in contrast to pathological cardiac hypertrophy that occurs in cardiovascular disease. Initially, the hypertrophy is a beneficial response, but when prolonged, the heart muscle is weakened, leading to decreased contractility and ultimately heart failure – a condition where the heart cannot sustain the supply of oxygenated blood to the body. It is known that, regardless of the species, the cardiomyocytes respond to the pathological hypertrophic stimulus with a characteristic succession of changes in gene expression. One of the first detectable changes is the activation of a program of immediate early genes. Genes such as c-fos, c-jun, and c-myc are transcribed as early as 30 minutes in response to mechanical stress [12]. Most of these genes are transiently over-transcribed, but the transcription normalises a few hours later, even though the stimulus persists. Cardiac hypertrophy is also associated with over-regulation of sarcoplasmic reticulum calcium pump (ATP2A2), myosin heavy chain 7 beta (MH7B) and atrial natriuretic peptide (ANP) amongst others [13-16]. The expression of these genes is delayed, usually taking place within 6 to 12 hours after the production

of the stimulus. Intriguingly, CT-1 has been shown to promote transcription of atrial natriuretic peptide and brain natriuretic peptide (BNP) [17, 18].

Until recently, the role of extracellular vesicles and particularly exosomes, as agents of cell-cell signaling both locally and remotely in cardiac physiology has been under-appreciated. Much emphasis had been placed on cytokines, peptides and other mediators as the main regulators of cardiac function. However, EV-dependent communication could be a superior mode of communication compared to the release of free soluble factors. First, molecules in the EV cargo are well protected by the vesicle membrane. Second, vesicle-mediated transport might be better targeted as EV could be specifically delivered to target cells.

Despite a significant body of work investigating cardiac hypertrophy, little is known about the molecular mechanisms that mediate pregnancy-induced hypertrophy. This may be because the heart is a dynamic network of various cell types, a physiological network not easily recapitulated in cell culture. Additionally, recreating the cytokine, chemokine and hormonal milieu of pregnancy for *in vitro* studies is technically very challenging. Notwithstanding this limitation, numerous studies have used *in vitro* model systems which have provided an initial skeleton of the potential signaling pathways that regulate cardiac genes during growth and hypertrophy.

We hypothesised that some cardiac changes in pregnancy e.g. cardiac hypertrophy might be mediated to a smaller or greater extent by the

trophoblast via the release of STB-EV. We explored the novel hypothesis that CT-1 is deported on STB-EV and that EV-bound CT-1 may alter gene expression in endothelial and cardiovascular cells in *in vitro* systems, thereby linking the placenta to the cardiac changes seen in pregnancy.

2.1.1. Aims

The aims of the work described in this chapter were to:

1. Investigate the expression of CT-1 on the human placenta by immunohistochemistry and Western blotting.
2. Isolate STB-EV using the ex-vivo dual perfusion technique and to characterise STB-EV by Western blotting, Nanoparticle Tracking Analysis (NTA), Electron Microscopy (EM) and flow cytometry.
3. Investigate the levels of CT-1 expression on PLAP positive STB-EX and STB-MV by Western blotting and flow cytometry.
4. Investigate the signaling mechanisms potentially effected by STB-EV-bound CT-1 *in vitro* by measuring intracellular molecules associated with CT-1 in cultured cells and to attenuate these effects by pharmacological inhibitors.
5. Study cardiac hypertrophy associated gene changes in endothelial cells and cardiomyocytes treated with CT-1 positive STB-EX.

2.2. MATERIALS AND METHODS

2.2.1. Patient information

For the isolation of syncytiotrophoblast extracellular vesicles (STB-EV) and human umbilical vein cells (HUVEC), placentas were collected from normal pregnant women undergoing elective caesarian section without labour. Normal pregnancy was defined as a healthy singleton pregnancy, without known fetal abnormality, natural conception and normal maternal blood pressures. Approval for these studies was obtained from Oxfordshire Research Ethics Committee C (Reference Number: 07/H0606/148). Informed written consent was obtained from all study subjects by a dedicated research mid-wife, who would also collect the placenta at the time of caesarean section and immediately deliver it to the laboratory for processing.

2.2.2. Immunohistochemistry

Paraffin embedded tissues from normal placental lobes, cut (5μm thickness) and processed by technicians at the Dunn's School of Pathology Oxford, were used for assessment of Cardiotrophin 1 (CT-1) expression. Tissues were deparaffinized and rehydrated in descending ethanol gradients (100%, 90%, 70%, 50% ethanol). For antigen retrieval, slides were boiled for 1 minute in sodium citrate (10mM, pH 6). Non- specific protein binding was blocked using 10% normal fetal calf serum (FCS) (Sigma, UK) for 1 hour at room temperature. Endogenous peroxidase activity was blocked using 0.3% hydrogen peroxidase (Sigma, UK). Tissue sections were probed with a monoclonal mouse primary antibody (1:100) to CT-1 (Abcam, UK) in 1% FCS

in 0.01% Phosphate Buffered Saline-Tween (PBS-T) (Sigma, UK) overnight at 4° C. Negative control sections were incubated overnight at 4° C in PBS containing 10% mouse serum (Sigma, UK). Slides were washed three times between treatments. The sections were subsequently incubated for 1 hour at room temperature (RT) with a mouse HRP-linked secondary antibody (New England Biolabs, UK). Finally, slides were treated with substrate and chromogen 3, 3'- diaminobenzidine (DAB) (Vector Laboratories, USA) and counterstained with hematoxylin (Sigma, UK). Coverslips were mounted in aqueous mounting medium (Vectashield) (Vector Laboratories, USA). The sections were viewed under a Leica DM2500 optical microscope (Leica Microsystems), and images were taken using a digital camera (Micropublisher 5.0 RTV).

2.2.3. Isolation of STB-EV by Ex-vivo Dual Placental Lobe Perfusion

To generate STB-EV, a dual placental perfusion system, [214] modified as previously described, [215] was used. Briefly, an intact peripheral lobule with no visible signs of postpartum villus breakage was identified, and an associated branch of the umbilical artery and vein were cannulated at the chorionic plate and perfused with 0.1 μM filtered tissue culture medium (Medium 199 with L-glutamine and Earle's salts, containing 0.8% Dextran 20, 0.5% Bovine Serum Albumin (BSA) (Sigma, UK) and 5000 U/L sodium heparin (Fannin, UK) at a rate of 5 mL/min. The whole placenta was turned upside down (with the maternal surface facing up) and laid inside a Perspex water jacket maintained at 37° C (Figure 2.1). The maternal surface was then perfused with tissue culture medium (Medium 199 with L-glutamine and Earle's

salts, containing 0.5% BSA, 5000 U/L sodium heparin) through six 1.7 mm fetal feeding tubes (Pennine Healthcare, UK) at a controlled rate of 20 ml/min. The lobule was perfused for 20 minutes to equilibrate the system, after which time the maternal circuit was closed with a total volume of perfusion medium of 600 ml. The volume of fetal effluent was continuously measured to ensure the stability of the preparation.

At the end of the 3-hour perfusion period, the maternal perfusate was centrifuged (Figure 2.2) to remove red blood cells and large cellular debris in a Beckman Coulter Avanti J-20XP centrifuge using a Beckman Coulter JS-5.3 swing out rotor at 200 x *g* for 10 minutes at 4° C. To generate microvesicles (STB-MV), the supernatant was then further centrifuged in a Beckman L80 ultracentrifuge and Sorvall TST28.39 swing out rotor at 10,000 x *g* for 30 minutes at 4° C. The supernatant was removed for further processing and the pellets were resuspended and pooled in sterile phosphate buffered saline (PBS) before being centrifuged again at 10,000 x *g* for 30 minutes at 4° C to wash the pellet, further reducing contamination by soluble proteins. The resultant washed pellet containing enriched microvesicles was then resuspended in sterile PBS for subsequent analysis. The remaining supernatant was passed through a 0.22 μm Stericup filtration device (Sigma, UK) to remove any large material before being centrifuged in a Beckman L80 ultracentrifuge with a Sorvall TST28.39 swing out rotor at 150,000 x *g* for 2 hours at 4° C. The pellets were pooled and washed in sterile PBS before finally being resuspended in PBS to give an enriched exosome fraction (STB-EX). The protein concentration (5 mg/ml) of each resuspended STB–MV and STB-

EX preparation was assessed using a Pierce BCA protein assay kit (Thermofisher Scientific, UK) before aliquots were stored at −80° C until subsequent use.

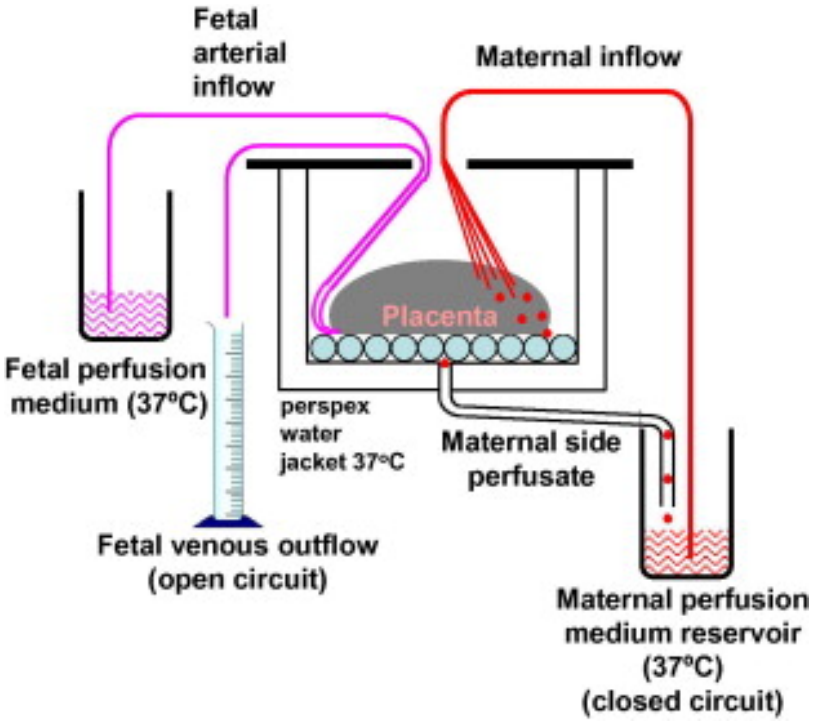


Figure 2.1. Schematic diagram of dual placental lobe perfusion system.
Adapted from Dragovic et al 2015

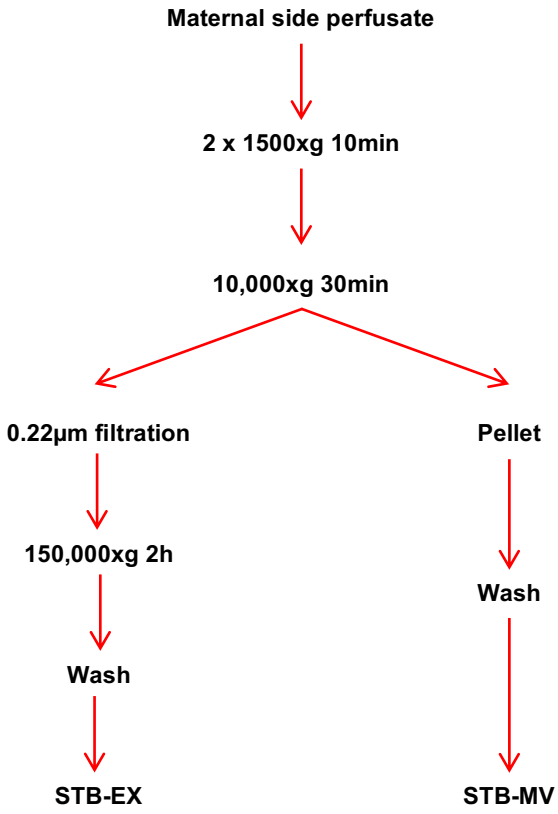


Figure 2.2. Schematic diagram of the sequential centrifugation and filtration protocol for the isolation and fractionation of placental EV from maternal perfusate collected using the *ex vivo* dual placental lobe perfusion method. Abbreviations: STB-EX: Syncytiotrophoblast-derived exosomes. STB-MV: Syncytiotrophoblast derived microvesicles.

2.2.4. Assessment of STB-EV size and concentration by Nanoparticle Tracking Analysis (NTA)

STB-EV size distribution profiles and concentration measurements of fresh microvesicle and exosomal fractions were analysed by nanoparticle tracking analysis (NTA) using a NanoSight NS500 instrument (Malvern, UK) as previously described [216]. STB-EV samples were diluted in PBS to give approximately 5 x 10^8 EV/ml. The samples were automatically introduced into the Nanosight sample chamber and then a finely focused laser beam was shone into the sample through a glass prism (Figure 2.3) [217]. The beam is refracted at a low angle as it enters the sample, resulting in a thin beam of laser light that illuminates vesicles through the sample. Light scattered by the

samples was then visualised using a conventional optical microscope, fitted with a video camera scientific complementary metal-oxide-semiconductor (sCMOS) at level 12 (camera shutter speed; 15 ms and camera gain; 350) collecting light scattered from all particles in the field of view. A 60 seconds long video was taken, with a frame rate of 30 frames per second . The PRIME, DELAY 5, CAPTURE 60, REPEAT 4 script was used for EV measurements. The NTA software then identified and tracked individual nanoparticles moving under Brownian motion and related the movement to the particle size according to a formula derived from the Stokes-Einstein equation:

$$< x, y >^2 = \frac{K_B T t_s}{3\pi\eta d_h}$$

where $< x, y >^2$ is the mean squared displacement, K_B is Boltzmann's constant, T is the temperature of the solvent in Kelvin, t_s is the sampling time (i.e. 33 msec), η is the viscosity and d_h is the hydrodynamic diameter.

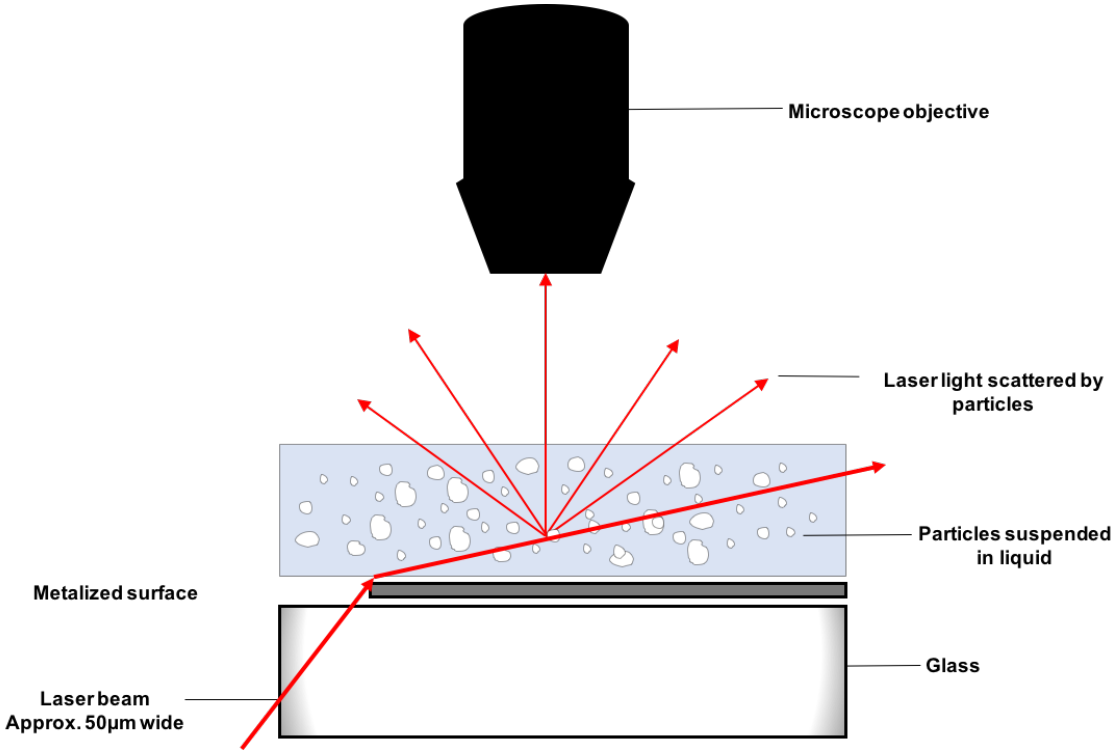


Figure 2.3. NanoSight instrument configuration. Nanoparticle tracking analysis (NTA) uses a finely focused laser beam that is introduced to the sample (a liquid containing a dilute suspension of particles) through a glass prism. The beam refracts at a low angle as it enters the sample, resulting in a thin beam of laser light that illuminates particles through the sample. Particles resident within the beam are visualized using a conventional optical microscope, fitted with a video camera, aligned normally to the beam axis, which collects light scattered from all particles in the field of view.

Silica 100nm calibration microspheres (Polysciences, Inc., USA) were routinely analysed to check instrument performance. Each video recording was analysed to determine EV size and concentration measurements using Nanoparticle Tracking Analysis (NTA) software version 2.3, Build 0033 (Malvern, UK).

2.2.5. Characterisation of STB-MV by Flow Cytometry

For characterization of STB-MV, multi-colour flow cytometry using a BD LSRII flow cytometer (BD Biosciences, UK) was carried out on freshly isolated STB-MV preparations using the method previously described [215]. Prior to use, all

antibodies, FcR blocking agent (Miltenyi Biotech, UK) and Biomaleimide were filtered through Nanosep 0.2 μm centrifugal devices (Sigma, UK). PBS was filtered through Whatman Anotop 0.1 μm filters.

Prior to running vesicle samples, Trucount beads (BD Biosciences, UK) were used to calculate vesicle concentrations using a method optimized in our laboratory. Briefly, 500 μl PBS was added to a BD Trucount tube and data acquired for two minutes on the "LO" flow rate setting (~12 μl/min) setting. To determine the flow rate in two minutes (A), the number of positively gated BD Trucounts beads (X) was divided by the number of BD Trucounts beads per tube (Y) and then multiplied by volume (A= X/Y x V). Next, fluorescence compensation was carried out using BD^{TM} CompBeads (BD Biosciences, UK) according to the manufacturer's instructions. Compensation was done to correct for the spillover of the fluorescence emission of one fluorochrome detected in a detector designed to measure a signal from another fluorochrome. To determine spillover from the FITC channel, STB-MV were labeled with the pan lipid membrane marker, BODIPY FL N-(2-aminoethyl)-maleimide (505/513 nm) (Molecular Probes, UK) which binds biological membranes via cysteine residues and thiol groups in proteins [218].

The level of background contaminating events was determined using filtered PBS and these were subsequently deducted from the total vesicle counts. Next, the volume of vesicles that would need to be labeled was determined by diluting samples with a given volume of PBS that would result in 20,000 – 30,000 total events being analysed in two minutes. Subsequently, 50 μl of

vesicle sample was incubated with 10 µl Fc receptor blocking reagent for 10 minutes at 4° C.

For the study of STB-MV, samples were labeled with the pan lipid membrane marker 0.5 µM Bio-maleimide to exclude particles which were not vesicles from the analysis. STB-MV were then identified using 0.5 µg/ml of the monoclonal antibody NDOG2 [215], which labels placental alkaline phosphatase (PLAP), a syncytiotrophoblast specific marker [219] and a marker for STB-EV. A panel of antibodies to markers of potential contaminating EV was used in parallel. These were to platelet EV (0.25 µg/ml anti-CD41 - PECy7) (Biolegend, UK), red blood cell (RBC) EV (0.05 µg/ml anti-CD235a/b - PECy5) (Biolegend, UK) and HLA-class I (2.5 µg/ml anti-W6/32 - Alexa 647) (AbD Serotec, UK) positive EV, which labels all EV from all cell types except those from STB and RBC, which are HLA class I negative [220].

A fluorescence minus one (FMO) control was used which contained all the fluorochromes in a panel, except for the one that was being measured. Following incubation, samples were diluted with PBS and transferred to flow cytometry tubes for analysis. Thirty thousand events were acquired and vesicles were identified by their forward and side scatter optical characteristics. Gates set on single parameter histograms, using the FMO controls, were used to determine the positive populations.

Data were analysed using FACSDiva software version 8.0 (BD Biosciences, UK) and figures generated using FlowJo version 10 (Tree Star Inc., Ashland, OR, USA).

2.2.6. Assessment of CT-1 expression on STB-MV by Flow Cytometry

For the detection of CT-1 by flow cytometry, an unconjugated antibody against CT-1 (R & D Systems, UK) was purchased and Lightning-Link antibody labeling kit (Innova Biosciences, UK) was used to conjugate the antibody to Allophycocyanin (APC). The APC conjugated CT-1 antibody was then titrated using single staining on HepG2 cells (prepared as described in section 2.2.9.1 below) which are known to the express CT-1. Aliquots containing 1 x 10^6 cells per 100 µl in 1.5 ml Eppendorf tubes were blocked with an FcR blocker for 10 minutes at 4° C. The APC conjugated CT-1 antibody was then titrated at 2.5, 5, and 10 µg/ml and incubated with the cells for 30 minutes. Additionally, aliquots containing the same concentration of cells were incubated for 30 minutes with APC conjugated isotype negative controls. After this time, 250 µl of PBS was added to each sample and transferred to flow cytometry tubes for analysis. Ten thousand events were collected by flow cytometry. Cells were identified by their forward and side scatter optical characteristics. Gates set on single parameter histograms, using the isotype-negative controls were used to determine the positive populations.

For the assessment of the expression of Cardiotrophin 1 on STB-MV, 50 µl of vesicle sample was incubated with 10 µl FcR blocker for 10 minutes at 4° C before being labeled with an antibody cocktail: 5 µg/ml APC conjugated CT-1,

0.5 μg/ml Phycoerythin (PE)-conjugated PLAP (NDOG2), 0.25 μg/ml Phycoerythrin Cyanine 7 (PE-CY7) CD41 (Biolegend, UK) and 0.05 μg/ml Phycoerythrin Cyanine 5 (PE-CY5) CD235a (Biolegend, UK) or 5 μg/ml APC IgG2A isotype control (Biolegend, UK), 0.5 μg/ml PE IgG1 isotype control (Biolegend, UK), 0.25 μg/ml PECY7 IgG1 isotype control (Biolegend, UK), 0.05 μg/ml PE-CY5 IgG2b isotype control (Biolegend, UK) for 15 minutes at room temperature in the dark and analysed by flow cytometry as described in section 2.2.5 above.

2.2.7. Western Blotting

Extracellular vesicle samples, cell lysates and cell extracts were diluted in reducing buffer (Bio-Rad, UK) to give a final protein concentration of 10-30 μg/well. For the study of CT-1 expression on placental lysates and STB-EV, 1 μg/ml recombinant CT-1 (R & D Systems, UK) was used as a positive control. Samples were then boiled at 96° C and centrifuged at 13,000 x *g* for 1 minute prior to separation by denaturing sodium dodecyl sulphate polyacrylamide gel electrophoresis (SDS-PAGE) under reducing conditions using Tris-HCl ready-made gels (Bio-Rad, UK). Proteins were transferred to Polyvinylidene difluoride (PVDF) (Bio-Rad, UK) membrane and subsequently incubated in blocking buffer containing 5% BLOTTO (Alpha Diagnostic International, US) in Tris-buffered saline with tween (TBST) (12.1g Tris, 87.6g NaCl, 0.1% Tween) (all from Sigma, UK) for 45 minutes at room temperature.

To study CT-1 expression on placental lysates and STB-EV, membranes were incubated with 1:500 anti-CT-1 (R&D Systems, UK) and 1: 1000 anti-PLAP (NDOG2) in 5% BLOTTO blocking buffer overnight at 4° C.

To determine whether samples were enriched with exosomes, membranes were incubated with 1:1000 anti-Alix (New England Biolabs, UK), 1:1000 anti-Syntenin (Abcam, UK) and 1:200 anti-CD9 (Santa Cruz, UK).

For the study of cell signaling pathways, membranes were incubated in 1:10 phospho/total-gp130 (Santa Cruz, UK), 1:1000 phospho/total-ERK (New England Biolabs, UK), 1:1000 phospho/total-Akt (New England Biolabs, UK) and 1:1000 phospho/total-STAT 3 (New England Biolabs, UK) in 5% BSA (Sigma, UK) and 0.1% TBST.

Reactions were visualized using an appropriate horseradish peroxidase conjugated secondary antibody (New England Biolabs, UK) in blocking buffer at room temperature for 1 hour and protein bands visualised using an enhanced chemiluminescence (ECL) reagent (Pierce, UK) and exposed on CL-XPosure^{TM} Film (Thermofisher Scientific, USA).

For lysates and cell extracts, to confirm that the same protein has been loaded in each lane, 1:10000 beta-actin (Abcam, UK), a constitutively expressed protein that maintains cell viability, was used as a loading control. However, we have found (in common with other groups) [221], that beta-actin is variable between vesicle preparations and therefore may not be an appropriate loading

control. We reverted to loading equal amounts of protein quantified using the Bicinchoninic acid (BCA) assay kit (Pierce, UK).

2.2.8. Immunoprecipitation of PLAP and CT-1 positive STB-EX determined by Western blotting and Flow Cytometry

To demonstrate that CT-1 is present on PLAP positive STB-EX, immunoprecipitation with pan mouse IgG Dynabeads (Life Technologies, UK) was carried out according to the manufacturer's instructions, with minor modification as described by Dragovic et al [215]. 50 μl of Dynabeads were coated with a saturating concentration (6 μg/ml) of either anti-PLAP antibody (NDOG2), anti-CT 1 antibody, IgG1 -MOPC-21 (Biolegend, UK) or IgG2A (Dako, UK). 25 μg STB-EX were incubated with FcR blocking reagent (10 μl, 10 minutes at 4° C), followed by overnight rotation at 4° C with either anti- CT-1, anti-PLAP, IgG1 or IgG2A beads in a total volume of 1 ml PBS. Bound and unbound EV were then separated using a magnet and retained for further analysis.

For Western blotting, using an optimized protocol [215], the supernatant (20 μl) was mixed with 3x reducing buffer, while EV bound to beads were washed with PBS and eluted in 1x reducing buffer before removal of beads by centrifugation (11,500 x *g* for 1 minute). An equivalent amount of the starting EV sample was also loaded onto the gels and Western blotting was carried out as described in section 2.2.7 above.

To determine the number of total and unbound STB-EX, untreated pools of STB-EX samples and their corresponding supernatants were diluted in PBS to approximately 5 x 10^8 EV/mL and analysed by NTA as described above in section 2.2.4.

Currently, only STB-MV can be analysed by conventional flow cytometry [66]. To overcome this limitation, and to study the expression of CT-1 on PLAP positive STB-EV, immunoprecipitation was carried out as described above. Briefly, STB-EX were captured using PLAP-coated Dynabeads. STB-EX-bound to the Dynabeads were subsequently interrogated with either an APC conjugated anti-CT antibody or negative isotype control and analysed on flow cytometry as described in section 2.2.6 above.

2.2.9. Cell Culture

2.2.9.1. HepG2 cells – Human Hepatocellular liver carcinoma cell line used as a positive control for APC-conjugated CT-1 antibody

HepG2 cells, a generous donation by Dr. Charlotte Green (Nuffield Department of Obstetrics and Gynaecology), were cultured as sub-confluent monolayers in T25 cell culture flasks (Nunc^{TM}) and maintained in Dulbecco's modified Eagle's medium (DMEM) (Sigma, UK) supplemented with 10% fetal calf serum (Sigma, UK), 2mM L-glutamine 100 units/ml penicillin plus 100 µg/ml streptomycin (Sigma, UK) at 37° C in 5% CO_2 in air. For cell dissociation, 0.25% Trypsin-EDTA (Sigma, UK), thawed overnight, was added to cover all the cells. Cells were subsequently incubated for 2 minutes at 37° C and the trypsin was quenched with 10 ml supplemented culture medium. The

cells were then pelleted at 200 x *g* for 5 minutes at room temperature and resuspended in 1 ml culture medium for live cell density determination by trypan blue (Life technologies, UK) exclusion. Cells were subsequently pelleted at 200 x *g* for 5 minutes at room temperature, washed in cold PBS and kept on ice prior to flow cytometric analysis.

2.2.9.2. HUVEC – Human endothelial umbilical vein cells used for the study of changes in gp130 in response to treatment with STB-EX

Human Umbilical Vein Endothelial Cells (HUVEC) were isolated from human umbilical cords by collagenase digestion of the interior of the umbilical vein as previously described by Jaffe et al [222]. Three HUVEC preparations from different umbilical cords were used. Briefly, placentas were collected from normal pregnant women undergoing elective caesarian section and processed within 10 minutes. Umbilical cords were clamped and cut from their placentas. These were subsequently immersed in warm PBS (Sigma, UK) to remove contaminating red blood cells. Next, the cords were inspected and only the length of the cord without evidence of post-partum trauma or bleeding was used. The umbilical vein of each cord was cannulated and flushed with 20 ml of warm PBS to ensure its patency, and the opposite end of the vein was then clamped. The vein was subsequently infused with 5 ml of 1x collagenase type 1a (1 mg/ml) (Sigma, UK). The cord was then incubated at 37° C for 15 minutes in 5% CO_2 for maximal digestion of extracellular matrix and detachment of endothelial cells. This was followed by flushing of the cord with

30 ml endothelial cell growth media (EGM-2) (Lonza, UK) containing 2% FBS, basic fibroblast growth factor (bFGF), epidermal growth factor (EGF), insulin-like growth factor-1 (IGF-1), vascular endothelial growth factor (VEGF), hydrocortisone, ascorbic acid, heparin, gentamicin, and amphotericin-B (all from Lonza, UK). Cells were then collected in a 50 ml Falcon tube and the cell suspension was pelleted at 500 x *g* for 5 minutes at room temperature.

The pellet was then re-suspended in 4 ml of supplemented cell growth medium (Lonza, UK) seeded onto a T25 cell culture flasks (Nunc^{TM}). Cells were left overnight to settle and adhere before the EGM-2 was changed. Cell culture medium was subsequently changed every two days until the cells were approximately 80-90% confluent and passaged for further study or storage in liquid nitrogen.

During a period of limited availability, it was necessary to expand HUVEC stocks. Cells were cultured to confluency until they reached passage 2 or 3. Culture medium was removed, and cells were washed with warm PBS. Trypsin-EDTA (Sigma, UK), thawed overnight, was added to cover all the cells and aspirated following evidence of detachment (round and floating cells). Trypsin was quenched with 10 ml supplemented culture medium and the cells were pelleted at 500 x *g* for 5 minutes at room temperature. Cells were resuspended in 1 ml culture medium and live cell density was determined by trypan blue (Life technologies, UK) exclusion.

For further expansion, cells were split into two T25 flasks (Nunc^{TM}) at a seeding density of 7 x 10^5 cells/ml or one T75 flask (Nunc^{TM}) at a seeding

density 2 x 10^6 cells/ml.

For storage, pellets were resuspended in 5% (v/v) Dimethyl sulfoxide (DMSO) (Sigma, UK) and 2 x 10^6 cells/ml were aliquoted into ice-cold cryovials and placed in a cell cryopreservation container at -80° C to freeze gradually. The following day, cells were stored in liquid nitrogen.

When cells were needed for further study, a vial containing 2 x 10^6 cells/ml of cryopreserved HUVEC was removed from the liquid nitrogen tank, disinfected with 70% ethanol and placed in a pre-heated (37° C) water bath. Cells were then transferred into a sterile 15 ml centrifuge tube containing 5 ml of pre-warmed supplemented EGM 2, before being pelleted at 500 x *g* for 5 minutes, counted and plated as described above.

2.2.9.3. HCAEC – Human coronary artery endothelial cells used for the study of gene changes in response to treatment with STB-EX

Human Coronary Artery Endothelial Cells (HCAEC) were purchased from cell applications (USA), and temporarily stored in liquid nitrogen until further use. For studying gene changes in response to treatment with STB-EX, cells were cultured according to the manufacturer's instructions (Cell Applications, USA). Briefly, a vial containing cryopreserved HCAEC was removed from the liquid nitrogen tank, disinfected with 70% ethanol and placed in a pre-heated (37° C) water bath. Cells were then transferred into a sterile 15 ml centrifuge tube and 5 ml of pre-warmed EGM -2 containing 5% FBS, human fibroblast growth factor beta (hFGF-β), human epidermal EGF (hEGF), R3-insulin-like growth

factor-1 (R3-IGF-1), human vascular endothelial growth factor (VEGF), hydrocortisone, ascorbic acid, gentamicin, and amphotericin-B (all from Lonza, UK). Due to the delicate nature of HCAEC, cells were not centrifuged. Cells were then seeded into T25 cell culture flasks (Nunc^{TM}), left overnight to settle and adhere before the culture medium was changed. Culture medium was subsequently changed every two days until cells had reached approximately 80-90% confluency.

2.2.9.4. Rat cardiomyocytes –used for the study of genes associated with cardiac myocytes hypertrophy in response to treatment with STB-EX

For the study of genes associated with cardiac hypertrophy, ventricular cardiomyocytes, isolated from neonatal Sprague-Dawley rats were purchased from Lonza, UK and immediately stored in liquid nitrogen for later use.

First, cell culture medium was prepared by adding SingleQuots^{TM} Kit containing 7.5% Horse Serum, 7.5% Fetal Bovine Serum (FBS), gentamicin, and amphotericin-B that were thawed overnight at 4° C and to rat cardiac basal medium (Lonza, UK). To prevent overgrowth of fibroblasts, culture medium was further supplemented with 40 mM 5-bromo-2'-deoxyuridine (BrdU) (Sigma, UK) to a final concentration of 200 μM.

Next, to facilitate cell adherence and survival, 15 wells of a 24-well plate were coated with nitrocellulose (Sigma, UK). Nitrocellulose Stock Solution was prepared by dissolving 1 cm^2 of nitrocellulose paper in 10 ml methanol and filtered through a 0.22 μM syringe filter (Sarstedt, Germany), and further

diluted to create a 1:10 nitrocellulose working solution. 10 μl of the working solution was added to each well and the plate was incubated at room temperature for 5 minutes until the solution had dried. The cells were plated immediately afterwards.

Finally, a vial containing cryopreserved rat cardiomyocytes was removed from the liquid nitrogen tank, disinfected with 70% ethanol and placed in a pre-heated (37° C) water bath. Cells were then transferred into a sterile 15 ml centrifuge tube and 4.3 ml of pre-warmed culture medium (without BrdU) was added to make a total volume of 5.3 ml. Due to the delicate nature of cardiomyocytes, cells were not centrifuged. 200 μl of cell suspension was pipetted into each well at a cell density of 3×10^5 cells/ml and incubated at 37° C in 5% CO_2. After 4 hours, 80% of the medium was removed from the cells and replaced with fresh, pre-warmed medium containing 200 μM BrdU and cultured for a further 24 hours.

2.2.10. Determining the non-toxic concentration of STB-EX for functional studies

Previous work by us and others has demonstrated that placental derived extracellular vesicles have a concentration-dependent cytotoxic effect on endothelial cells [112, 113, 115, 223]. Therefore, the non-toxic concentration of STB-EX that could be used to treat cells in functional studies was determined using the CellTox™ Green (Promega, UK) assay according to the manufacturer's instructions. The assay used a cyanine dye that preferentially stained the DNA released by dead cells following disruption of the plasma membrane. When the dye bound DNA in compromised cells, the dye's

fluorescent properties were substantially enhanced [224]. Viable cells produce no appreciable increases in fluorescence. The fluorescent signal produced by the dye binding to the dead-cell DNA was proportional to cytotoxicity [225].

For this study, triplicates of 3 x 10^4 cells/ml HUVEC were seeded into a 96-well plate and incubated overnight at 37° C in 5% CO_2 before being treated with STB-EX concentrations ranging from 1 x 10^6 EV/ml – 1 x 10^{10} EV/ml. The CellTox^{TM} Green dye was added to each sample at the time of treatment. The cells were then incubated at 37° C in 5% CO_2 in a FLUOstar Omega (BMG Labtech) plate reader for 12 hours, and the fluorescence measured at 485–500 nm excitation wavelength and 520–530nm emission wavelength. Positive and negative controls were used by adding cell lysis buffer and equal volumes of PBS/cell culture medium to the cells, respectively.

2.2.11. Cell treatment with STB-EX

2.2.11.1. For the study of changes in in gp130, ERK 1/2 and Akt in HUVEC

For the study of changes in gp130 in response to treatment with STB-EX, HUVEC were seeded into 6-well plates at a seeding density of 3 x 10^5 cells/ml and cultured to 80 -90% confluency as described in section 2.2.9.2 above. Cells were subsequently cultured in serum-free endothelial growth media at 37° C in 5% CO_2 for 24 hours before being treated with a vehicle (5 μl PBS), recombinant CT-1 (100 ng/ml) (R & D Systems, UK), 1 x 10^8 STB-EX in 5 μl of PBS, and STB-EX pre-treated with a neutralising antibody against CT-1 (R & D Systems, UK). Following treatment, cells were incubated at 37° C for 15

minutes in 5% CO_2. After incubation, cells were washed with ice-cold PBS. All subsequent treatments were carried out on ice. Cells were then treated with non-denaturing 1x cell lysis buffer (New England Biolabs, UK) containing protease and phosphatase inhibitors (Roche, Germany). To remove cell debris, the cell suspension was centrifuged at 13,000 x g for 10 minutes. The supernatants were transferred to 1.5 ml Eppendorf tubes for protein quantification (Pierce, UK) and further study of intracellular pathways were carried out by Western Blotting as previously described.

2.2.11.2. To demonstrate internalisation of STB-EX by HUVEC and rat cardiomyocytes

To determine whether STB-EX are taken up by endothelial cells and/or cardiomyocytes, 5 x 10^4 HUVEC or rat cardiomyocytes were seeded into a 2-well glass bottom µ-slide (Ibidi, Germany) pre-coated with 0.1% fibronectin (Sigma, UK) and nitrocellulose (Sigma, UK) respectively, and allowed to settle and adhere overnight. HUVEC were subsequently treated with 1 x 10^8 STB-EX labeled with PKH26 (Sigma, UK) and rat cardiomyocytes with 1 x 10^8 STB-EX labeled with FITC-conjugated Biomaleimide for one hour. Next, cells were washed with 0.01% PBS-T and fixed with 4% Paraformaldehyde (Sigma, UK) in PBS for 10 minutes at room temperature. After three washes with 0.01% PBS-T, cells were labeled with 2 µg/ml Hoescht 33342 (Life technologies, USA) for 15 minutes at room temperature and washed again with 0.01% PBST. Finally, five drops of Ibidi mounting medium (Ibidi, Germany) was added to the cells before microscopic analysis. Imaging was performed using either a Leica DM2500 optical microscope (Leica Microsystems), and captured

with a digital camera (Micropublisher 5.0 RTV) or a Zeiss LSM 780 inverted laser confocal microscope under the supervision of Dr Christoffer Lagerholm from the Weatherall Institute of Molecular Medicine. Fluorescence microscope images were collected under a X40 objective and confocal images were collected under a X100 oil immersion objective lens. ImageJ version 2.0 (NIH) software was used to process and analyse collected images.

2.2.11.3. The study of gene changes caused by STB-EX in HCAEC

For the study of gene changes in response to treatment with STB-EX, human coronary arterial endothelial cells (HCAEC) were seeded in triplicates into 12 wells of a 24-well plate at a seeding density of 2 x 10^5 cells/ml and cultured overnight to ensure adherence and confluency at 80 -90% as described in section 2.2.9.3 above. Cells were subsequently cultured in serum-free endothelial growth medium at 37° C in 5% CO_2 for 24 hours. The culture medium was then replaced with serum free EGM-2 containing 5 μl sterile PBS (vehicle), recombinant CT-1 (100 ng/ml) (R & D Systems, UK), 1 x 10^8 STB-EX in 5 μl of PBS, or STB-EX pre-treated with 5 μl neutralising antibody against CT-1 (R & D Systems, UK) and cells were cultured at 37° C in 5% CO_2. After 24 hours of treatment, cells were washed with PBS and lysed with 350 μl of cell lysis buffer (Qiagen, Germany) and immediately processed for RNA isolation.

2.2.11.4. The study of gene changes caused by STB-EX in rat cardiomyocytes

For the study of gene changes associated with cardiac hypertrophy in response to treatment with STB-EX, rat cardiomyocytes were seeded in triplicates into 12 wells of a nitrocellulose coated 24-well plate at a seeding density of 3 x 10^5 cells/ml as described in section 2.2.9.4 above, before being cultured in serum-free culture medium at 37° C in 5% CO_2 for 24 hours. The culture medium was then replaced with serum free cardiomyocytes medium containing 5 μl sterile PBS (vehicle), recombinant CT-1 (100 ng/ml) (R & D Systems, UK), 1 x 10^8 STB-EX in 5 μl of PBS, or STB-EX pre-treated with 5 μl neutralising antibody against CT-1 (R & D Systems, UK) and cells were cultured at 37° C in 5% CO_2. After 24 hours of treatment, cells were washed with PBS and lysed with 350 μl of cell lysis buffer (Qiagen, Germany) and immediately processed for RNA isolation.

2.2.12. Real-Time Quantitative Polymerase Chain Reaction (RT-qPCR)

2.2.12.1. RNA isolation

For RNA isolation, the Qiagen RNeasy mini kit (Qiagen, Germany) was used according to the manufacturer's instructions. Briefly, following cell culture (described in section 2.2.9 above) and cell treatment (described in section 2.2.11) the culture medium was aspirated and each well was washed once with PBS. Next, cells were lysed with 350 μl Buffer RLT (Qiagen, Germany). To homogenize the cells, the lysate was passed eight times through a blunt 20-gauge needle fitted with a RNA-free syringe. For RNA precipitation, 350 μl

of 70% ethanol was added to the lysate and passed through an RNeasy spin column placed in a 2 ml collection tube and centrifuged at 8,000 x g for 15 seconds. The spin column was subsequently washed with 700 μl Buffer RW1(Qiagen, Germany) at 8,000 x g for 15 seconds. Finally, the spin column was washed with 500 μl Buffer RPE (with 70% ethanol) (Qiagen, Germany) at 8,000 x g for 15 seconds and washed again with 500 μl Buffer RPE at 8,000 x g for 2 minutes to ensure that no residual ethanol was carried over during RNA elution. The flow-through was discarded after each spin. To elute the RNA, 30 μl of RNase free water was added to the spin column and centrifuged at 8,000 x g for 1 minute. The eluent was collected in a RNase free tube (Qiagen, Germany) and placed on ice until quantification by ultraviolet spectroscopy at 260 nm/ 280 nm with a NanoDrop® ND-1000 Spectrophotometer (Thermo Fisher Scientific, USA) and storage at -80° C.

2.2.12.2. Taqman® Gene expression assay

To generate cDNA, 50 ng of high-quality total RNA was reverse transcribed using High Capacity cDNA Reverse Transcription Kit (Applied Biosystems, USA). The High Capacity cDNA Reverse Transcription Kit uses the random primer scheme for initiating cDNA synthesis which anneal to any complement site of RNA transcripts. After thawing on ice, a 1X RT reaction mix was made up using 2 μl 10X RT buffer, 0.8 μl of 100 mM dNTP mix, 2 μl 10X Random Primers, and 1 μl Multiscribe Reverse Transcriptase. Thereafter, 5.8 μl of RT mix was added to 14.2 μl of RNA sample to make up a total volume of 20 μl before being processed in a G-Storm^{TM} (G-storm, UK) thermocycler using the

following settings: 16° C for 30 minutes, 42° C for 30 minutes, followed by 85° C for 5 minutes and a final hold at 4°C.

For RT-qPCR, the Taqman® assay (Applied Biosystems, USA) was used for its simplicity, specificity and reproducibility. The Taqman® used a single-stranded probe complementary to the template sequence. The probe has a fluorescent reporter and quencher dye covalently attached at the 5' and 3' end, respectively. At "rest", the quencher dye is in close proximity to the reporter. Thus, when the fluorophore on the reporter is excited with a laser, the energy released by the reporter is absorbed by the quencher preventing detection of a fluorescent signal [226]. During PCR amplification, the probe hydrolyses to its complementary sequence. *Taq* polymerase extends the DNA strand from primers bound to the amplicon and displaces the 5' end of the probe. As the *Taq* polymerase exonuclease activity continues, the probe is degraded, permanently separating the reporter from the quencher [227]. Consequently, when the fluorophore on the reporter is excited a fluorescence signal is emitted which corresponds to the increase in DNA concentration with each amplification.

To evaluate gene changes following treatment of endothelial cells with STB-EX, RT- qPCR with a predesigned Taqman® expression assay was used. After thawing on ice, a 1x PCR reaction mix was made up using 1 μl 20x Taqman® expression assay, 10 μl 2x Taqman® gene expression Master Mix, 1.36 μl (5 ng) of cDNA, and 7.64 μl RNase-free water for total volume of 20 μl. All mixes were pipetted into the wells of a gene disc (Qiagen, Germany) using a CAS-1200 pipetting robot (Corbett Life Science Sceince, UK). At the end of

each automated pipetting cycle, the gene discs were sealed with a Rotor-Disc Heat Sealer (Qiagen, Germany) before further processing. For, RT-PCR 40 cycles were carried out on the Rotor-Gene 6000 analyser (Corbett Life Science, UK) using the following settings: hold- 50° C for 2 minutes, hold - 95° C for 10 minutes, followed by forty 95° C for 5 seconds/ 60° C for 6 seconds' cycles acquiring to FAM™. The results were analysed with the Rotor-Gene Q Series software (Qiagen, Germany).

Table 1: Details of genes investigated

Gene	Species	Assay ID	Gene name
GAPDH	Rat	Rn99999916_s1	glyceraldehyde-3-phosphate dehydrogenase
ATP2A2	Rat	Rn00568762_m1	ATPase, Ca++ transporting, cardiac muscle, slow twitch 2
MYH7B	Rat	Rn01536269_m1	myosin, heavy chain 7B, cardiac muscle, beta
NPPB	Rat	Rn00580641_m1	natriuretic peptide B
NPPA	Rat	Rn00664637_g1	natriuretic peptide A
GAPDH	Human	Hs99999905_m1	glyceraldehyde-3-phosphate dehydrogenase
FLT1	Human	Hs01052961_m1	fms related tyrosine kinase 1
EDN1	Human	Hs00174961_m1	endothelin 1
CCNA2	Human	Hs00996788_m1	cyclin A2
IL6	Human	Hs00174131_m1	interleukin 6

2.2.13. Statistical analysis

Data are shown as mean ± SEM. The results generated from the intracellular signaling and RT-qPCR experiments were analysed using a two-sample t-test. The Mann Whitney non-parametric test was used on all other comparisons. Statistical analyses were carried out using Prism software (GraphPad Software, San Diego California USA, www.graphpad.com). Values of $p<0.05$ were considered statistically significant.

2.3. RESULTS

2.3.1. Cardiotrophin 1 is expressed on the syncytiotrophoblast layer of the human placenta

First, to determine whether CT-1 is expressed by the syncytiotrophoblast (STB), immunostaining of sections of three normal placentas was performed. Strong staining of the STB was seen (Figure 2.4-A). The expression of CT -1 and PLAP from normal placentas was then analysed by Western blotting of six normal placental lysates (Figure 2.4-B). This showed a 25KD band corresponding to CT-1, and a 60KD band consistent with PLAP, confirming that CT-1 was expressed on the human placenta (Figure 2.4-C).

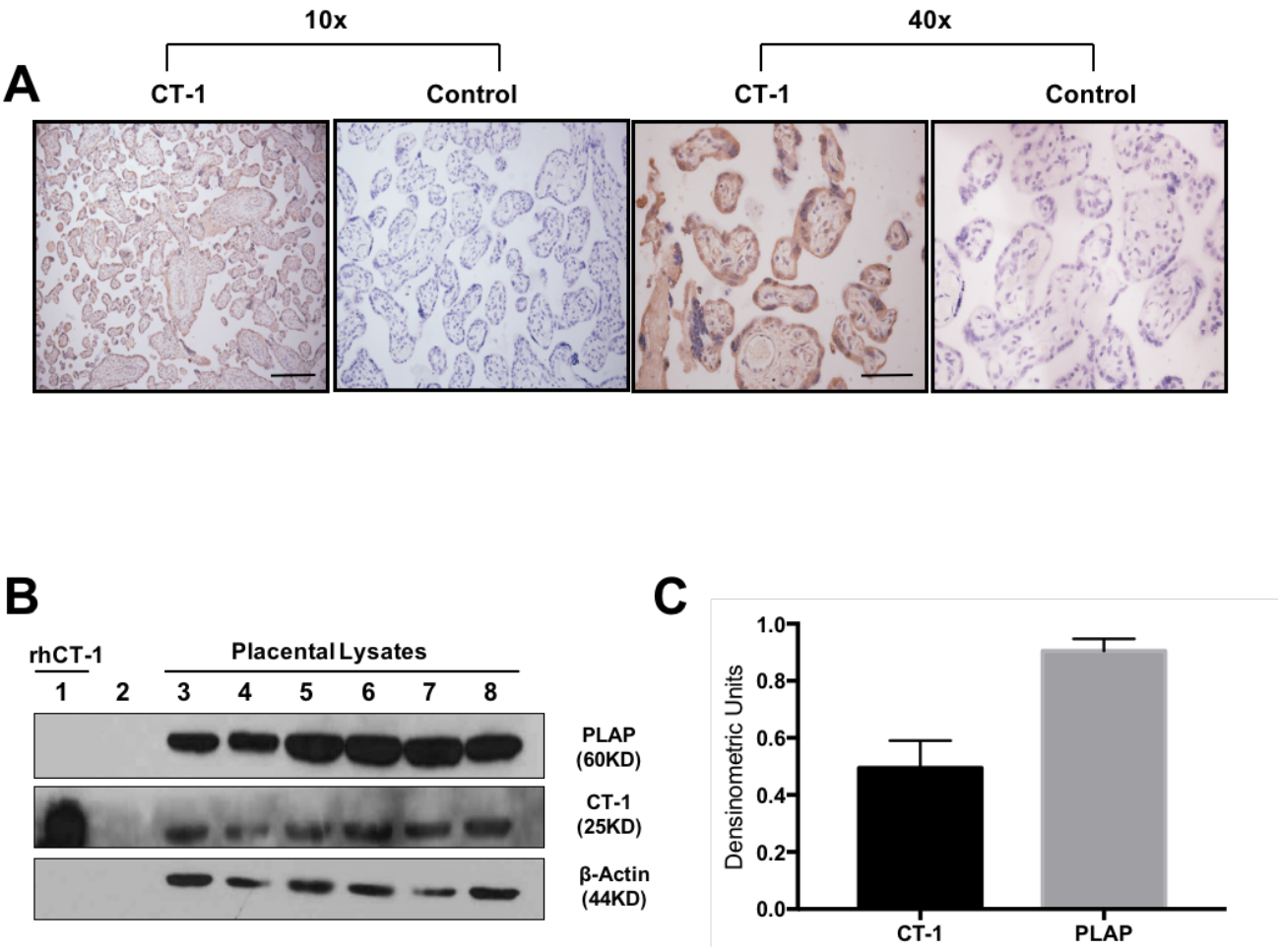


Figure 2.4. Cardiotrophin 1 is expressed on the human placenta. (A) Immunohistochemistry demonstrating the expression of CT-1 on the syncytiotrophoblast layer of the human placenta at 40x magnification and 10x magnification with the corresponding negative control sections. Scale bar:100 µm. **(B)** Western Blot demonstrating the expression of placental alkaline phosphatase (PLAP) and CT-1 on placental lysates, Lane 1: Recombinant CT-1(rhCT-1); Lanes 3-8: Placental Lysates. **(C)** Corresponding densinometric analysis of PLAP and CT-1 in placental lysates.

2.3.2. Isolation and characterisation of STB-EV

Next, to study the expression of CT-1 on placental extracellular vesicles (EV), STB-EV were isolated from the placenta using a dual perfusion system and subjected to differential ultracentrifugation before being analysed by Nanoparticle Tracking Analaysis (NTA), Transmission Electron Microscopy (TEM) and Western blotting. Vesicle preparations isolated from the 10 000 x g

centrifugation spin were analysed by NTA. These were found to have a peak modal size of 345 nm ±5 (Figure 2.5-A) which is consistent with that of microvesicles, whilst preparations from the 150 000 x g spin showed a peak modal size of 170 nm ±5.9 (Figure 2.5-A) consistent with that of exosomes. TEM confirmed the NTA data: showing that the STB-MV was enriched for EV >300 nm which were heterogeneous in size and appearance (Figure 2.5-B) while the STB-EX contained a small and more homogeneous population of EV (approximately 50–200 nm), in the reported size range of exosomes.

Western blotting of the placental lysates, STB-MV and STB-EX from the same placentas was also carried out for PLAP, Alix, Syntenin and CD 9, to validate their syncytiotrophoblast origin and the presence of exosomes (Figure 2.5-C). All lysates, STB-MV and STB-EX samples had a 60KD band consistent with PLAP (Figure 2.5-D), thus confirming their STB origin. 96KD, 34KD and 23KD bands consistent with Alix (Figure 2.5-E), Syntenin (Figure 2.5-F) and CD9 (Figure 2.5-G) respectively, were observed in the STB-EX preparations which suggests that they were highly enriched with exosomes compared to the placental lysates and the STB-MV preparations.

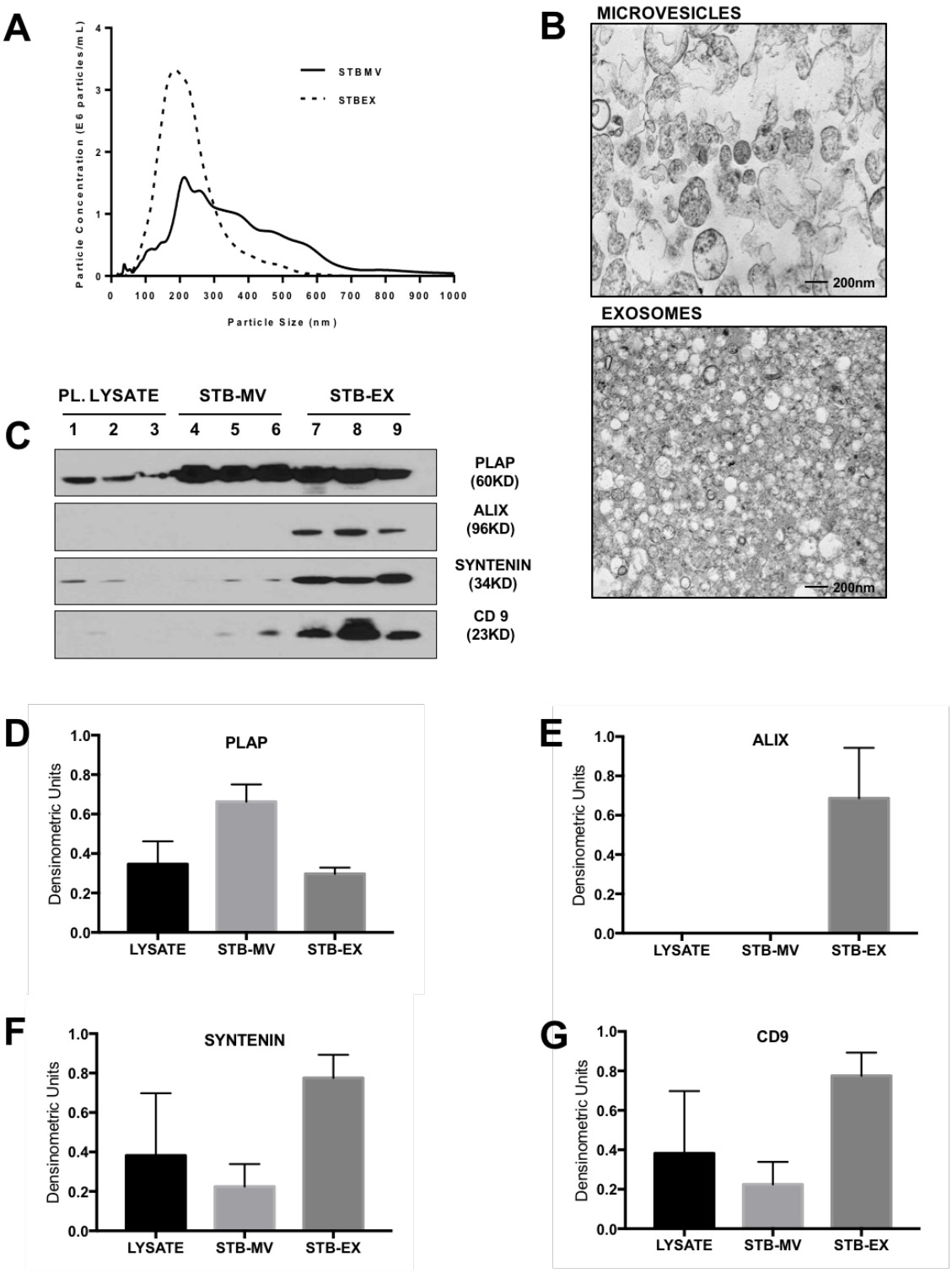


Figure 2.5. Characterization and quantification of Syncytiotrophoblast Extracellular Vesicles (STB-EV). Representative Images. **(A)** Representative results of nanoparticle tracking analysis (NTA) demonstrating the size distribution in diluted samples of exosomes and microvesicles. **(B)** Transmission electron micrographs of microvesicle and exosomes. Scale bars represent 200 nm **(C)** Western Blot confirming the presence of exosomal proteins Alix, Syntenin and CD9. Lanes 1-3: Placental Lysates; Lane 4-6: Placental Microvesicles; Lane 7-9: Placental Exosomes. Corresponding densinometric analysis of **(D)** PLAP, and exosome markers **(E)** Alix **(F)** Syntenin **(G)** CD9.

2.3.3. Characterisation of STB-MV by Flow Cytometry

STB-EV preparations were also characterised by flow cytometry. Currently, this can only be done for microvesicles, as this technique is not sensitive enough to measure antigen expression on the much smaller exosome population.

Phenotyping of STB-MV was carried out as follows: the total microvesicle population was identified on the forward scatter (FSC) vs. side scatter (SCC) plot as being $\leq$1 μm using reference beads. Results are presented as percentages (mean$\pm$ standard error of the mean). Figure 2.6-A shows that 97.7 % (97.97$\pm$0.54) of the population was <1 µm. Next, vesicles labeling positive for biomaleimide (a lipid membrane marker present in all extracellular vesicles) were gated. Figure 2.6-B and C show that 86.1 % (86.93$\pm$1.17) of the particles analysed labeled positively with biomaleimide and were therefore vesicles.

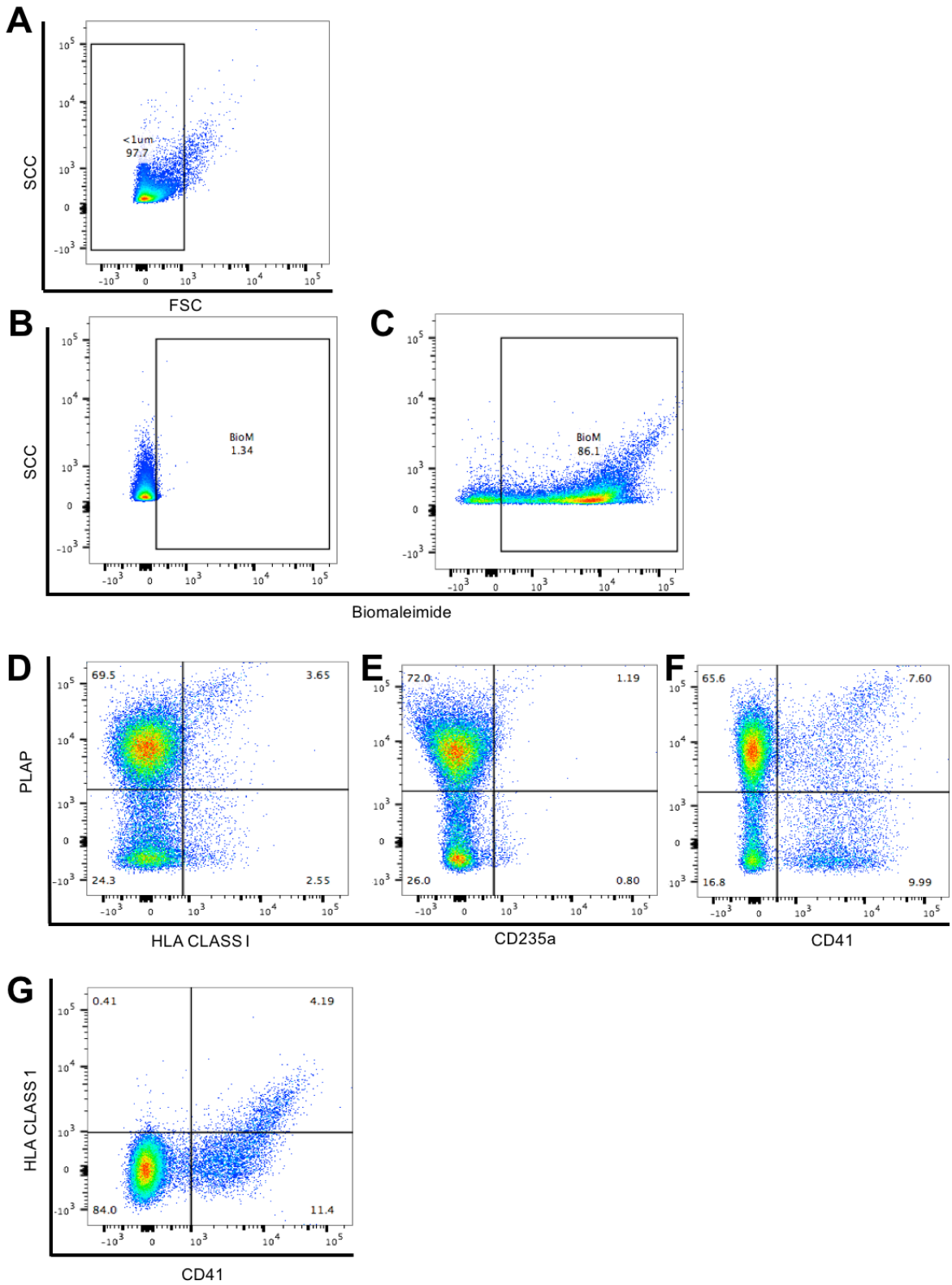


Figure 2.6. Representative flow cytometric analyses of STB-MV generated from *ex-vivo* dual placental perfusion that are biomaleimide positive. (A) Forward scatter (FSC) vs. side scatter (SSC) profile. **(B)** and **(C)** Gating of Biomaleimide positive vesicles. Extracellular Vesicles (EV) displayed on two-parameter plots and phenotype identified: **(D)** STB-MV, $PLAP^{+}$/HLA Class I^{-} **(E)** RBC EV, $CD235a/b^{+}/PLAP^{-}$**(F)** Platelet EV ($CD41^{+}/PLAP^{-}$) **(G)** Leukocyte/endothelial EV (HLA Class $I^{+}/CD41^{-}$).

STB-MV were then displayed on PLAP vs HLA class I quadrant plots to identify STB-MV ($PLAP^+$, HLA $Class^-$) and non-STB-MV ($PLAP^-$, HLA Class I^+) populations. Figure 2.6-D shows that 69.5% (67.83±4.83) of these EV were positive for the STB specific antibody against PLAP and negative for HLA Class 1 (which is not expressed on the STB) confirming their syncytiotrophoblast origin.

To determine whether cross contamination from RBC and platelet vesicles had occurred, EV were labeled for CD235a and CD41 respectively. Figure 2.6-E shows 1.99% (3.47±1.36) RBC vesicle contamination whilst Figure 2.6-F shows 17.59% (17.91±3.734) platelet contamination suggesting, again that placental preparations are enriched for syncytiotrophoblast EV with some contamination from RBC and platelet EV. Finally, to exclude leukocyte/endothelial EV contamination, the EV were stained for HLA Class I and CD41 (we would expect these to be HLA Class I positive and CD41 negative). The results show 0.41% (0.98±0.24) of the vesicles were HLA Class I positive (Figure 2.6-G) suggesting that leukocyte/endothelial EV contamination is negligible. The small populations of EV that are $PLAP^+$/HLA Class I^+, $PLAP^+/CD41^+$ and $PLAP^+/CD235a^+$ suggest that during sample processing, STB-MV aggregate to a limited extent, with other blood-derived vesicles.

2.3.4. Determination of level of CT-1 expression on STB-MV and STB-EX by Western blotting

Having fully characterized the STB-MV and STB-EX preparations, CT-1 and PLAP expression was studied on three STB-MV and three STB-EX samples by Western blotting. A 25KD positive band corresponding to CT-1 and a positive band at 60KD consistent with PLAP (Figure 2.7-A and B) were observed. Figure 2.7-C showed that CT-1 was weakly expressed on the STB-MV but highly expressed on STB-EX.

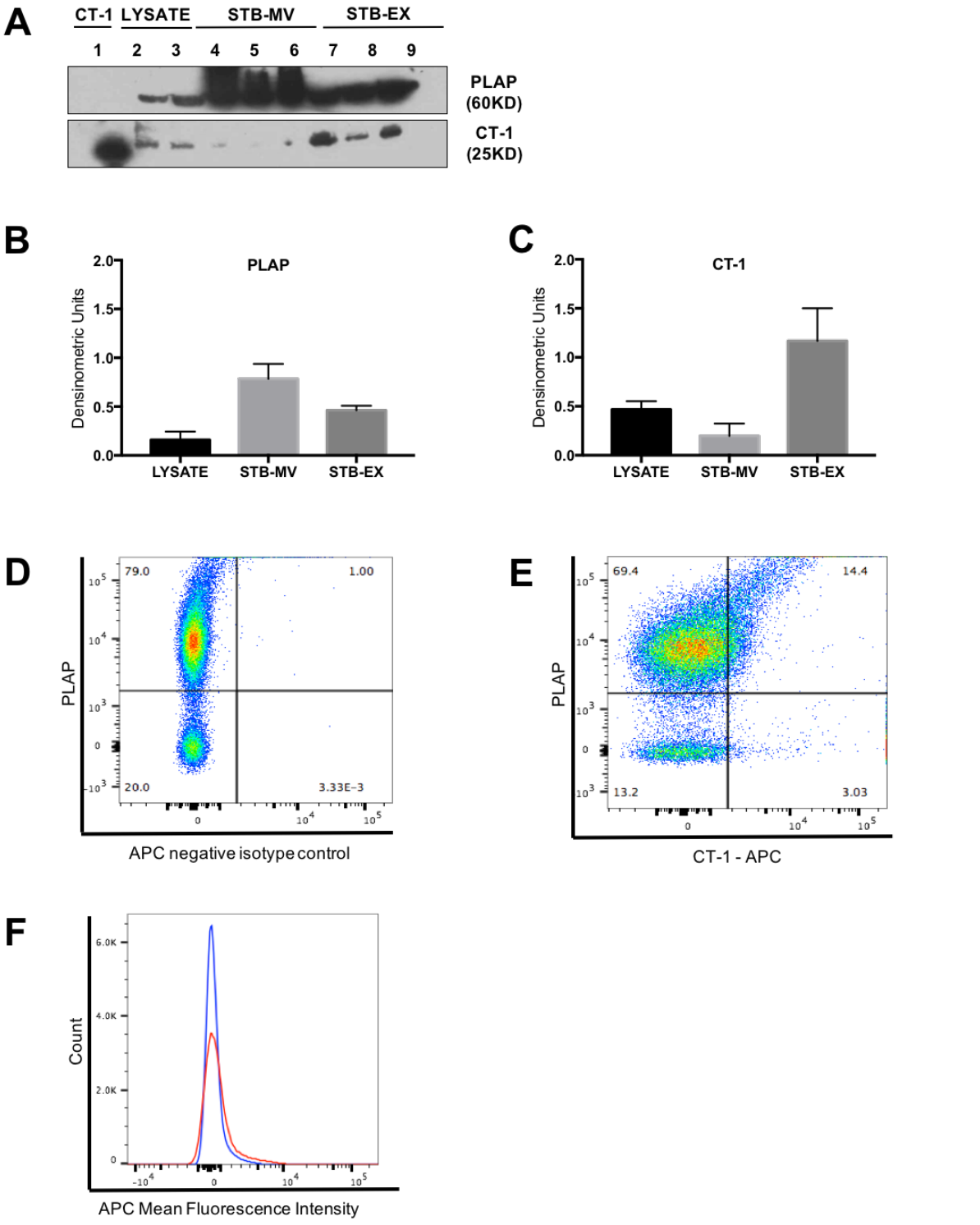


Figure 2.7. Cardiotrophin 1 expression on STB-EX and STB-MV. **(A)** Western Blot demonstrating the expression of PLAP and CT-1 on placental lysates, microvesicles and exosomes. Lane 1: Recombinant CT-1; Lanes 2-3: Placental Lysates; Lane 4-6: STB-MV; Lane 7-9: STB-EX. Corresponding densinometric analysis of **(B)** PLAP and **(C)** CT-1. Flow cytometric analysis of STB-MV isolated by placental perfusion labeled with **(D)** PLAP antibody AND negative isotype control, and **(E)** both PLAP and CT-1 antibody. **(F)** MFI for APC showing that there is no significant difference in the expression of CT-1 on vesicles compared to isotype negative control. Representative images.

2.3.5. Validation of in-house conjugation of anti - CT-1 antibody for use on flow cytometry

To study the expression of CT-1 on STB-MV by flow cytometry an antibody conjugated to a fluorophore was needed. However, antibodies validated for use in flow cytometry were not commercially available and therefore an in-house conjugation of Allophycocyanin (APC) to an anti-CT-1 antibody was done. This was first tested on the HepG2 cells, a cell line known to express CT-1 [228].

HepG2 cells were identified on their FSC and SCC profile (Figure 2.8–A). Titration using single staining for CT-1 showed marked expression of CT-1 compared to the negative isotype control (Figure 2.8–B). This data confirmed that CT-1 was expressed as a cell surface antigen. Furthermore, CT-1 positivity on HepG2 confirmed that the conjugation was successful and that the CT-1 conjugated antibody could be used for interrogation of STB-MV on flow cytometry.

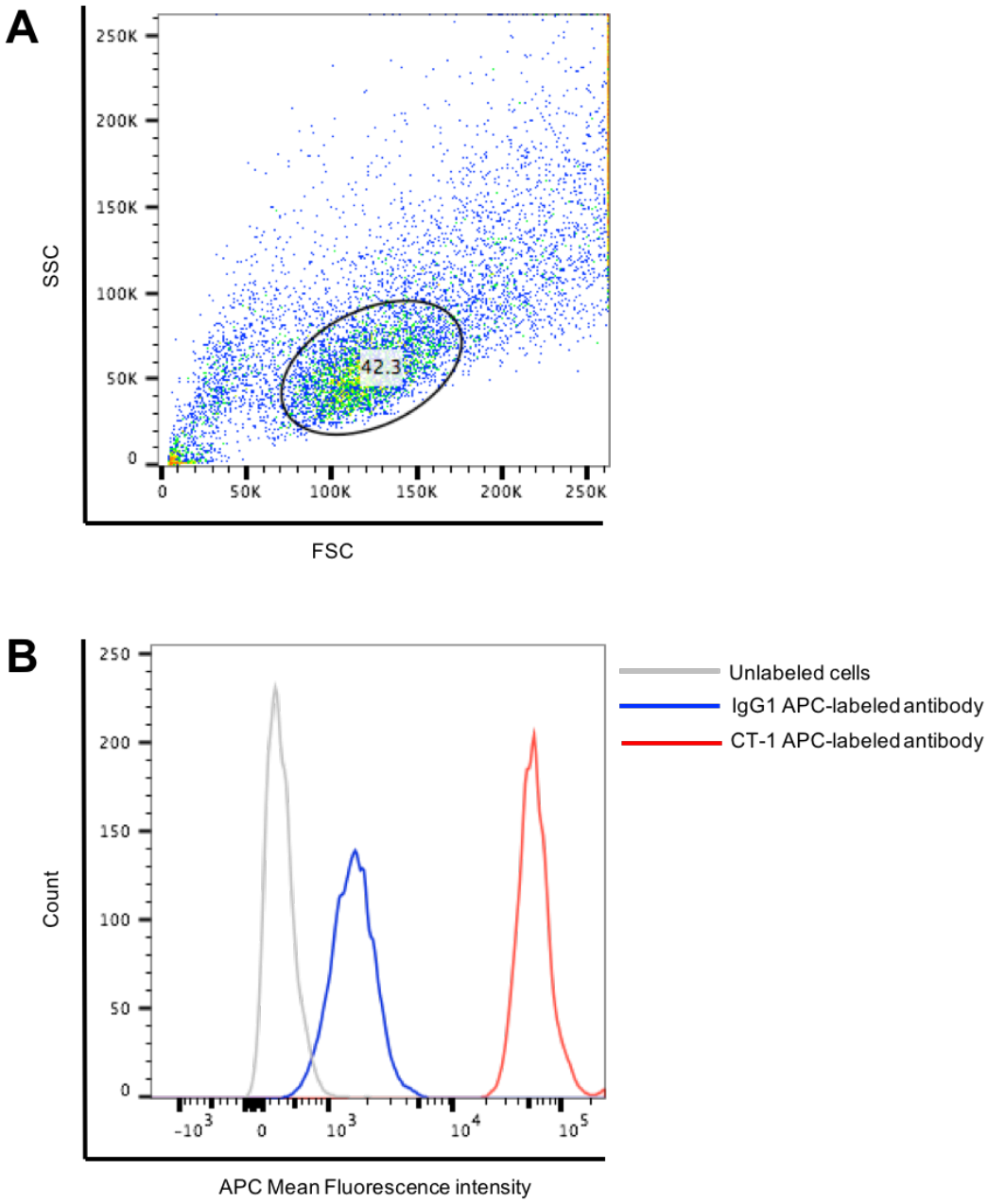


Figure 2.8. Validation of in-house conjugation of anti-CT-1 antibody be single-staining of HepG2 cells. (A) Forward scatter (FSC) vs. side scatter (SSC) profile. **(B)** Mean Fluorescence Intensity (MFI) for APC showing that CT-1 is carried as a surface receptor on HepG2 cells.

2.3.6. Determination of levels of CT-1 expression on STB-MV by Flow Cytometry

Having validated the APC conjugation to a CT-1 antibody, the levels of expression of CT-1 on STB-MV were studied by flow cytometry. To determine the proportion of STB-MV that co-express the STB-EV-specific marker, PLAP

and CT-1, samples were labeled with antibodies conjugated to Phycoerythrin (PE) and APC respectively. Figure 2.7 D and E show that 14.40% of PLAP positive microvesicles were also CT-1 positive.

The mean fluorescence intensity (MFI) for CT-1 was also investigated. The MFI indicates the amount of CT-1 carried on each STB-MV. There was no significant difference in the MFI for CT-1 (Figure 2.7–F) compared to the negative isotype control suggesting low level antigen expression.

To exclude potential contamination from blood-derived vesicles in the placental preparations that might express CT-1, six STB-MV samples were used to measure CT-1 expression. Fluorescence minus-one (FMO) control experiments were conducted using a marker for RBC EV (Figure 2.9).
The total microvesicle population was identified on the FSC vs. SCC plot as being ≤ 1 μm and only vesicles labeling positive for biomaleimide were gated. Figure 2.9-A and B show that 96.80% of vesicles were ≤ 1 μm and 90.52% labeled positively with biomaleimide.

Figure 2.9-C shows that though STB-MV were weakly enriched of CT-1 ($PLAP^+/CT\text{-}1^+$: 14.9 $\pm$0.83% there were very low levels of contamination from RBC vesicles ($CD235a^+/CT\text{-}1^+$:1.79$\pm$0.24%, Figure 2.9-D). Statistical analysis showed that in placental preparations, significantly more STB-MV expressed CT-1 compared to RBC vesicles. This analysis shows that placental-derived vesicles independently express CT-1 (Figure 2.9-E).

Western blotting shows that very little CT-1 is expressed on STB-MV. Similarly, flow cytometry using an antibody to CT-1 only labels a very small population of STB-MV. Given that CT-1 expression was much higher on STB-EX it was decided to focus on this population from this point on.

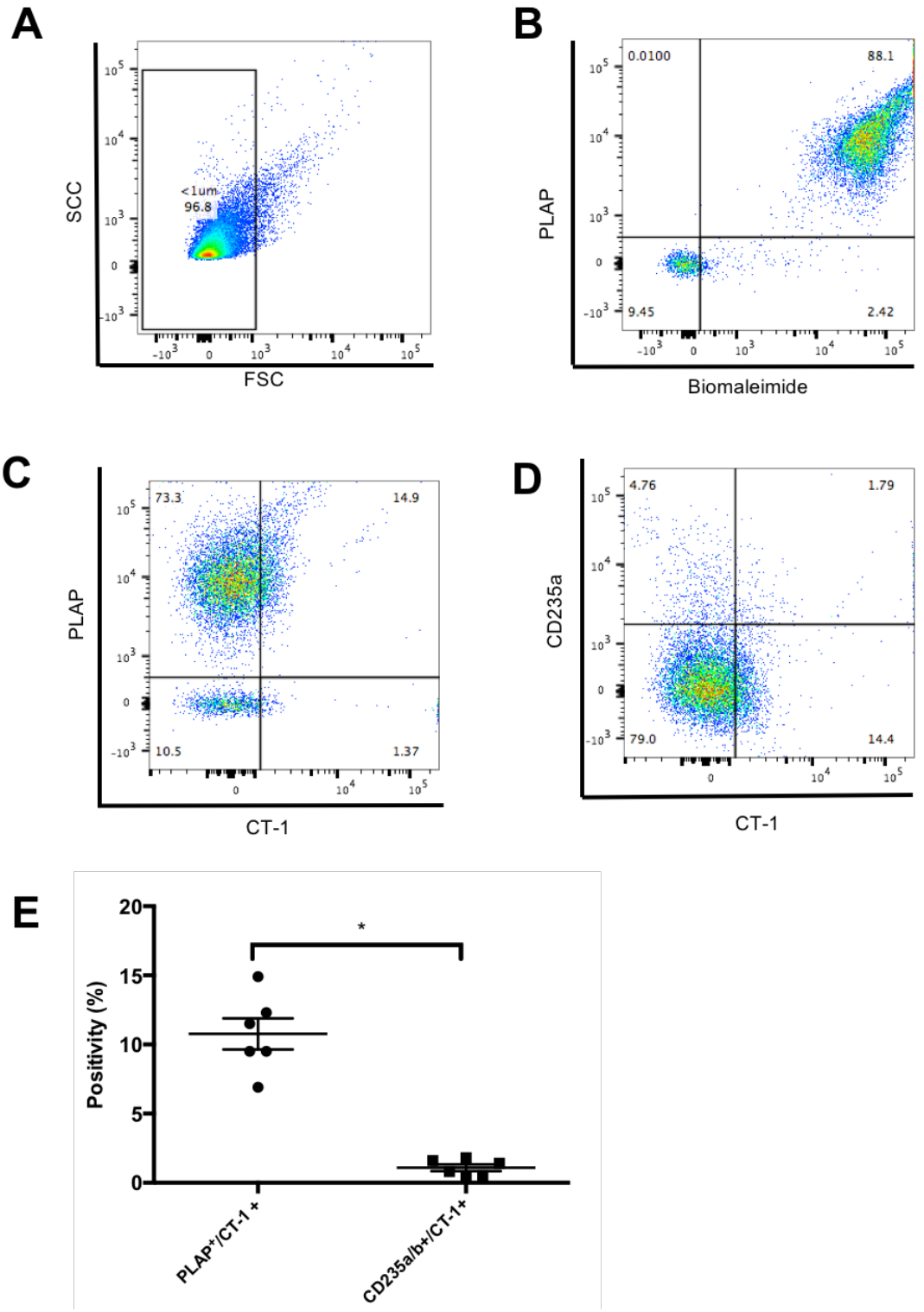


Figure 2.9. Figure 2.9. To exclude potential contamination from blood-derived vesicles. Representative flow cytometric images showing **(A)** Forward scatter (FSC) vs. side scatter (SSC) profile of microvesicles. **(B)** The vesicles were biomaleimide positive and placentally derived (PLAP positive). Two-parameter plots showing **(C)** CT-1 positive STB-MV ($PLAP^+/CT\text{-}1^+$) and **(D)** CT-1 positive RBC EV $CD235a/b^+/CT\text{-}1^+$). **(E)** Corresponding analysis of STB-MV and RBC EV. Bars = mean ± standard error of the mean, *= $p<0.05$

2.3.7. Determination of CT-1 expression on PLAP positive STB-EX

To further investigate that CT-1 was present on PLAP positive STB-EX, immunoprecipitation of CT-1 and PLAP positive vesicles was carried out on STB-EX preparations.

First, STB-EX were immunoprecipitated using Dynabeads coated with either an anti- CT-1 or an anti-PLAP antibody. Precipitated exosomes and the corresponding supernatant were analysed by Western blotting. Figure 2.10 –A shows a 25KD positive band corresponding to CT-1 and a positive band at 60KD consistent with PLAP in untreated (positive control) STB-EX. Figure 2.10–B also shows that on the one hand, STB-EX pulled down using a CT-1 antibody (CT-1 pull down) were positive for PLAP, but not all PLAP positive vesicles were pulled down by CT-1 coated beads, as evidenced by the 60KD band consistent with PLAP in the corresponding supernatant (CT-1 S/N). On the other hand, virtually all STB-EX pulled down by PLAP coated beads (PLAP pull down) were positive for CT- 1 (Figure 2.10–C). The 25KD band seen in the PLAP S/N shows that there is a small proportion of PLAP negative vesicles that express CT-1. These findings demonstrate that both species are present on the same population of STB-EX.

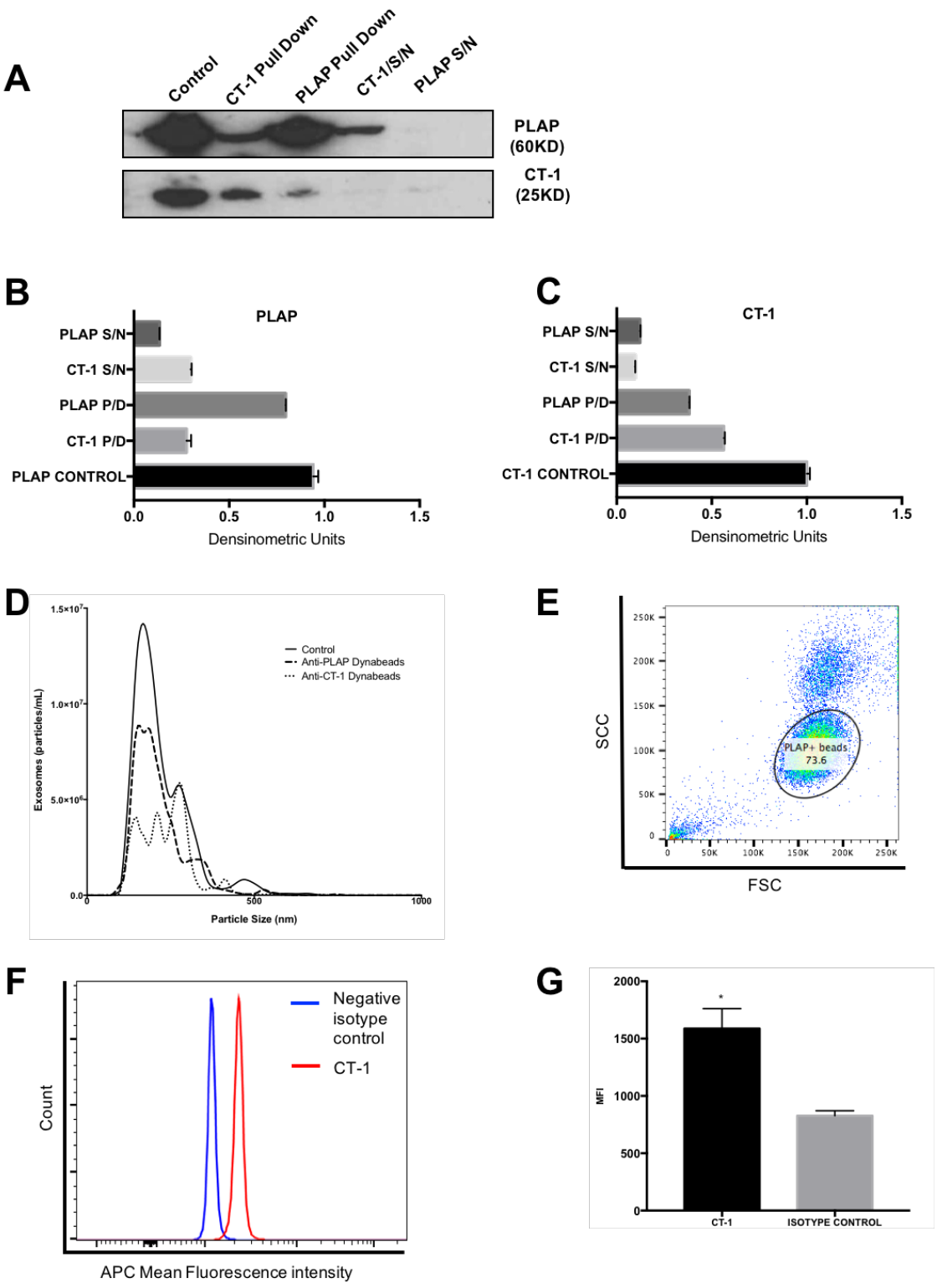


Figure 2.10. Immunoprecipitation of CT-1 and PLAP using Dynabeads to demonstrate co-localisation of these molecules on STB-EX. (A) Western Blot demonstrating expression of PLAP and CT-1 in STB-EX control exosomes, exosomes immunoprecipitated using CT-1 and PLAP, and the corresponding supernatants. Lane 1: Pooled STBEV, Lanes 2: CT-1 Pull Down, Lane 3: PLAP Pull Down; Lane 4: CT-1 Supernatant; Lane 5: PLAP supernatant. Corresponding Bar graphs of STB-EX treated **(B)** PLAP coated Dynabeads and **(C)** CT-1 coated Dynabeads relative to control **(D)** Nanoparticle Tracking Analysis of supernatants from control exosomes and vesicles treated with

Dynabeads coated with CT-1 and PLAP following magnetic bead depletion of placental exosome samples using PLAP and PLAP coated Dynabeads. **(E)** Flow cytometric analysis showing FSC vs SCC profile of bead-exosome complex – STB-EX captured with PLAP coated Dynabeads and interrogated with fluorescently labeled anti-CT-1. **(F)** Histograms showing MFI for APC showing that CT-1 is carried as a surface receptor on STB-EX with **(G)** corresponding bar charts an analysis of three STB-EX samples. *p < 0.05.

Furthermore, we compared the EV concentrations in supernatants of samples treated with anti-CT-1 and anti-PLAP Dynabeads using NTA. It was postulated that a reduction in EV concentration in the experimental samples relative to the untreated control would reflect the number of vesicles that expressed that molecule. Figure 2.10–D shows a 35.07± 3.5% and 55.7± 0.6% reduction in the vesicle concentration compared to control, corresponding to the number of CT-1 and PLAP positive STB-EX, respectively (n = 3).

Lastly, to further characterise the expression of CT-1 on PLAP positive STB-EX, immunoprecipitation was carried out as described (in section 2.2.8) and analysed by flow cytometry. STB-EX captured using PLAP-coated Dynabeads were interrogated with either an anti-CT antibody or negative isotype control. Initially, the bead-vesicle complex was gated on size on the FSC and SCC plot (Figure 2.10–E). Next, the difference in mean fluorescence intensity (MFI) was studied on three STB-EX preparations (Figure 2.10–F). This data showed that CT-1 was expressed on STB-EX (Figure 2.10–G).

2.3.8. Determining the non-toxic concentration of STB-EX for function studies

Several authors have reported on the concentration-dependent cytotoxic effects of STB-EV [112, 113, 115, 223]. Before studying the downstream

functional effects of STB-EX, we investigated the non-toxic concentration of STB-EX that could be used to treat cells. The CellTox^{TM} Green assay, in which a cyanine dye binds DNA released by dead cells following disruption of the plasma membrane, was used.

Experiments were set up using a wide range of STB-EX concentrations (1 x 10^6 EV/ml – 1 x 10^{10} EV/ml), each in 3 replicates. Figure 2.11 shows that after 12 hours of treatment, there was no difference in the fluorescence emitted by cells treated with STB-EX 1 x 10^6 – 1 x 10^{10} EV/ml compared to PBS control (vehicle). However, cells treated with 1 x 10^{10} EV/ml showed marked fluorescence intensity and therefore, cytotoxicity (Figure 2.11). Additionally, light microscopy revealed that the control HUVEC formed a smooth flat monolayer (data not shown). This was no different to the HUVEC treated with vesicle ranges 1 x 10^6 EV/ml – 1 x 10^8 EV/ml. In contrast, the HUVEC treated with 1 x 10^{10} EV/ml showed marked disruption of the monolayer. This data corroborates the findings that STB-EV have a concentration-dependent cytotoxic effect on endothelial cells. Lower EV concentrations, however, did not result in cytotoxicity. Thus, it was resolved that 1 x 10^8 EV/ml, the median EV concentration, which had no cytotoxic effects, would be used for downstream experiments.

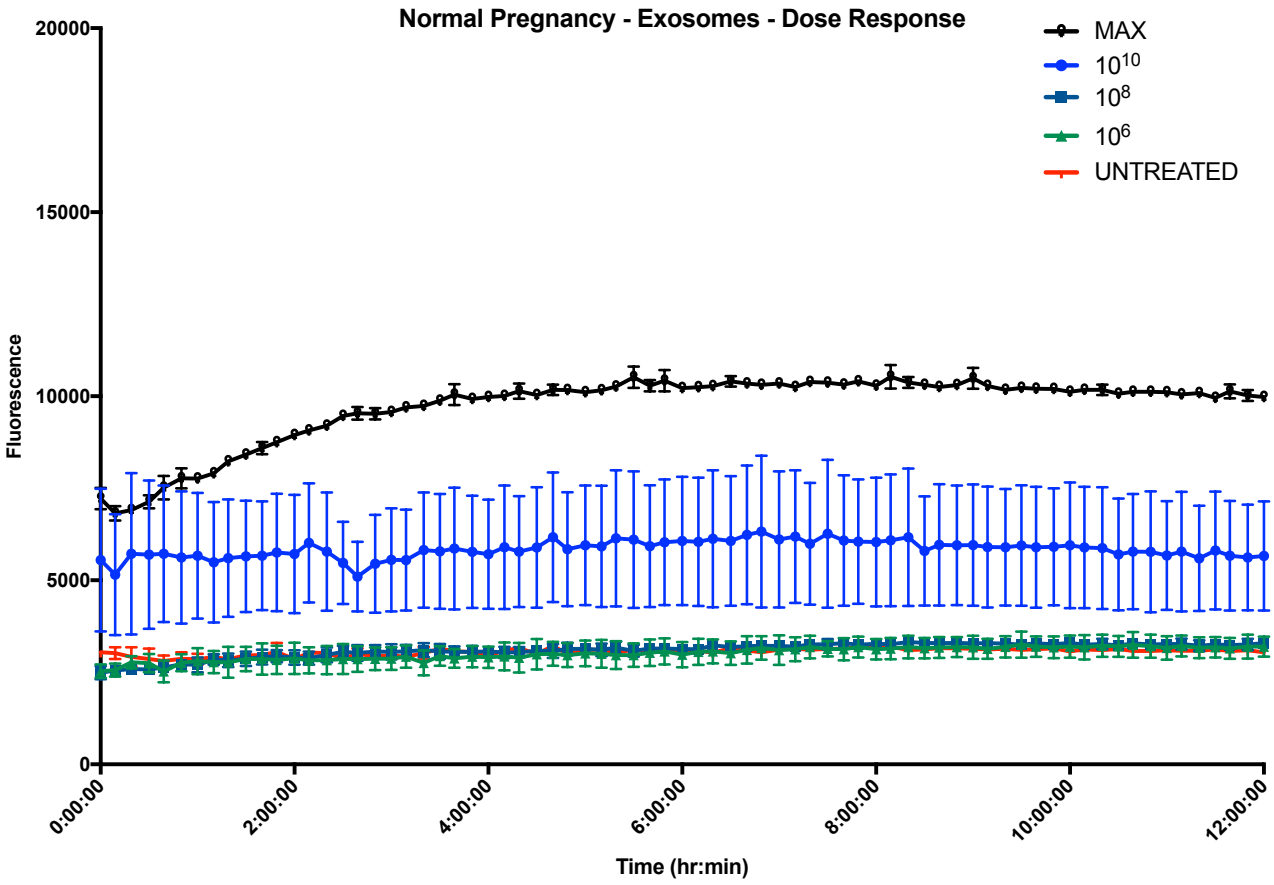


Figure 2.11. Figure 2.11. Determining the effective, non -toxic concentration of STB-EX. The effect of varying concentrations of STB-EX on HUVEC cell viability assessed using CellTox green® MT Cell Viability Assay. Average results of triplicates at the indicated concentrations of STB-EX. MAX = Maximal cell lysis induced with cell lysis buffer.

2.3.9. STB-EX-bound CT-1 phophorylates gp130, ERK 1/2 and STAT 3 but not Akt.

Having determined the non-cytotoxic concentration of STB-EX, the biological effects of STB-EX bound CT-1 *in vitro* were investigated on HUVEC cells as a model for vesicle-endothelial interaction. Intracellular pathways previously shown to mediate CT-1 signaling were studied and the results were analysed by Western blotting (Figure 2.12-A).

First, to investigate the extracellular and intracellular effects of CT-1, the activation of the gp130 transmembrane receptor was studied. HUVEC were treated with a 5μl of PBS (vehicle), 100 ng/ml recombinant CT-1, 1 x 10^8 STB-EX (from three different donors) in 5μl of PBS, or STB-EX pre-treated with a neutralising antibody against CT-1, each in 3 replicates (three technical replicates from 3 pooled biological samples). Western blot analysis showed that adding STB-EX to endothelial cells resulted in a significant phosphorylation of gp130 compared to those treated with PBS alone. This was consistent with the effect induced by recombinant CT-1 (Figure 2.12-B). Furthermore, the phosphorylation could be attenuated by the addition of CT-1 neutralising antibody, thus ascribing gp130 phosphorylation to STB-EX bound CT-1 (Figure 2.12-B).

Downstream of gp130, are classic pathways involved in the intracellular signaling of CT-1, namely, the mitogen-activated protein kinases/extracellular signal-regulated kinases (MAPK/ERK) pathways, signal transducer and activator of transcription 3 (STAT 3) and protein kinase B (also known as AKT). The ability of the CT-1 positive STB-EX to activate these pathways was also studied. This data also showed that adding STB-EX to HUVEC resulted in the activation of STAT 3 (Figure 2.12-C) and ERK (Figure 2.12-D). However, no AKT phosphorylation was observed after STB-EX treatment (Figure 2.12-A). Like the phosphorylation of gp130, the phosphorylation of ERK and STAT 3 could also be attenuated by the addition of a CT-1 neutralising antibody, showing specificity to CT-1. Conversely, the CT-1 neutralising antibody did not completely reduce the phosphorylation of STAT 3 and ERK, suggesting insufficient neutralization of CT-1 or that there may be other molecules

deployed on STB-EX that also activate these pathways. More importantly, these data suggest that STB-EX bound CT-1 induces an intracellular signaling cascade following a ligand –receptor interaction between the STB-EX and gp130. The lack of AKT phosphorylation suggests that STB-EX do not activate insulin receptor signaling in endothelial cells.

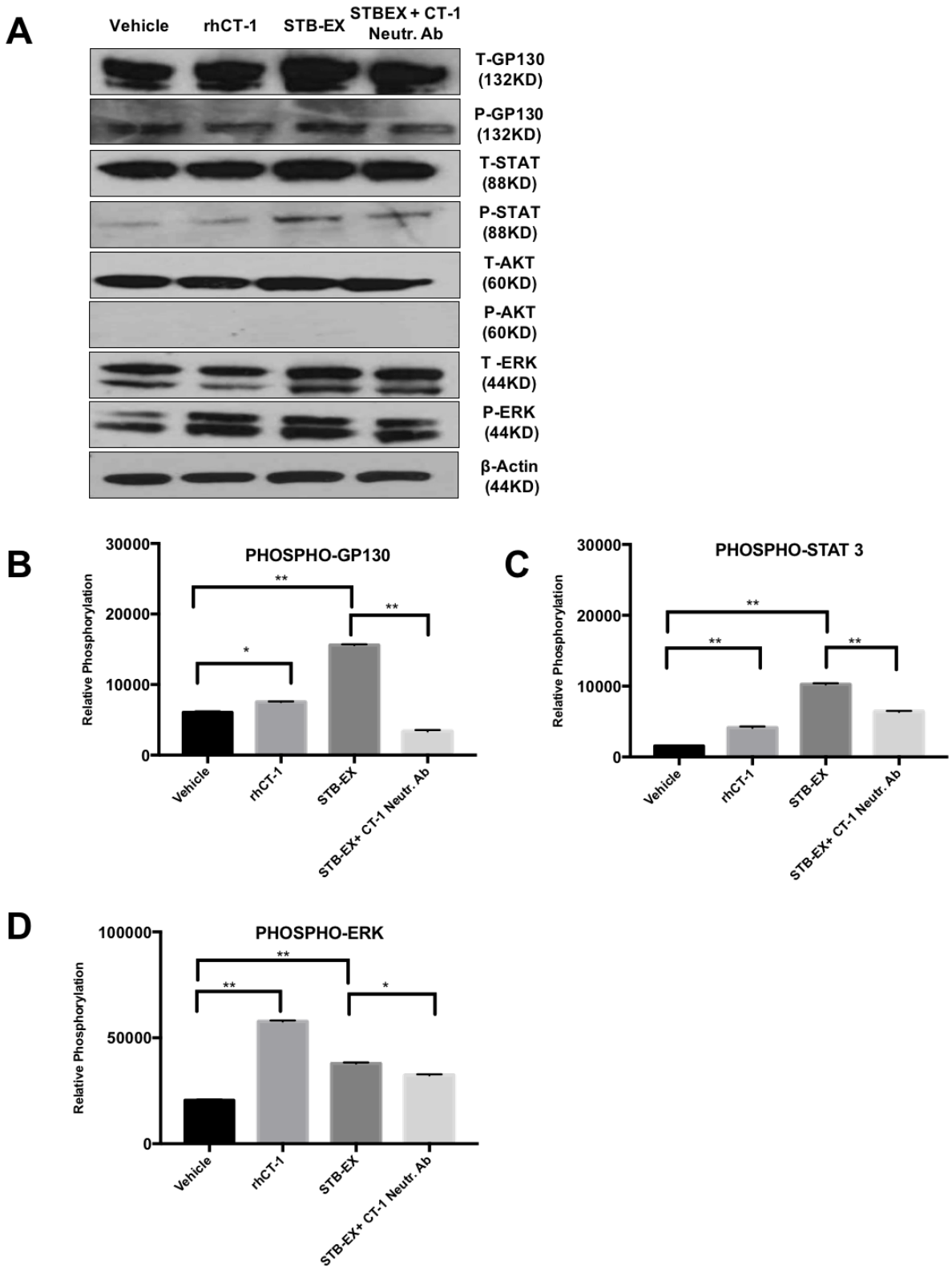


Figure 2.12. Investigating effects of STB-EV bound CT-1 phosphorylates gp130, STAT 3, AKT and ERK in HUVEC. **(A)** Western Blot demonstrating phosphorylation of gp130, STAT 3, ERK but not AKT on HUVECS treated with PBS (vehicle), recombinant CT-1 (rhCT-1), STB-EX and STBEX pre-treated with a CT-1 neutralising antibody. Corresponding densinometric analysis of **(B)** P-gp130, **(C)** STAT 3 and **(D)** ERK. N=3 *p<0.05 **p<0.0001

2.3.10. Internalisation of STB-EX by endothelial cells and cardiomyocytes

To further characterize the mechanisms by which STB-EX might interact with the heart, two cells lines were used. HUVEC and rat cardiomyocytes were incubated with fluorescent STB-EX for 1 hour, washed and examined by fluorescence and confocal microscopy. These experiments showed that STB-EX were taken up by endothelial cells (Figure 2.13-A) and cardiomyocytes (Figure 2.13-B). Our group previously demonstrated by flow cytometry that STBEV were internalized by HUVEC. This is the first study to show that cardiomyocytes can take up STB-EV. The mechanisms by which STB-EV are taken up by endothelial cells and cardiomyocytes are yet to be elucidated.

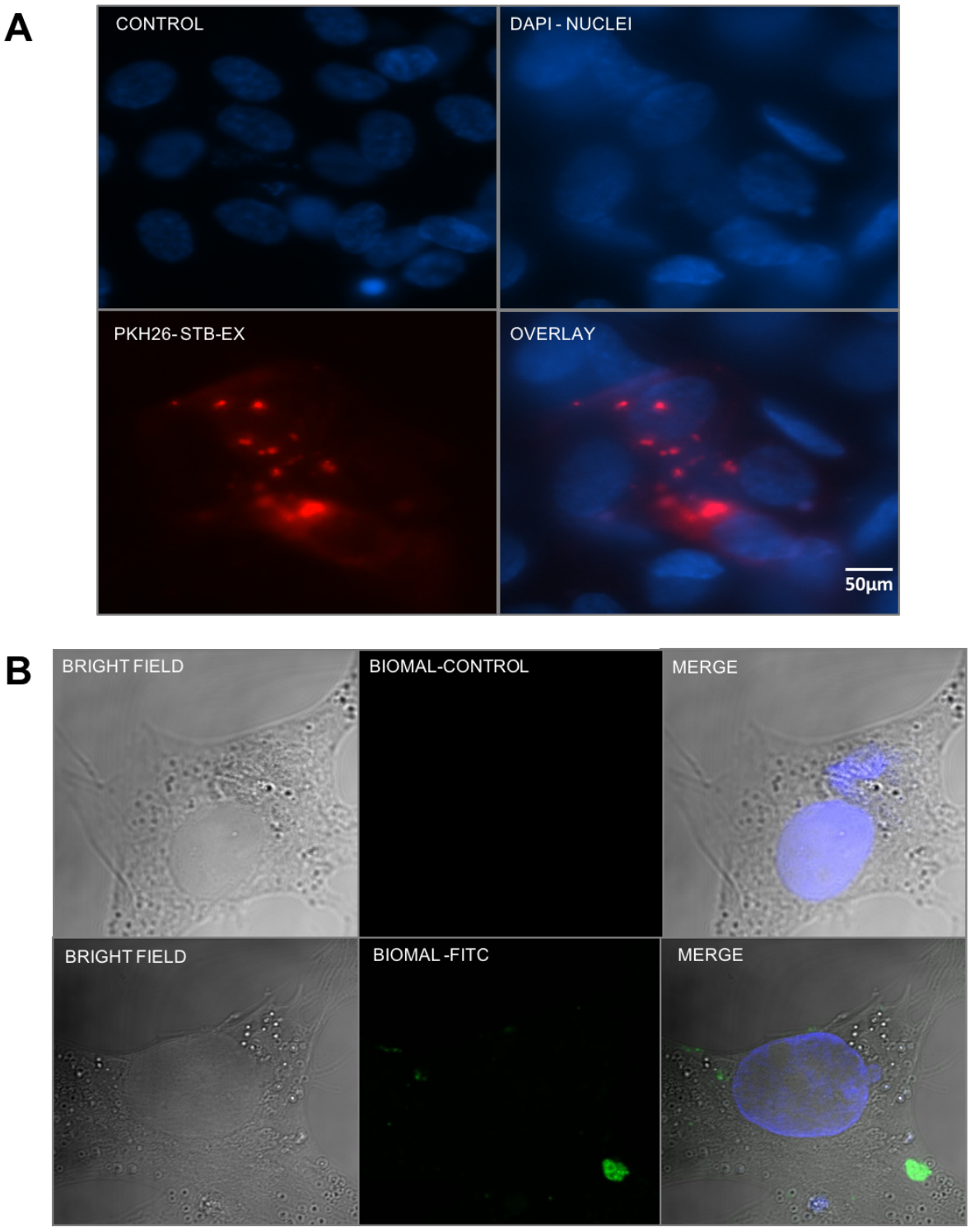


Figure 2.13. Internalization of STB-EX by HUVEC and rat cardiomyocytes. (A) Fluorescence microscopic image at X40 magnification showing PKH26 labeled STB-EX inside the HUVEC monolayer. **(B)** Confocal microscopic image at X100 magnification showing Biomaleimide labeled STB-EX inside the rat cardiomyocyte. Representative images.

2.3.11. Gene changes associated with treatment of cardiomyocytes with STB-EX

Having demonstrated that STB-EX are taken up by both endothelial and cardiac cells, the ability of STB-EX to induce gene changes associated with cardiac hypertrophy was studied by real time quantitative PCR (RT-qPCR). It was hypothesized that these studies would help determine whether the effects (if any) induced by STB-EX on the heart were due to direct (on cardiac cells) or indirect (endothelial cells acting on cardiac cells) vesicle-cardiomyocyte interaction. To achieve this, four cardiac genes: sarcoplasmic reticulum calcium pump (ATP2A2), myosin heavy chain 7 beta (MH7B), atrial natriuretic peptide (ANP or NPPA) and brain natriuretic peptide (BNP or NPPB) were investigated. These were previously shown to be altered as early as 2 hours of treatment following stimulation of cardiac cells with inducers of cardiac hypertrophy [229-231]. Similarly, five genes, previously shown to induce cardiac hypertrophy were examined by treating human coronary arterial endothelial cells (HCAEC) with STB-EX. These were: fms-related tyrosine kinase 1 (FLT), endothelin 1 (EDN 1), cyclin A2 (CCNA2) and interleukin 6 (IL-6) [232-235]. Cardiac and endothelial genes were normalized to rat and human glyceraldehyde-3-phosphate dehydrogenase (GAPDH), respectively. Cells were stimulated with a 5 μl of PBS (untreated cells), 100 ng/ml recombinant CT-1, 1 x 10^8 STB-EX (from three different donors) in 5 μl of PBS, or STB-EX pre-treated with a neutralising antibody against CT-1, each in 3 replicates (three technical replicates from 3 pooled biological samples).

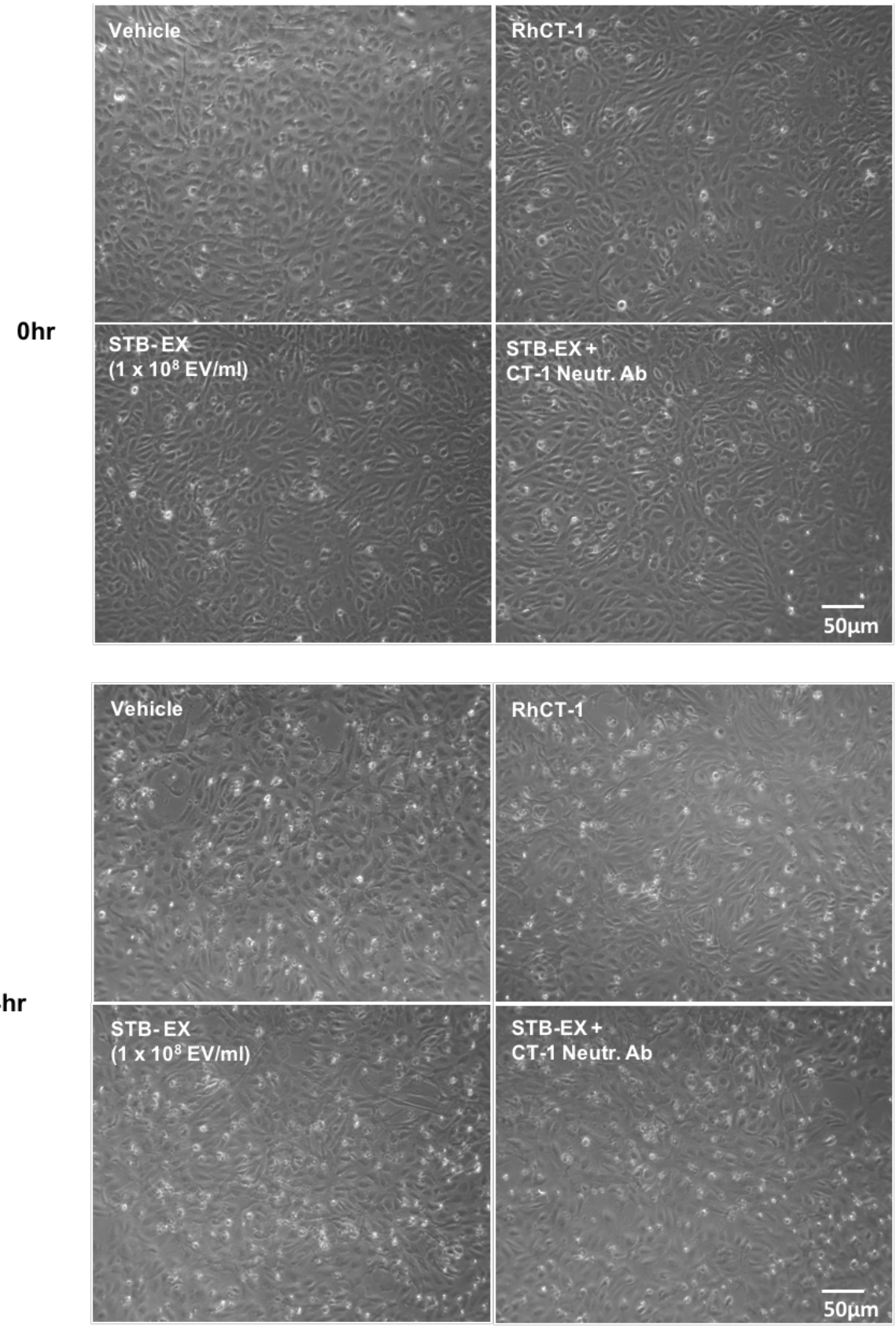


Figure 2.14. Microscopic of images of human coronary artery endothelial cell (HCAEC) monolayer at X10 magnification. Images show HCAEC at 0 hours and after 24 hours of treatment with PBS (vehicle), recombinant CT-1 (rhCT-1), STB-EX and STBEX pre-treated with a CT-1 neutralising antibody. Representative images.

Figure 2.14 shows that after 24 hours of treatment, there were no phenotypic changes microscopically between the various groups. Figure 2.15-A shows that, relative to untreated cardiomyocytes, recombinant CT-1 and STB-EX resulted in a 6-fold and 4-fold increase in the expression of NPPB. Furthermore, the transcription of NPPB could be attenuated by the addition of CT-1 neutralising antibody, thus ascribing the changes seen in NPPB transcription to STB-EX bound CT-1. The addition of recombinant CT-1 and STB-EX to rat cardiac cells, however, did not induce significant changes in the expression of APT2A2, MYH7B, NPPA after 24 hours of treatment. Figure 2.15-B shows that relative to untreated HCAEC cells, recombinant CT-1 upregulated IL-6. However, treating the cells with STB-EX did not result in a significant change in the expression of IL-6.

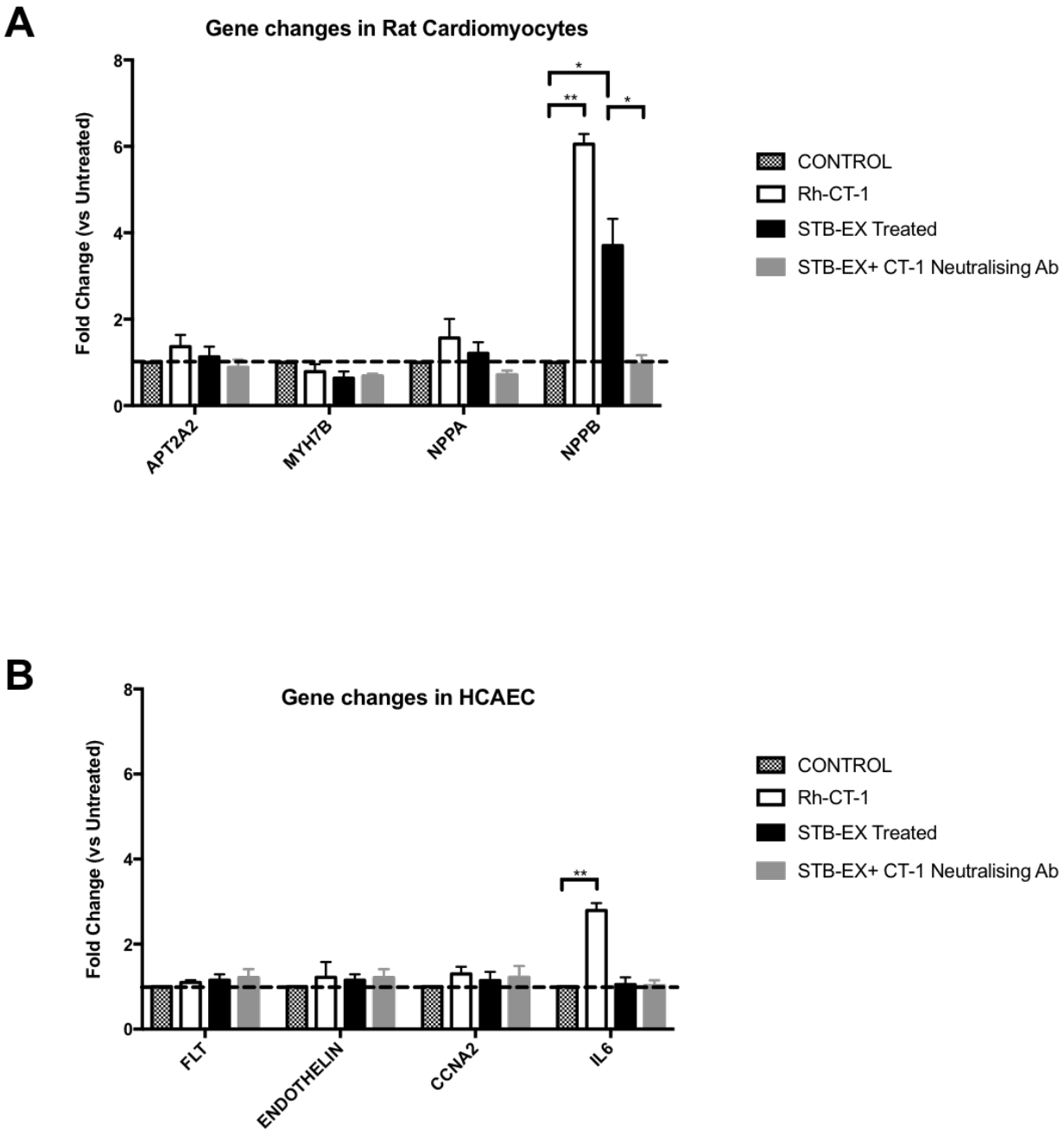


Figure 2.15 Gene changes caused by STB-EX in (A) rat cardiomyocytes and **(B) HCAEC.** Data are from simple t-test and are expressed as fold changes of genes. Sarcoplasmic reticulum calcium pump (ATP2A2), myosin heavy chain 7 beta (MH7B), atrial natriuretic peptide (ANP) and brain natriuretic peptide (BNP), fms-related tyrosine kinase 1 (FLT), endothelin 1 (END 1), cyclin A2 (CCNA2) and interleukin 6 (IL-6). * $p < 0.05$ vs untreated; ** $p < 0.01$ vs untreated.

2.4. DISCUSSION

This chapter studied the expression of CT-1 on the placenta and investigated the hypothesis that the expression of CT-1 on STB-EV may be a novel mechanism by which the placenta engages the maternal cardiovascular system during pregnancy. CT- 1 was originally discovered based on its ability to induce cardiomyocyte hypertrophy [121, 145]. Its expression has been detected in the heart, kidney, lung, aorta and skeletal muscle [122]. This is the first study to demonstrate its expression in the human placenta.

The human placenta is of the haemochorial type, so the fetal syncytiotrophoblast is direct contact with the maternal blood. Therefore, material released from the syncytiotrophoblast can enter the maternal circulation and effect tissue function. It is known that extracellular vesicles (STB-EV) are released by the syncytiotrophoblast and the amount of STB-EV shed into the maternal blood has been shown to increase with increasing gestational age, most likely reflecting increasing placental size as gestation progresses [105, 236]. Various techniques for the isolation of STB-EV and their characterization have been described [97]. The dual placental lobe perfusion technique was adopted because it is the most physiological and representative of the in vivo environment. We fractionated STB-EV by differential ultracentrifugation to produce two populations, the larger STB-MV and the smaller STB-EX. As previously discussed in the introduction of this chapter, Microvesicles are thought to be derived from the budding of the plasma membrane of cells [63] and are believed to play a role in the

pathophysiology of disease. In contrast, Exosomes are secreted vesicles of endosomal origin and thought to be involved in cell signaling processes [237]. Several studies have shown that exosomes are enriched with proteins such as tetraspanins and syndecan heparan sulfate proteoglycans which are increasingly being used as exosomal markers. With relevance to the placenta, exosomal proteins have been shown to play a major role in target cell selection in endothelial cells [238, 239], tethering of exosome to macrophages [240] and facilitating the uptake of vesicles by cytotrophoblasts [241]. Our results show that compared to placental lysates and the STB-MV preparations, STB-EX, are highly enriched in heparan sulfate proteoglycans, Alix and Syntenin, and CD 9, a tetraspanin.

Having successfully isolated STB-EV, we investigated the expression of CT-1 on STB-EV. We show for the first time that CT-1 is expressed on STB-EV. Furthermore, we confirmed by immunoprecipitation, that CT-1 and PLAP are co-expressed on STB-EX. Additionally, Western blotting and flow cytometry demonstrated that CT-1 was weakly expressed on STB-MV. However, it is thought that there are PLAP negative STB-MV. Considering the weak expression of CT-1 on STB-MV, only functional effects of STB-EX bound CT-1 was studied further.

An area of placental vesicular biology that has sparked increased interest but remains relatively unexplored is whether any signals exist on placental vesicles that target organs or cell types, especially those in the heart. First, we studied whether STB-EX bound CT-1 was biologically active, by investigating

the ability of STB-EX to activate intracellular signaling pathways. A review of the literature revealed four key pathways that CT-1 has been documented to activate. Our goal was to demonstrate that CT-1 on exosomes was capable of interacting with cells and induce a downstream signal, therefore suggesting a biological role. Our results show that indeed, STB-EX can phosphorylate the transmembrane receptor, gp130, as well as STAT 3 and ERK. Moreover, the activation of these proteins could be attenuated by pre-treating STB-EX with a CT-1 specific neutralising antibody.

Tian et al. investigated the contribution of the JAK/STAT 3 pathway, (ERK1/2) pathway, and the PI3K/Akt pathway to rat cardiomyocyte hypertrophy induced by cardiotrophin-1 (CT-1) [155]. They found in CT-1-induced cardiomyocyte hypertrophy, STAT 3 pathway played a predominant role, ERK1/2 pathway served as a negative regulator via inhibiting the activity of STAT 3, and the PI3K pathway was not involved in this process [155]. Moreover, Chung et al., found that in mid and late pregnancy, the pro-survival signaling cascades of Akt and ERK1/2 were activated in the hearts of mice [242].

Our signaling experiments, conducted on HUVEC seem to demonstrate that STB-EX-bound CT-1 activate similar pathways to those described by Tian et al [155]. Furthermore, Fritzenwanger et al. demonstrated that in quiescent confluent layers of HUVEC, CT-1 induced IL-6 via JAK2 activation and STAT 3 phosphorylation [198, 243]. They also found that in HUVEC, the MAPK and PI3K pathways were not necessary for IL-6 expression. So, concerning STB-

EX bound CT-1, our data are in good agreement with data published in the literature.

It is evident from our results that there are other molecules deployed on the vesicles capable of activating these pathways, but blocking CT-1 on STB-EX showed that a significant proportion of signaling was CT-1 dependent. Our study is not the first to demonstrate that exosome-bound surface proteins can induce intracellular signaling. Interestingly, Vicencio et al. have recently shown that exosomal HSP70 from rats and human stimulated toll-like receptor 4 (TLR4) signaling, and leading to the activation of ERK1/2, P38 MAPK, and subsequent HSP27 phosphorylation in cardiomyocytes [244]. STB-EV, like many extracellular vesicles studied, carry a complex cargo of proteins, lipids and miRNA. It is known that exosomes carry specific patterns of ligands and receptors on their surface, which likely allows targeting of specific cell types bearing the right counter-ligands. Our results demonstrate the ligand-receptor interaction created by CT-1 positive exosomes and gp130 is robust enough to initiate an intracellular cascade. However, we contend that the interaction reflects a small component of a much more sophisticated mechanism by which vesicles interact with target cells. The role of CT-1 on STB-EX would, therefore, be to target specific cells expressing its receptor. To test this hypothesis, we investigated whether fluorescently labeled STB-EX are taken up by HUVEC and rat cardiomyocytes, cells that abundantly express gp130. Our results show that endothelial cells and cardiomyocytes internalise STB-EX. Attempts to inhibit this uptake using CT-1 neutralising antibody did not show a significant decrease in uptake. This may indicate that different

mechanisms may mediate vesicle uptake, or that a reduction in uptake is not able to be detected by fluorescent/confocal microscopy. Our results demonstrated STB-EX uptake by HUVEC is consistent with previous work published by our laboratory that demonstrated by flow cytometry that STB-EV rapidly internalized by HUVEC (reviewed in [245]). Recently, work published by Tong et al. showed that placental vesicles isolated from cultured human first-trimester placental explants not only rapidly interact with human microvascular endothelial cells (HMEC) and but also localise to different organs in vivo [246]. Our laboratory has recently discovered that STB-EX carry non-coding RNA, some of which have been shown to be involved in cardiovascular physiology (unpublished). Therefore, the data presented in this chapter suggests that STB-EX may have their biological effect acutely, via ligand-receptor interaction, but also capable of delivering longer term effects to cardiomyocytes via known miRNA.

Cardiomyocytes lie subjacent to coronary endothelial cells. One hypothesis is that vesicles are taken up by endothelial cells and transferred to cardiomyocytes where they effect change. Alternatively, vesicles may be taken up by endothelial cells which in turn release factors that act on cardiomyocytes. To test these hypotheses, we studied gene changes in endothelial cells and cardiomyocytes following exposure to STB-EX. Placental vesicles have been shown to induce gene changes in endothelial cells [114, 116]. Wei et al. investigated the transcriptional and proteomic changes that occur in HMEC-1 following exposure to placental vesicles from normal first-trimester placentas and showed that vesicles alter the phenotype of

endothelial cells in a manner that may help induce the cardiovascular changes necessary for healthy pregnancy [116]. This work, however, was primarily focused on endothelial cell function in pregnancy. To date, no one has looked at the circulating placental vesicles and how these could affect the cardiac microenvironment.

Cardiac myocytes are known to react to increased hypertrophic neuro-humoral stimuli by reinitiating expression of fetal forms of structural genes e.g. ANP and BNP. We studied four genes which are altered in cardiac hypertrophy. We show, for the first time, that rat cardiomyocytes exposed to STB-EX generated by ex vivo perfusion of healthy term pregnancy placentas upregulate the expression of BNP in rat cardiomyocytes. This finding is consistent with the findings of Kuwahara et al. who demonstrated that CT-1 promotes transcription of BNP in cultured neonatal rat cardiac myocytes [247]. The NPPB gene encodes BNP and comprises three exons separated by two introns [248, 249]. The second and third exons contain the sequence encoding the biologically active peptide [248, 249]. In humans, NPPB mRNA translates proBNP, precursor protein and is transcribed in response to cardiac stress states such as volume overload [248, 249]. This prohormone is cleaved within the secretory granule, before or at the time of secretion, a C-terminal fragment (BNP) and an N-terminal fragment (ntBNP), which is thought to be functionally inactive [248, 249]. N-terminal fragment is stable in plasma, and it accumulates at very high levels in states of increased BNP secretion, such as heart failure [250, 251]. Tsutamoto et al. found that patients with a BNP level that exceeded 73 pg/ml (median value in their heart failure cohort) had a survival rate that

was significantly lower than that of the group with BNP levels falling below this level [252]. Similar results have been reported by others, supporting the notion that higher BNP levels, perhaps indicative of more severe cardiac dysfunction, correlate with increased cardiovascular morbidity and mortality. In rat models, Eghbali et al. and later Chung et al. found that in the hearts of pregnant mice, BNP expression did not change in mid- and late pregnancy [59, 242]. A different study, however, found that BNP expression was decreased in late pregnancy [253]. In humans, Hameed et al. demonstrated that circulating BNP levels were approximately 2-fold higher than their non-pregnant counterparts in their study cohort, and do not significantly fluctuate during pregnancy [254] whilst others found that BNP levels are markedly increased in pregnant patients with cardiac disease and those with preeclampsia [255, 256][58]. Interestingly, pharmacologically, BNP has ameliorative effects on patients with acute heart failure [257] [258] [259] [260] with symptom and haemodynamic improvement after a short infusion [261]. Given the very high levels of BNP that circulate in the plasma of heart failure patients, it remains unclear as to why infusions of BNP have any effect at all.

Our data shows that CT-1 did not significantly increase ANP, ATP2A2, and β-MyHC (MYH7 gene) expression in rat cardiomyocytes. This result is inconsistent with previous results obtained from isolated neonatal rat cardiac myocytes. For example, Wollert et al. demonstrated that CT-1 upregulates the ANP gene but does not affect skeletal α-actin or myosin light chain-2v expression [146]. Conversely, in hearts isolated from pregnant mice throughout gestation, ANP gene levels are significantly decreased in mid-

pregnancy [7]. Furthermore, ATP2A2 and β-MyHC (MYH7 gene) do not change in mid- and late pregnancy [59, 242]. A different study found that β-MyHC expression was increased in late pregnancy [253].

Our results also showed that while HCAEC exposed to recombinant CT-1 upregulated the expression of IL-6, HCAEC exposed to STB-EX did not significantly alter IL-6 gene expression. Fritzenwanger et al. showed that CT-1 induces IL-6 expression in a dose-dependent manner requiring at least 100 ng/ml to induce significant expression [243]. Given the fact that we do not know the concentration of CT-1 on STB-EX, and treatment of HCAEC was based on EV concentration instead of the concentration of CT-1, it possible that the lack of IL-6 expression may be due to inadequate, insufficient amounts of CT-1 on vesicles. FLT, END 1, and CCNA2, were not significantly altered by the treatment of HCAEC with STB-EX.

Based on these findings we decided to study the effects of STB-EX directly on human cardiomyocytes which will be explored in Chapter 4 of this thesis.

Considering these new findings of CT-1 on STB-EX, we attempted to study the circulating levels of total CT-1 in the plasma of women who had normal pregnancies using commercially available CT-1 ELISA kits. However, we were unable to detect CT-1 in either normal pregnancy women or non-pregnant controls. It is possible that the fact that CT-1 is encapsulated in a membrane prevented the secondary (detection) antibody from binding and giving a signal. Some authors in the field have attempted to use placental alkaline

phosphatase as a secondary detection system [236]; however, we were concerned that non-specific binding might give an artificially inflated result and decided not to proceed along this route. This lack of standardisation in tools used for the detection of CT-1 could account for the variation in our findings.

2.5. SUMMARY

The findings of this thesis chapter make it clear that CT-1 is expressed on the syncytiotrophoblast and is differentially deployed on STB-EX. Furthermore, we found in vitro evidence that STB-EX bound CT-1 stimulated gp130 signaling leading to the activation of STAT 3 and ERK 1/2 but not Akt. We also showed that STB-EX are internalised by endothelial cells and cardiomyocytes. Finally, we demonstrated that STB-EX induce the transcription of BNP.

CHAPTER 3

THE STUDY OF GENE CHANGES IN RESPONSE TO THE TREATMENT OF HUMAN INDUCED PLURIPOTENT STEM CELL-DERIVED CARDIOMYOCTYES WITH CT-1 POSITIVE STB-EV

3.1. INTRODUCTION

In Chapter 2 we demonstrated that Cardiotrophin 1 (CT-1) present on syncytiotrophoblast-derived exosomes (STB-EX) activate gp130 signaling leading to the activation of STAT 3 and ERK 1/2. Furthermore, we demonstrated that STB-EX-bound CT-1 can induce gene changes in rat cardiomyocytes. However, we were interested in whether STB-EX could induce gene changes in human cardiac myocytes.

In this chapter of the thesis, we investigate the effects of STB-EX on human cardiomyocyte gene expression. To achieve this, human induced pluripotent stem cell derived cardiomyocytes (hiPSC-CM) were used. HiPSC-CM have previously been shown to resemble cardiomyocytes in contractile protein expression, and myofibril structure, electrophysiology, calcium handling and force generation [262-265]. Thus, they have been shown to be excellent models for the study of cardiac specific pharmacodynamics and kinetics and safety of several therapeutic agents [266-268].

We cultured hiPSC-CM for 24 hours in the presence of CT-1 positive STB-EX or STB-EX pre-treated with a CT-1 neutralising antibody. Thereafter, total RNA was purified from cultures and analysed on microarrays (Affymetrix GeneChips, Affymetrix, USA) for specific gene expression. The expression levels of some of the genes that were found to be differentially expressed (i.e. expressed at different levels between two states) following STB-EX treatment were then verified by RT-qPCR.

3.2. MATERIALS AND METHODS

3.2.1. Cell culture

Human induced pluripotent stem cell derived cardiomyocytes (hiPSC-CM) were purchased from Axol biosciences (UK), and temporarily stored in liquid nitrogen until further use. For studying gene changes in response to treatment with STB-EX, cells were cultured according to the manufacturer's instructions (Axol Biosciences, UK). HiPSC-CM are ventricular cardiomyocytes that were derived from induced pluripotent stem cells through proprietary differentiation and purification protocols. First, cardiomyocyte maintenance cell culture medium was prepared by adding cardiomyocyte supplement (Axol Biosciences, UK) to 500 ml cardiomyocyte medium (Axol bioscience, UK). Next, plating medium was constituted by adding 10% (v/v) fetal bovine serum (FBS) (Sigma, UK) to an aliquot of cardiomyocyte maintenance medium.

Next, to facilitate cell adherence and survival, 12 wells of a 24-well plate were coated with fibronectin (Axol bioscience, UK). Fibronectin Stock Solution was diluted to create a 1:100 working solution. 200 μl per cm^2 of the working solution was added to each well and the plate was placed in a humidified incubator at 37° C. After overnight incubation, the solution was removed and cells were plated immediately afterwards.

For plating, a vial containing cryopreserved hiPSC-CM was removed from the liquid nitrogen tank, disinfected with 70% ethanol and placed in a pre-heated (37° C) water bath. Cells were then gently transferred into a sterile 15 ml centrifuge tube containing 10 ml of pre-warmed plating culture medium. The

cells were pelleted at 200 x *g* for 5 minutes at room temperature and resuspended in 1 ml culture medium for live cell density determination by trypan blue (Life technologies, UK) exclusion. Next, 1000 μl of cell suspension was pipetted into each well at a cell density of 1.2 x 10^5 cells/ml and incubated at 37° C in 5% CO_2. The day after, to remove dead cells and debris, the plating medium was removed from the cells and replaced with fresh, pre-warmed cardiomyocyte maintenance medium. The cells were maintained in culture for 8 days with cardiomyocyte maintenance medium was changed every two days.

3.2.2. The study of gene changes caused by STB-EX in hiPSC-CM.

For the study of gene changes associated with cardiac function in response to treatment with STB-EX, hiPSC-CM were seeded in triplicates into 12 wells of a fibronectin coated 24-well plate and maintained in culture as described in section 3.2.1. above, before being cultured in serum-free cardiomyocyte culture medium at 37° C in 5% CO_2 for 24 hours (Figure 3.1). The culture medium was then replaced with serum free cardiomyocyte medium containing either 5 μl sterile PBS (vehicle), or recombinant CT-1 (100 ng/ml) (R & D Systems, UK), or 1 x 10^8 STB-EX in 5 μl of PBS, or STB-EX pre-treated with a neutralising antibody against CT-1 (R & D Systems, UK) and cells were cultured at 37° C in 5% CO_2. After 24 hours of treatment, cells were washed with PBS and lysed with 350 μl of cell lysis buffer (Qiagen, Germany) and immediately processed for RNA isolation.

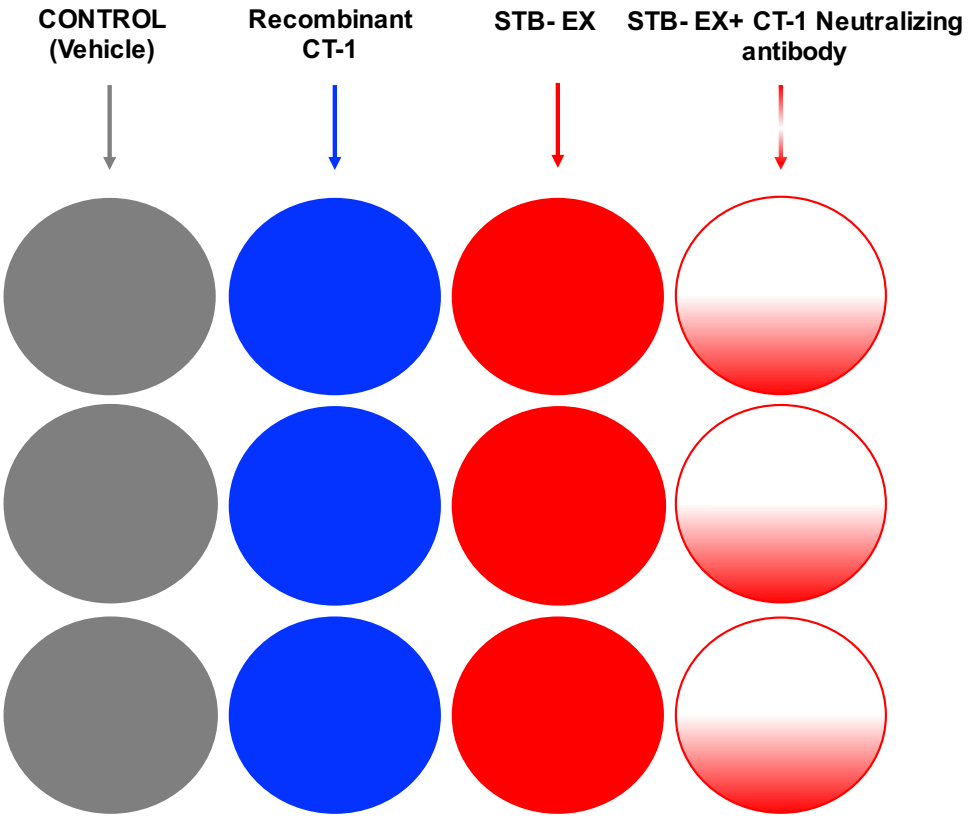


Figure 3.1. Schematic representation of the different groups used to treat human induced pluripotent stem cell -derived cardiomyocytes. HiPSC-CM seeded in triplicates into 12 wells of a 24-well fibronectin coated plate were treated with containing PBS (vehicle), recombinant CT-1 (100 ng/ml), 1 x 10^8 STB-EX in PBS or STB-EX pre-treated with a neutralising antibody against CT-1.

3.2.3. RNA isolation

For RNA isolation, the Qiagen RNeasy micro kit (Qiagen, Germany) was used according to the manufacturer's instructions. Briefly, following cell culture (described in section 3.1.1 above) and cell treatment (described in section 3.1.2), the culture medium was aspirated and each well was washed once with PBS. Next, cells were lysed with 350 μl Buffer RLT (Qiagen, Germany). To homogenize the cells, the lysate was vortexed for 1 minute. For RNA precipitation, 350 μl of 70% ethanol was added to the lysate and passed through an RNeasy spin column placed in a 2 ml collection tube and

centrifuged at 8,000 x g for 15 seconds. The spin column was subsequently washed with 700 μl Buffer RW1 (Qiagen, Germany) at 8,000 x g for 15 seconds. For DNase digestion, 10 μl of DNase incubation mix (prepared as 10 μl of DNase stock solution to 70 μl Buffer RDD (Qiagen, Germany) was added directly to the RNeasy spin column membrane and left on the bench for 15 minutes followed by a washing step with 350 μl Buffer RW1 (Qiagen, Germany) at 8,000 x g for 15 seconds. Afterwards, the spin column was washed twice, first, with 500 μl Buffer RPE (with 70% ethanol) (Qiagen, Germany) at 8,000 x g for 15 seconds and again with 500 μl Buffer RPE at 8,000 x g for 2 minutes. The flow-through was discarded after each spin. Finally, 500 μl of 80% ethanol was added to the spin column and centrifuged at 8,000 x g for 2 minutes followed by centrifugation with an open lid at 8,000 x g for 5 minutes to ensure that no residual ethanol was carried over during RNA elution. To elute the RNA, 14 μl of RNase free water was added to the spin column and centrifuged at 8,000 x g for 1 minute. The eluent was collected in a RNase-free tube (Qiagen, Germany) and placed on ice until quantification by ultraviolet spectroscopy at 260 nm/ 280 nm with a NanoDrop® ND-1000 Spectrophotometer (Thermo Fisher Scientific, USA) and storage at -80° C.

3.2.4. Microarray gene expression profiling and data analysis

Microarray analysis was conducted by the High-Throughput Genomics Group at the Wellcome Trust Centre for Human Genetics according to the standard Affymetrix protocol using the high-throughput Affymetrix system. 12 total RNA samples extracted from hiPSC-CM using the GeneChip© WT PLUS assay kit (Affymetrix, USA) which generates amplified and biotinylated sense-strand

DNA targets from total RNA. Labeled ss-cDNA was hydridised to the Human Gene 2.1 ST 16-Array Plate and processed on the Affymetrix GeneTitan platform. The GeneChip© WT PLUS assay kit uses a reverse transcription priming method that primes the entire length of RNA, including both poly(A) and non-poly(A) mRNA to provide complete and unbiased coverage of the transcriptome.

First, total RNA concentration was assessed using the Quant-iT™ RiboGreen® RNA Assay Kit (Thermofischer, UK) according to the manufacturer's instructions. Samples were normalised to 90 ng in a total volume of 3 µl for processing. The Affymetrix RNA control sample at 50 ng/µl concentration was also included in the process.

Next, the quality of the RNA was checked for integrity in the Agilent BioAnalyser (Agilent, UK) prior to processing and was also used for hybridization, after all the quality control (QC) was completed. The RNA integrity Number (RIN) value and samples with integrity number > 9 were used to generate microarray data (n = 3 per group). The latest version of Affymetrix Genechip Command Console software for GeneTitan was used to carry out QC checks of the procedure and to produce reports.

Controls for Sample Labelling (polyadenylated mRNA Spike): Eukaryotic Poly-A RNA labelling controls contains four exogenous, pre-mixed, polyadenylated prokaryotic controls namely: lys, phe, thr, and dap with final concentration of 1:100 000, 1:50 000, 1:25 000 and 1:7 500 respectively that were spiked

directly into RNA samples before target labelling. Their resultant signal intensities on the arrays served as sensitive indicators of target preparation and the labelling reaction efficiency, independent from starting sample quality.

Array Hybridization Controls: BioB, bioC, and bioD are genes of the biotin synthesis pathway from the bacteria E. coli, and cre is the recombinase gene from P1 bacteriophage. A ready-prepared mixture of these biotinylated controls at staggered concentrations were added with labelled eukaryotic RNA samples to hybridize onto GeneChip probe arrays. Signal intensities obtained on these genes provided information on how well the hybridization, washing, and staining procedures were performed.

Presence of spiked control cRNAs: Bio-B, C, D and CRE serve as positive controls for hybridization and are spiked at different concentrations as follows: BioB: 1.5 pm, BioC: 5 pM, BioD: 25 pM, CRE: 100 pM. At 1.5 pM, bioB is at the detection limit for most expression arrays and is anticipated to be called “Present”, at least 70% of the time. In contrast, the other controls should be called Present all of the time, with increasing signal values (bioC, bioD, and cre, respectively). Absent calls, or relatively low Signal values, indicate a potential problem with the hybridization reaction or subsequent washing and staining steps.

Background v signal Check: Signal levels were assessed using the un-normalised .CEL files and were considerably higher than background. There was no official signal intensity value for this but the difference between the two

were similar between arrays and showed the same signal fluctuation pattern when compared all arrays that were processed at the same time.

Intron v Exon signal check: This was based on 100 specific genes with probes to exons and introns. The ideal is signal on all exon generated and not at intron level. The ideal value = 1.0. The cut off is 0.8. and checks sample quality to ensure no DNA contamination.

Raw microarray data was deposited on http://www.well.ox.ac.uk/customer-downloads/Manu_Vatish_P170290/ (P170290).

The microarray data was analysed in conjunction with Assistant Professor Muhammad Furqan Bari from Dow University of Health Sciences. First, for background correction and to normalise data, processing and transformation was performed using R statistical program (Software for Data Analysis: Programming with R) and performed as follows: The Affymetrix raw data (CEL files) were background corrected using Robust Multi-Array analysis (RMA) [269] and quantile normalized [270] using method implemented in bioconductor packages oligo [271] in R statistical program.

The probes to genes were matched using NetAffx Alignment Files (HuGene-2_0-st-v1) from the Affymetrix website Release 36 (dated 7/6/16) [272]. To identify differentially expressed genes, a linear model was fitted to the data sets using the LIMMA package as previously described by Smyth [273].

To identify the relationships between selected genes, the Ingenuity Pathway Analysis (IPA) (Ingenuity Systems, USA) was used. Excel datasheets containing gene IDs with the assigned gene expression values were uploaded onto the program. The software then analyses the information by comparing the uploaded data to the information found on its database called the Ingenuity Pathways Knowledge Base (IPKB). The IPKB is derived from the literature and provides information about known functions and interactions which have been published in the literature. A built-in statistical tool calculates a p-value to determine the probability that each biological function or canonical pathway assigned to the data set was due to chance alone. For the representation of the relationships between the genes, the 'Pathway Designer' tool of the IPA software was used.

3.2.5. Taqman® Gene expression assay for gene validation by RT-qPCR

First, cDNA was generated as previously described in section 2.2.12.2. Briefly, 150 ng of high-quality total RNA was reverse transcribed using High Capacity cDNA Reverse Transcription Kit (Applied Biosystems, USA). After thawing on ice, a 1X RT reaction mix was made up using 2 μl 10X RT buffer, 0.8 μl of 100 mM dNTP mix, 2 μl 10X Random Primers, and 1 μl Multiscribe Reverse Transcriptase. Thereafter, 5.8 μl of RT mix was added to 14.2 μl of RNA sample to make up a total volume of 20 μl before being processed in a Veriti (Applied Biosystems, USA) thermocycler using the following settings: 16° C for 30 minutes, 42° C for 30 minutes, followed by 85° C for 5 minutes and a final hold at 4°C.

To validate genes changes following treatment of hiPSC-CM with STB-EX, RT-qPCR with a predesigned Taqman® expression assay was used. After thawing on ice, a 1x PCR reaction mix was made up using 1 μl 20x Taqman® expression assay, 11 μl 2x Taqman® gene expression Master Mix and 9 μl (10 ng) of cDNA, total volume of 20 μl. All mixes were pipetted into the wells of a gene disc (Qiagen, Germany) using a CAS-1200 pipetting robot (Corbett Life Science, UK). At the end of each automated pipetting cycle, the gene discs were sealed with a Rotor-Disc Heat Sealer (Qiagen, Germany) before further processing. For, RT-qPCR 40 cycles were carried out on the Rotor-Gene 6000 analyser (Corbett Life Science, UK) using the following settings: hold- 50° C for 2 minutes, hold - 95° C for 10 minutes, followed by forty 95° C for 5 seconds/ 60° C for 6 seconds' cycles acquiring to FAM™. The results were analysed with the Rotor-Gene Q Series software (Qiagen, Germany).

3.2.6. Statistical Analysis

Data are shown as mean ± SEM. The results generated from the RT-qPCR experiments were analysed using a two-sample t-test. Statistical analyses were carried out using Prism software (GraphPad Software, San Diego California USA, www.graphpad.com). Values of $p<0.05$ were considered statistically significant.

3.3. RESULTS

3.3.1. Total RNA quality assessment

Having isolated total RNA from hiPSCs, a quality assessment was conducted. Figure 3.2 shows the bioanalyzer gel image showing distinct RNA bands and that each sample had a RIN number that was above 9 (Figure 3.2). Furthermore, electropherograms for the RNA of purified from all hiPSCs samples show distinct 18S and 28S peaks preceded by an area of low background indicating the presence of intact RNA (Figure 3.3).

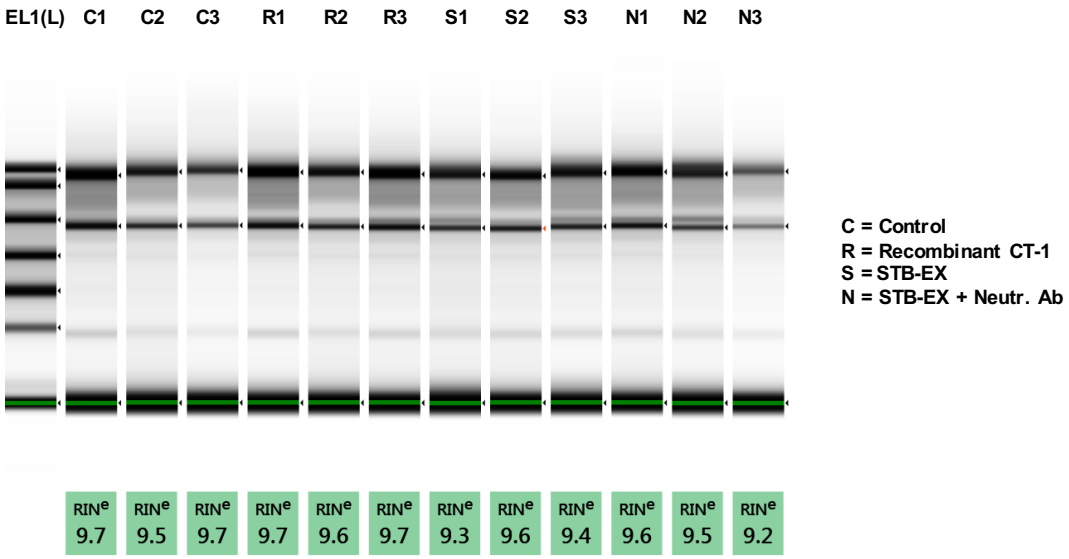


Figure 3.2. Bioanalyzer gel image of RNA quality among samples extracted from hiPSC-CM.

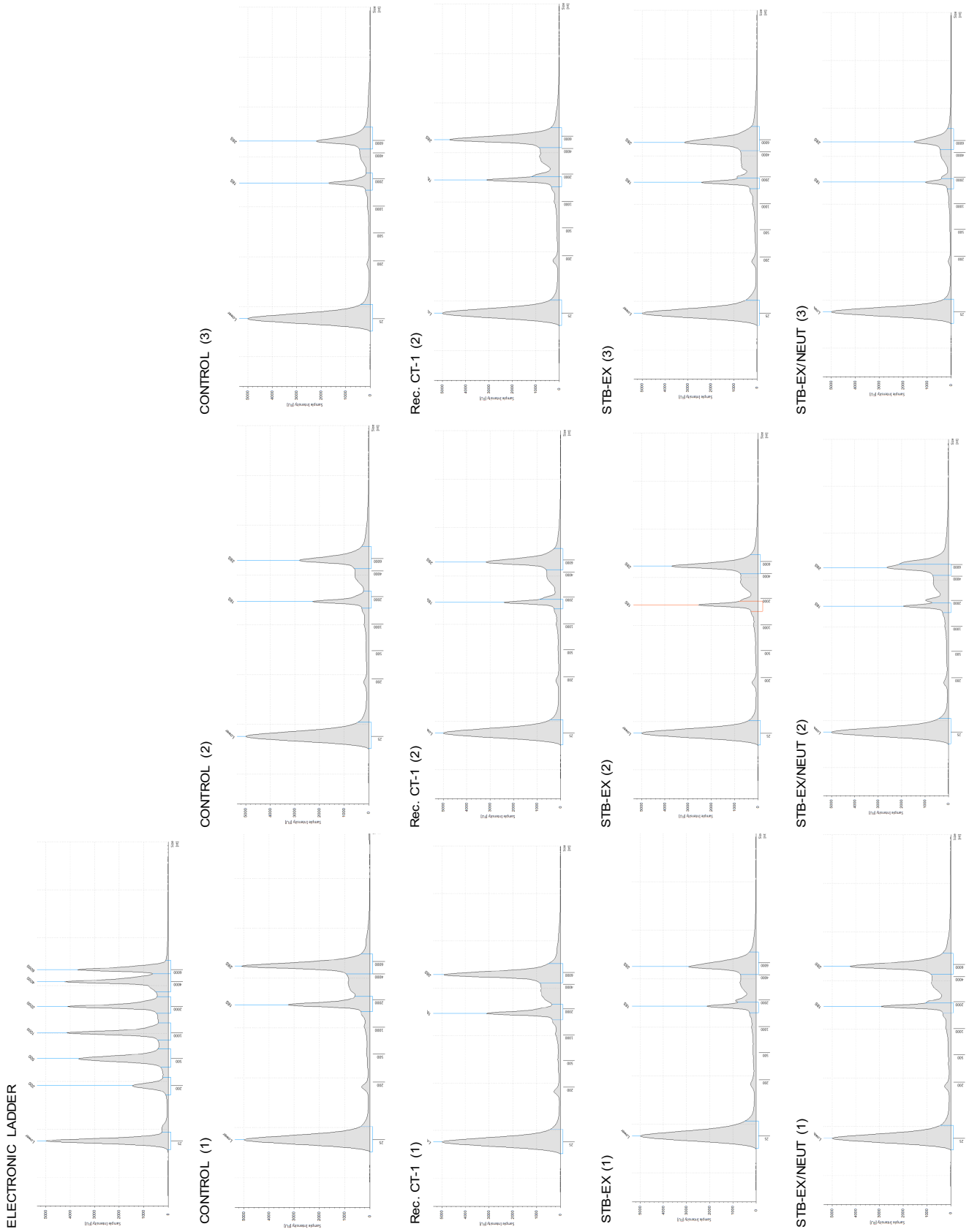


Figure 3.3. Electropherograms of RNA quality among samples extracted from hiPSC-CM.

3.3.2. Hierarchical Clustering

Next, hierarchical clustering was conducted to group together samples with similar properties based on gene expression levels. There was space on the overall chip for two duplicates, so additional runs were performed using RNA from STB-EX and STB-EX/Neutralising antibody samples. The clustering showed that there was not a vast difference amongst the various groups (Figure 3.4). However, the technical replicate (STB-EX/NEUTR (2) _repeat) was identified as an outlier (having shown a much lower intensity level than other samples during the processing) and was removed from the analysis.

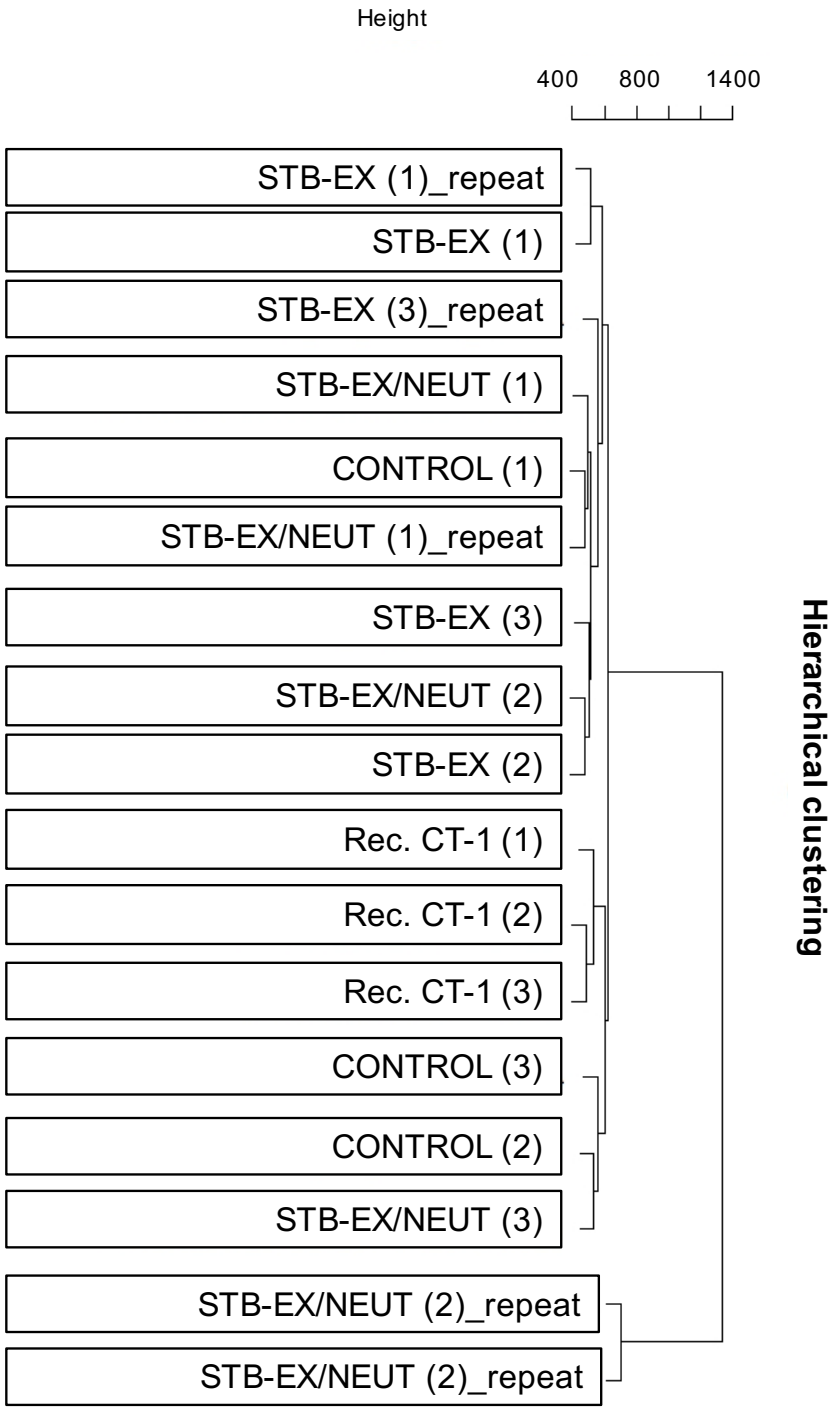


Figure 3.4. Hierarchical clustering of gene expression data from hiPSC-CM

3.3.3. Gene array and IPA analysis

A microarray based transcriptional profiling was used to compare samples treated with CT-1 positive STB-EX to STB-EX pre-treated with a CT-1

neutralising antibody (STB-EX/NEUTR). The intensity profiles of the background corrected, normalized and log2 transformed signal values of 352859 probes were obtained and analysed using the contrast: [(STB-EX – CONTROL) - (STB-EX_NEUTRAL – CONTROL)], out of which 7759 and 7737 transcripts had a more than 2-fold up-regulated and down-regulated genes, respectively ($n = 3$, $p < 0.05$).

Table 3.1. The most upregulated canonical pathways found in hiPSC-CM treated with STB-EX compared to those treated STB-EX+CT-1 neutralising antibody.

Top Canonical Pathways		
Name	p-value	Overlap
Remodeling of Epithelial Adherens Junctions	4.94E-04	11.6 % 8/69
Hepatic Fibrosis / Hepatic Stellate Cell Activation	5.25E-04	7.5 % 14/187
Epithelial Adherens Junction Signaling	6.39E-04	8.1 % 12/148
Hepatic Cholestasis	8.37E-04	7.5 % 13/174
Neuregulin Signaling	8.56E-04	9.7 % 9/93

Top Upstream Regulators		
Upstream Regulator	p-value of overlap	Predicted Activation
U0126	6.04E-08	Inhibited
TNF	8.04E-08	Activated
BDNF	1.32E-07	
PDGF BB	6.14E-07	Activated
TGFB1	9.39E-07	Activated

Table 3.2. The most upregulated toxicological functions found in hiPSC-CM treated with STB-EX compared to those treated STB-EX+CT-1 neutralising antibody.

Top Tox Functions		
Assays: Clinical Chemistry and Hematology		
Name	p-value	#Molecules
Increased Levels of Creatinine	2.19E-02 - 2.19E-02	5
Decreased Levels of Potassium	4.90E-02 - 4.90E-02	3
Increased Levels of Albumin	2.97E-01 - 5.27E-02	3
Increased Levels of Bilirubin	1.16E-01 - 5.27E-02	2
Increased Levels of Blood Urea Nitrogen	1.16E-01 - 1.16E-01	2
Cardiotoxicity		
Name	p-value	#Molecules
Heart Failure	4.92E-01 - 6.75E-03	13
Cardiac Damage	3.52E-01 - 7.44E-03	7
Cardiac Degeneration	5.27E-02 - 9.95E-03	2
Cardiac Dysfunction	4.42E-02 - 1.96E-02	10
Cardiac Enlargement	1.00E00 - 1.96E-02	17
Hepatotoxicity		
Name	p-value	#Molecules
Liver Hyperplasia/Hyperproliferation	5.44E-01 - 1.31E-08	241
Liver Hyperbilirubinemia	5.27E-02 - 7.44E-05	3
Hepatocellular Carcinoma	5.44E-01 - 9.93E-04	42
Liver Inflammation/Hepatitis	3.86E-01 - 5.50E-03	23
Liver Cirrhosis	1.73E-01 - 9.39E-03	16
Nephrotoxicity		
Name	p-value	#Molecules
Nephrosis	4.18E-01 - 9.34E-04	8
Glomerular Injury	5.56E-01 - 3.24E-03	16
Renal Necrosis/Cell Death	5.56E-01 - 1.79E-02	23
Renal Damage	2.43E-01 - 2.59E-02	12
Kidney Failure	4.70E-01 - 2.67E-02	11

Tables 3.1 – 3.6 summarize the most affected signaling pathways identified by the IPA software based on the significant expression of genes in the STB-EX treatment group. Of the upregulated genes, the top canonical pathways included genes involved in remodeling of epithelial adherence junctions, hepatic fibrosis, epithelial adherence junction signaling, hepatic cholestasis and neuregulin signaling (Table 3.1). IPA could determine the cardiac specific diseases or toxicological pathways (Table 3.2) from the significantly changed expression levels of groups of genes: 17 molecules were found to be involved in cardiac enlargement, 13 in heart failure, 10 in cardiac dysfunction, 7 in cardiac damage and 2 in cardiac degeneration. Some of the signaling pathways were also related to biological functions and diseases (Table 3.3)

such as induction of cancer and reproductive system disease but also gastrointestinal disease, haematological disease, and organismal injury and abnormalities. In terms of molecules involved in physiological system development and function, most were involved in organism development, followed by tissue development, nervous system development and function, organism survival and cardiovascular system development and function.

Table 3.3. The most upregulated biological functions found in hiPSC-CM treated with STB-EX compared to those treated STB-EX+CT-1 neutralising antibody.

Top Diseases and Bio Functions

Diseases and Disorders

Name	p-value	#Molecules
Cancer	7.13E-04 - 2.97E-26	557
Organismal Injury and Abnormalities	7.13E-04 - 2.97E-26	562
Reproductive System Disease	3.94E-04 - 6.53E-18	301
Gastrointestinal Disease	7.13E-04 - 8.63E-18	484
Hematological Disease	7.13E-04 - 1.31E-13	177

Molecular and Cellular Functions

Name	p-value	#Molecules
Cellular Assembly and Organization	6.28E-04 - 2.74E-14	156
Cellular Function and Maintenance	6.34E-04 - 2.74E-14	139
Cell Morphology	7.13E-04 - 9.81E-13	187
Post-Translational Modification	7.13E-04 - 1.50E-08	64
Cellular Development	6.99E-04 - 5.76E-08	112

Physiological System Development and Function

Name	p-value	#Molecules
Nervous System Development and Function	7.13E-04 - 5.76E-08	124
Organismal Development	7.13E-04 - 5.76E-08	170
Tissue Development	6.21E-04 - 5.76E-08	140
Organismal Survival	2.13E-06 - 1.66E-06	144
Cardiovascular System Development and Function	7.13E-04 - 1.74E-05	59

Of the downregulated genes, the top canonical pathways included genes involved in autophagy, glycolysis 1, and HIPPO signaling amongst others (Table 3.4). In contrast to upregulated genes, fewer molecules were found to be involved in toxicological pathways (Table 3.5). However, from the significantly changed expression levels of groups of genes, 6 were found to be

involved in cardiac enlargement, 3 in cardiac dysfunction and 3 in cardiac inflammation. The signaling pathways related to biological functions and diseases (Table 3.6) included organismal injury and abnormalities, cardiovascular disease, neurological disease and connective tissue disorders. Finally, 36 molecules involved organismal survival and 26 involved in cardiovascular development and function were found to be downregulated.

Table 3.4. The most downregulated canonical pathways found in hiPSC-CM treated with STB-EX compared to those treated STB-EX+CT-1 neutralising antibody.

Top Canonical Pathways		
Name	p-value	Overlap
Role of IL-17A in Psoriasis	2.03E-03	15.4 % 2/13
autophagy	4.58E-03	4.7 % 3/64
HIPPO signaling	1.10E-02	3.4 % 3/88
Glycolysis I	2.03E-02	4.8 % 2/42
Gluconeogenesis I	2.51E-02	4.3 % 2/47

Top Upstream Regulators		
Upstream Regulator	p-value of overlap	Predicted Activation
MYC	2.50E-08	
hydroxyl radical	8.79E-05	
D-glucose	1.45E-04	
butyric acid	2.21E-04	Inhibited
beta-estradiol	3.35E-04	Inhibited

Next, we compared selected genes that were upregulated and downregulated in all the different conditions. Figure 3.5 shows the heatmap of the top 100 upregulated (red) and 100 downregulated (green) which demonstrates a distinction between the various groups.

We were also interested to determine which of the genes was directly related to CT-1 and which of the genes might be altered by other potential proteins/miRNAs deployed on vesicles. To achieve this, we selected genes that were changed in the samples treated with STB-EX (compared to the

STBEX/NEUTR), and compared these to the genes that were changed in response to treatment with recombinant CT-1 (versus control). Figure 3.6-A shows the genes and their subcellular location, that were most upregulated in both STB-EX and recombinant CT-1. Using IPA, we then connected these genes to look for particular hubs or networks. Figure 3.6-B shows that *myc* appears to be a hub for most of the networks. However, when we introduced and networked CT-1 (Figure 3.8-A), we noticed that STAT 3 became apparent and linked to a number of key genes, including *myc* (Figure 3.7). Furthermore, we wondered whether ERK was involved in the pathways. However, when ERK was added, only two networks were created, suggesting that ERK was not a major contributor to the network and that STAT 3 is the major driver of CT-1 mediated gene expression in this group (Figure 3.8).

Table 3.5. The most downregulated toxicological functions found in hiPSC-CM treated with STB-EX compared to those treated STB-EX+CT-1 neutralising antibody.

Top Tox Functions

Assays: Clinical Chemistry and Hematology

Name	p-value	#Molecules
Decreased Levels of Albumin	7.55E-02 - 5.22E-03	2
Increased Levels of Creatinine	8.03E-02 - 8.03E-02	1
Increased Levels of LDH	1.80E-01 - 1.80E-01	1
Increased Levels of Hematocrit	3.96E-01 - 3.96E-01	1
Increased Levels of Alkaline Phosphatase	4.20E-01 - 4.20E-01	1

Cardiotoxicity

Name	p-value	#Molecules
Cardiac Enlargement	5.80E-01 - 3.61E-03	6
Cardiac Dysfunction	1.72E-01 - 5.22E-03	3
Pulmonary Hypertension	3.69E-02 - 5.22E-03	2
Cardiac Inflammation	2.51E-02 - 1.56E-02	3
Congenital Heart Anomaly	2.26E-01 - 3.60E-02	1

Hepatotoxicity

Name	p-value	#Molecules
Liver Inflammation/Hepatitis	4.61E-01 - 1.04E-02	3
Liver Cirrhosis	4.38E-01 - 1.12E-02	6
Liver Damage	3.32E-01 - 1.14E-02	5
Liver Necrosis/Cell Death	2.36E-01 - 2.07E-02	2
Hepatocellular Carcinoma	1.41E-01 - 2.67E-02	10

Nephrotoxicity

Name	p-value	#Molecules
Renal Necrosis/Cell Death	1.18E-01 - 1.33E-03	10
Nephrosis	1.18E-01 - 5.22E-03	2
Renal Inflammation	6.03E-01 - 5.22E-03	3
Renal Nephritis	6.03E-01 - 5.22E-03	3
Glomerular Injury	1.80E-01 - 1.00E-02	3

Table 3.6. The most upregulated biological functions found in hiPSC-CM treated with STB-EX compared to those treated STB-EX+CT-1 neutralising antibody.

Top Diseases and Bio Functions

Diseases and Disorders

Name	p-value	#Molecules
Neurological Disease	1.14E-02 - 1.68E-05	45
Cardiovascular Disease	1.04E-02 - 2.95E-05	18
Ophthalmic Disease	5.32E-03 - 1.23E-04	16
Organismal Injury and Abnormalities	1.14E-02 - 1.23E-04	111
Connective Tissue Disorders	1.05E-02 - 2.41E-04	24

Molecular and Cellular Functions

Name	p-value	#Molecules
Cellular Assembly and Organization	1.07E-02 - 5.64E-06	37
Cell Death and Survival	1.11E-02 - 1.58E-05	46
Cellular Function and Maintenance	1.04E-02 - 1.82E-05	49
Cell-To-Cell Signaling and Interaction	1.07E-02 - 2.70E-05	27
Cellular Movement	1.11E-02 - 2.70E-05	32

Physiological System Development and Function

Name	p-value	#Molecules
Hematological System Development and Function	1.07E-02 - 2.70E-05	17
Immune Cell Trafficking	1.11E-02 - 2.70E-05	16
Organismal Functions	5.83E-03 - 2.70E-05	8
Cardiovascular System Development and Function	1.04E-02 - 4.08E-05	26
Organismal Survival	4.40E-04 - 1.13E-04	36

We then analysed genes that were downregulated in the samples treated with STB-EX (compared to the STBEX/NEUTR), and compared these to the genes that were changed in response to treatment with recombinant CT-1 (versus control). Figure 3.9-A shows fewer genes and their subcellular location. We then networked these genes and found caveolin 1 (Cav -1) to be a major hub (Figure 3.8-B). When CT-1 was introduced and networked, we found that STAT 3 became apparent once again and linked with several key genes including Cav-1, suggesting that STAT 3 drove most the Cav-1 changes. When ERK was added to the equation, no links with other genes were created.

This data suggests that most of the genes changes that are CT-1 dependent are largely driven by STAT 3.

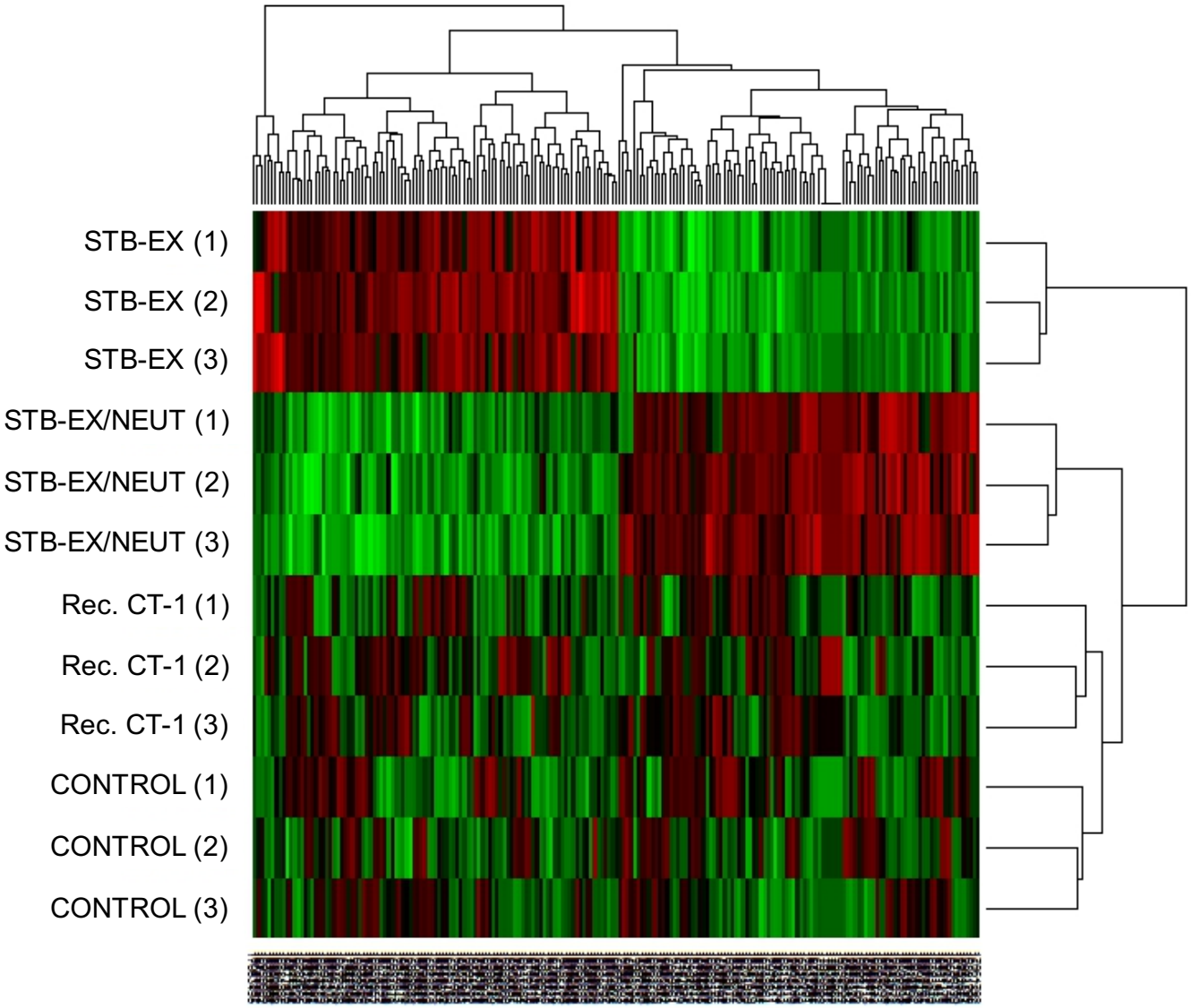


Figure 3.5. Heatmap representing the distribution of 200 significantly differentially expressed genes in hiPSC-CM (top 100 upregulated and top 100 downregulated).

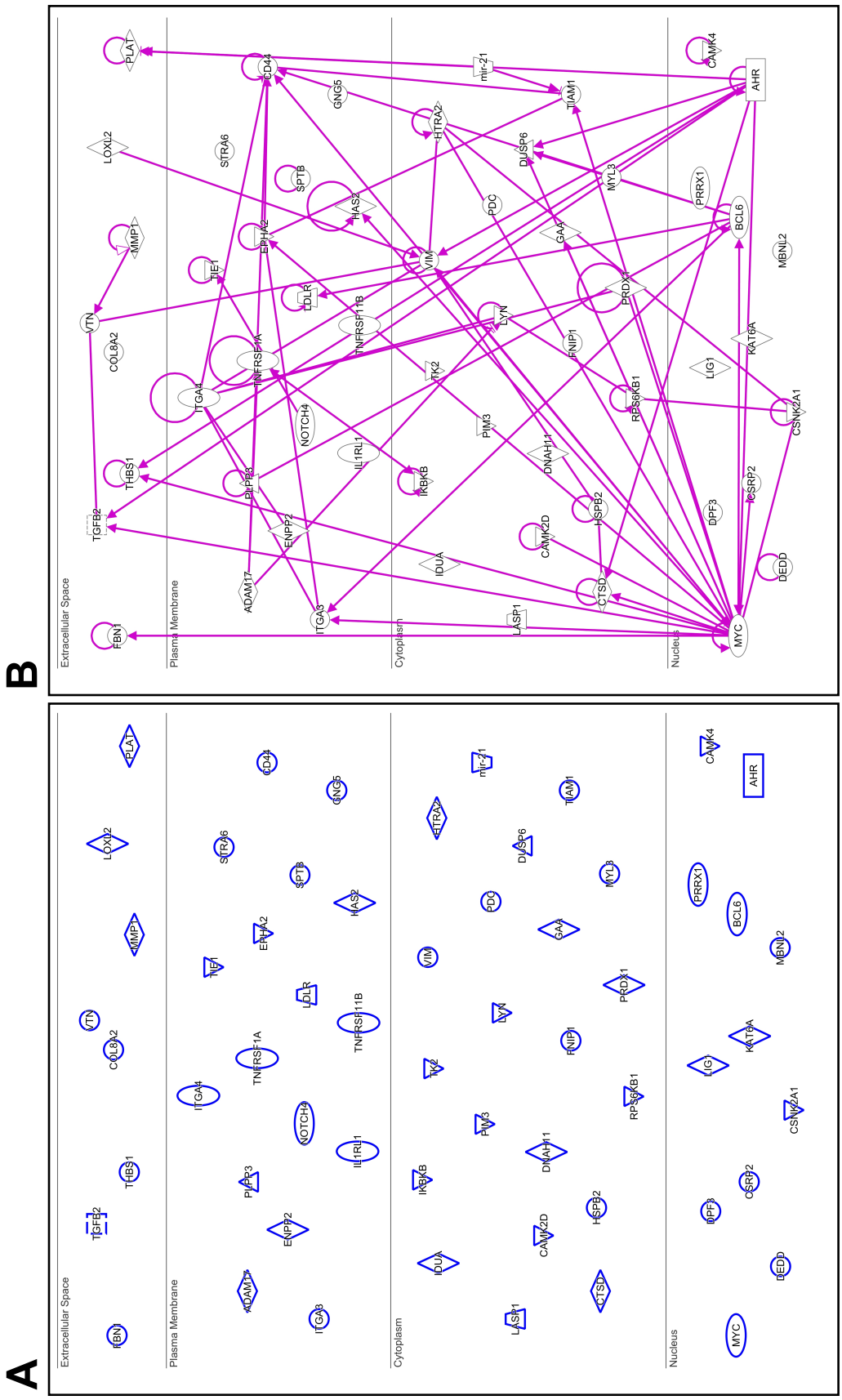


Figure 3.6. Networking of upregulated genes using Ingenuity pathway analyses (IPA). A) Upregulated genes in response to treatment of hiPSC-CM with STB-EX. **B)** Networking upregulated genes showing *myc* as a hub.

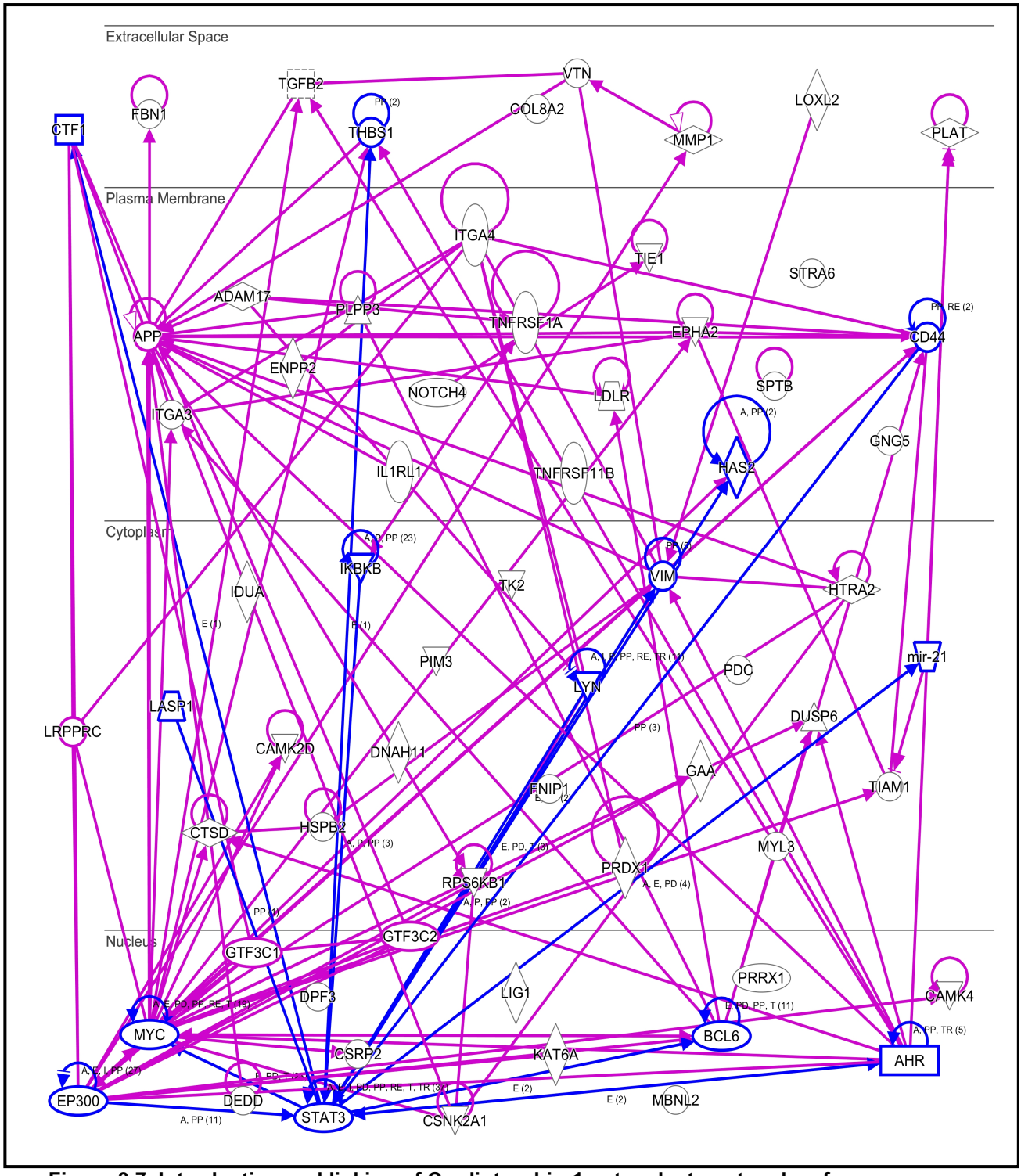


Figure 3.7. Introduction and linking of Cardiotrophin-1 networks to networks of upregulated genes using IPA.

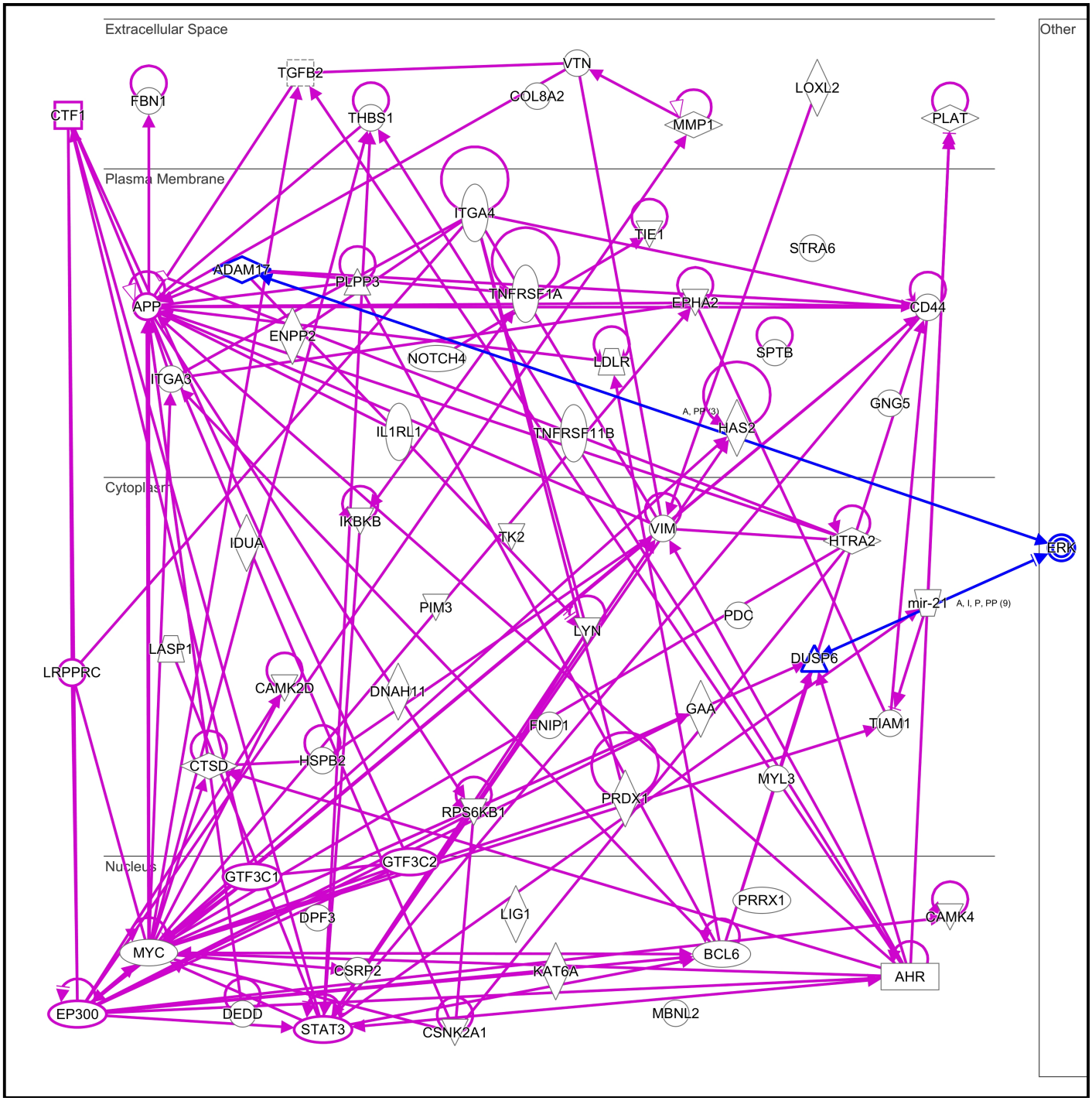


Figure 3.8. Introduction and linking of ERK to Cardiotrophin-1 networks and networks of upregulated genes using IPA.

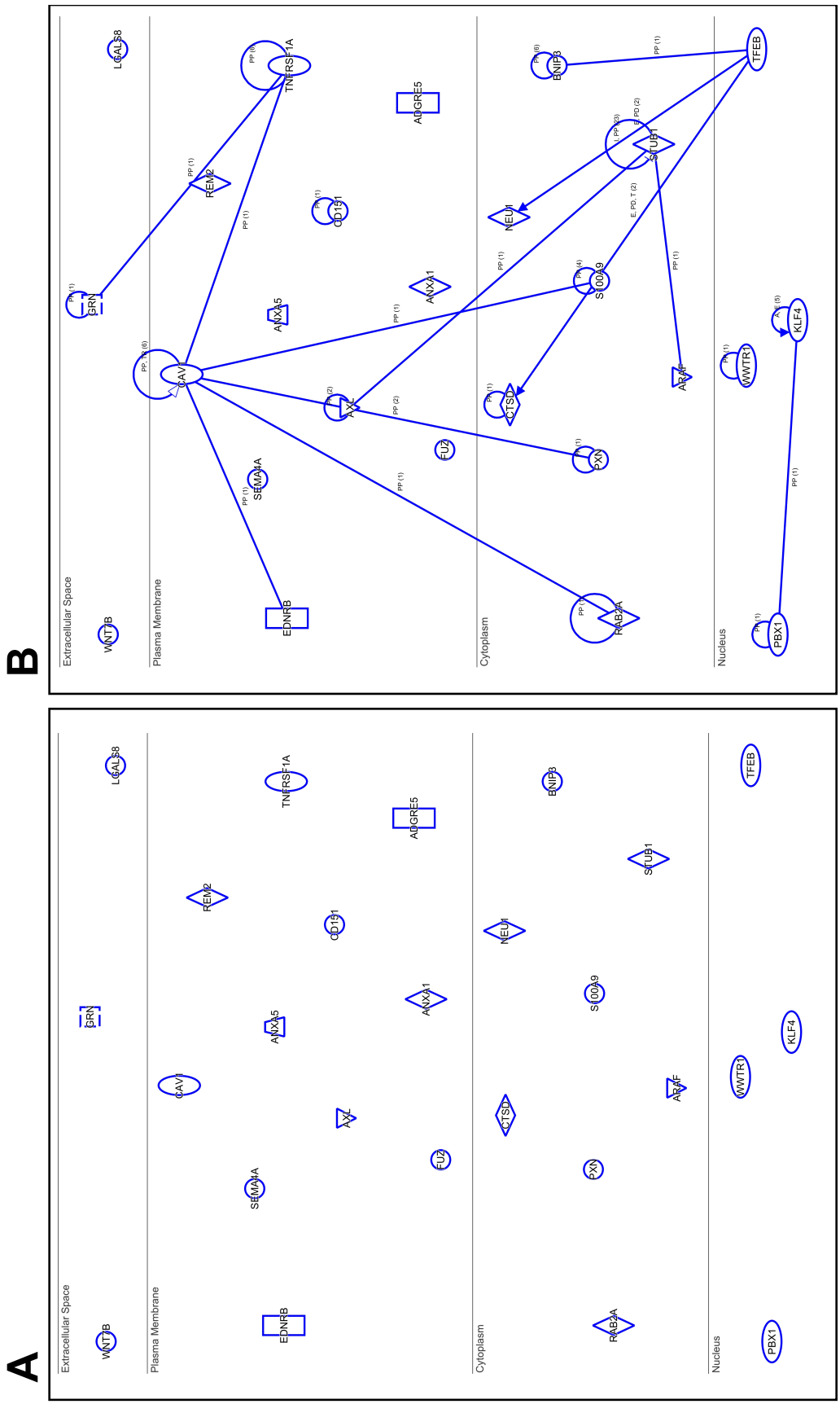


Figure 3.9. Networking of downregulated genes in Ingenuity Pathway Analyses (IPA). A) Downregulated genes in response to treatment of hiPSC-CM with STB-EX. **B)** Networking downregulated regulated genes showing Caveolin -1 as a hub.

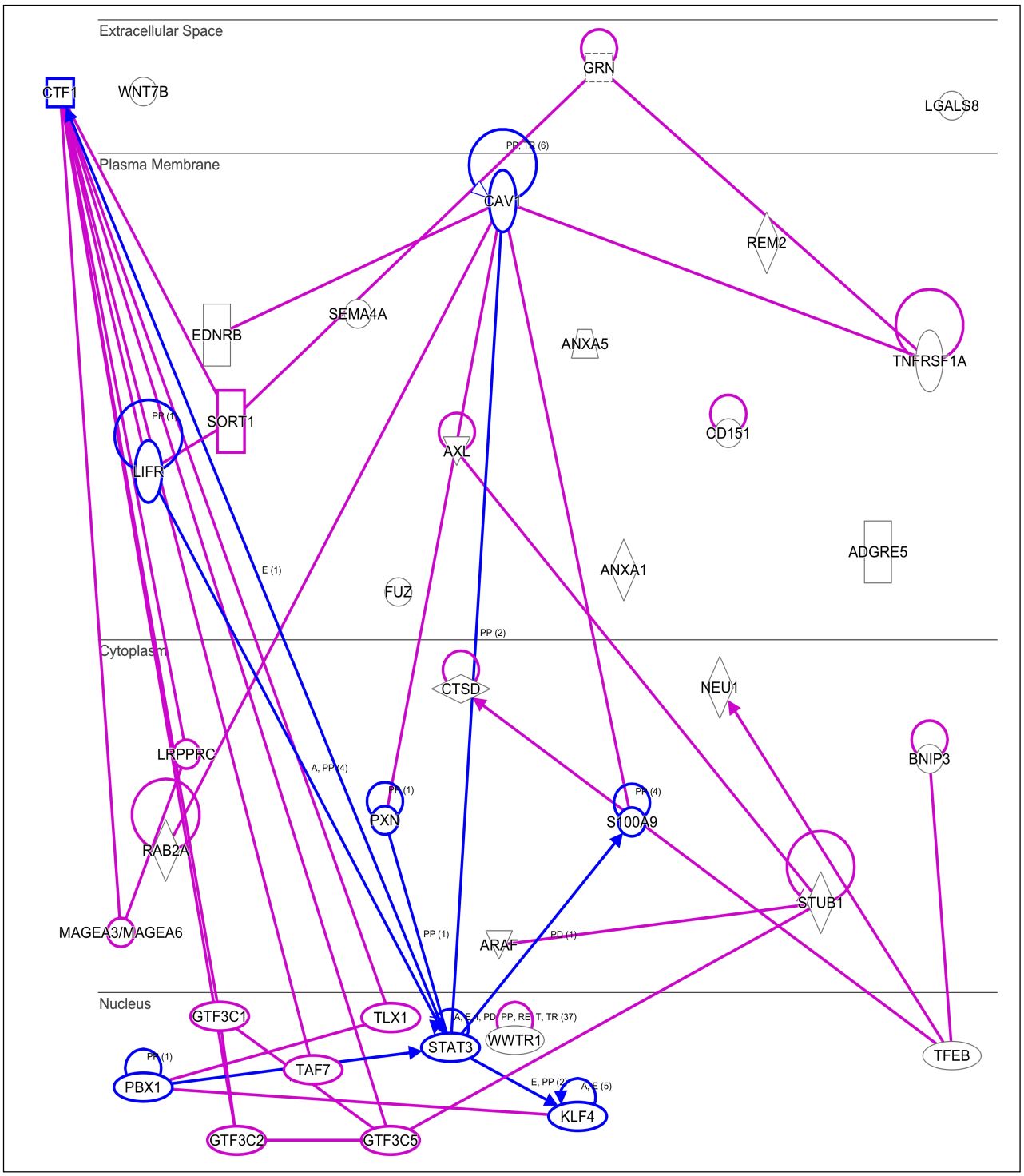


Figure 3.10. Introduction and linking of Cardiotrophin-1 networks to networks of downregulated genes using IPA.

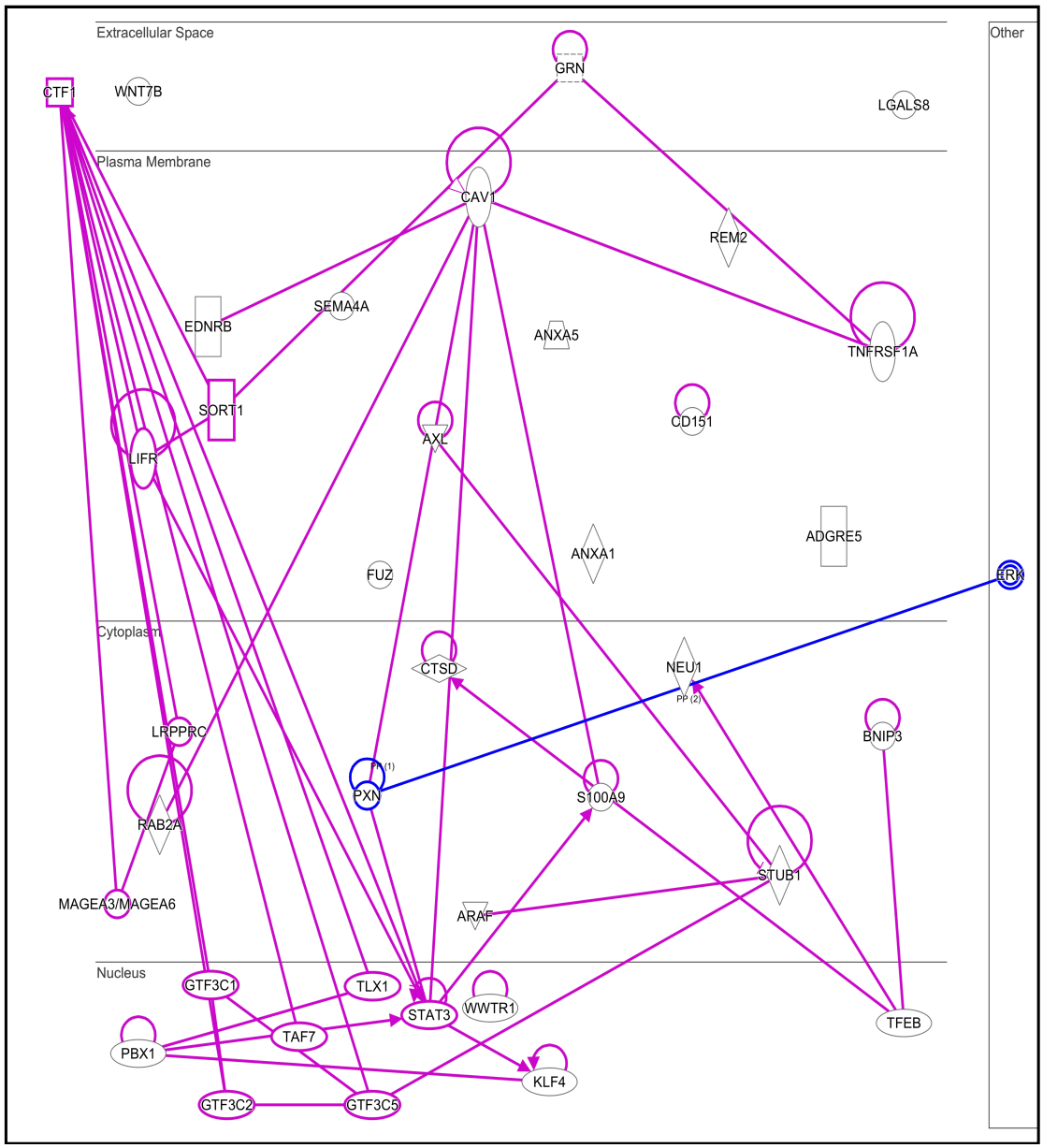


Figure 3.11. Introduction and linking of ERK to Cardiotrophin-1 networks and networks of downregulated genes using IPA.

3.3.4. Gene validation by RT-qPCR

To validate the microarray and the gene changes described above, we selected a few genes previously shown to be involved in cardiac physiology and pathophysiology. These included 3 upregulated genes (endothelin 1, thrombospondin-1, and ADAM17) and 1 downregulated gene (caveolin-1) in the microarray analysis.

Our data shows that, relative to untreated cardiomyocytes, STB-EX resulted in a 3.5 -fold increase in the expression of thrombospondin-1 (Figure 3.12-A). Recombinant CT-1 also resulted in a 4-fold upregulation in thrombospondin-1 gene expression. Furthermore, the transcription of thrombospondin-1 could be attenuated by pre-treating STB-EX with a CT-1 neutralising antibody, thus ascribing thrombospondin-1 gene expression to STB-EX-bound CT-1. These findings mirror the results in our microarray analysis.

We also noticed that when cardiomyocytes were treated with STB-EX, there was 3-fold induction of endothelin 1 gene expression, which could be attenuated by the addition of a CT-1 neutralising antibody (Figure 3.12-B). However, we noted that recombinant CT-1 did not change the expression of endothelin 1 relative to control. These data suggest, that perhaps endothelin 1 gene expression may be mediated by other cargo on CT-1 positive vesicles, an effect which is abrogated by the addition of a CT-1 neutralising antibody thus preventing vesicle uptake.

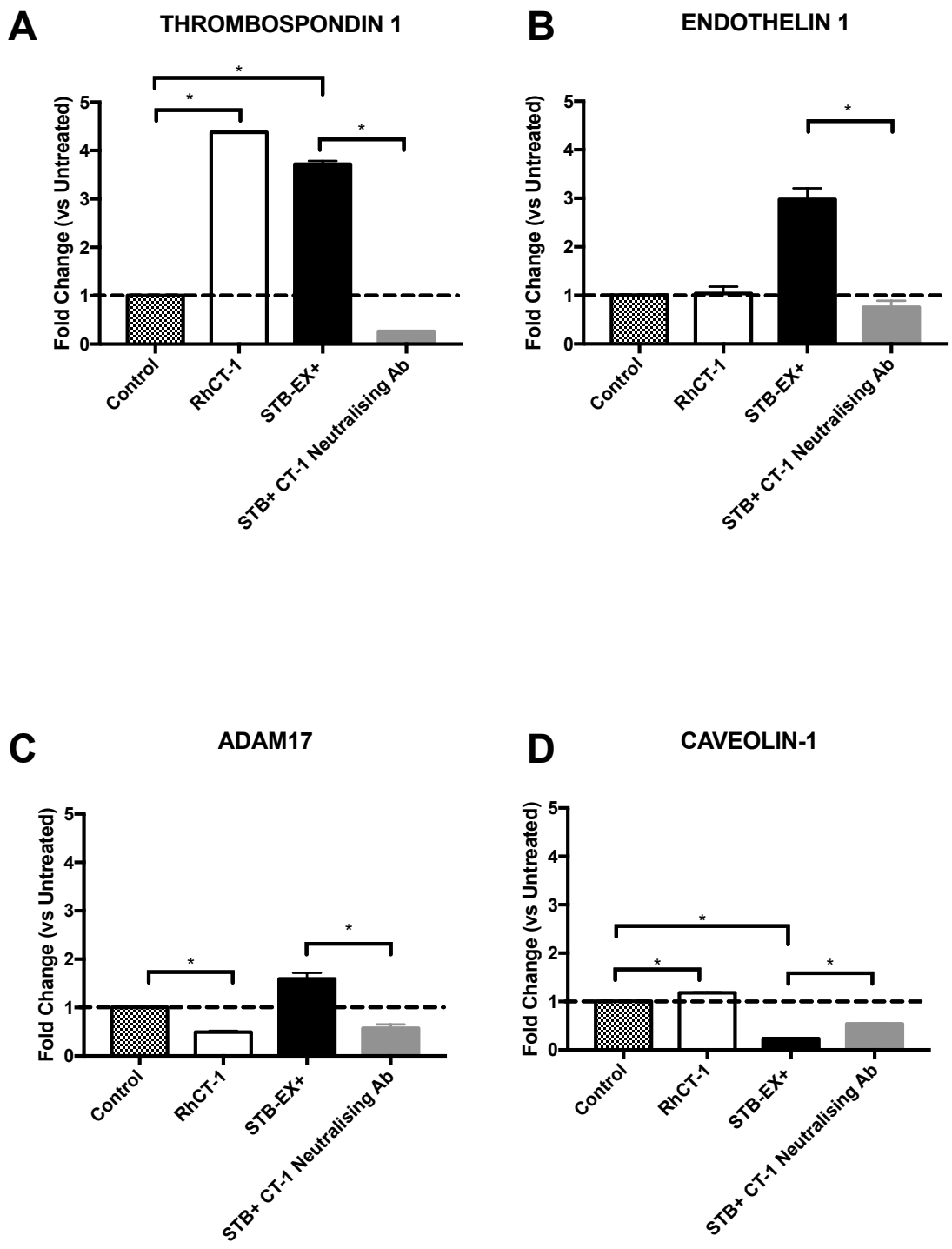


Figure 3.12. Figure 3.12. RT-qPCR validated gene changes caused by treatment of hiPSC-CM with vehicle, recombinant CT-1, STB-EX, and STB-EX pre-treated with a CT-1 neutralising antibody. Data are from simple t-test and are expressed as fold changes of genes. * $P < 0.05$ vs untreated; ** $P < 0.01$ vs untreated.

When investigating the gene expression of ADAM17, another gene that was found to be upregulated in the microarray analysis, we noticed that the addition

of recombinant CT-1 and STB-EX (with and without CT-1 neutralisation) to cardiomyocytes resulted in different effects (Figure 3.12-C). First, we noticed that recombinant CT-1 downregulated ADAM17 gene expression. Secondly, STB-EX did not result in a change in expression of ADAM17 relative to control. However, when STB-EX pretreated with a CT-1 neutralising antibody were added to cardiomyocytes, there was a downregulation of ADAM17. These data reflect that ADAM17 gene expression is in fact not CT-1 dependent.

We also investigated the gene expression of Caveolin-1. Our data shows in contrast to the microarray data, recombinant CT-1 resulted in a marginal increase in the gene expression of Caveolin-1 (Figure 3.12-D). What was consistent with our microarray findings however, was that STB-EX caused a downregulation of Caveolin-1 gene expression which could be partially inhibited by the addition of a CT-1 neutralising antibody.

3.4. DISCUSSION

This Chapter investigated the effects of STB-EX generated from ex vivo perfusion of the human placenta, on human induced pluripotent stem cell-derived cardiomyocytes (hiPSC-CM), by studying gene changes in these cells in response to treatment with CT-1 positive STB-EX or STB-EX pre-treated with a neutralising antibody to CT-1. We show for the first time that exosomes, derived from the placenta, result in differential expression of genes associated with many physiological and pathophysiological processes including cardiovascular pathophysiology.

In our study, we treated hiPSC-CM with Cardiotrophin 1 (CT-1) positive STB-EX, recombinant CT-1 STB-EX pre-treated with a CT-1 neutralising antibody as well as recombinant CT-1 and controls. We then isolated the RNA and conducted a microarray analysis to determine genes that were altered by these treatment conditions. However, we were particularly interested in genes that were altered by CT-1 positive vesicles. Our analysis yielded results that show that CT-1 positive STB-EX alter genes involved in different diseases and physiological states including cardiac development, cardiac failure and cardiac enlargement. Furthermore, we found that most of the CT-1 dependent genes, upregulated and downregulated were largely driven by STAT 3.

According to our IPA analysis, STB-EX appeared to have both detrimental and beneficial effects. We selected Thrombospondin-1-1, Endothelin 1, ADAM 17 and Caveolin 1 for our validation.

The thrombospondin-1 gene encodes the protein thrombospondin (TSP-1), a calcium-binding protein that regulates cellular adhesion and migration; cytoskeletal organisation; and cell proliferation and apoptosis [274, 275]. TSP-1 belongs to the thrombospondin family, a group of matricellular proteins, which have been shown to strongly increase during cardiac stress or injury and play a crucial role in cardiac remodeling [276]. Furthermore, a number of studies have implicated TSP-1 in the pathogenesis of a range of cardiovascular diseases [276-278]. With a particular focus on the role of TSP-1 in myocardial function, Xia et al. induced pressure overload in mice by transverse aortic constriction and showed that TSP-1 is markedly upregulated in the myocardial interstitial space [279]. Moreover, they showed that TSP-1 gene disruption causes adverse cardiac remodeling in the pressure-overloaded heart, a process which seems to be mediated by transforming growth factor beta (TGF-β) signaling [279]. In humans, studies assessing the association of human TSP-1 polymorphisms and cardiovascular disease showed a biological link between TSP-1 variation and early onset coronary artery disease [280-282].

Endothelin-1 is a potent inducer of vasoconstriction [283] and growth factor for a variety of cells, including cardiomyocytes [284-288]. Additionally, endothelin-1 is produced by endothelial and epithelial cells, macrophages, fibroblasts, and many other types of cells, including cardiac myocytes [22[136, 289-291]. Moreover, endothelin-1 has been shown to have cardiovascular effects including positive cardiac inotropic effects in animals and humans [292-296]. However, MacCarthy et al. showed that the positive cardiac inotropic effects of

endothelin-1 are only effected in patients with healthy hearts and that endothelin-1 may in fact cause negative inotropic effects in the failing heart [297]. In cultured cells, it has been shown that endothelin-1 mRNA is upregulated by inflammatory factors such as TGF-β, tumor necrosis factor alpha (TNF-α), interleukins, insulin, and angiotensin II, and downregulated by nitric oxide, prostacyclin, and shear stress [298-302]. Furthermore, Yamazaki et al. also reported increased endothelin-1 mRNA levels after mechanical stretching of rat neonatal cardiomyocytes [303].

Activation of a disintegrin and metalloproteinase-17 (ADAM17) is also termed TNF-α converting enzyme (TACE), based on its ability to release pro-TNF-α and TNF receptors from cell surface [304, 305]. TNF-α activity independently influences cell death and aggravates left ventricular remodeling and myocardial dysfunction [306-308]. Satoh et al. have shown that myocardial ADAM17 and TNF-α expression in both mRNA and protein levels are increased in humans with dilated cardiomyopathy [309]. Simultaneously, TNF-α is also involved in cardioprotective processes in ischemic conditioning [310]. Ischemic conditioning is a phenomenon in which several brief episodes of ischemia/reperfusion precede a prolonged period of ischemia and then followed by reperfusion, resulting in a markedly enhanced ability of the heart to withstand the resulting insult, including arrhythmias, contractile dysfunction and myocardial infarction [311]. It is thought that TNF-α activates ADAM17 through epidermal growth factor receptor (EGFR) and through the non-receptor tyrosine kinase, Src. [312-314]. Furthermore, Shi et al. demonstrated

that ADAM17 possibly regulates cardiomyocyte proliferation during the late fetal stage of cardiac development via an EGFR-mediated pathway [315].

Caveolin-1 is the first of a member of a gene family consisting of three structurally related proteins (Caveolin-2 and 3) that transcribes Cav-1, a structural protein of caveolae [316-319]. Caveolae, or “little caves”, are cholesterol and sphingolipid-enriched invaginations of the plasma membrane [320]. Caveolins function as chaperones and scaffolds for signaling molecules in caveolae by providing temporal and spatial regulation of signal transduction [321]. Cav-1 has been reported to be co-expressed with caveolin-2 in a variety of cells and tissue types but are abundantly expressed in fibroblasts and endothelial cells [316, 322-324]. Recently, however, Cho et al. reported the expression of Cav-1 in mouse ventricular cardiomyocytes [325]. In the cardiovascular endothelium, Cav-1 is a key regulator of nitric oxide (NO) by endothelial nitric oxide synthase (eNOS), calcium, and vascular growth and remodeling [326]. Furthermore, Frank et al. reported that genetic ablation of caveolin-1 confers protection against atherosclerosis [327]. With reference to the role of Cav-1 on myocardial function, two independent studies reported that Cav-1 null mice develop dilated cardiomyopathy and pulmonary hypertension and cardiac hypertrophy [328, 329]. The findings that mice lack Cav-1 develop cardiac hypertrophy were also corroborated by Augustus et al. [330]. Furthermore, Cohen et al. demonstrated that Cav-1-deficient mice that develop cardiac hypertrophy also show hyperactivation of the p42/44 MAP kinase cascade *in vivo* and in isolated cardiac fibroblasts in culture [329]. Thus, Cav-1 expression in the heart is thought to negatively regulate the

p42/44 MAP kinase cascade, and the loss of caveolin-1 leads to the development of cardiac myocyte hypertrophy.

In our study, STB-EX resulted in induction of thrombospondin 1 mRNA, an effect which was attenuated by the addition of a CT-1 neutralising antibody. Upregulation of thrombospondin-1 by recombinant CT-1 supports the finding that STB-EX-bound CT-1 induces the gene expression of thrombospondin 1 in cardiomyocytes. This is the first study to demonstrate Thrombospondin-1 gene induction by STB-EX-bound CT-1 in human induced pluripotent stem cell-derived cardiomyocytes.

Furthermore, we found that STB-EX upregulated the expression of endothelin 1 in cardiomyocytes, and this effect was attenuated by the addition of a CT-1 neutralising antibody, a finding that was consistent with the microarray analysis. However, endothelin 1 gene expression was not affected by treatment of cardiomyocytes with recombinant CT-1. We also noted that, ADAM17 gene expression, though not significantly altered by treatment of cardiomyocytes with STB-EX (relative to control), adding a CT-1 neutralising antibody resulted in the downregulation of this gene. However, this change does not seem to be mediated by CT-1 because adding recombinant CT-1 to cardiomyocytes resulted in the downregulation of CT-1. Several studies have reported that gp130 and LIF-R can be endocytosed [331-336]. Furthermore, in Chapter 2 of this thesis, we showed that cardiomyocytes internalize STB-EX after 1 hour of treatment. Therefore, it is possible that endothelin 1 gene expression may be mediated by other cargo on CT-1 positive vesicles rather

the CT-1 itself, an effect which is abrogated by the addition of CT-1 neutralising antibody and thus preventing vesicle uptake. Finally, consistent with the microarray data, adding STB-EX to cardiomyocytes resulted in the downregulation of Cav-1. This effect could be blocked with the addition of a CT-1 neutralising antibody. However, when recombinant CT-1 was used to treat the cardiomyocytes, there was upregulation of Cav-1. Clearly, there is other cargo deployed on STB-EX that overwhelm the ability of STB-EX-bound CT-1 to cause upregulation of Cav-1 (as in the case of recombinant CT-1).

In contrast to our IPA analysis, our RT-qPCR data highlights the complexity of using programs designed to assess the effects of a single molecule when, in fact, a vesicle carries more complex moieties. RT-qPCR data confirmed that gene changes seen in the treatment with Cardiotrophin-1 positive vesicles mirrored those seen in the array. However, contrasting the RT-qPCR vesicle derived data with RT-qPCR recombinant CT-1 data showed no variance with the vesicle data, precisely echoing the microarray findings, but not being replicated by the recombinant CT-1. It is likely therefore, that these gene changes are partly being mediated by CT-1 (in the case of thrombospondin 1) and partly by the cargo that the vesicles are carrying (Endothelin 1, Cav-1 and ADAM17). Further work, beyond the scope of this thesis, where the other molecular “passengers” of CT-1 positive vesicles might be identified (either by proteomics or next generation sequencing) might shed light on the moieties responsible for these changes. Thus, in this chapter whilst we studied the effects of CT-1 positive vesicles, our results clearly show that gene changes induced in hiPSC-CM could not be due to CT-1 alone.

3.5. SUMMARY

Previously considered to be “debris”, extracellular vesicles are increasingly becoming understood as mediators of intercellular communication. In this chapter, we tested the hypothesis that STB-EX-bound CT-1 can induce gene changes in human induced pluripotent stem cell derived cardiomyocytes (hiPSC-CM). We found that indeed, STB-EX induce a host of gene changes involved cardiovascular and other pathophysiological states. Moreover, we demonstrated by RT-qPCR a CT-1 dependent upregulation of Thrombospondin-1 gene expression, and that the upregulation of Endothelin-1, and ADAM17 as well as the downregulation of Caveolin-1 gene expression in hiPSC-CM. Taken together, these results reflect the complex nature of vesicular biology and that gene expression induced by extracellular vesicles cannot easily be mapped out using conventional gene networking platforms such as IPA.

CHAPTER 4

CHARACTERISATION OF THE EXPRESSION AND FUNCTION PLATELET-DERIVED EXTRACELLULAR VESICLE BOUND CT-1 ON ENDOTHELIAL CELLS *IN VITRO*

4.1. INTRODUCTION

Whilst performing Western blots an unexpected finding was that platelet-derived extracellular vesicles (EV), initially used as negative controls, express cardiotrophin 1 (CT-1). Thus, in this thesis chapter we characterise the expression of CT-1 expression on platelets and platelet-derived EV and investigate its biological function *in vitro*.

The fundamental role of platelets in hemostasis was first identified by the Italian pathologist and pioneering medical researcher, Bizzozzero in 1882 [337]. However, recent evidence has shown that platelets also play an important role in a range of other processes, microbial adhesion, angiogenesis and tissue generation [338]. Furthermore, platelets are key players in mediating a diverse range of immune, inflammatory, and malignant diseases [339-347].

Human platelets are small anucleate cellular fragments derived from megakaryocytes [348]. Resting platelets are approximately 2–5 μm in diameter, 0.5 μm in thickness and ~6–10 femtolitres in mean cell volume and once released into the circulation, have an average lifespan of 10 days [349, 350]. In the resting state, platelets have a unique biconcave discoid shape cell, in part, due to their robust cytoskeletal structure encompassed by several loops of the microtubular coils (Figure 4.1). Additionally, they are rich in functional organelles such as endoplasmic reticulum, Golgi apparatus, mitochondria and mRNA, platelets are metabolically active cells and capable of synthesizing their own proteins.

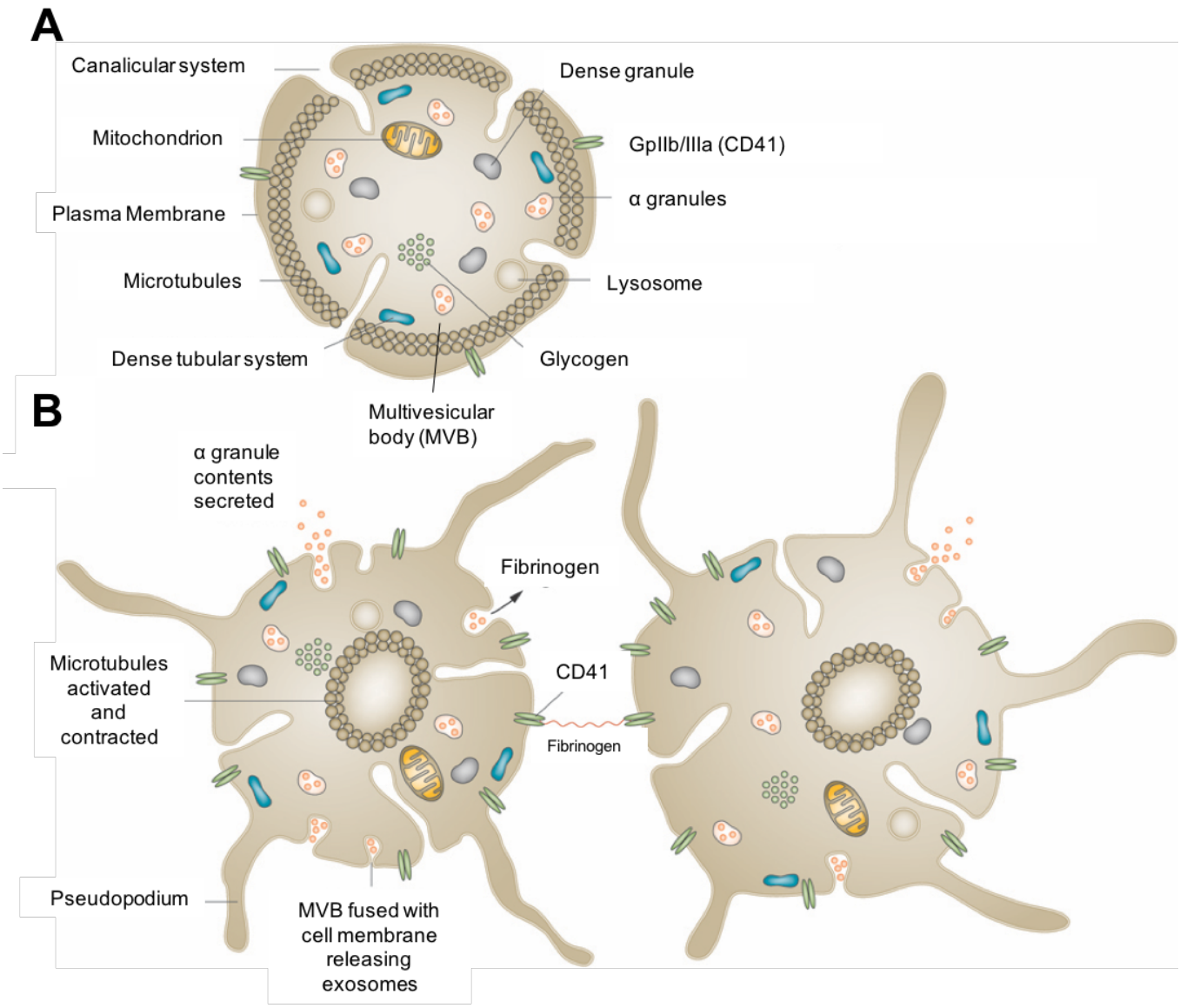


Figure 4.1. Schematic diagram of the platelet in a resting and activated state.
Adapted from Martin, J. F. et al. (2012)

Although the physiological and pathological stimuli that activate platelets both *in vivo* and *in vitro* are diverse, the platelet response to these stimuli usually follow the same pattern (Figure 4.1): platelets change their shape (the cytoskeletal rearrangement transforms the resting oblate spheroid to a more-stellate form with long pseudopodia), then they become sticky so that they aggregate and finally release α-granules, dense granules, lysosomes and

extracellular vesicles which contain pre-formed molecules (synthesized de novo and inherited from megakaryocytes) [351-353].

Like all other cell types, platelets release extracellular vesicles. Fifty years ago, Peter Wolf identified platelet-derived EV and called them “platelet dust”. Initially thought to be cell debris, decades of research have shown that platelet-derived EV participate in coagulation, cellular signaling, vascular injury, and homeostasis [354]. They serve as mediators of intercellular communication, directly affecting the biology of target cells or delivering bioactive molecules [355]. Additionally, their quantity has been shown to increase in many pathological conditions [221, 346, 356-361].

EV biogenesis, isolation and characterisation has already been discussed in Chapter 1 of this thesis. However, given that platelets are endowed with different types of granules, it is important to highlight some of the properties of these granules as they overlap with those of extracellular vesicles, more specifically, exosomes. Furthermore, most currently used techniques cannot completely obtain pure EV populations, and provide a mixture of exosomes, microvesicles, granules and apoptotic bodies [362].

Amongst the different type of granules, the α-granules are the most abundant. These are 200–500 nm in diameter and contain molecules involved in platelet adhesion, aggregation and coagulation [363]. Additionally, α-granules contain hundreds of distinct proteins, including substances with opposing physiological roles. Some examples of α-granule contents include fibrinogen, von Willebrand

factor (VWF), vitronectin, fibronectin, thrombospondin, factor V, factor VIII, and cell adhesion molecules like integrins GPIIb/IIIa (CD41) and P-selectin (CD62P), which is expressed on the platelet surface following platelet activation of platelets [364].

Dense granules (based on their dense appearance on electron microscopy), are approximately 150 nm in diameter and are less abundant than α-granules [365, 366]. Dense granules contain serotonin which mediates vascular tone and neutrophil recruitment at site of inflammation, calcium and magnesium which support signal transduction and nucleotides adenosine triphosphate (ATP) and adenosine diphosphate (ADP), which are believed to be involved in the modulation of inflammatory pathways by activating dendritic cells and providing a feedback mechanism that activates platelets [367, 368].

Lysomes are 200–250 nm in diameter and contain proteases like carboxylpeptidases, cathepsin D and E that contribute to the inflammatory potential of platelets and enzymes that remodel the extracellular matrix [367, 369, 370]. Lysosomes contain the lysosomal-associated membrane proteins (LAMP) 1, LAMP 2 and LAMP-3 (CD63) [371].

In Chapter 1, we discussed that exosomes are formed in structures called multivesicular bodies, using the machinery of the endocytic pathway, and express tetraspanins, particularly CD63, which is involved in exosome biogenesis. The multivesicular bodies then fuse with the plasma membrane and release the cargo of exosomes into the extracellular space. Heijnen et al. studied the biogenesis of α-granules and also identified multivesicular bodies and a subclass of α-granules as multivesicular compartments [372].

Furthermore, α-granules contained several proteins including CD62P and CD63 [372]. All these properties qualify α-granules as exosomes. In fact, in a later study, Heijnen et al. also reported that following platelet activation, exosomes are derived from exocytosis of multivesicular compartments and α-granules [373]. Therefore, in this thesis, α-granules will be included in the broader definition of platelet-derived extracellular vesicles.

The vesicle type that has been extensively studied are platelet microvesicles (PMV). For historical reasons, the term “microparticles” is the most commonly used to describe PMV [374]. Although the term platelet microvesicle will be used in this thesis, we also considered the more commonly used term microparticle while performing relevant literature searches. Microvesicles are larger than exosomes with a size range of 100 nm – 1 μm, and they are formed by direct budding of plasma membrane ultimately resulting in pinching of the plasma membrane bound vesicles with subsequent release into the extracellular space [88]. PMV are produced in response to many stimuli such as collagen, thrombin, the complement membrane attack complex C5b-9, liposaccharide and immune complexes [375, 376]. Furthermore, in response to platelet activation by agonists like thrombin, collagen or ADP, or by the calcium ionophore A-23187, an increase in intracellular calcium induces the activation of scramblase, a bidirectional phospholipid transporter, leading to rapid exposure of the negatively charged phospholipid phosphatidylserine and platelet-derived glycoprotein such as CD41 and activation markers such as CD62P at the platelet surface [84, 355, 377].

PMV formation is closely connected to the formation of surface phosphatidylserine (PS), an anionic phospholipid, found on platelets [83]. The outer leaflet of the platelet plasma membrane is enriched in phosphatidylcholine and sphingomyelin [84]. PS is normally located on the inner leaflet of the cellular membrane. Membrane asymmetry is actively regulated by a “flip-flop” mechanism which is mediated by phospholipid transporters [83]. Aminophospholipid translocases also called flippases and floppases ensure the inward “flip” and outward “flop” traffic of phospholipids at the membrane bilayer [83]. The exact molecular mechanisms implicated in PS exposure are not completely understood, but molecules such as the transmembrane proteins 16 (TMEM16) family and the proteasome have been described in PMV production [85-87]. Considering the pro-coagulatory role of PS, PMV are believed to serve as a mechanism by which a thrombus is propagated and sustained. However, a large proportion of circulating PMV are PS negative [378], thus, given the heterogeneity of PMV with regards to content and size distribution, membrane scrambling and PS may not be the only mechanism involved and thus, their role in pathophysiology cannot be limited to hemostasis and coagulation [379-382]. In fact, the involvement of PMV in inflammation, infection, immunity and malignant disease have been well described [347, 383-401].

With relevance to this thesis chapter, is the potential role that the pleiotropic cytokine, CT-1, found expressed on platelet-derived EV, plays in vascular pathophysiology. Platelets are small cells, and owing to their small size, under laminar flow conditions, they are pushed to the periphery forcing them in close contact with the vessel wall. This allows to them to respond efficiently and

effectively through the release of platelet-derived EV and other substances upon activation. Given the effect that platelets, platelet derived EV and CT-1 have been shown to have in vascular pathophysiology, we decided to further investigate and characterise the expression of CT-1 on platelet-derived EV and its endothelial cell function.

4.1.1. Aims

The aims of the work described in this chapter were to:

1) Characterise the expression of CT-1 on the human platelets by immunocytochemistry and Western blotting.
2) Isolate platelet-derived EV by differential ultracentrifugation and to characterise them by Western blotting and Nanoparticle Tracking Analysis (NTA).
3) Investigate the levels of CT-1 expression on CD41 positive EV by Western blotting and flow cytometry.
4) Investigate the signaling mechanisms potentially effected by PEV-bound CT-1 *in vitro* by measuring intracellular molecules associated with CT-1 in cultured endothelial cells and to attenuate these effects using pharmacological inhibitors.
5) Study the effects of CT-1 positive platelet-derived EV on endothelial cells with a focus on the potential cytoprotective effects of CT-1.

4.2. MATERIALS AND METHODS

4.2.1. Subject Information

For the isolation of platelets, red blood cells (RBC), platelet extracellular vesicles (EV) and RBC EV, venous blood was drawn from healthy non-pregnant volunteers who had given their informed consent. Approval for these studies was obtained from Oxfordshire Research Ethics Committee C (Reference Number: 07/H0606/148).

4.2.2. Platelet isolation and activation

Platelets were isolated as previously described by Cazenave et al. [402], with slight modification (Figure 4.2). Peripheral blood was drawn through a 21-gauge needle into a 4.5 ml 0.105M buffered sodium citrate vacutainer and processed immediately. To generate platelet rich plasma (PRP), blood was centrifuged at 200 x *g* for 2 minutes at room temperature (RT). The PRP was then centrifuged at 1000 x g for 20 minutes at RT to generate a platelet pellet which was subsequently resuspended in 10 ml of Tyrode buffer (pH 6.5) containing 0.25% w/v bovine serum albumin (BSA), 136.9mmol/l NaCl, 11.9mmol/l $NaHCO_3$, 5.6mmol/L glucose, 2.7mmol/l KCl, 1.0mmol/l, $MgCl_2H_2O$, 0.36mmol/L Na_2HPO_4 and 2mmol/L Ethylenediaminetetractacetic acid (EDTA) (all from Sigma). The platelet suspension was then washed by centrifugation at 1000 x *g* for 20 minutes at RT and the platelet pellet was resuspended in 0.5 ml Tyrode buffer (pH 7.4) containing 2mmol/L $CaCl_2$. The supernatant was discarded after each centrifugation step. Platelets were counted by flow cytometry using TruCount Beads (BD Biosciences, UK) following the manufacturer's instructions, before being used for further study.

For platelet activation, 200 µl aliquots containing 1 x 10^7 platelets were used. These were activated using 2.5µmol/L calcium ionophore A-23187 (Sigma, UK) and incubated at 37° C for 20 minutes. Calcium ionophore A-23187, which acts by increasing the intracellular calcium concentration of cells, is a potent inducer of platelet activation and a universal stimulus for EV formation irrespective of the cell type [362, 403, 404]. After 20 minutes, 5mmol/L EDTA (Sigma, UK) was added to each tube to stop the activation process and the platelets were pelleted by centrifugation at 1000 x *g* for 20 minutes at RT. The protein concentration was assessed using a Pierce BCA protein assay kit (Thermofisher Scientific, USA).

Platelet pellets were then studied by immunocytochemistry, flow cytometry and Western blotting, and the supernatant was further processed for the isolation of the platelet extracellular vesicles as described in section 4.2.4 below.

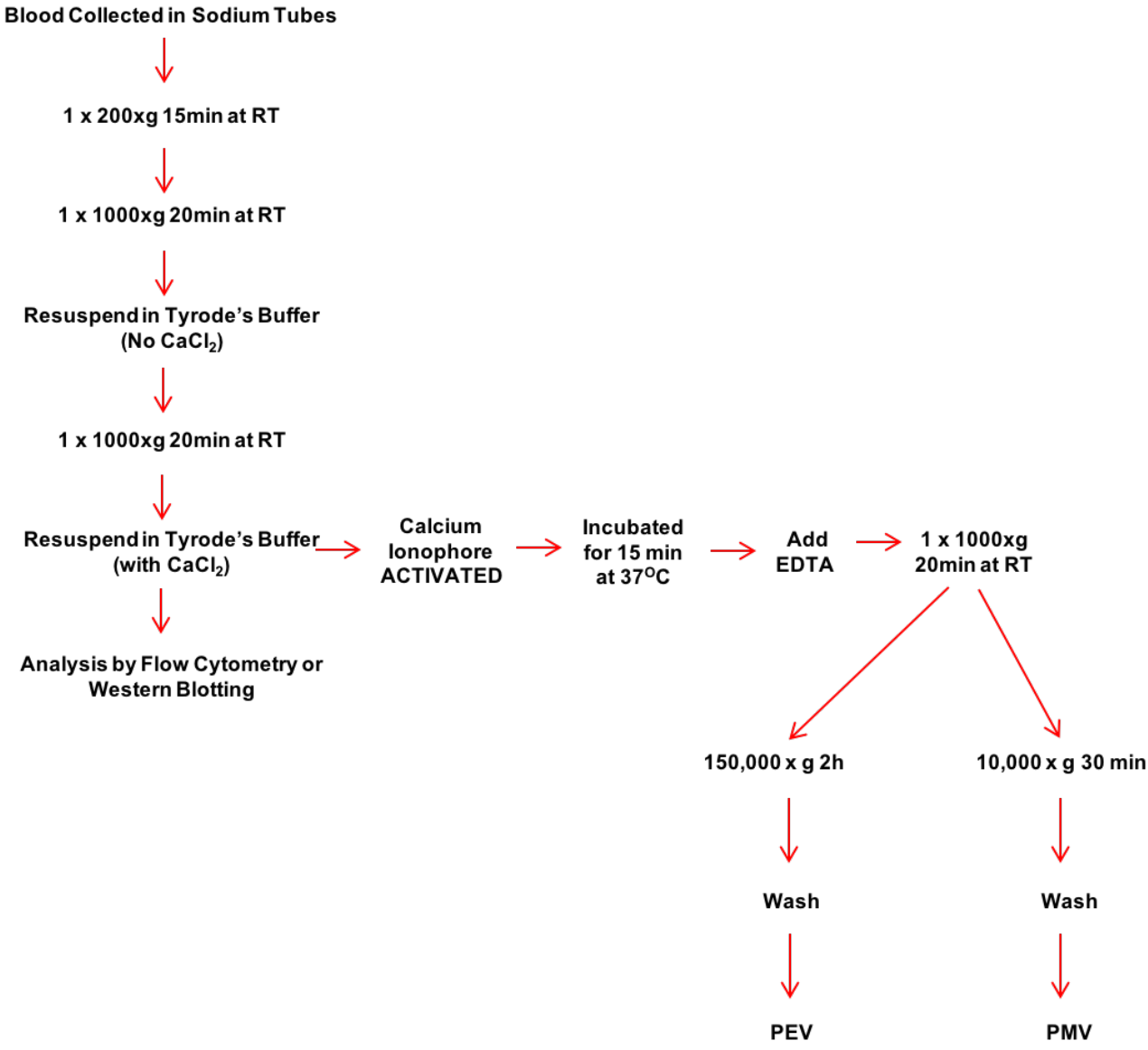


Figure 4.2. Schematic diagram of the sequential centrifugation protocol for the isolation and fractionation of platelet EV from peripheral blood plasma.

4.2.3. Immunocytochemistry

Freshly isolated non-stimulated and activated platelets were prepared from PRP as described in section 4.2.2. above and were diluted in PBS to give a concentration of 1 x 10^6 cells/ml. To layer the platelets onto Superfrost™ Plus cover slides (VWR, USA), 200 µl of the dilute cell suspension was loaded into a reusable Cytofunnel (Thermofisher Scientific, USA) that was pre-attached to a white disposable filter card (Thermofisher Scientific, USA) and held in place

by a Shandon Cytoclip (Thermofisher Scientific, USA) and centrifuged at 500 revolutions per minute (rpm) for 5 minutes at RT in a Shandon Cytospin® (Thermofisher Scientific, USA). Next, slides containing layered cells were left to dry for 5 minutes before being fixed and permeabilised with methanol. For staining, first, non- specific protein binding was blocked using 1% normal fetal calf serum (FCS) (Sigma, UK) for 1 hour at RT. Then, platelets were probed with a monoclonal mouse primary antibody (1:100) to CT-1 (Abcam, UK) in 1% FCS in 0.01% PBS-Tween (PBS-T) (Sigma, UK) and (1:500) polyclonal antibody to CD41 (Abcam, UK) in 1% FCS in 0.01% PBS-T (Sigma, UK) overnight at 4° C. Negative control sections were incubated overnight at 4° C in PBS containing 1% mouse serum and 1% rabbit serum, respectively. Following overnight incubation, slides were washed three times with 0.01% PBS-T and the samples were subsequently incubated for 1 hour at RT with a donkey anti-mouse Alexa647 (Life technologies, USA) and goat anti-rabbit Alexa488 secondary antibody (Life technologies, USA). After three washes with 0.01% PBS-T, slides were mounted in Ibidi mounting medium (Ibidi, Germany). Imaging was performed using a Zeiss LSM 780 inverted laser confocal microscope under the supervision of Dr Christoffer Lagerholm from the Weatherall Institute of Molecular Medicine under a X100 oil immersion objective lens. ImageJ version 2.0 (NIH) software was used to process and analyse collected images.

4.2.4. Isolation of Platelet extracellular vesicles

Platelet vesicles were derived as previously described by Aatonen et al. [362] and Abid et al. in 2003 [404], with slight modification (Figure 4.2).

Aatonen et al. found that following isolation of microvesicles by differential ultracentrifugation, a large EV population is lost during the filtration step of this process, decreasing the EV concentration of exosomes [362]. Furthermore, the size distribution profiles between the total EV (which omits the filtration step) and the exosomal fractions were similar, suggesting that the two populations either overlap in size, or that they cannot be separated by differential centrifugation [362].

Thus, to generate platelet microvesicles (PMV), one batch of the supernatant generated from platelet activation (described in section 4.2.2. above), was pooled and subjected to ultracentrifugation in a Beckman L80 ultracentrifuge and Sorvall TST28.39 swing out rotor at 10,000 x *g* for 30 minutes at 4° C. The supernatant was removed for further processing and the pellets were resuspended and pooled in sterile phosphate buffered saline (PBS) before being centrifuged again at 10,000 x *g* for 30 minutes at 4° C to wash the pellet, further reducing contamination by soluble proteins. The resultant washed pellet containing enriched microvesicles was then resuspended in sterile PBS for subsequent analysis. For the purposes of this thesis, the population was called platelet microvesicle (PMV).

We were also interested in studying the expression of CT-1 on the total platelet-derived EV population and thus, the method described by Abid et al. in

2003 [404] was used. Essentially, this protocol allowed for the harvesting of a pellet enriched with all vesicle types including exosomes. For the purposes of this thesis, the term platelet extracellular vesicles (PEV) will be used to described this population.

Thus, to generate PEV, another batch of the supernatant generated from platelet activation was pooled and centrifuged in a Beckman L80 ultracentrifuge with a Sorvall TST28.39 swing out rotor at 150,000 x *g* for 2 hours at 4° C. The pellets were pooled and washed in sterile PBS before finally being resuspended in PBS to give a pellet enriched for PEV.

The protein concentration of each resuspended PMV and PEV preparations were assessed using a Pierce BCA protein assay kit (Thermofisher Scientific, USA) before aliquots (final concentration 5 mg/ml) were stored at −80° C until subsequent use.

4.2.5. Isolation of Red blood cells (RBC) and RBC extracellular vesicles

RBC vesicles, used a negative controls, were derived as described by Hugel et al. [358] but with slight modification. Briefly, peripheral blood from healthy non-pregnant volunteers was drawn through a 21-gauge needle into 4.5 ml 0.105M buffered sodium citrate vacutainer and centrifuged at 200 x *g* for 15 minutes to pellet red blood cells. The supernatant was discarded and the pelleted RBC were washed twice with PBS. To isolate RBC EV, 1 x 10^7/ml RBC was resuspended in PBS containing 2 mmol/L $CaCl_2$ and stimulated with 5µmol/L

calcium ionophore- A23187 (Sigma, UK) for 30 minutes at 37° C. After incubation, 5mmol/L EDTA was added to stop activation process. For analysis by flow cytometry, RBC were separated from derived vesicles by centrifugation at 12, 000 x *g* for 30 seconds. To isolate RBC EV for further analysis, the supernatant was pooled and centrifuged in a Beckman L80 ultracentrifuge with a Sorvall TST28.39 swing out rotor at 150,000 x *g* for 2 hours at 4° C.

4.2.6. Assessment of extracellular vesicles by Nanoparticle Tracking Analysis

Platelet extracellular vesicle size distribution profiles and concentration measurements were analysed by NTA as previously described in section 2.2.4. Briefly, vesicles were visualised by light scattering using a light microscope. Samples were automatically introduced into the sample chamber and a video was taken using a high sensitivity camera. The NTA software tracked the Brownian motion of individual vesicles and calculated the vesicle size and concentration [217]. Each sample was diluted in PBS to give approximately 5 x 10^8 EV/ml. A shutter speed and gain of 15 ms and 350 respectively, were used. The post-acquisition settings were kept constant between samples and each video was analysed to give the vesicles sizes and sample concentrations.

4.2.7. Assessment of CT-1 by flow cytometry

The expression of CT-1 on platelets was studied by flow cytometry using a BD LSRII flow cytometer (BD Biosciences, UK). Freshly isolated platelet

preparations were isolated and processed as described in section 4.2.2. and counted by flow cytometry using TruCount Beads (BD Biosciences, UK) following the manufacturer's instructions. Compensation was determined using BD^{TM} CompBeads (BD Biosciences, UK) as described in section 2.2.5. Next, 50 µl containing 1 x10^9/ml of platelets was incubated with 10 µl Fc Receptor blocker (Miltenyi Biotech, UK) for 10 minutes at 4° C before being labeled with 0.25 µg/ml anti-CD41 monoclonal antibody conjugated phycoerythrin-cyanine 7 (PE-Cy7) (Biolegend, UK) which detects the glycoprotein IIb/IIIa complex on the surface of platelets and megakaryocytes, and 5 µg/ml anti-CT-1 monoclonal antibody (R & D Systems, UK) conjugated to allophycocyanine (APC) and their respective isotype controls for 15 minute at RT in the dark. RBC were labeled with 0.05 µg/ml anti-CD235a/b conjugated to phycoerythrin-cyanine 5 (PE-Cy5), a sialoglycoprotein present in the cell membranes of erythroid precursors and erythrocytes. PBS was added to each sample to create a staining volume of 100 µl. Fluorescence minus one Control (FMO control) was used to accurately identify and gate cell populations in multicolour flow cytometry**.** Thirty thousand events were collected by flow cytometry. Cells were identified by their forward and side scatter optical characteristics. Data were analysed using FACSDiva software version 8.0 (BD Biosciences, UK) and figures generated using FlowJo version 10 (Tree Star Inc., Ashland, OR).

For the assessment of the expression of CT-1 on PMV, the BD LSR II flow cytometer was set up as described in section 2.2.5. Briefly, the flow rate of ~12 µl/min was determined using BD Trucount beads (BD Biosciences, UK) and BD^{TM} CompBeads (BD Biosciences, UK) were used to calculate

compensation. Next, the level of background contaminating events was determined using filtered PBS and these were subsequently deducted from the total vesicle counts. The Fc receptor was blocked by adding 10 µl Fc receptor blocking reagent (Miltenyi Biotech, UK) to 50 µl vesicle sample and the suspension incubated for 10 minutes at 4° C. Next, samples were labeled with 0.5 µM of the pan lipid membrane marker, Bio-maleimide, to exclude particles which were not extracellular vesicles from the analysis. PMV were then double-labeled using 0.25 µg/ml PECy7 conjugated CD41 antibody and 5 µg/ml APC conjugated CT-1 and their respective isotype controls for 15 min at RT in the dark. Following incubation, samples were diluted with PBS and transferred to flow cytometry tubes for analysis. Thirty thousand events were collected by flow cytometry. PMV were identified by their forward and side scatter optical characteristics. Gates set on single parameter histograms, using the FMO controls were used to determine the positive populations. Data were analysed using FACSDiva software version 8.0 (BD Biosciences, UK) and figures generated using FlowJo version 10 (Tree Star Inc., Ashland, OR).

4.2.8. Western blotting

Western blotting was carried out as described in section 2.2.7. Briefly, vesicle samples, cell lysate controls and cell extracts were lysed and diluted in reducing buffer (Bio-Rad, UK) and non-reducing buffer (CD63) to give a final concentration of 30 µg/well. Samples were then boiled at 96° C and centrifuged (13,000 x *g* for 1 minute) prior to separation by denaturing SDS-PAGE (Bio-Rad, UK) and semi-dry transfer to Polyvinylidene difluoride (PVDF)

membrane (Bio-Rad, UK). Non-specific binding was blocked in Tris-buffered saline (TBS) with 5% BLOTTO (Alpha Diagnostic International, US) and 0.1% Tween for 45 minutes at RT. Membranes were incubated overnight at 4° C with antibodies against CT-1(1:500) (R&D Systems, UK), Alix (1:1000) (New England Biolabs, UK), Syntenin (1:1000), CD9 (1:200) (Santa Cruz, UK), CD63 (1:1000) (Abcam, UK) and CD41 (1:1000) (Abcam, UK) in milk blocking buffer. For the study of cell signaling pathways, membranes were incubated with antibodies against phospho/total-GP130 (Santa Cruz, UK), phospho/total-ERK, phospho/total-Akt and phospho/total-STAT 3 (all from New England Biolabs, UK) in 5% BSA (Sigma, UK) and 0.1% TBST. Membranes were then washed in TBS-T before incubation with the appropriate horseradish peroxidase-conjugated secondary antibody (New England Biolabs, UK) in blocking buffer at RT for 2 hours. After washing, the membranes were treated with an enhanced chemiluminescence system (Pierce, UK) and exposed on CL-XPosure^{TM} Film (Thermofisher Scientific, USA). Beta-actin (1:1000) (Abcam, UK) was used as a loading control for lysates and cell extracts. The resultant band densities were quantified using Image J ImageJ version 2.0 (NIH) software.

4.2.9. HUVEC treatment with platelet extracellular vesicles for the study of changes in GP130, STAT 3, ERK and AKT.

Human umbilical vein cells (HUVEC) were used for the study of changes in gp130 in response to treatment with platelet extracellular vesicles. Briefly, HUVEC were seeded into 6-well plates at a seeding density of 3 x 10^5 cells/ml

and cultured to 80 -90% confluency as described in section 2.2.9.2Cells were subsequently cultured in serum-free endothelial growth media at 37° C in 5% CO_2 for 24 hours before being treated with a vehicle (5 μl PBS), recombinant CT-1 (100 ng/ml) (R & D Systems, UK), 1 x 10^{10} PEV in 5 μl of PBS, and PEV pre-treated with a neutralising antibody against CT-1 (R & D Systems, UK). Following treatment, cells were incubated at 37° C for 15 minutes in 5% CO_2 and samples processed as described in section 2.2.11.1.

4.2.10. Cytotoxicity/ Survival Assay – to determine whether PEV bound CT-1 has protective effects on endothelial cell *in vitro*

The cytoprotective effects of CT-1 are well reported [405, 406]. Therefore, we studied the effects of early apoptosis of HUVEC in response to PEV in the presence and absence of a CT-1 neutralising antibody using the CellTox™ Green (Promega, UK) assay according to the manufacturer's instructions. The assay used a cyanine dye that preferentially stained the DNA released by dead cells following disruption of the plasma membrane. When the dye bound DNA in compromised cells, the dye's fluorescent properties were substantially enhanced [224]. Viable cells produce no appreciable increases in fluorescence. The fluorescent signal produced by the dye binding to the dead-cell DNA was proportional to cytotoxicity [225].

For this study, triplicates of 3 x 10^4 cells/ml HUVEC were seeded into a 96-well plate and incubated overnight at 37° C in 5% CO_2 before being treated with recombinant CT-1 and PEV concentrations ranging from 1 x 10^6 EV/ml – 1 x 10^{10} EV/ml. The CellTox™ Green dye was added to each sample at the time of

treatment. The cells were then incubated at 37° C in 5% CO_2 in a FLUOstar Omega (BMG Labtech) plate reader for 20 hours, and the fluorescence measured at 485–500 nm excitation wavelength and 520–530nm emission wavelength. Positive and negative controls were used by adding cell lysis buffer and equal volumes of PBS (vehicle) to the cells, respectively.

4.2.11. Statistical Analysis

Data are shown as mean ± SEM. The results generated from the intracellular signaling experiments were analysed using a two-sample t-test. The Mann Whitney non-parametric test was used on all other comparisons. Statistical analyses were carried out using Prism software (GraphPad Software, San Diego California USA, www.graphpad.com). Values of $p<0.05$ were considered statistically significant.

4.3. RESULTS

4.3.1. Determination of CT-1 expression on human platelets by immunocytochemistry and Western blotting

Since the detection of CT-1 on platelet extracellular vesicles was incidental, we decided to further characterise the expression of platelet EV-bound CT-1. First, we studied the expression of CT-1 on Cytospin preparations of non-stimulated and calcium ionophore activated platelets which were double-labeled with platelet marker, CD41 and CT-1, and analysed these by confocal microscopy. Figure 4.3-A shows intense fluorescence of CD41 on preparations from non-stimulated platelets and minimal fluorescence of CT-1 on smaller populations (200–500 nm in diameter) was observed. When platelets were activated, the fluorescence intensity of CT-1 on the smaller population was increased and a subset was seen to be co-localized with CD41. Given the size, the small population was likely to be platelet-derived extracellular vesicles.

Next, we studied the expression of CT -1 and CD41 on non-stimulated platelets by Western blotting of four platelet lysates isolated from healthy subjects. This showed a 25KD band corresponding to CT-1, and a 130KD band consistent with CD41, confirming that CT-1 was expressed on the human platelets (Figure 4.3-B and C).

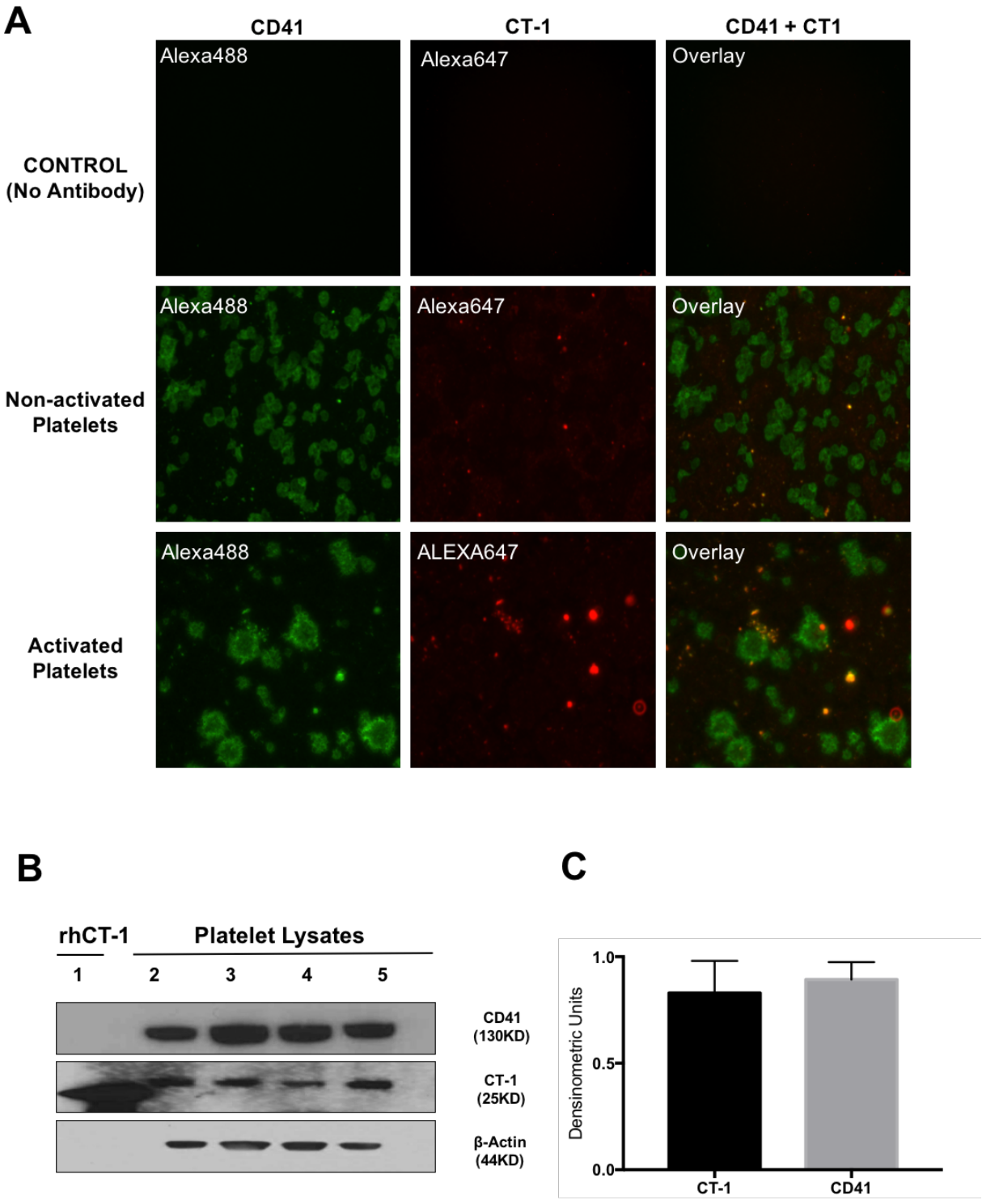


Figure 4.3. Cardiotrophin 1 expression on platelets (A) Immunocytochemistry demonstrating the expression of CT-1 on the non-stimulated and calcium ionophore activated platelets at 63x magnification negative control. **(B)** Western Blot demonstrating the expression of CD41 and CT-1 on platelet lysates, Lane 1: Recombinant CT-1(rhCT-1); Lanes 3-8: Platelet Lysates. **(C)** Corresponding densinometric analysis of CD41 and CT-1 in platelet lysates.

4.3.2. Determination of CT-1 expression on human platelets by flow cytometry

To determine the proportion of platelets that co-express the platelet marker, CD41 and CT-1, six non-stimulated platelet samples were labeled with antibodies conjugated to PE-Cy7 and APC respectively and were analysed by flow cytometry.

First, platelets were identified based on their forward scatter (FSC) vs. side scatter (SCC) profiles. Figure 4.4-A. shows that the platelet population was greater than $\geq$1 μm. This was consistent with the average size of non-stimulated platelets which are 2-5 μm in the greatest diameter. The mean fluorescence intensity (MFI) for CD41 was also evaluated. The MFI indicates the amount of antigen carried on each platelet. Figure 4.4–B and C show that platelets abundantly expressed CD41 and thus confirming their origin. Platelets were then displayed on CD41 vs CT-1 quadrant plots to identify the proportion of platelets that co-express CD41 and CT-1. Figure 4.4- D and E show that 51.40 $\pm$3.49% of CD41 positive platelets were also CT-1 positive. The MFI for CT-1 was 740.5 ± 84.77 compared to 63.75 ± 10.99 (Figure 4.4–F and G, n=6) on the isotype negative control, further confirming that CT-1 expression on platelets is not due to non-specific antibody binding.

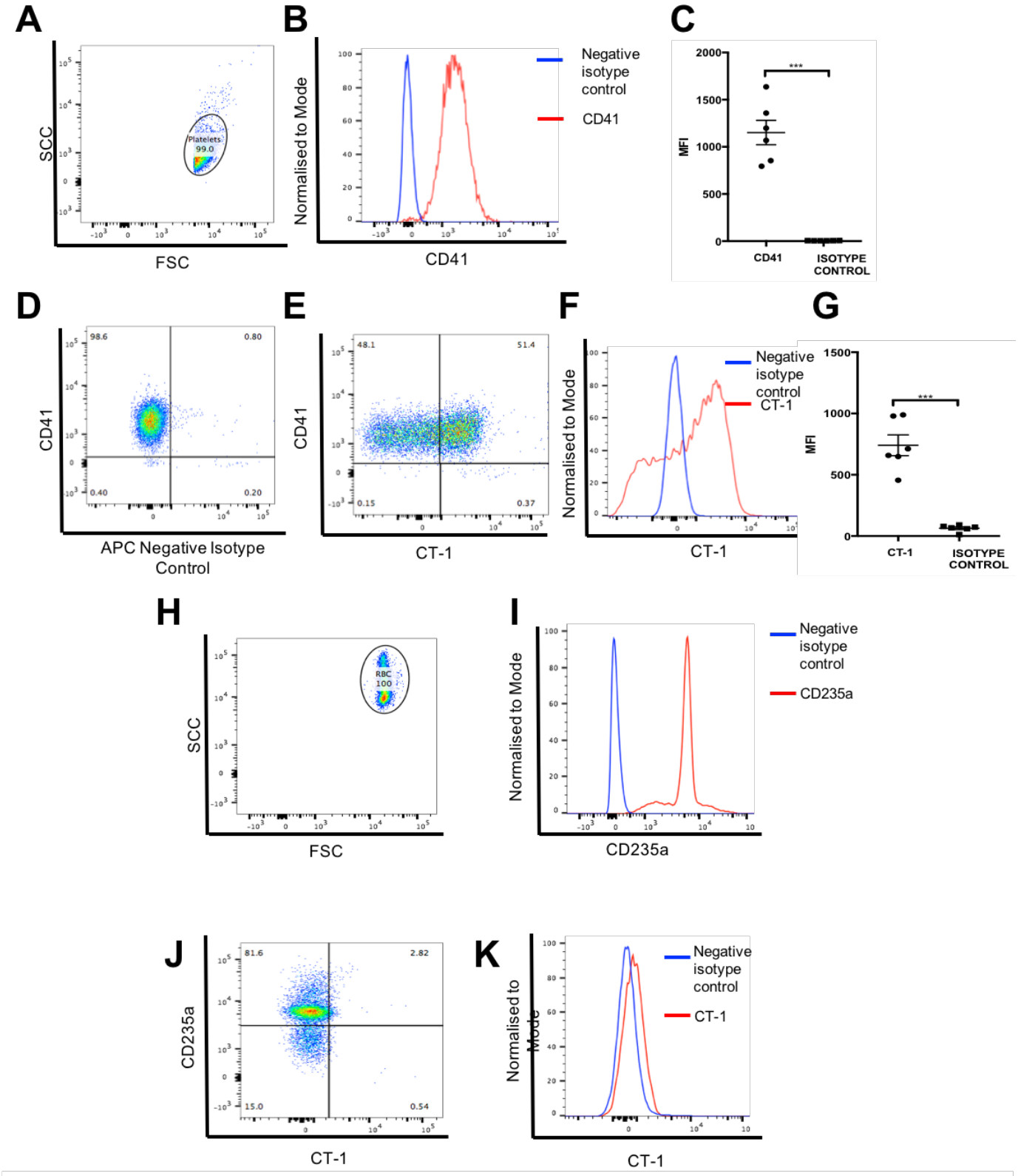


Figure 4.4. Representative flow cytometric analyses of non-stimulated platelets from peripheral blood plasma. (A) Forward scatter (FSC) vs. side scatter (SSC) profile for platelets. **(B)** Mean Fluorescence Intensity (MFI) for CD41 showing a significant difference in the expression of CD41 on platelets compared to isotype negative control. **(C)** Corresponding analysis of six platelet samples. Two-parameter plots showing **(D)** CD41 positive platelets

(CD41$^+$/APC control) and **(E)** CT-1 positive platelets **(F)** MFI for CT-1 showing a significant difference in the expression of CT-1 on platelets compared to isotype negative control (CT1$^+$/CD41$^+$) and **(G)** Corresponding analysis of six platelet samples. *= p<0.05 Red blood cells (RBC) used as a negative control for CT-1 expression. **(H)** Forward scatter (FSC) vs. side scatter (SSC) profile for RBC. **(I)** MFI for CD235a showing a significant difference in the expression of CD235a on RBC compared to isotype negative control. Two-parameter plots showing for **(J)** CD235a and CT-1; and **(H)** MFI for CT-1 showing no difference in CT-1 expression on RBC. Bars = mean ± standard error of the mean, *= p<0.05

We also studied the expression of CT-1 on RBC (used as a negative control), the most abundant cell type in the circulation, by flow cytometry. RBC were identified on their SCC and FSC profile (Figure 4.7-H). The expression of erythrocyte marker, CD235a on RBC confirmed their origin (Figure 4.7-I). RBC were also displayed on CD235a vs CT-1 quadrant plots. Figure 4.7-J shows that virtually no RBC were positive for CT-1. This was also evidenced by the MFI for CT-1 which showed no significant difference in the expression of CT-1 (Figure 4.7–K) compared to the negative isotype control.

4.3.3. Isolation and characterisation of platelet extracellular vesicles

We learned from our immunohistochemistry findings that more CT-1 was expressed on platelet preparations upon activation, and that CT-1 was localized on populations that were smaller than the activated platelets in size. We hypothesized that this small population consisted of extracellular vesicles. To test the hypothesis that platelet derived extracellular vesicles expressed CT-1, fresh platelet preparations isolated from human plasma were activated with calcium ionophore –A23187 and subjected to differential ultracentrifugation before being analysed by Nanoparticle Tracking Analysis (NTA) and Western blotting. Vesicle preparations isolated from the 10 000 x g centrifugation spin were analysed by NTA. These were found to have a peak

modal size of 305 nm ±6 (Figure 4.5-A) which is consistent with that of microvesicles. Interestingly, vesicle preparation generated from the 150 000 x g spin showed a peak modal size of 129 nm ±7.4 which is consistent with the theoretical size range for exosomes.

Western blotting of the platelet lysates, PMV and PEV was also carried out for Alix, Syntenin and CD 9, to validate their platelet origin and to determine presence of exosomes (Figure 4.5-B). Interestingly, PEV, but not PMV and platelet lysates showed positive bands at 96KD, 34KD bands consistent with Alix (Figure 4.5-D) and Syntenin (Figure 4.5-E), respectively. This suggests that, PEV, but not PMV and platelet lysates are enriched for exosomes. A further interrogation using exosomal marker, CD63, underscored this finding. Furthermore, a 23KD band consistent with CD9 (Figure 4.5-F), a molecule known to be expressed on platelets (but highly enriched in exosomes), was observed on all samples, but stronger bands were seen in the PEV samples further validating that PEV were enriched in exosomes.

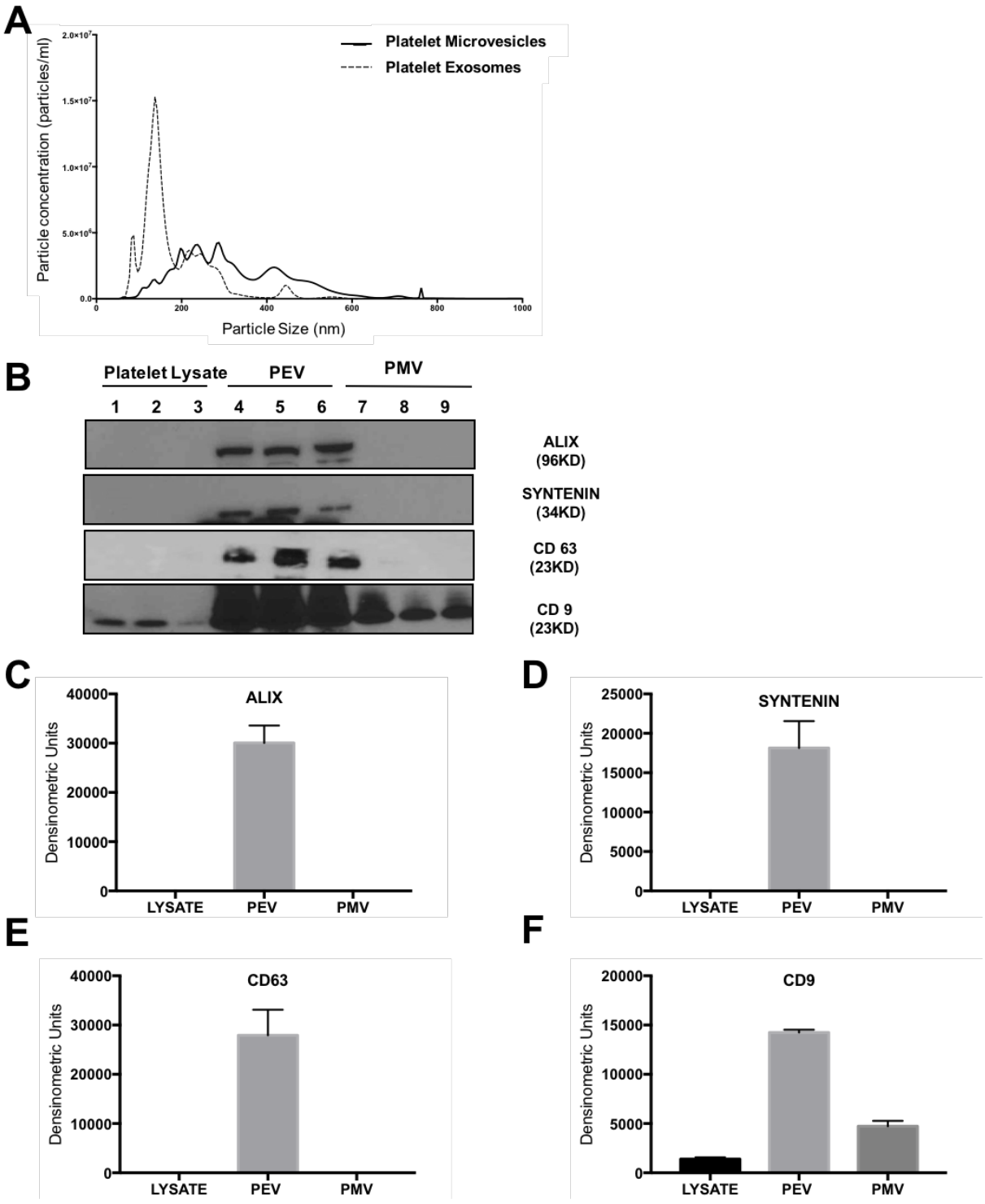


Figure 4.5. Characterization and quantification of platelet extracellular vesicles generated from calcium ionophore activated platelets. (A) Representative results of nanoparticle tracking analysis (NTA) demonstrating the size distribution in diluted samples of exosomes and microvesicles. **(B)** Western Blot confirming the presence of exosomal proteins Alix, Syntenin and CD9. Lanes 1-3: Platelet Lysates; Lane 4-6: Platelet Microvesicles; Lane 7-9: Platelet Exosomes. Corresponding densinometric analysis of exosome markers **(C)** Alix **(D)** Syntenin **(E)** CD63 and **(F)** CD9. Bars = mean ± standard error of the mean, *= $p<0.05$

4.3.4. Determining the expression on CT-1 on PMV and PEV by Western blotting

Having successfully isolated and fully characterized the PMV and PEV preparations, we studied the expression of CT-1 and CD41 on three PMV and three PEV samples by Western blotting. A 25KD positive band corresponding to CT-1 and a positive band at 130KD consistent with CD41 (Figure 4.6-A) were observed. We also noted that CT-1 was highly expressed on PEV (Figure 4.6-B) but weakly expressed on the PMV samples (Figure 4.6-C). Given that the PEV samples contain microvesicles and is highly enriched for exosomes, this data suggests that more CT-1 might be expressed on exosomes.

Given that CT-1 expression was much higher on PEV it was decided to focus on this population from this point on.

Having determined the expression of CT-1 on PEV compared to PMV, we were interested in whether more CT-1 was expressed on PEV (released on platelet activation) compared to non-stimulated platelets. Thus, we compared the expression of CT-1 and CD41 on platelets and PEV by Western blotting. Figure 4.6-D and E showed that on one hand, compared to non-stimulated platelets, the expression of CD41 was significantly lower on PEV. On the other hand, CT-1 expression was marginally higher on PEV than non-stimulated platelets, though not statistically significant (Figure 4.6 D and F).

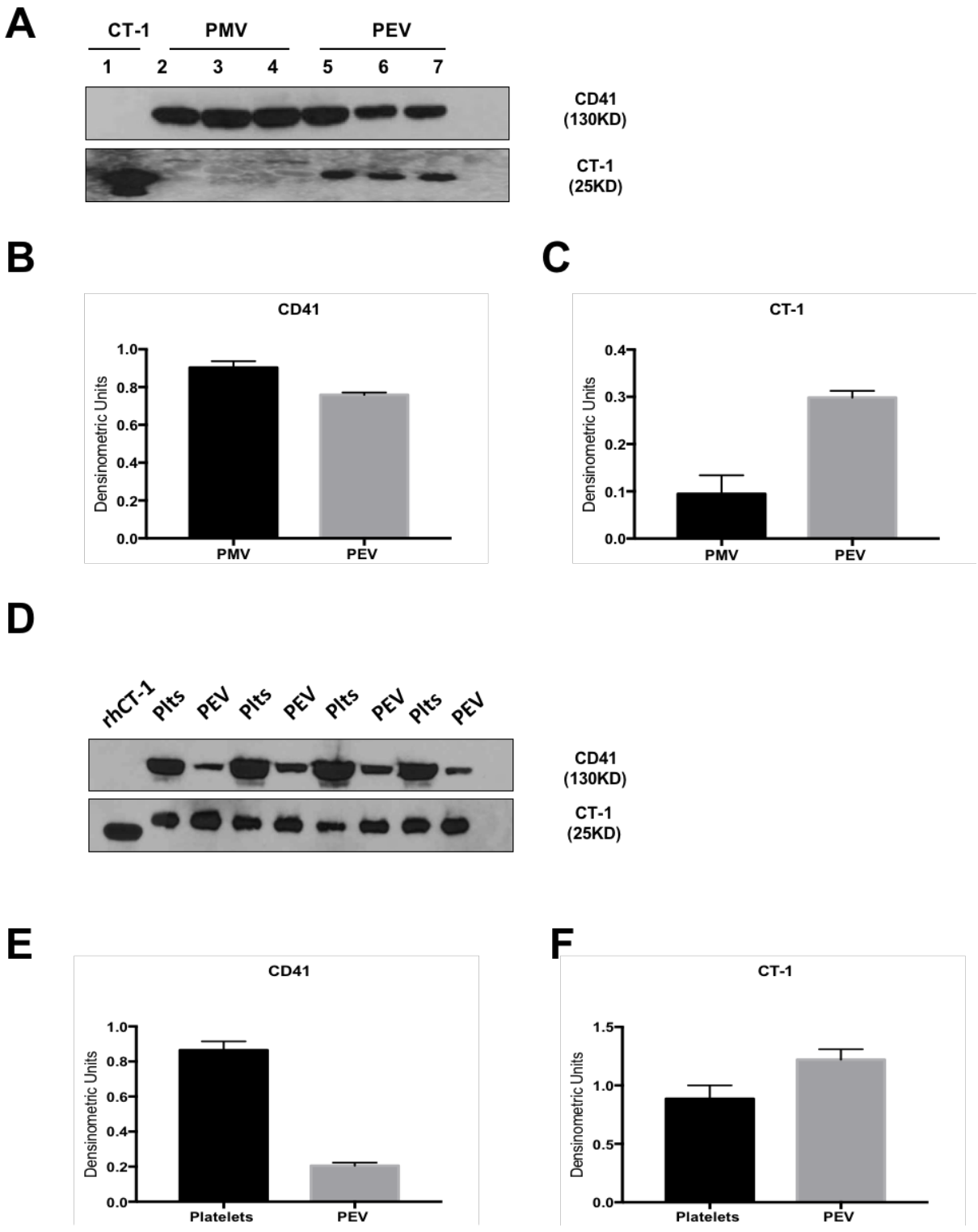


Figure 4.6. Cardiotrophin 1 expression on P-EX and PMV. (A) Western Blot demonstrating the expression of CD41 and CT-1 on platelet lysates, microvesicles and exosomes. Lane 1: Recombinant CT-1; Lanes 2-3: Platelet Lysates; Lane 4-6: P-MV; Lane 7-9: P-EX. Corresponding densinometric analysis of **(B)** CD41 and **(C)** CT-1. **(D)** Western Blot comparing the expression of CD41 and CT-1 on platelet lysates and microvesicles and exosomes and the corresponding densinometric analysis **(E)** CD41 and **(F)** CT-1. Bars = mean ± standard error of the mean, *= $p<0.05$

4.3.5. Determining the expression on CT-1 on PMV by flow cytometry

We were also interested in studying the levels of expression of CT-1 on extracellular vesicles by flow cytometry. As previously indicated in Chapter 2 of this thesis, only microvesicles can be studied by flow cytometry, as this technique is not sensitive enough to measure antigen expression on the much smaller exosome population.

Six PMV preparations were analysed by flow cytometry. Phenotyping of PMV was carried out as follows: the total microvesicle population was identified on the FSC vs. SCC plot as being $\leq$1 μm using reference beads. Results are presented as percentages (mean$\pm$ standard error of the mean). Figure 4.7-A shows that 71.2 % (77.05$\pm$3.09) of the population was <1 µm. Next, vesicles labeling positive for biomaleimide (a lipid membrane marker present in all extracellular vesicles) were gated. Figure 4.7-B and C show that 96.9 % (98.8$\pm$1.02) of the particles analysed labeled positively with biomaleimide and were therefore vesicles.

To determine the proportion of PMV that co-express the platelet marker, CD41 and CT-1, samples were labeled with monoclonal antibodies conjugated to PECY7 and APC respectively and displayed on CD41 vs CT-1 quadrant plots. Figure 4.7 D and E shows that 45.4% (44.3$\pm$2.61) of CD41 positive microvesicles were also CT-1 positive. The MFI for CT-1 was 830.12 ± 64.43 compared to 54.26 ± 8.41, n=6). This data suggests there are relatively high levels of CT-1 carried on each PMV.

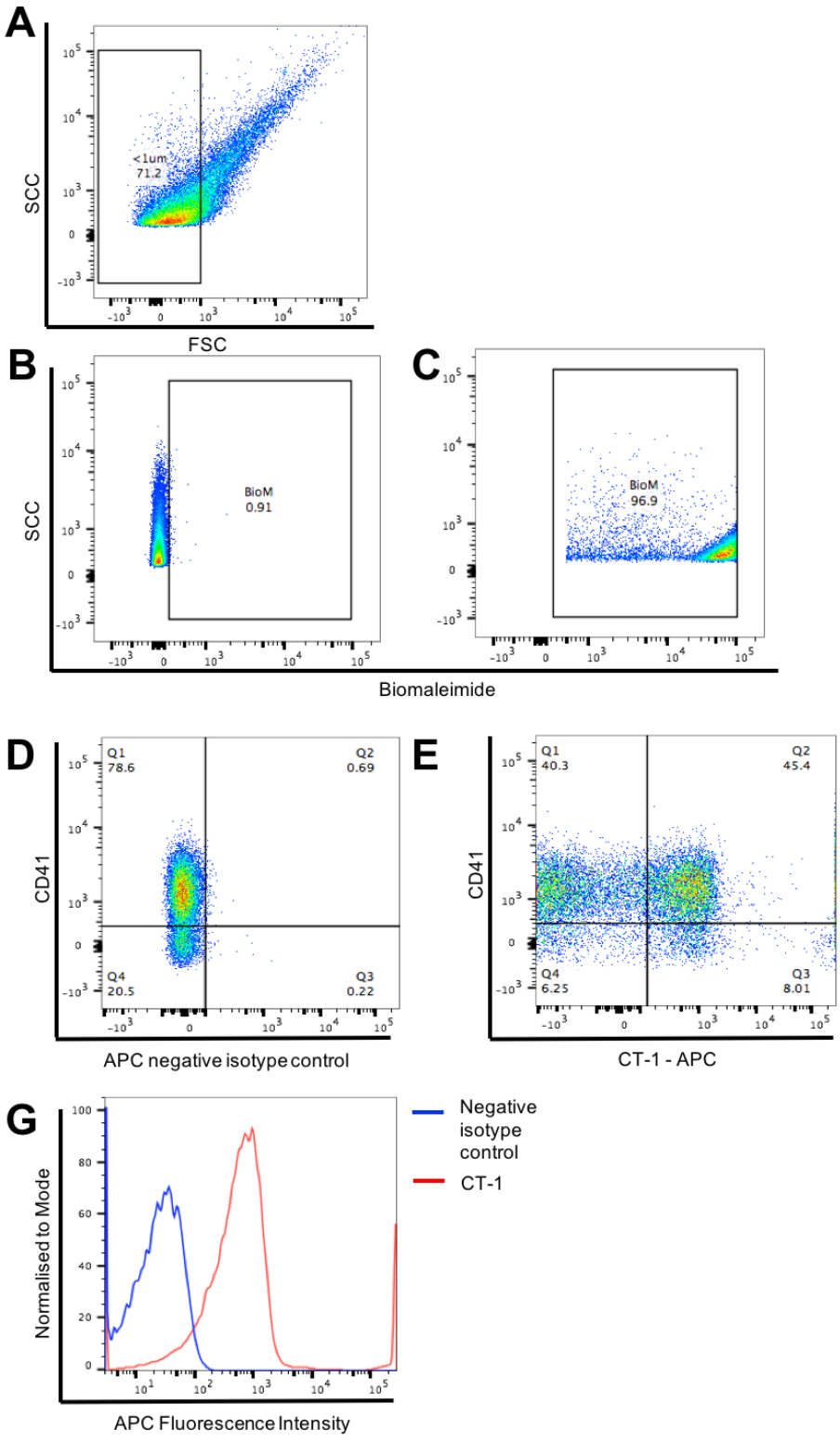


Figure 4.7. Representative flow cytometric analyses of PMV generated from calcium ionophore activated platelets. (A) Forward scatter (FSC) vs. side scatter (SSC) profile. **(B)** and **(C)** Gating of Biomaleimide positive vesicles. PMV displayed on two-parameter plots and phenotype identified: **(D)** CD41 antibody positive AND CT-1 negative isotype control, and **(E)** both CD41 and CT-1 antibody. **(F)** MFI for APC showing a significant difference in the expression of CT-1 on vesicles compared to isotype negative control**.**

4.3.6. PEV-bound CT-1 phosphorylates gp130 and STAT 3 but not ERK and Akt

The biological effects of PEV bound CT-1 *in vitro* were investigated on HUVEC by studying intracellular pathways previously shown to mediate CT-1 signaling.

First, we studied the effects of PEV-bound CT-1 on gp130, a transmembrane receptor that signals as a heterodimer with Leukemia Inhibitory Factor Receptor (LIF-R). HUVEC were treated with a 5 μl of PBS (vehicle), 100 ng/ml recombinant CT-1, 1 x 10^8 PEV in 5 μl of PBS, or PEV pre-treated with a neutralising antibody against CT-1, each in 3 replicates. Western blot analysis showed that adding PEV to endothelial cells resulted in a significant phosphorylation of gp130 compared to those treated with PBS alone. This was consistent with the effect induced by recombinant CT-1 (Figure 4.8-B). Furthermore, the phosphorylation of gp130 could be attenuated by the addition of CT-1 neutralising antibody, thus ascribing gp130 phosphorylation to PEV bound CT-1 (Figure 4.8-B).

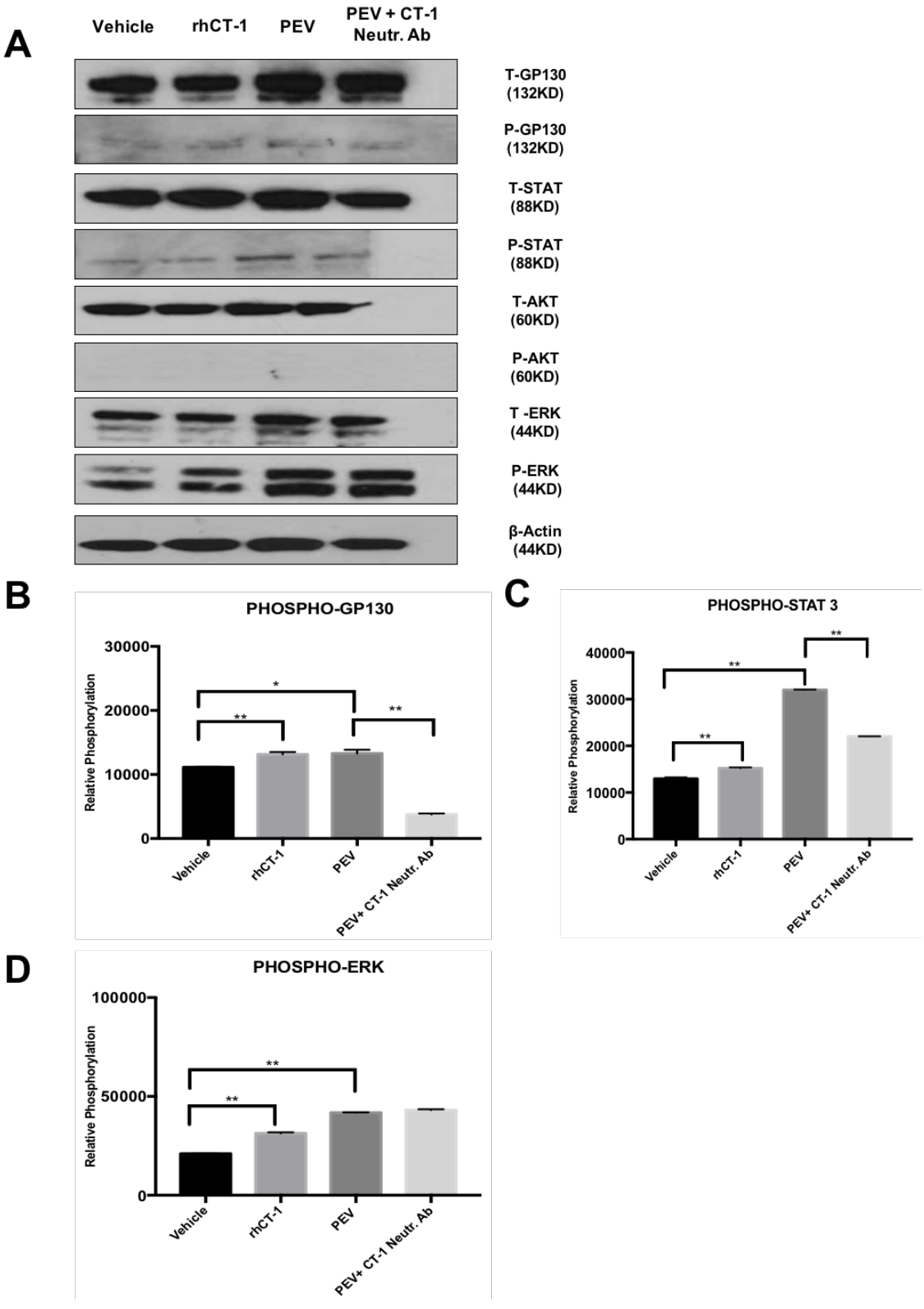


Figure 4.8. Investigating effects of PMV bound CT-1 phosphorylates gp130, STAT 3, AKT and ERK in HUVEC. **(A)** Western Blot demonstrating phosphorylation of gp130, STAT 3, ERK but not AKT on HUVECS treated with PBS (vehicle), recombinant CT-1 (rhCT-1), PMV and PMV pre-treated with a CT-1 neutralising antibody. Corresponding densinometric analysis of **(B)** p-gp130, **(C)** STAT 3 and **(D)** ERK. N=3 *p<0.05 **p<0.0001

Intracellularly, classic pathways involved in CT-1 signaling, namely, the mitogen-activated protein kinases/extracellular signal-regulated kinases (MAPK/ERK) pathways, signal transducer and activator of transcription 3 (STAT 3) and protein kinase B (also known as AKT) were also studied. This data also showed that adding PEV to HUVEC resulted in the activation of STAT 3 (Figure 4.8-C) and ERK (Figure 4. 8-D). However, no AKT phosphorylation was observed after PEV treatment (Figure 4.8-A) which suggests that PEV do not activate insulin receptor signaling in endothelial cells. Like the phosphorylation of gp130, the phosphorylation of STAT 3 could also be attenuated by the addition of a CT-1 neutralising antibody, showing specificity to CT-1. Conversely, the CT-1 neutralising antibody did not reduce the phosphorylation of ERK. This could be due to insufficient neutralization of CT-1 or that there may be other molecules deployed on PEV that also activate this pathway. Taken together these data suggest that PEV-bound CT-1 induces an intracellular signaling cascade following a ligand –receptor interaction between the PEV and gp130.

4.3.7. Determining the cytoprotective effects of PEV-bound CT-1 on endothelial cells *in vitro*.

HUVEC are known to rapidly undergo apoptosis when deprived of complete endothelial cell growth medium [407]. Furthermore, STAT 3 and ERK mediated cytoprotective effects induced by CT-1 have been previously reported [405]. Thus, we investigated the role of PEV bound CT-1 as a likely mediator of endothelial cell protection *in vitro*. The CellTox^{TM} Green assay, in which a

cyanine dye binds DNA released by dead cells following disruption of the plasma membrane, was used.

HUVEC were treated using a wide range of PEV concentrations (1 x 10^4 EV/ml – 1 x 10^{10} EV/ml) and PEV blocked with a specific neutralising antibody to CT-1 and cultured for 20 hours. PBS (vehicle), 100 ng/ml recombinant CT-1 and cell lysis buffer (for maximal cell death) were used as controls. First, we tested the effects of recombinant CT-1 on endothelial cell cultivated in unsupplemented cultured medium. The area under the curve (AUC) was calculated for each condition and results are represented as mean± standard error of the mean. Figure 4.9 shows that the addition of recombinant CT-1 (9535±357.2) acutely prevented HUVEC apoptosis compared to vehicle (11576±444.6). Next, we added 1 x 10^{10} EV/ml CT-1 positive PEV to HUVEC. This resulted in a marginal increase (13769±498) in the rate of apoptosis compared to vehicle (11576±444.6). Moreover, these findings corroborate the current understanding of the anti-angiogenic effects of PEV. Interestingly, when PEV pretreated with a CT-1 neutralising antibody were added, there was an increase (20638±661.2) in the rate of apoptosis compared to vehicle (11576±444.6), an effect that was more pronounced in the first 6 hours of culture. These data suggest that PEV-bound CT-1 provides endothelial cell protection from cytotoxic effects induced by other molecules deployed on PEV.

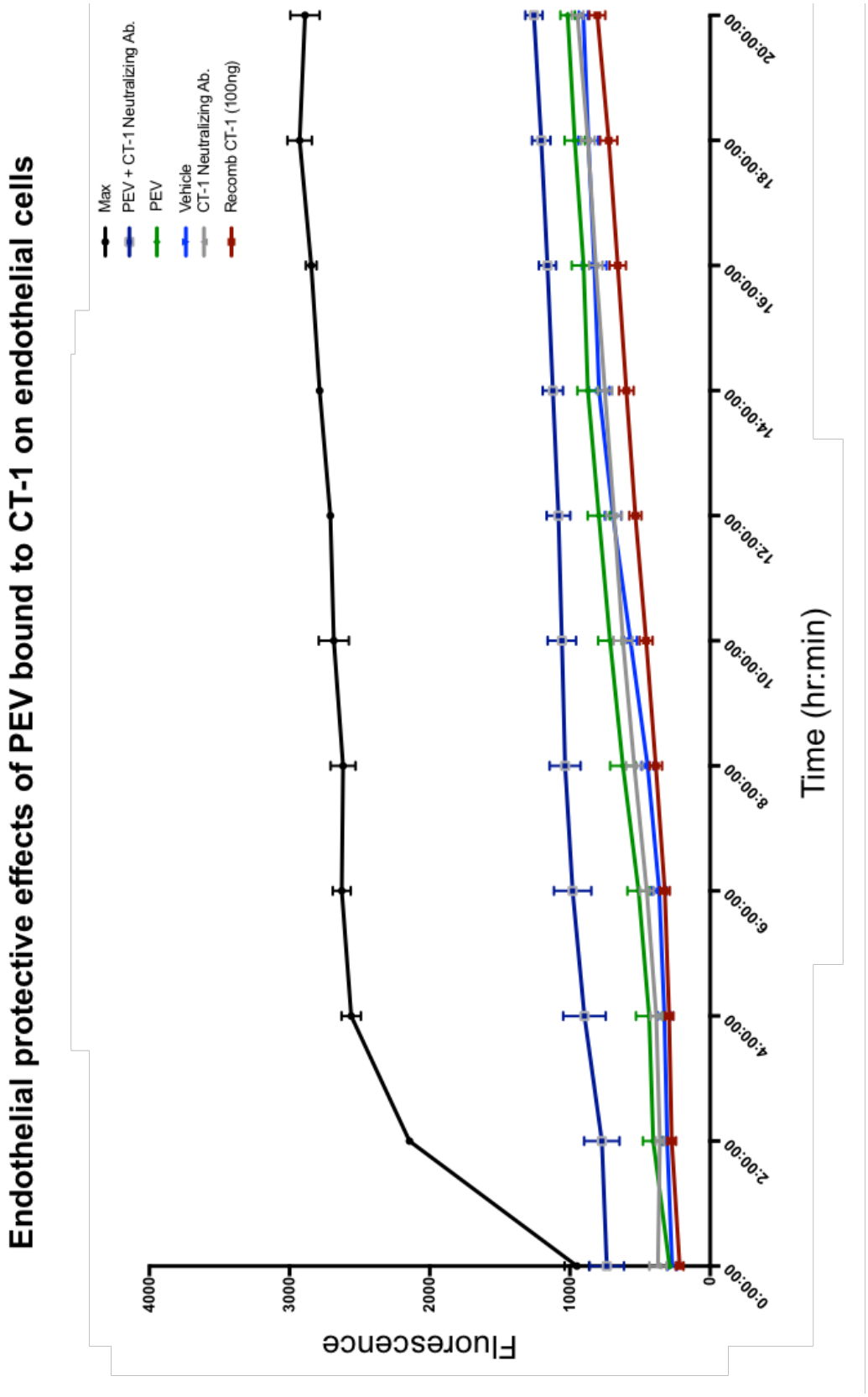


Figure 4.9. Effects of Platelet Extracellular vesicles have endothelial protective effects. Platelet extracellular vesicles were cultured with 10^{10} EV/ml and were culture for 20 hours in serum free medium in the presence of and absence of CT-1 neutralising antibody. Maximum cytotoxicity was induced with a cell lysis buffer. Effects of PEV, PEV Recombinant CT-1 and CT-1 neutralising antibody

4.4. DISCUSSION

Having incidentally discovered that platelets and platelet extracellular vesicles (PEV) express Cardiotrophin 1, in this thesis chapter, we characterised the levels of CT-1 expression on platelets and PEV. Additionally, we investigated the functional relevance of PEV-bound CT-1 on endothelial cell *in vitro*.

Platelets normally circulate through the vasculature in a quiescent state. However, after breaches of the vasculature or alteration to normal blood flow, platelets become activated - they rapidly decelerate, roll on the injured endothelium and several highly reactive sub-endothelial matrix proteins become exposed which form receptor-ligand interactions that initiate a cascade of intracellular responses resulting in amplification of the platelet activation response [408]. Furthermore, platelets are endowed with hundreds of pre-formed and pre-packaged proteins which, when platelets become activated, are secreted in granules and platelet-derived EV to the extracellular milieu, or expressed on the platelet surface [409, 410]. We now report for the first time that platelets express CT-1 and that when platelets become activated, biologically active CT-1 is released in platelet-derived EV.

First, we localized CT-1 on non-stimulated and activated platelets by immunocytochemistry. Confocal microscopy observations confirmed the presence of CT-1 in non-stimulated platelets and its expression on smaller population with an average size of 200 nm. Furthermore, we demonstrated CT-1 co-localization with the more abundant platelet marker, CD41,

particularly after activation. We also demonstrated CT-1 expression on platelet lysates by Western blotting and flow cytometry. Furthermore, we studied the expression of CT-1 on red blood cells, the most abundant cell type in the circulation. Flow cytometric analysis and Western blotting (results not shown) revealed no detectable CT-1 on red blood cells and red blood cell vesicles which express erythrocyte marker, CD235a, contrasting with the high levels of co-expression of CT-1 and CD41 labels observed in platelets.

It has long been established that platelets contain pre-stored proteins in their granules or on their membrane which are thought to play a role in haemostasis. However, despite findings by Warshaw et al. in 1967 [411], it has only recently been accepted that platelets can also synthesize proteins, despite lacking a nucleus [412]. For example, activated platelets have be shown to synthesize interleukin-1β, a portion of which is shed in its mature form in membrane microvesicles and promotes an inflammatory response by inducing adhesiveness of human endothelial cells for neutrophils [408, 413]. Activated platelets also secrete several chemokines such as chemokine ligand (CXCL1), platelet factor 4 (PF4) also known as chemokine ligand 4 (CXCL4), chemokine ligand 5 (CXCL5), chemokine ligand 7 (CXCL7), interleukin (IL) -8 (also known as CXCL8), CXCL12, macrophage inflammatory protein- (MIP-) 1α (also known as CCL3), and regulated on activation, normal T cell expressed and secreted (RANTES), also known as chemokine ligand 5 (CCL5) [390, 414-416]. These chemokines have no apparent role in hemostasis. We show evidence suggesting that CT-1 is a new addition to this group.

We also found that CT-1 was expressed on platelet-derived EV. Platelet-derived EV are released as part of the **p**latelet activation process which encompasses a variety of cellular responses, including shape change, translocation of membrane glycoproteins, and exocytosis of granule contents. In vitro, platelet activation and the release of PEV has been demonstrated after stimulation with the agonists such as calcium ionophore A23187, thrombin, collagen, the thrombin receptor agonist peptide SFLLRN and lipopolysaccharide (LPS) [362, 417, 418]. Recently, Aatonen et al. studied PEV that were generated from platelets activated by thrombin and collagen, LPS or calcium ionophore A23187 and isolated by differential centrifugation [362]. They compared the quantity and the protein content of the EV subpopulation induced by different platelet activators [362]. They found that the activation pathways induced by the various agonists vary in their efficacy to produce EV, with calcium ionophore A23187 being the most potent of these [362].

In this study, we used calcium ionophore A23187 for platelet activation and vesiculation. Calcium ionophore A23187 is a widely-used platelet agonist that transports divalent cations across cell membranes into the cytoplasm and releases cations from intracellular storage sites [404, 419-421]. Our preliminary work included a comparison of activation patterns of calcium ionophore A23187 and thrombin receptor-activating peptide (TRAP) (results not shown). We noticed that calcium ionophore A23187 did indeed yield a higher number of vesicles compared to TRAP which is consistent with previous reports [362]. Proteomic analysis conducted by Aatonen et al. on EV showed

that each agonist resulted in distinct protein contents, which changed over time [362]. In light of these findings and to ensure consistency in the quality of EV and protein content generated from vesiculation, we resolved to use calcium ionophore A23187 in all our subsequent experiments. Interestingly, in contrast to the findings by Aatonen et al. (who reported that calcium ionophore A23187 yielded protein-poor vesicles) [362], we found that vesicles generated using calcium ionophore A23187 had relatively high concentrations of protein averaging 5 mg/ml.

There is no standardized method for the isolation of platelet-derived EV. Some groups have reported successful isolation and purification microvesicles and exosomes [373] and others report a difficulty in distinguishing microvesicles and exosomes by differential centrifugation [362]. In our studies, we isolated populations, PEV and PMV, with different size distributions based on their NTA profiles. Upon further interrogation of these vesicle populations by Western blotting, we found that the vesicle samples with smaller size distribution profiles (PEV) were highly enriched in heparan sulfate proteoglycans, Alix and Syntenin, and tetraspanins, CD9 and CD63. These molecules are routinely employed as exosome markers given their role in exosome biogenesis. In contrast, the larger vesicle population (PMV) was not enriched in exosomal molecules. CD9 was also present on platelet lysates and PMV because it is commonly detected on the platelet cells surface after activation, including release on microvesicles but found highly enriched on exosomes [422].

The enrichment of certain molecules on exosomes suggest that such molecules are selectively sorted from other glycoproteins via the formation of small internal vesicles [373]. The role of exosome molecules is complex and an area of increased study. For example, tetraspanin proteins are believed to function cooperatively with each other in complex formation with cell surface proteins and can interact with integrins [422-425]. Platelet derived extracellular vesicles may have the potential to excite signaling at a distance from the site of platelet activation and such signaling role may occur through specific association of CD63 [373]. Additionally, integrins have a key role in anchoring endothelial cells to matrix proteins, allowing flexible responses to changes in the microenvironment [426].

Having successfully isolated and characterised platelet-derived EV, we investigated the expression of CT-1 on these vesicles. We show for the first time that CT-1 is expressed on PEV and PMV. Further analysis of CT-1 expression on PMV by flow cytometry showed that CT-1 was expressed as a surface protein and co-expressed with platelet marker, CD41. Despite evidence of CT-1 expression on PMV on flow cytometry, Western blotting demonstrated that CT-1 was weakly expressed on the PMV. Considering the weak expression of CT-1 on PMV, only functional effects of PEV bound CT-1 was studied further.

In Chapter 2 of thesis, we demonstrated that STB-EX bound CT-1 stimulated gp130 signaling leading to the activation of STAT 3 and ERK 1/2 in HUVEC. There have also been reports that platelet-derived EV induced effects on cells

that are mediated by signaling proteins. Thus, we studied whether PEV bound CT-1 could induce intracellular signaling pathways by investigating the activation of four key molecules that CT-1 has been documented to activate viz. gp130, STAT 3, ERK 1/2 and Akt. Our results show that indeed, PEV can phosphorylate the transmembrane receptor, gp130, as well as STAT 3 and ERK in endothelial cells. Interestingly, adding PEV to HUVEC resulted in a phosphorylation of STAT 3 that exceeded that induced by recombinant CT-1. Moreover, the activation of gp130 and STAT 3 could be attenuated by pre-treating PEV with a CT-1 specific neutralising antibody. The CT-1 neutralising antibody did not reduce the phosphorylation of ERK. This makes it difficult to ascribe ERK activation to PEV-bound CT-1. Perhaps there may be other molecules deployed on PEV capable of activating ERK. Equally, not being able to inhibit ERK levels may simply be a consequence of insufficient neutralization.

The STAT 3 and ERK signaling pathway plays an essential role in regulating proliferation, differentiation and apoptosis in endothelial cells [427, 428]. Furthermore, STAT 3 signaling in endothelial cells has been linked to anti-inflammatory action and protection against LPS-induced inflammation [429-431]. Kim et al. have reported that treatment of HUVEC with platelet-derived EV resulted in protection from apoptosis, enhanced proliferation, and angiogenesis [432]. CT-1 also mediates its cytoprotective properties through STAT 3 signaling [405, 406]. Considering our signaling data, we hypothesised that CT-1 may be responsible for the STAT 3 mediated cytoprotective effects induced by PEV on endothelial cells *in vitro*. To test this hypothesis, we

cultured HUVEC in unsupplemented culture medium, in the presence of PBS (vehicle), recombinant CT-1 (100 ng/ml), PEV (1 x 10^{10} EV/ml) or PEV pre-treated with a CT-1 neutralising antibody. We show for the first time that recombinant CT-1 promotes the cell survival of cultured endothelial cells. When PEV were added to HUVEC, there was a marginal increase in cell cytotoxicity compared to vehicle. Intriguingly, the cytotoxic effects were significantly increased when CT-1 on PEV was blocked with a CT-1 specific neutralising antibody. To ensure that cell death was not a consequence of bacterial or endotoxin contamination of the neutralising antibody, HUVEC were treated with CT-1 neutralising antibody alone. Our data showed no difference in endothelial cell death compared to control.

It must be noted that to study the effects of all vesicles, PEV used for this study were harvested after a single 150 000 x g spin. Whilst our data shows that our PEV samples were enriched in exosomes, it is possible that other vesicle population were also isolated including platelet microvesicles, granules and apoptotic bodies. Microvesicles and exosomes have different biological functions, cargos and mode of production. It is therefore not surprising to see endothelial cell dysfunction and death when a composite mixture of vesicles is added to them. Though our experimental conditions may not be entirely representative of normal physiology, when platelets become activated, all these different type of vesicles are released [373]. Therefore, these data take together, reflect the multifaceted nature of platelet vesicular biology and the delicate balance that is required when vesicles carrying complex cargo are released. It is however, evident that PEV-bound CT-1 plays an important role

in the maintenance of this balance, more specifically, endothelial cell protection.

Most of the research regarding platelet-derived EV has largely been focused on their role in pathological conditions. Consequently, these vesicles can easily be mistaken as purely detrimental. Although their relative concentrations are determined by the pathophysiological context, circulating platelet-derived EV are found in the plasma of healthy subjects [433]. In fact, in this study, extracellular vesicles were isolated from platelets of healthy subjects.

Platelet-derived EV are the most abundant of all circulating extracellular vesicle pool and contribute to many biological processes [434]. Moreover, circulating platelet-derived EV have been considered as biological markers in conditions associated with platelet activation. With particular relevance to cardiovascular disease, previous studies have reported that the levels of circulating platelet-derived EV were increased in patients with various diseases such as hypertension [357, 360, 361], obesity [435], atherosclerosis [360], and stroke [357]. Furthermore, high concentrations of circulating platelet-derived extracellular vesicles (ranging from ~3,000–11,000/μL) have been reported in patients with coronary heart disease including acute coronary syndrome [436-438]. Additionally, Jung et al. found that circulating levels of platelet-derived EV reflect the size of myocardium at risk in patients with ST-elevation myocardial infarction [359]. Intriguingly, CT-1 plasma concentration levels are altered in all these conditions [126, 137, 204, 209, 210, 439-446]. To date, no studies have reported the relationship between circulating levels of platelet-

derived EV and CT-1 plasma levels. Perhaps, this novel link between platelets, platelet-derived EV and CT-1 expression may improve our understanding of cardiac pathophysiology.

4.5. SUMMARY

This thesis chapter investigated the expression of CT-1 on platelets and platelet-derived EV. We found in vitro evidence that PEV bound CT-1 activated gp130 signaling leading to the activation of STAT 3 and ERK 1/2 but not Akt. Furthermore, we tested the hypothesis that CT-1 may be responsible for cytoprotective effects induced by PEV on endothelial cells *in vitro* and these could be mediated by STAT 3 and/or ERK 1/2.

CHAPTER 5

GENERAL DISCUSSION

5.1. GENERAL DISCUSSION

Maternal cardiovascular adaptions during pregnancy have been well described and include characteristic changes in cardiac morphology and function. However, the mechanisms that mediate these changes are still being elucidated but clearly require orchestrated communication between cells and tissues. Recently, immense interest has developed regarding the role of extracellular vesicles in cardiac physiology. In particular, exosomes have been proposed to stimulate beneficial signaling pathways in cardiovascular disease [447]. Furthermore, exosomes can ferry the intravesicular cargo (e.g. miRNAs) and protein through the blood stream and represent a potential mode of intercellular communication throughout the entire circulatory system [448]. Seminal studies conducted in our laboratory (and those of others) have demonstrated that the placent also releases extracellular vesicles (STB-EV) into the maternal circulation throughout gestation. In this thesis, we tested the hypothesis that STB-EV may have a role in cardiac specific changes seen in normal pregnancy and thereby linking the placenta to the cardiac changes seen in pregnancy.

5.1.1. Characterisation of STB-EV- bound CT-1

Following a systematic approach to identify potential cardiac specific molecules that might be deployed, we found CT-1, a pleiotropic cytokine known for its ability to induce cardiac hypertrophic and protective effects. In Chapter 2 of this thesis we demonstrated, for the first time, that this molecule was preferentially expressed on the placenta and was deployed on STB-EV. Furthermore, we showed that it was differentially expressed on STB-EX and

that it was co-localized with the specific placental marker, placental alkaline phosphatase (PLAP). More importantly, we demonstrated that STB-EX- bound CT-1 was biologically active and can induce intracellular signaling.

In our intracellular signaling studies, only the major known pathways were investigated. We recognize that there may well be other pathways involved in STB-EX- bound CT-1 signaling. These could, in theory, be tested using a Proteome Profiler™ Antibody Array which allows for the measurement of up to 119 proteins in a single sample. The problem with that approach is that vesicles carry multiple cargo which can technically activate several pathways. This would make it incredibly difficult to ascribe changes to the pathways to vesicles carrying CT-1 as being directly due to CT-1. Secondly, these profiler arrays are not sensitive enough to detect low abundant proteins and would therefore miss out on signaling pathways that are marginally activated. We therefore resolved to focus on key molecules involved in CT-1 signaling, viz. STAT 3, ERK 1/2 and Akt.

Activation of a signaling cascade is, however, not the only way that STB-EX might mediate their putative effects on their target cells. We demonstrated that endothelial cells and cardiac myocytes internalise STB-EX after one hour of treatment. Endocytosis of exosomes has been demonstrated in several studies and molecules such as clarithrin have been implicated [449]. However, it has been previously shown the gp130 and LIF receptor are endocytosed. This could present a novel mechanism by which CT-1 positive vesicles are internalised. It would be interest to see whether blocking gp130 would result in

the decrease in the uptake of vesicles by endothelial and cardiomyocytes, perhaps more specifically, whether pretreating vesicles with a CT-1 neutralising antibody would decrease the uptake of vesicles. There are, however, pitfalls to this, as quantitating vesicle uptake is challenging. Unless gp130/LIF-R endocytosis is the main player involved in vesicle uptake, subtle reduction in vesicle endocytosis may not be easily detected using conventional methods such as confocal microscopy.

We also investigated the effects on STB-EX-bound CT-1 on cardiomyocyte gene expression. Using a simple experiment in which we treated human coronary artery endothelial cells and rat cardiomyocytes and then compared the expression of key genes associated with CT-1. We determined that STB-EX would probably mediate their effects directly on cardiomyocytes versus an indirect effect i.e. through endothelial cells. Thus, in Chapter 3, we presented the findings of the microarray analysis of total RNA from human induced pluripotent stem cell–derived cardiomyocytes (hiPSC-CM) treated with CT-1 positive STB-EX, recombinant CT-1 or STB-EX pretreated with a CT-1 neutralising antibody. We demonstrated for the first time, that CT-1 positive STB-EX resulted in the activation of differentially expressed genes. When this data was further analysed using Ingenuity Pathway Analysis (IPA), we showed that STB-EX activated groups of genes that are involved in the physiological and pathophysiological processes of different organ systems including the cardiovascular system. Moreover, we validated the microarray data by RT-qPCR of key genes involved in cardiac physiology and pathophysiology. This analysis showed that indeed STB-EX resulted in the upregulation of three

genes viz. Thrombospondin -1, Endothelin 1, and ADAM17, and the down regulation of Caveolin -1. Most notably, we showed that the CT-1 present on the CT-1 positive vesicles may be involved in the induction of some, but not all gene changes.

5.1.2. Characterisation of PEV- bound CT-1

In Chapter 4, we demonstrated that CT-1 is expressed on platelet and platelet extracellular vesicles (PEV) upon platelet activation using similar methodologies described above. First, we localized the expression of CT-1 by immunocytochemistry in activated and inactivated platelets. Next we demonstrated the expression of CT-1 on platelets by Western blotting and flow cytometry and showed that it was co-expressed with CD41. It would be interesting to investigate whether CT-1 is co-localized with other platelet markers such as CD42 and CD62P to help determine a global assessment of CT-1 levels on platelets.

We then isolated platelet extracellular vesicles and confirmed that CT-1 was indeed deployed on them. Furthermore, we showed for the first time that PEV-bound CT-1 is biologically active, activates intracellular signaling of STAT 3 and ERK 1/2. Finally, we tested the cytoprotective effects of CT-1 on endothelial cells cultured in serum free medium, and we showed for the first time that recombinant CT-1 offers cytoprotective properties to endothelial cells. In confirmation of this, we also found that PEV increased endothelial cell death

which was markedly enhanced by the addition of CT-1 neutralising antibody, suggesting a regulatory role of PEV-bound CT-1 in endothelial cell survival.

5.1.3. Future work

In pregnancy, pathological cardiac remodeling is a known feature of preeclampsia; it would be interesting to see if we can optimize the measurement of vesicular levels of CT-1 in the plasma of healthy pregnancy and preeclampsia e.g. by flow cytometry or ELISA, to determine whether CT-1 levels can predict which patients would develop cardiovascular disease in pregnancy.

In Chapter 4 we reported that platelet extracellular vesicles are increased in a variety of cardiovascular conditions and that circulating CT-1 has also been modulated in those conditions. It would therefore be interesting to determine whether CT-1 levels could be directly correlated with vesicular levels of CT-1 in the plasma of patients with cardiac disease, and whether this would be of predictive value. The same caveats of identifying specific “vesicular” CT-1 in STB-EV would also apply here, and use of CD41 as a secondary, whilst immediately attractive, might deliver non-specific results.

Additionally, it would be most interesting to see if we can isolate CT-1 positive and negative vesicles and interrogate their cargo to determine the specific molecules that mediate their biological effects. This could be achieved using immunomagnetic beads coupled to an anti-placental alkaline phosphatase antibody (PLAP) antibody (in the case of STB-EV) or CD41 (in the case of

platelets) and to then use CT-1 coupled beads to pull all CT-1 positive vesicles. These could then be subjected to high throughput 'omics analysis.

Finally, having demonstrated that endothelial cells and cardiomyocytes internalize CT-1 positive vesicles, gp130/LIF-R might ultimately be exploited as a way of delivering therapeutic agents to endothelial cells and cardiac myocytes. Furthermore, it would also be interesting to learn whether administrating CT-1 positive vesicles would improve the cardiovascular performance in patients with poor cardiac outcomes in either the pregnant or non-pregnant state.

REFERENCES

1. Tan, E.K. and E.L. Tan, *Alterations in physiology and anatomy during pregnancy.* Best Pract Res Clin Obstet Gynaecol, 2013. **27**(6): p. 791-802.
2. Pritchard, J.A., *Changes in the blood volume during pregnancy and delivery.* Anesthesiology, 1965. **26**: p. 393-9.
3. Chesley, L.C., *Plasma and red cell volumes during pregnancy.* Am J Obstet Gynecol, 1972. **112**(3): p. 440-50.
4. Hytten, F., *Blood volume changes in normal pregnancy.* Clin Haematol, 1985. **14**(3): p. 601-12.
5. Pirani, B.B., D.M. Campbell, and I. MacGillivray, *Plasma volume in normal first pregnancy.* J Obstet Gynaecol Br Commonw, 1973. **80**(10): p. 884-7.
6. Bernstein, I.M., W. Ziegler, and G.J. Badger, *Plasma volume expansion in early pregnancy.* Obstet Gynecol, 2001. **97**(5 Pt 1): p. 669-72.
7. Finn, W.L., et al., *Sodium and volume dysregulation after apparently normal pregnancy is suggested by abnormal levels of atrial natriuretic peptide, renin and aldosterone.* Clin Exp Pharmacol Physiol, 1991. **18**(5): p. 269-73.
8. Milman, N., et al., *Serum erythropoietin during normal pregnancy: relationship to hemoglobin and iron status markers and impact of iron supplementation in a longitudinal, placebo-controlled study on 118 women.* Int J Hematol, 1997. **66**(2): p. 159-68.
9. Zeeman, G.G., F.G. Cunningham, and J.A. Pritchard, *The magnitude of hemoconcentration with eclampsia.* Hypertens Pregnancy, 2009. **28**(2): p. 127-37.
10. Silversides, C.K. and J.M. Colman, *Physiological Changes in Pregnancy*, in *Heart Disease in Pregnancy*. 2007, Blackwell Publishing. p. 6-17.
11. Vincent, J.L., *Understanding cardiac output.* Crit Care, 2008. **12**(4): p. 174.
12. Robson, S.C., et al., *Serial study of factors influencing changes in cardiac output during human pregnancy.* Am J Physiol, 1989. **256**(4 Pt 2): p. H1060-5.
13. Mabie, W.C., et al., *A longitudinal study of cardiac output in normal human pregnancy.* Am J Obstet Gynecol, 1994. **170**(3): p. 849-56.
14. Ouzounian, J.G. and U. Elkayam, *Physiologic changes during normal pregnancy and delivery.* Cardiol Clin, 2012. **30**(3): p. 317-29.
15. Gilson, G.J., et al., *Changes in hemodynamics, ventricular remodeling, and ventricular contractility during normal pregnancy: a longitudinal study.* Obstet Gynecol, 1997. **89**(6): p. 957-62.
16. Buttrick, P.M., et al., *Effects of pregnancy on cardiac function and myosin enzymology in the rat.* Am J Physiol, 1987. **252**(4 Pt 2): p. H846-50.
17. Umar, S., et al., *Cardiac structural and hemodynamic changes associated with physiological heart hypertrophy of pregnancy are reversed postpartum.* J Appl Physiol (1985), 2012. **113**(8): p. 1253-9.

18. Geva, T., et al., *Effects of physiologic load of pregnancy on left ventricular contractility and remodeling.* Am Heart J, 1997. **133**(1): p. 53-9.
19. Clark, S.L., et al., *Central hemodynamic assessment of normal term pregnancy.* Am J Obstet Gynecol, 1989. **161**(6 Pt 1): p. 1439-42.
20. Duvekot, J.J., et al., *Early pregnancy changes in hemodynamics and volume homeostasis are consecutive adjustments triggered by a primary fall in systemic vascular tone.* Am J Obstet Gynecol, 1993. **169**(6): p. 1382-92.
21. Osol, G. and M. Mandala, *Maternal uterine vascular remodeling during pregnancy.* Physiology (Bethesda), 2009. **24**: p. 58-71.
22. Carbillon, L., M. Uzan, and S. Uzan, *Pregnancy, vascular tone, and maternal hemodynamics: a crucial adaptation.* Obstet Gynecol Surv, 2000. **55**(9): p. 574-81.
23. Conrad, K.P., *Maternal vasodilation in pregnancy: the emerging role of relaxin.* Am J Physiol Regul Integr Comp Physiol, 2011. **301**(2): p. R267-75.
24. Liu, L.X. and Z. Arany, *Maternal cardiac metabolism in pregnancy.* Cardiovasc Res, 2014. **101**(4): p. 545-53.
25. Cohn, J.N., R. Ferrari, and N. Sharpe, *Cardiac remodeling--concepts and clinical implications: a consensus paper from an international forum on cardiac remodeling. Behalf of an International Forum on Cardiac Remodeling.* J Am Coll Cardiol, 2000. **35**(3): p. 569-82.
26. Melchiorre, K., R. Sharma, and B. Thilaganathan, *Cardiac structure and function in normal pregnancy.* Curr Opin Obstet Gynecol, 2012. **24**(6): p. 413-21.
27. Mone, S.M., S.P. Sanders, and S.D. Colan, *Control mechanisms for physiological hypertrophy of pregnancy.* Circulation, 1996. **94**(4): p. 667-72.
28. Grossman, W., D. Jones, and L.P. McLaurin, *Wall stress and patterns of hypertrophy in the human left ventricle.* J Clin Invest, 1975. **56**(1): p. 56-64.
29. Li, J., et al., *New frontiers in heart hypertrophy during pregnancy.* Am J Cardiovasc Dis, 2012. **2**(3): p. 192-207.
30. Hutcheon, J.A., S. Lisonkova, and K.S. Joseph, *Epidemiology of pre-eclampsia and the other hypertensive disorders of pregnancy.* Best Pract Res Clin Obstet Gynaecol, 2011. **25**(4): p. 391-403.
31. Ghossein-Doha, C., et al., *Hypertension after preeclampsia is preceded by changes in cardiac structure and function.* Hypertension, 2013. **62**(2): p. 382-90.
32. Melchiorre, K., et al., *Maternal cardiac dysfunction and remodeling in women with preeclampsia at term.* Hypertension, 2011. **57**(1): p. 85-93.
33. Nag, A.C., *Study of non-muscle cells of the adult mammalian heart: a fine structural analysis and distribution.* Cytobios, 1980. **28**(109): p. 41-61.
34. Zak, R., *Development and proliferative capacity of cardiac muscle cells.* Circ Res, 1974. **35**(2): p. suppl II:17-26.
35. Popescu, L.M., et al., *Insights into the interstitium of ventricular myocardium: interstitial Cajal-like cells (ICLC).* J Cell Mol Med, 2006. **10**(2): p. 429-58.

36. Soonpaa, M.H., et al., *Cardiomyocyte DNA synthesis and binucleation during murine development.* Am J Physiol, 1996. **271**(5 Pt 2): p. H2183-9.
37. Booz, G.W., *Putting the brakes on cardiac hypertrophy: exploiting the NO-cGMP counter-regulatory system.* Hypertension, 2005. **45**(3): p. 341-6.
38. Dorn, G.W. and T. Force, *Protein kinase cascades in the regulation of cardiac hypertrophy.* J Clin Invest, 2005. **115**(3): p. 527-37.
39. Molkentin, J.D., *Calcineurin-NFAT signaling regulates the cardiac hypertrophic response in coordination with the MAPKs.* Cardiovasc Res, 2004. **63**(3): p. 467-75.
40. Zhang, T. and J.H. Brown, *Role of Ca2+/calmodulin-dependent protein kinase II in cardiac hypertrophy and heart failure.* Cardiovasc Res, 2004. **63**(3): p. 476-86.
41. Arai, M., et al., *Endothelin-1 and its binding sites are upregulated in pressure overload cardiac hypertrophy.* Am J Physiol, 1995. **268**(5 Pt 2): p. H2084-91.
42. Rapacciuolo, A., et al., *Important role of endogenous norepinephrine and epinephrine in the development of in vivo pressure-overload cardiac hypertrophy.* J Am Coll Cardiol, 2001. **38**(3): p. 876-82.
43. Schunkert, H., et al., *Increased rat cardiac angiotensin converting enzyme activity and mRNA expression in pressure overload left ventricular hypertrophy. Effects on coronary resistance, contractility, and relaxation.* J Clin Invest, 1990. **86**(6): p. 1913-20.
44. Mehta, P.K. and K.K. Griendling, *Angiotensin II cell signaling: physiological and pathological effects in the cardiovascular system.* Am J Physiol Cell Physiol, 2007. **292**(1): p. C82-97.
45. Gray, M.O., et al., *Angiotensin II stimulates cardiac myocyte hypertrophy via paracrine release of TGF-beta 1 and endothelin-1 from fibroblasts.* Cardiovasc Res, 1998. **40**(2): p. 352-63.
46. Serneri, G.G., et al., *Cardiac angiotensin II formation in the clinical course of heart failure and its relationship with left ventricular function.* Circ Res, 2001. **88**(9): p. 961-8.
47. Reiss, K., et al., *Overexpression of insulin-like growth factor-1 in the heart is coupled with myocyte proliferation in transgenic mice.* Proc Natl Acad Sci U S A, 1996. **93**(16): p. 8630-5.
48. Delaughter, M.C., et al., *Local insulin-like growth factor I expression induces physiologic, then pathologic, cardiac hypertrophy in transgenic mice.* Faseb j, 1999. **13**(14): p. 1923-9.
49. Shioi, T., et al., *The conserved phosphoinositide 3-kinase pathway determines heart size in mice.* Embo j, 2000. **19**(11): p. 2537-48.
50. Koziris, L.P., et al., *Serum levels of total and free IGF-I and IGFBP-3 are increased and maintained in long-term training.* J Appl Physiol (1985), 1999. **86**(4): p. 1436-42.
51. Perrino, C., et al., *Intermittent pressure overload triggers hypertrophy-independent cardiac dysfunction and vascular rarefaction.* J Clin Invest, 2006. **116**(6): p. 1547-60.
52. Sakamoto, M., et al., *Upregulation of heat shock transcription factor 1 plays a critical role in adaptive cardiac hypertrophy.* Circ Res, 2006. **99**(12): p. 1411-8.

53. Bedotto, J.B., et al., *Cardiac hypertrophy induced by thyroid hormone is independent of loading conditions and beta adrenoceptor blockade.* J Pharmacol Exp Ther, 1989. **248**(2): p. 632-6.
54. Kodama, H., et al., *Leukemia inhibitory factor, a potent cardiac hypertrophic cytokine, activates the JAK/STAT pathway in rat cardiomyocytes.* Circ Res, 1997. **81**(5): p. 656-63.
55. Pellegrini, S. and I. Dusanter-Fourt, *The structure, regulation and function of the Janus kinases (JAKs) and the signal transducers and activators of transcription (STATs).* Eur J Biochem, 1997. **248**(3): p. 615-33.
56. McMullen, J.R. and P.Y. Jay, *PI3K(p110alpha) inhibitors as anti-cancer agents: minding the heart.* Cell Cycle, 2007. **6**(8): p. 910-3.
57. Gonzalez, A.M., et al., *Hypertrophy signaling during peripartum cardiac remodeling.* Am J Physiol Heart Circ Physiol, 2007. **293**(5): p. H3008-13.
58. Hilfiker-Kleiner, D., et al., *A cathepsin D-cleaved 16 kDa form of prolactin mediates postpartum cardiomyopathy.* Cell, 2007. **128**(3): p. 589-600.
59. Eghbali, M., et al., *Molecular and functional signature of heart hypertrophy during pregnancy.* Circ Res, 2005. **96**(11): p. 1208-16.
60. Jankowski, M., et al., *Pregnancy alters nitric oxide synthase and natriuretic peptide systems in the rat left ventricle.* J Endocrinol, 2005. **184**(1): p. 209-17.
61. Harrison, P., C. Gardiner, and I.L. Sargent, *Extracellular Vesicles in Health and Disease*. 2014: Pan Stanford.
62. Raposo, G. and W. Stoorvogel, *Extracellular vesicles: Exosomes, microvesicles, and friends.* The Journal of Cell Biology, 2013. **200**(4): p. 373-383.
63. Raposo, G. and W. Stoorvogel, *Extracellular vesicles: exosomes, microvesicles, and friends.* J Cell Biol, 2013. **200**(4): p. 373-83.
64. Conde-Vancells, J., et al., *Characterization and comprehensive proteome profiling of exosomes secreted by hepatocytes.* J Proteome Res, 2008. **7**(12): p. 5157-66.
65. Yuana, Y., et al., *Atomic force microscopy: a novel approach to the detection of nanosized blood microparticles.* J Thromb Haemost, 2010. **8**(2): p. 315-23.
66. Dragovic, R.A., et al., *Sizing and phenotyping of cellular vesicles using Nanoparticle Tracking Analysis.* Nanomedicine, 2011. **7**(6): p. 780-8.
67. van der Pol, E., et al., *Recent developments in the nomenclature, presence, isolation, detection and clinical impact of extracellular vesicles.* J Thromb Haemost, 2016. **14**(1): p. 48-56.
68. Colombo, M., et al., *Analysis of ESCRT functions in exosome biogenesis, composition and secretion highlights the heterogeneity of extracellular vesicles.* J Cell Sci, 2013. **126**(Pt 24): p. 5553-65.
69. Kalra, H., G.P.C. Drummen, and S. Mathivanan, *Focus on Extracellular Vesicles: Introducing the Next Small Big Thing.* Int J Mol Sci, 2016. **17**(2).
70. Henne, W.M., N.J. Buchkovich, and S.D. Emr, *The ESCRT pathway.* Dev Cell, 2011. **21**(1): p. 77-91.

71. Stuffers, S., et al., *Multivesicular endosome biogenesis in the absence of ESCRTs.* Traffic, 2009. **10**(7): p. 925-37.
72. Stenmark, H., *Rab GTPases as coordinators of vesicle traffic.* Nat Rev Mol Cell Biol, 2009. **10**(8): p. 513-25.
73. Savina, A., M. Vidal, and M.I. Colombo, *The exosome pathway in K562 cells is regulated by Rab11.* J Cell Sci, 2002. **115**(Pt 12): p. 2505-15.
74. Ostrowski, M., et al., *Rab27a and Rab27b control different steps of the exosome secretion pathway.* Nat Cell Biol, 2010. **12**(1): p. 19-30; sup pp 1-13.
75. Hsu, C., et al., *Regulation of exosome secretion by Rab35 and its GTPase-activating proteins TBC1D10A-C.* J Cell Biol, 2010. **189**(2): p. 223-32.
76. Baietti, M.F., et al., *Syndecan-syntenin-ALIX regulates the biogenesis of exosomes.* Nat Cell Biol, 2012. **14**(7): p. 677-85.
77. Friand, V., G. David, and P. Zimmermann, *Syntenin and syndecan in the biogenesis of exosomes.* Biol Cell, 2015. **107**(10): p. 331-41.
78. Colombo, M., G. Raposo, and C. Thery, *Biogenesis, secretion, and intercellular interactions of exosomes and other extracellular vesicles.* Annu Rev Cell Dev Biol, 2014. **30**: p. 255-89.
79. Thery, C., M. Ostrowski, and E. Segura, *Membrane vesicles as conveyors of immune responses.* Nat Rev Immunol, 2009. **9**(8): p. 581-93.
80. Pasquet, J.M., J. Dachary-Prigent, and A.T. Nurden, *Calcium influx is a determining factor of calpain activation and microparticle formation in platelets.* Eur J Biochem, 1996. **239**(3): p. 647-54.
81. Pizzirani, C., et al., *Stimulation of P2 receptors causes release of IL-1beta-loaded microvesicles from human dendritic cells.* Blood, 2007. **109**(9): p. 3856-64.
82. Del Conde, I., et al., *Tissue-factor-bearing microvesicles arise from lipid rafts and fuse with activated platelets to initiate coagulation.* Blood, 2005. **106**(5): p. 1604-11.
83. Zwaal, R.F., et al., *Loss of membrane phospholipid asymmetry during activation of blood platelets and sickled red cells; mechanisms and physiological significance.* Mol Cell Biochem, 1989. **91**(1-2): p. 23-31.
84. Bevers, E.M., P. Comfurius, and R.F. Zwaal, *Changes in membrane phospholipid distribution during platelet activation.* Biochim Biophys Acta, 1983. **736**(1): p. 57-66.
85. Fujii, T., et al., *TMEM16F is required for phosphatidylserine exposure and microparticle release in activated mouse platelets.* Proc Natl Acad Sci U S A, 2015. **112**(41): p. 12800-5.
86. Suzuki, J., et al., *Calcium-dependent phospholipid scrambling by TMEM16F.* Nature, 2010. **468**(7325): p. 834-8.
87. Gupta, N., et al., *Proteasome proteolysis supports stimulated platelet function and thrombosis.* Arterioscler Thromb Vasc Biol, 2014. **34**(1): p. 160-8.
88. Muralidharan-Chari, V., et al., *ARF6-regulated shedding of tumor cell-derived plasma membrane microvesicles.* Curr Biol, 2009. **19**(22): p. 1875-85.

89. Di Vizio, D., et al., *Oncosome formation in prostate cancer: association with a region of frequent chromosomal deletion in metastatic disease.* Cancer Res, 2009. **69**(13): p. 5601-9.
90. Bianco, F., et al., *Acid sphingomyelinase activity triggers microparticle release from glial cells.* Embo j, 2009. **28**(8): p. 1043-54.
91. Berckmans, R.J., et al., *Cell-derived microparticles in synovial fluid from inflamed arthritic joints support coagulation exclusively via a factor VII-dependent mechanism.* Arthritis Rheum, 2002. **46**(11): p. 2857-66.
92. Kerr, J.F., A.H. Wyllie, and A.R. Currie, *Apoptosis: a basic biological phenomenon with wide-ranging implications in tissue kinetics.* Br J Cancer, 1972. **26**(4): p. 239-57.
93. Hristov, M., et al., *Apoptotic bodies from endothelial cells enhance the number and initiate the differentiation of human endothelial progenitor cells in vitro.* Blood, 2004. **104**(9): p. 2761-6.
94. Thery, C., et al., *Proteomic analysis of dendritic cell-derived exosomes: a secreted subcellular compartment distinct from apoptotic vesicles.* J Immunol, 2001. **166**(12): p. 7309-18.
95. Bilyy, R.O., et al., *Macrophages discriminate glycosylation patterns of apoptotic cell-derived microparticles.* J Biol Chem, 2012. **287**(1): p. 496-503.
96. Xu, R., et al., *Extracellular vesicle isolation and characterization: toward clinical application.* J Clin Invest, 2016. **126**(4): p. 1152-62.
97. Dragovic, R.A., et al., *Isolation of syncytiotrophoblast microvesicles and exosomes and their characterisation by multicolour flow cytometry and fluorescence Nanoparticle Tracking Analysis.* Methods, 2015. **87**: p. 64-74.
98. Livshits, M.A., et al., *Isolation of exosomes by differential centrifugation: Theoretical analysis of a commonly used protocol.* Sci Rep, 2015. **5**: p. 17319.
99. Redman, C.W., et al., *Review: Does size matter? Placental debris and the pathophysiology of pre-eclampsia.* Placenta, 2012. **33 Suppl**: p. S48-54.
100. Burton, G.J. and A.L. Fowden, *The placenta: a multifaceted, transient organ.* Philos Trans R Soc Lond B Biol Sci, 2015. **370**(1663): p. 20140066.
101. Attwood, H.D. and W.W. Park, *Embolism to the lungs by trophoblast.* J Obstet Gynaecol Br Commonw, 1961. **68**: p. 611-7.
102. Askelund, K.J. and L.W. Chamley, *Trophoblast deportation part I: review of the evidence demonstrating trophoblast shedding and deportation during human pregnancy.* Placenta, 2011. **32**(10): p. 716-23.
103. Tannetta, D., et al., *Extracellular vesicles and reproduction–promotion of successful pregnancy.* Cell Mol Immunol, 2014. **11**(6): p. 548-63.
104. Johansen, M., et al., *Trophoblast deportation in human pregnancy--its relevance for pre-eclampsia.* Placenta, 1999. **20**(7): p. 531-9.
105. Germain, S.J., et al., *Systemic inflammatory priming in normal pregnancy and preeclampsia: the role of circulating syncytiotrophoblast microparticles.* J Immunol, 2007. **178**(9): p. 5949-56.
106. Sabapatha, A., C. Gercel-Taylor, and D.D. Taylor, *Specific isolation of placenta-derived exosomes from the circulation of pregnant women and*

their immunoregulatory consequences. Am J Reprod Immunol, 2006. **56**(5-6): p. 345-55.
107. Salomon, C., et al., *A gestational profile of placental exosomes in maternal plasma and their effects on endothelial cell migration.* PLoS One, 2014. **9**(6): p. e98667.
108. Reddy, A., et al., *The effect of labour and placental separation on the shedding of syncytiotrophoblast microparticles, cell-free DNA and mRNA in normal pregnancy and pre-eclampsia.* Placenta, 2008. **29**(11): p. 942-9.
109. Tannetta, D.S., et al., *Characterisation of syncytiotrophoblast vesicles in normal pregnancy and pre-eclampsia: expression of Flt-1 and endoglin.* PLoS One, 2013. **8**(2): p. e56754.
110. Southcombe, J., et al., *The immunomodulatory role of syncytiotrophoblast microvesicles.* PLoS One, 2011. **6**(5): p. e20245.
111. Cronqvist, T., et al., *Syncytiotrophoblast derived extracellular vesicles transfer functional placental miRNAs to primary human endothelial cells.* Sci Rep, 2017. **7**(1): p. 4558.
112. Smarason, A.K., et al., *The effect of placental syncytiotrophoblast microvillous membranes from normal and pre-eclamptic women on the growth of endothelial cells in vitro.* Br J Obstet Gynaecol, 1993. **100**(10): p. 943-9.
113. Gupta, A.K., et al., *A comparative study of the effect of three different syncytiotrophoblast micro-particles preparations on endothelial cells.* Placenta, 2005. **26**(1): p. 59-66.
114. Hoegh, A.M., et al., *Effect of syncytiotrophoblast microvillous membrane treatment on gene expression in human umbilical vein endothelial cells.* Bjog, 2006. **113**(11): p. 1270-9.
115. Cockell, A.P., et al., *Human placental syncytiotrophoblast microvillous membranes impair maternal vascular endothelial function.* Br J Obstet Gynaecol, 1997. **104**(2): p. 235-40.
116. Wei, J., et al., *Trophoblastic debris modifies endothelial cell transcriptome in vitro: a mechanism by which fetal cells might control maternal responses to pregnancy.* Sci Rep, 2016. **6**: p. 30632.
117. Gupta, A.K., et al., *Syncytiotrophoblast micro-particles do not induce apoptosis in peripheral T lymphocytes, but differ in their activity depending on the mode of preparation.* J Reprod Immunol, 2005. **68**(1-2): p. 15-26.
118. Thibault, G., et al., *The inhibitory effect of human syncytiotrophoblast plasma membrane vesicles on in vitro lymphocyte proliferation is associated with reduced interleukin 2 receptor expression.* Cell Immunol, 1991. **138**(1): p. 165-74.
119. von Dadelszen, P., G. Hurst, and C.W. Redman, *Supernatants from co-cultured endothelial cells and syncytiotrophoblast microvillous membranes activate peripheral blood leukocytes in vitro.* Hum Reprod, 1999. **14**(4): p. 919-24.
120. Messerli, M., et al., *Feto-maternal interactions in pregnancies: placental microparticles activate peripheral blood monocytes.* Placenta, 2010. **31**(2): p. 106-12.

121. Pennica, D., et al., *Expression cloning of cardiotrophin 1, a cytokine that induces cardiac myocyte hypertrophy.* Proc Natl Acad Sci U S A, 1995. **92**(4): p. 1142-6.
122. Pennica, D., et al., *Human cardiotrophin-1: protein and gene structure, biological and binding activities, and chromosomal localization.* Cytokine, 1996. **8**(3): p. 183-9.
123. Lopez-Yoldi, M., M.J. Moreno-Aliaga, and M. Bustos, *Cardiotrophin-1: A multifaceted cytokine.* Cytokine Growth Factor Rev, 2015.
124. Ishikawa, M., et al., *cDNA cloning of rat cardiotrophin-1 (CT-1): augmented expression of CT-1 gene in ventricle of genetically hypertensive rats.* Biochem Biophys Res Commun, 1996. **219**(2): p. 377-81.
125. Sheng, Z., et al., *Cardiotrophin-1 displays early expression in the murine heart tube and promotes cardiac myocyte survival.* Development, 1996. **122**(2): p. 419-28.
126. Song, K., et al., *Plasma cardiotrophin-1 levels are associated with hypertensive heart disease: a meta-analysis.* J Clin Hypertens (Greenwich), 2014. **16**(9): p. 686-92.
127. Limongelli, G., et al., *Cardiotrophin-1 and TNF-alpha circulating levels at rest and during cardiopulmonary exercise test in athletes and healthy individuals.* Cytokine, 2010. **50**(3): p. 245-7.
128. Funamoto, M., et al., *Isolation and characterization of the murine cardiotrophin-1 gene: expression and norepinephrine-induced transcriptional activation.* J Mol Cell Cardiol, 2000. **32**(7): p. 1275-84.
129. Pennica, D., W.I. Wood, and K.R. Chien, *Cardiotrophin-1: a multifunctional cytokine that signals via LIF receptor-gp 130 dependent pathways.* Cytokine Growth Factor Rev, 1996. **7**(1): p. 81-91.
130. Natal, C., et al., *Cardiotrophin-1 is expressed in adipose tissue and upregulated in the metabolic syndrome.* Am J Physiol Endocrinol Metab, 2008. **294**(1): p. E52-60.
131. Jougasaki, M., et al., *Cardiotrophin-1 stimulates endothelin-1 via gp130 in vascular endothelial cells.* Peptides, 2002. **23**(8): p. 1441-7.
132. Jougasaki, M., et al., *Augmented cardiac cardiotrophin-1 in experimental congestive heart failure.* Circulation, 2000. **101**(1): p. 14-7.
133. Kuwahara, K., et al., *Involvement of cardiotrophin-1 in cardiac myocyte-nonmyocyte interactions during hypertrophy of rat cardiac myocytes in vitro.* Circulation, 1999. **100**(10): p. 1116-24.
134. Asai, S., et al., *The heart is a source of circulating cardiotrophin-1 in humans.* Biochem Biophys Res Commun, 2000. **279**(2): p. 320-3.
135. Pan, J., et al., *Involvement of gp130-mediated signaling in pressure overload-induced activation of the JAK/STAT pathway in rodent heart.* Heart Vessels, 1998. **13**(4): p. 199-208.
136. Pan, J., et al., *Mechanical stretch activates the JAK/STAT pathway in rat cardiomyocytes.* Circ Res, 1999. **84**(10): p. 1127-36.
137. Pemberton, C.J., et al., *Plasma cardiotrophin-1 is elevated in human hypertension and stimulated by ventricular stretch.* Cardiovasc Res, 2005. **68**(1): p. 109-17.
138. Hishinuma, S., et al., *Hypoxic stress induces cardiotrophin-1 expression in cardiac myocytes.* Biochem Biophys Res Commun, 1999. **264**(2): p. 436-40.

139. Ateghang, B., et al., *Regulation of cardiotrophin-1 expression in mouse embryonic stem cells by HIF-1alpha and intracellular reactive oxygen species.* J Cell Sci, 2006. **119**(Pt 6): p. 1043-52.
140. Kishimoto, T., et al., *Interleukin-6 family of cytokines and gp130.* Blood, 1995. **86**(4): p. 1243-54.
141. Hibi, M., et al., *Molecular cloning and expression of an IL-6 signal transducer, gp130.* Cell, 1990. **63**(6): p. 1149-57.
142. Narazaki, M., et al., *Soluble forms of the interleukin-6 signal-transducing receptor component gp130 in human serum possessing a potential to inhibit signals through membrane-anchored gp130.* Blood, 1993. **82**(4): p. 1120-6.
143. Gearing, D.P., et al., *Leukemia inhibitory factor receptor is structurally related to the IL-6 signal transducer, gp130.* Embo j, 1991. **10**(10): p. 2839-48.
144. Gearing, D., et al., *Leukemia inhibitory factor receptor is structurally related to the IL-6 signal transducer, gp130.* The EMBO journal, 1991. **10**(10): p. 2839.
145. Pennica, D., et al., *Cardiotrophin-1. Biological activities and binding to the leukemia inhibitory factor receptor/gp130 signaling complex.* J Biol Chem, 1995. **270**(18): p. 10915-22.
146. Wollert, K.C., et al., *Cardiotrophin-1 activates a distinct form of cardiac muscle cell hypertrophy. Assembly of sarcomeric units in series VIA gp130/leukemia inhibitory factor receptor-dependent pathways.* J Biol Chem, 1996. **271**(16): p. 9535-45.
147. Robledo, O., et al., *Signaling of the cardiotrophin-1 receptor. Evidence for a third receptor component.* J Biol Chem, 1997. **272**(8): p. 4855-63.
148. Cheng, J.G., D. Pennica, and P.H. Patterson, *Cardiotrophin-1 induces the same neuropeptides in sympathetic neurons as do neuropoietic cytokines.* J Neurochem, 1997. **69**(6): p. 2278-84.
149. Kurdi, M. and G.W. Booz, *Jak inhibition, but not Stat1 knockdown, blocks the synergistic effect of IFN-gamma on Fas-induced apoptosis of A549 human non-small cell lung cancer cells.* J Interferon Cytokine Res, 2007. **27**(1): p. 23-31.
150. Kumar, G., et al., *Involvement of Janus kinases, p52shc, Raf-1, and MEK-1 in the IL-6-induced mitogen-activated protein kinase cascade of a growth-responsive B cell line.* J Immunol, 1994. **153**(10): p. 4436-47.
151. Nakafuku, M., T. Satoh, and Y. Kaziro, *Differentiation factors, including nerve growth factor, fibroblast growth factor, and interleukin-6, induce an accumulation of an active Ras.GTP complex in rat pheochromocytoma PC12 cells.* J Biol Chem, 1992. **267**(27): p. 19448-54.
152. Sheng, Z., et al., *Cardiotrophin 1 (CT-1) inhibition of cardiac myocyte apoptosis via a mitogen-activated protein kinase-dependent pathway. Divergence from downstream CT-1 signals for myocardial cell hypertrophy.* J Biol Chem, 1997. **272**(9): p. 5783-91.
153. Takahashi, N., et al., *Hypertrophic responses to cardiotrophin-1 are not mediated by STAT3, but via a MEK5-ERK5 pathway in cultured cardiomyocytes.* J Mol Cell Cardiol, 2005. **38**(1): p. 185-92.

154. Li, Y.J., et al., *Crosstalk between ERK1/2 and STAT3 in the modulation of cardiomyocyte hypertrophy induced by cardiotrophin-1.* Chin Med J (Engl), 2004. **117**(8): p. 1135-42.
155. Tian, Z.J., et al., *Different contributions of STAT3, ERK1/2, and PI3-K signaling to cardiomyocyte hypertrophy by cardiotrophin-1.* Acta Pharmacol Sin, 2004. **25**(9): p. 1157-64.
156. He-nan, Z., et al., *Relation of Cardiotrophin-1 (CT-1) and cardiac transcription factor GATA4 expression in rat's cardiac myocytes hypertrophy and apoptosis.* Pathol Res Pract, 2009. **205**(9): p. 615-25.
157. Ochiai, W., et al., *Astrocyte differentiation of fetal neuroepithelial cells involving cardiotrophin-1-induced activation of STAT3.* Cytokine, 2001. **14**(5): p. 264-71.
158. Barnabe-Heider, F., et al., *Evidence that embryonic neurons regulate the onset of cortical gliogenesis via cardiotrophin-1.* Neuron, 2005. **48**(2): p. 253-65.
159. Oppenheim, R.W., et al., *Cardiotrophin-1, a muscle-derived cytokine, is required for the survival of subpopulations of developing motoneurons.* J Neurosci, 2001. **21**(4): p. 1283-91.
160. Oberle, S., et al., *Loss of leukemia inhibitory factor receptor beta or cardiotrophin-1 causes similar deficits in preganglionic sympathetic neurons and adrenal medulla.* J Neurosci, 2006. **26**(6): p. 1823-32.
161. Bordet, T., et al., *Adenoviral cardiotrophin-1 gene transfer protects pmn mice from progressive motor neuronopathy.* J Clin Invest, 1999. **104**(8): p. 1077-85.
162. Wen, T.C., et al., *Cardiotrophin-1 protects cortical neuronal cells against free radical-induced injuries in vitro.* Neurosci Lett, 2005. **387**(1): p. 38-42.
163. Sola, A., et al., *Animal models of neonatal stroke and response to erythropoietin and cardiotrophin-1.* Int J Dev Neurosci, 2008. **26**(1): p. 27-35.
164. Moreno-Aliaga, M.J., et al., *Cardiotrophin-1 is a key regulator of glucose and lipid metabolism.* Cell Metab, 2011. **14**(2): p. 242-53.
165. Lopez-Yoldi, M., et al., *Cardiotrophin-1 Regulates Adipokine Production in 3T3-L1 Adipocytes and Adipose Tissue From Obese Mice.* J Cell Physiol, 2017. **232**(9): p. 2469-2477.
166. Zvonic, S., et al., *Effects of cardiotrophin on adipocytes.* J Biol Chem, 2004. **279**(46): p. 47572-9.
167. Peters, M., et al., *A new hepatocyte stimulating factor: cardiotrophin-1 (CT-1).* FEBS Lett, 1995. **372**(2-3): p. 177-80.
168. Beraza, N., et al., *Interplay among cardiotrophin-1, prostaglandins, and vascular endothelial growth factor in rat liver regeneration.* Hepatology, 2005. **41**(3): p. 460-9.
169. Iniguez, M., et al., *Cardiotrophin-1 defends the liver against ischemia-reperfusion injury and mediates the protective effect of ischemic preconditioning.* J Exp Med, 2006. **203**(13): p. 2809-15.
170. Marques, J.M., et al., *Cardiotrophin-1 is an essential factor in the natural defense of the liver against apoptosis.* Hepatology, 2007. **45**(3): p. 639-48.

171. Tunon, M.J., et al., *Cardiotrophin-1 promotes a high survival rate in rabbits with lethal fulminant hepatitis of viral origin.* J Virol, 2011. **85**(24): p. 13124-32.
172. Ho, D.W., et al., *Therapeutic potential of cardiotrophin 1 in fulminant hepatic failure: dual roles in antiapoptosis and cell repair.* Arch Surg, 2006. **141**(11): p. 1077-84; discussion 1084.
173. Yang, Z.F., et al., *Cardiotrophin-1 enhances regeneration of cirrhotic liver remnant after hepatectomy through promotion of angiogenesis and cell proliferation.* Liver Int, 2008. **28**(5): p. 622-31.
174. Garcia-Cenador, M.B., et al., *Cardiotrophin-1 administration protects from ischemia-reperfusion renal injury and inflammation.* Transplantation, 2013. **96**(12): p. 1034-42.
175. Song, Y., et al., *Photoreceptor protection by cardiotrophin-1 in transgenic rats with the rhodopsin mutation s334ter.* Invest Ophthalmol Vis Sci, 2003. **44**(9): p. 4069-75.
176. Walker, E.C., et al., *Cardiotrophin-1 is an osteoclast-derived stimulus of bone formation required for normal bone remodeling.* J Bone Miner Res, 2008. **23**(12): p. 2025-32.
177. Nishikawa, J., et al., *Increase of Cardiotrophin-1 immunoreactivity in regenerating and overloaded but not denervated muscles of rats.* Neuropathology, 2005. **25**(1): p. 54-65.
178. Railson, J.E., et al., *Cardiotrophin-1 and urocortin cause protection by the same pathway and hypertrophy via distinct pathways in cardiac myocytes.* Cytokine, 2002. **17**(5): p. 243-53.
179. Jin, H., et al., *In vivo effects of cardiotrophin-1.* Cytokine, 1996. **8**(12): p. 920-6.
180. Jamshidi, Y., et al., *Signal-transduction pathways involved in the hypertrophic effect of hsp56 in neonatal cardiomyocytes.* J Mol Cell Cardiol, 2004. **36**(3): p. 381-92.
181. Lopez, N., J. Diez, and M.A. Fortuno, *Characterization of the protective effects of cardiotrophin-1 against non-ischemic death stimuli in adult cardiomyocytes.* Cytokine, 2005. **30**(5): p. 282-92.
182. Hirota, H., et al., *Loss of a gp130 cardiac muscle cell survival pathway is a critical event in the onset of heart failure during biomechanical stress.* Cell, 1999. **97**(2): p. 189-98.
183. Stephanou, A., et al., *Cardiotrophin-1 induces heat shock protein accumulation in cultured cardiac cells and protects them from stressful stimuli.* J Mol Cell Cardiol, 1998. **30**(4): p. 849-55.
184. Heads, R.J., D.S. Latchman, and D.M. Yellon, *Stable high level expression of a transfected human HSP70 gene protects a heart-derived muscle cell line against thermal stress.* J Mol Cell Cardiol, 1994. **26**(6): p. 695-9.
185. Cumming, D.V., et al., *Differential protection of primary rat cardiocytes by transfection of specific heat stress proteins.* J Mol Cell Cardiol, 1996. **28**(12): p. 2343-9.
186. Kuwahara, K., et al., *Cardiotrophin-1 phosphorylates akt and BAD, and prolongs cell survival via a PI3K-dependent pathway in cardiac myocytes.* J Mol Cell Cardiol, 2000. **32**(8): p. 1385-94.

187. Zha, J., et al., *Serine phosphorylation of death agonist BAD in response to survival factor results in binding to 14-3-3 not BCL-X(L).* Cell, 1996. **87**(4): p. 619-28.
188. del Peso, L., et al., *Interleukin-3-induced phosphorylation of BAD through the protein kinase Akt.* Science, 1997. **278**(5338): p. 687-9.
189. Ghosh, S., et al., *Cardiotrophin-1 protects the human myocardium from ischemic injury. Comparison with the first and second window of protection by ischemic preconditioning.* Cardiovasc Res, 2000. **48**(3): p. 440-7.
190. Brar, B.K., et al., *Cardiotrophin-1 can protect cardiac myocytes from injury when added both prior to simulated ischaemia and at reoxygenation.* Cardiovasc Res, 2001. **51**(2): p. 265-74.
191. Craig, R., et al., *p38 MAPK and NF-kappa B collaborate to induce interleukin-6 gene expression and release. Evidence for a cytoprotective autocrine signaling pathway in a cardiac myocyte model system.* J Biol Chem, 2000. **275**(31): p. 23814-24.
192. Ruixing, Y., Y. Dezhai, and L. Jiaquan, *Effects of cardiotrophin-1 on hemodynamics and cardiomyocyte apoptosis in rats with acute myocardial infarction.* J Med Invest, 2004. **51**(1-2): p. 29-37.
193. Oshima, Y., et al., *STAT3 mediates cardioprotection against ischemia/reperfusion injury through metallothionein induction in the heart.* Cardiovasc Res, 2005. **65**(2): p. 428-35.
194. Drobic, V., et al., *Differential and combined effects of cardiotrophin-1 and TGF-beta1 on cardiac myofibroblast proliferation and contraction.* Am J Physiol Heart Circ Physiol, 2007. **293**(2): p. H1053-64.
195. Freed, D.H., et al., *Cardiotrophin-1: expression in experimental myocardial infarction and potential role in post-MI wound healing.* Mol Cell Biochem, 2003. **254**(1-2): p. 247-56.
196. Freed, D.H., et al., *Induction of protein synthesis in cardiac fibroblasts by cardiotrophin-1: integration of multiple signaling pathways.* Cardiovasc Res, 2003. **60**(2): p. 365-75.
197. Ichiki, T., et al., *Cardiotrophin-1 stimulates intercellular adhesion molecule-1 and monocyte chemoattractant protein-1 in human aortic endothelial cells.* Am J Physiol Heart Circ Physiol, 2008. **294**(2): p. H750-63.
198. Fritzenwanger, M., et al., *Cardiotrophin-1 induces monocyte chemoattractant protein-1 synthesis in human umbilical vein endothelial cells.* Cytokine, 2006. **33**(1): p. 46-51.
199. Jin, H., et al., *Effects of cardiotrophin-1 on haemodynamics and cardiac function in conscious rats.* Cytokine, 1998. **10**(1): p. 19-25.
200. Hamanaka, I., et al., *Effects of cardiotrophin-1 on hemodynamics and endocrine function of the heart.* Am J Physiol Heart Circ Physiol, 2000. **279**(1): p. H388-96.
201. Yao, L., et al., *Acute effect of human cardiotrophin-1 on hemodynamic parameters in spontaneously hypertensive rats and Wistar Kyoto rats.* Hypertens Res, 2001. **24**(6): p. 717-21.
202. Lopez, B., et al., *Is plasma cardiotrophin-1 a marker of hypertensive heart disease?* J Hypertens, 2005. **23**(3): p. 625-32.

203. Lopez, B., et al., *Association of increased plasma cardiotrophin-1 with inappropriate left ventricular mass in essential hypertension.* Hypertension, 2007. **50**(5): p. 977-83.
204. Lopez, B., et al., *Association of plasma cardiotrophin-1 with stage C heart failure in hypertensive patients: potential diagnostic implications.* J Hypertens, 2009. **27**(2): p. 418-24.
205. Takimoto, Y., et al., *Increased expression of cardiotrophin-1 during ventricular remodeling in hypertensive rats.* Am J Physiol Heart Circ Physiol, 2002. **282**(3): p. H896-901.
206. Talwar, S., et al., *Elevated circulating cardiotrophin-1 in heart failure: relationship with parameters of left ventricular systolic dysfunction.* Clin Sci (Lond), 2000. **99**(1): p. 83-8.
207. Talwar, S., et al., *An immunoluminometric assay for cardiotrophin-1: a newly identified cytokine is present in normal human plasma and is increased in heart failure.* Biochem Biophys Res Commun, 1999. **261**(3): p. 567-71.
208. Ng, L.L., et al., *Non-competitive immunochemiluminometric assay for cardiotrophin-1 detects elevated plasma levels in human heart failure.* Clin Sci (Lond), 2002. **102**(4): p. 411-6.
209. Tsutamoto, T., et al., *Relationship between plasma level of cardiotrophin-1 and left ventricular mass index in patients with dilated cardiomyopathy.* J Am Coll Cardiol, 2001. **38**(5): p. 1485-90.
210. Talwar, S., et al., *The effect of valvular regurgitation on plasma Cardiotrophin-1 in patients with normal left ventricular systolic function.* Eur J Heart Fail, 2000. **2**(4): p. 387-91.
211. Wei, M., et al., *Perioperative plasma brain natriuretic peptide and cardiotrophin-1 in off-pump coronary artery bypass.* Scand Cardiovasc J, 2008. **42**(6): p. 399-404.
212. Khan, S.Q., et al., *Cardiotrophin-1 predicts death or heart failure following acute myocardial infarction.* J Card Fail, 2006. **12**(8): p. 635-40.
213. Cottone, S., et al., *Association between biomarkers of inflammation and left ventricular hypertrophy in moderate chronic kidney disease.* Clin Nephrol, 2007. **67**(4): p. 209-16.
214. Eaton, B.M. and M.P. Oakey, *Sequential preparation of highly purified microvillous and basal syncytiotrophoblast membranes in substantial yield from a single term human placenta: inhibition of microvillous alkaline phosphatase activity by EDTA.* Biochim Biophys Acta, 1994. **1193**(1): p. 85-92.
215. Dragovic, R.A., et al., *Isolation of syncytiotrophoblast microvesicles and exosomes and their characterisation by multicolour flow cytometry and fluorescence Nanoparticle Tracking Analysis.* Methods, 2015.
216. Gardiner, C., et al., *Extracellular vesicle sizing and enumeration by nanoparticle tracking analysis.* J Extracell Vesicles, 2013. **2**.
217. Soo, C.Y., et al., *Nanoparticle tracking analysis monitors microvesicle and exosome secretion from immune cells.* Immunology, 2012. **136**(2): p. 192-7.
218. Galush, W.J., J.A. Nye, and J.T. Groves, *Quantitative fluorescence microscopy using supported lipid bilayer standards.* Biophys J, 2008. **95**(5): p. 2512-9.

219. Sunderland, C.A., C.W. Redman, and G.M. Stirrat, *Monoclonal antibodies to human syncytiotrophoblast.* Immunology, 1981. **43**(3): p. 541-6.
220. Dragovic, R.A., et al., *Multicolor flow cytometry and nanoparticle tracking analysis of extracellular vesicles in the plasma of normal pregnant and pre-eclamptic women.* Biol Reprod, 2013. **89**(6): p. 151.
221. Yoshioka, Y., et al., *Comparative marker analysis of extracellular vesicles in different human cancer types.* J Extracell Vesicles, 2013. **2**.
222. Jaffe, E.A., et al., *Culture of human endothelial cells derived from umbilical veins. Identification by morphologic and immunologic criteria.* J Clin Invest, 1973. **52**(11): p. 2745-56.
223. Kertesz, Z., E.A. Linton, and C.W. Redman, *Adhesion molecules of syncytiotrophoblast microvillous membranes inhibit proliferation of human umbilical vein endothelial cells.* Placenta, 2000. **21**(2-3): p. 150-9.
224. S, M.M.a.D., *Nucleic acid Binding Dyes and Uses Therefore*, in *US Patent application* 2010: USA.
225. Zhang, J.H., T.D. Chung, and K.R. Oldenburg, *A Simple Statistical Parameter for Use in Evaluation and Validation of High Throughput Screening Assays.* J Biomol Screen, 1999. **4**(2): p. 67-73.
226. Suzuki, N., A. Yoshida, and Y. Nakano, *Quantitative analysis of multi-species oral biofilms by TaqMan Real-Time PCR.* Clin Med Res, 2005. **3**(3): p. 176-85.
227. Holland, P.M., et al., *Detection of specific polymerase chain reaction product by utilizing the 5'----3' exonuclease activity of Thermus aquaticus DNA polymerase.* Proc Natl Acad Sci U S A, 1991. **88**(16): p. 7276-80.
228. Abcam. *Cardiotrophin 1 expression on HepG2 cells* Available from: http://www.abcam.com/cardiotrophin-1-antibody-ab83176.html.
229. Chien, K.R., et al., *Regulation of cardiac gene expression during myocardial growth and hypertrophy: molecular studies of an adaptive physiologic response.* Faseb j, 1991. **5**(15): p. 3037-46.
230. Komuro, I., et al., *Expression of cellular oncogenes in the myocardium during the developmental stage and pressure-overloaded hypertrophy of the rat heart.* Circ Res, 1988. **62**(6): p. 1075-9.
231. Chien, K.R., et al., *Transcriptional regulation during cardiac growth and development.* Annu Rev Physiol, 1993. **55**: p. 77-95.
232. Seno, A., et al., *Suppressed Production of Soluble Fms-Like Tyrosine Kinase-1 Contributes to Myocardial Remodeling and Heart Failure.* Hypertension, 2016. **68**(3): p. 678-87.
233. Bupha-Intr, T., K.M. Haizlip, and P.M.L. Janssen, *Role of Endothelin in the Induction of Cardiac Hypertrophy In Vitro.* PLoS One, 2012. **7**(8).
234. Chaudhry, H.W., et al., *Cyclin A2 mediates cardiomyocyte mitosis in the postmitotic myocardium.* J Biol Chem, 2004. **279**(34): p. 35858-66.
235. Melendez, G.C., et al., *Interleukin 6 mediates myocardial fibrosis, concentric hypertrophy, and diastolic dysfunction in rats.* Hypertension, 2010. **56**(2): p. 225-31.
236. Sarker, S., et al., *Placenta-derived exosomes continuously increase in maternal circulation over the first trimester of pregnancy.* J Transl Med, 2014. **12**: p. 204.

237. Kowal, J., M. Tkach, and C. Thery, *Biogenesis and secretion of exosomes.* Curr Opin Cell Biol, 2014. **29**: p. 116-25.
238. Rana, S. and M. Zoller, *Exosome target cell selection and the importance of exosomal tetraspanins: a hypothesis.* Biochem Soc Trans, 2011. **39**(2): p. 559-62.
239. Rana, S., et al., *Toward tailored exosomes: the exosomal tetraspanin web contributes to target cell selection.* Int J Biochem Cell Biol, 2012. **44**(9): p. 1574-84.
240. Atay, S., et al., *Trophoblast-derived exosomes mediate monocyte recruitment and differentiation.* Am J Reprod Immunol, 2011. **65**(1): p. 65-77.
241. Vargas, A., et al., *Syncytin proteins incorporated in placenta exosomes are important for cell uptake and show variation in abundance in serum exosomes from patients with preeclampsia.* Faseb j, 2014. **28**(8): p. 3703-19.
242. Chung, E., F. Yeung, and L.A. Leinwand, *Akt and MAPK signaling mediate pregnancy-induced cardiac adaptation.* J Appl Physiol (1985), 2012. **112**(9): p. 1564-75.
243. Fritzenwanger, M., et al., *Cardiotrophin-1 induces interleukin-6 synthesis in human umbilical vein endothelial cells.* Cytokine, 2006. **36**(3-4): p. 101-6.
244. Vicencio, J.M., et al., *Plasma exosomes protect the myocardium from ischemia-reperfusion injury.* J Am Coll Cardiol, 2015. **65**(15): p. 1525-36.
245. Tannetta, D., et al., *Update of syncytiotrophoblast derived extracellular vesicles in normal pregnancy and preeclampsia.* J Reprod Immunol, 2017. **119**: p. 98-106.
246. Tong, M., et al., *In vivo targets of human placental micro-vesicles vary with exposure time and pregnancy.* Reproduction, 2017. **153**(6): p. 835-845.
247. Kuwahara, K., et al., *Endothelin-1 and cardiotrophin-1 induce brain natriuretic peptide gene expression by distinct transcriptional mechanisms.* J Cardiovasc Pharmacol, 1998. **31 Suppl 1**: p. S354-6.
248. Ogawa, Y., et al., *Molecular cloning of the complementary DNA and gene that encode mouse brain natriuretic peptide and generation of transgenic mice that overexpress the brain natriuretic peptide gene.* J Clin Invest, 1994. **93**(5): p. 1911-21.
249. Ogawa, Y., et al., *Molecular cloning and chromosomal assignment of the mouse C-type natriuretic peptide (CNP) gene (Nppc): comparison with the human CNP gene (NPPC).* Genomics, 1994. **24**(2): p. 383-7.
250. Mukoyama, M., et al., *Brain natriuretic peptide as a novel cardiac hormone in humans. Evidence for an exquisite dual natriuretic peptide system, atrial natriuretic peptide and brain natriuretic peptide.* J Clin Invest, 1991. **87**(4): p. 1402-12.
251. Mukoyama, M., et al., *Increased human brain natriuretic peptide in congestive heart failure.* N Engl J Med, 1990. **323**(11): p. 757-8.
252. Tsutamoto, T., et al., *Attenuation of compensation of endogenous cardiac natriuretic peptide system in chronic heart failure: prognostic role of plasma brain natriuretic peptide concentration in patients with*

chronic symptomatic left ventricular dysfunction. Circulation, 1997. **96**(2): p. 509-16.
253. Rimbaud, S., et al., *Stimulus specific changes of energy metabolism in hypertrophied heart.* J Mol Cell Cardiol, 2009. **46**(6): p. 952-9.
254. Hameed, A.B., et al., *Longitudinal changes in the B-type natriuretic peptide levels in normal pregnancy and postpartum.* Clin Cardiol, 2009. **32**(8): p. E60-2.
255. Resnik, J.L., et al., *Evaluation of B-type natriuretic peptide (BNP) levels in normal and preeclamptic women.* Am J Obstet Gynecol, 2005. **193**(2): p. 450-4.
256. Tanous, D., et al., *B-type natriuretic peptide in pregnant women with heart disease.* J Am Coll Cardiol, 2010. **56**(15): p. 1247-53.
257. Yoshimura, M., et al., *Hemodynamic, renal, and hormonal responses to brain natriuretic peptide infusion in patients with congestive heart failure.* Circulation, 1991. **84**(4): p. 1581-8.
258. Hobbs, R.E., et al., *Hemodynamic effects of a single intravenous injection of synthetic human brain natriuretic peptide in patients with heart failure secondary to ischemic or idiopathic dilated cardiomyopathy.* Am J Cardiol, 1996. **78**(8): p. 896-901.
259. Marcus, L.S., et al., *Hemodynamic and renal excretory effects of human brain natriuretic peptide infusion in patients with congestive heart failure. A double-blind, placebo-controlled, randomized crossover trial.* Circulation, 1996. **94**(12): p. 3184-9.
260. Mills, R.M., et al., *Sustained hemodynamic effects of an infusion of nesiritide (human b-type natriuretic peptide) in heart failure: a randomized, double-blind, placebo-controlled clinical trial. Natrecor Study Group.* J Am Coll Cardiol, 1999. **34**(1): p. 155-62.
261. Colucci, W.S., et al., *Intravenous nesiritide, a natriuretic peptide, in the treatment of decompensated congestive heart failure. Nesiritide Study Group.* N Engl J Med, 2000. **343**(4): p. 246-53.
262. Binah, O., et al., *Functional and developmental properties of human embryonic stem cells-derived cardiomyocytes.* J Electrocardiol, 2007. **40**(6 Suppl): p. S192-6.
263. Babiarz, J.E., et al., *Determination of the human cardiomyocyte mRNA and miRNA differentiation network by fine-scale profiling.* Stem Cells Dev, 2012. **21**(11): p. 1956-65.
264. Dolnikov, K., et al., *Functional properties of human embryonic stem cell-derived cardiomyocytes: intracellular Ca2+ handling and the role of sarcoplasmic reticulum in the contraction.* Stem Cells, 2006. **24**(2): p. 236-45.
265. Lundy, S.D., et al., *Structural and functional maturation of cardiomyocytes derived from human pluripotent stem cells.* Stem Cells Dev, 2013. **22**(14): p. 1991-2002.
266. Pointon, A., et al., *Assessment of cardiomyocyte contraction in human-induced pluripotent stem cell-derived cardiomyocytes.* Toxicol Sci, 2015. **144**(2): p. 227-37.
267. Braam, S.R., et al., *Repolarization reserve determines drug responses in human pluripotent stem cell derived cardiomyocytes.* Stem Cell Res, 2013. **10**(1): p. 48-56.

268. Reynolds, J.G., et al., *HER2-targeted liposomal doxorubicin displays enhanced anti-tumorigenic effects without associated cardiotoxicity.* Toxicol Appl Pharmacol, 2012. **262**(1): p. 1-10.
269. Irizarry, R.A., et al., *Exploration, normalization, and summaries of high density oligonucleotide array probe level data.* Biostatistics, 2003. **4**(2): p. 249-64.
270. Bolstad, B.M., et al., *A comparison of normalization methods for high density oligonucleotide array data based on variance and bias.* Bioinformatics, 2003. **19**(2): p. 185-93.
271. Carvalho, B.S. and R.A. Irizarry, *A framework for oligonucleotide microarray preprocessing.* Bioinformatics. **26**(19): p. 2363-7.
272. Affymetrix. Available from: http://www.affymetrix.com/support/technical/byproduct.affx?product=hugene-1_0-st-v1.
273. Smyth, G.K., *Linear models and empirical bayes methods for assessing differential expression in microarray experiments.* Stat Appl Genet Mol Biol, 2004. **3**: p. Article3.
274. Chen, H., M.E. Herndon, and J. Lawler, *The cell biology of thrombospondin-1.* Matrix Biol, 2000. **19**(7): p. 597-614.
275. Jimenez, B., et al., *Signals leading to apoptosis-dependent inhibition of neovascularization by thrombospondin-1.* Nat Med, 2000. **6**(1): p. 41-8.
276. Chatila, K., et al., *The role of the thrombospondins in healing myocardial infarcts.* Cardiovasc Hematol Agents Med Chem, 2007. **5**(1): p. 21-7.
277. Stenina, O.I., et al., *Coronary artery disease and the thrombospondin single nucleotide polymorphisms.* Int J Biochem Cell Biol, 2004. **36**(6): p. 1013-30.
278. Frangogiannis, N.G., et al., *Critical role of endogenous thrombospondin-1 in preventing expansion of healing myocardial infarcts.* Circulation, 2005. **111**(22): p. 2935-42.
279. Xia, Y., et al., *Endogenous thrombospondin-1 protects the pressure-overloaded myocardium by modulating fibroblast phenotype and matrix metabolism.* Hypertension, 2011. **58**(5): p. 902-11.
280. Stenina, O.I., E.J. Topol, and E.F. Plow, *Thrombospondins, their polymorphisms, and cardiovascular disease.* Arterioscler Thromb Vasc Biol, 2007. **27**(9): p. 1886-94.
281. Topol, E.J., et al., *Single nucleotide polymorphisms in multiple novel thrombospondin genes may be associated with familial premature myocardial infarction.* Circulation, 2001. **104**(22): p. 2641-4.
282. Zwicker, J.I., et al., *The thrombospondin-1 N700S polymorphism is associated with early myocardial infarction without altering von Willebrand factor multimer size.* Blood, 2006. **108**(4): p. 1280-3.
283. Yanagisawa, M., et al., *A novel potent vasoconstrictor peptide produced by vascular endothelial cells.* Nature, 1988. **332**(6163): p. 411-5.
284. Bobik, A., et al., *Growth factor activity of endothelin on vascular smooth muscle.* Am J Physiol, 1990. **258**(3 Pt 1): p. C408-15.
285. Ito, H., et al., *Endothelin-1 induces hypertrophy with enhanced expression of muscle-specific genes in cultured neonatal rat cardiomyocytes.* Circ Res, 1991. **69**(1): p. 209-15.

286. Gu, X.H., D.J. Casley, and W.G. Nayler, *Characterization of [125I]endothelin-1 binding sites in rat cardiac membrane fragments.* J Cardiovasc Pharmacol, 1989. **13 Suppl 5**: p. S171-3.
287. Shubeita, H.E., et al., *Endothelin induction of inositol phospholipid hydrolysis, sarcomere assembly, and cardiac gene expression in ventricular myocytes. A paracrine mechanism for myocardial cell hypertrophy.* J Biol Chem, 1990. **265**(33): p. 20555-62.
288. Suzuki, T., H. Hoshi, and Y. Mitsui, *Endothelin stimulates hypertrophy and contractility of neonatal rat cardiac myocytes in a serum-free medium.* FEBS Lett, 1990. **268**(1): p. 149-51.
289. Loennechen, J.P., et al., *Regional expression of endothelin-1, ANP, IGF-1, and LV wall stress in the infarcted rat heart.* Am J Physiol Heart Circ Physiol, 2001. **280**(6): p. H2902-10.
290. Wahl, J.R., et al., *Murine macrophages produce endothelin-1 after microbial stimulation.* Exp Biol Med (Maywood), 2005. **230**(9): p. 652-8.
291. Li, Z., et al., *Expression of endothelin-1 in macrophages and mast cells in hyperplastic human tonsils.* FEBS Lett, 1999. **457**(3): p. 381-4.
292. Kang, M. and J.W. Walker, *Endothelin-1 and PKC induce positive inotropy without affecting pHi in ventricular myocytes.* Exp Biol Med (Maywood), 2006. **231**(6): p. 865-70.
293. Katoh, H., et al., *Heterogeneity and underlying mechanism for inotropic action of endothelin-1 in rat ventricular myocytes.* Br J Pharmacol, 1998. **123**(7): p. 1343-50.
294. Kelly, R.A., et al., *Endothelin enhances the contractile responsiveness of adult rat ventricular myocytes to calcium by a pertussis toxin-sensitive pathway.* J Clin Invest, 1990. **86**(4): p. 1164-71.
295. Li, K., D.J. Stewart, and J.L. Rouleau, *Myocardial contractile actions of endothelin-1 in rat and rabbit papillary muscles. Role of endocardial endothelium.* Circ Res, 1991. **69**(2): p. 301-12.
296. Pieske, B., et al., *Functional effects of endothelin and regulation of endothelin receptors in isolated human nonfailing and failing myocardium.* Circulation, 1999. **99**(14): p. 1802-9.
297. MacCarthy, P.A., et al., *Contrasting inotropic effects of endogenous endothelin in the normal and failing human heart: studies with an intracoronary ET(A) receptor antagonist.* Circulation, 2000. **101**(2): p. 142-7.
298. Boulanger, C. and T.F. Luscher, *Release of endothelin from the porcine aorta. Inhibition by endothelium-derived nitric oxide.* J Clin Invest, 1990. **85**(2): p. 587-90.
299. Brunner, F., H. Stessel, and W.R. Kukovetz, *Novel guanylyl cyclase inhibitor, ODQ reveals role of nitric oxide, but not of cyclic GMP in endothelin-1 secretion.* FEBS Lett, 1995. **376**(3): p. 262-6.
300. Kohno, M., et al., *C-type natriuretic peptide inhibits thrombin- and angiotensin II-stimulated endothelin release via cyclic guanosine 3',5'-monophosphate.* Hypertension, 1992. **19**(4): p. 320-5.
301. Maemura, K., et al., *Production of endothelin-1 in vascular endothelial cells is regulated by factors associated with vascular injury.* Gerontology, 1992. **38 Suppl 1**: p. 29-35.

302. Prins, B.A., et al., *Prostaglandin E2 and prostacyclin inhibit the production and secretion of endothelin from cultured endothelial cells.* J Biol Chem, 1994. **269**(16): p. 11938-44.
303. Yamazaki, T., et al., *Endothelin-1 is involved in mechanical stress-induced cardiomyocyte hypertrophy.* J Biol Chem, 1996. **271**(6): p. 3221-8.
304. Schwarz, J., et al., *Polo-like kinase 2, a novel ADAM17 signaling component, regulates tumor necrosis factor alpha ectodomain shedding.* J Biol Chem, 2014. **289**(5): p. 3080-93.
305. Menghini, R., et al., *The role of ADAM17 in metabolic inflammation.* Atherosclerosis, 2013. **228**(1): p. 12-7.
306. Bradham, W.S., et al., *Tumor necrosis factor-alpha and myocardial remodeling in progression of heart failure: a current perspective.* Cardiovasc Res, 2002. **53**(4): p. 822-30.
307. Bradham, W.S., et al., *TNF-alpha and myocardial matrix metalloproteinases in heart failure: relationship to LV remodeling.* Am J Physiol Heart Circ Physiol, 2002. **282**(4): p. H1288-95.
308. Li, Y.Y., et al., *Myocardial extracellular matrix remodeling in transgenic mice overexpressing tumor necrosis factor alpha can be modulated by anti-tumor necrosis factor alpha therapy.* Proc Natl Acad Sci U S A, 2000. **97**(23): p. 12746-51.
309. Satoh, M., et al., *Tumor necrosis factor-alpha-converting enzyme and tumor necrosis factor-alpha in human dilated cardiomyopathy.* Circulation, 1999. **99**(25): p. 3260-5.
310. Heusch, G. and R. Schulz, *Endogenous protective mechanisms in myocardial ischemia: hibernation and ischemic preconditioning.* The American journal of cardiology, 1997. **80**(3): p. 26A-33A.
311. Murry, C.E., R.B. Jennings, and K.A. Reimer, *Preconditioning with ischemia: a delay of lethal cell injury in ischemic myocardium.* Circulation, 1986. **74**(5): p. 1124-36.
312. Ohtsu, H., et al., *ADAM17 mediates epidermal growth factor receptor transactivation and vascular smooth muscle cell hypertrophy induced by angiotensin II.* Arterioscler Thromb Vasc Biol, 2006. **26**(9): p. e133-7.
313. Takayanagi, T., et al., *Role of epidermal growth factor receptor and endoplasmic reticulum stress in vascular remodeling induced by angiotensin II.* Hypertension, 2015. **65**(6): p. 1349-55.
314. Niu, A., B. Wang, and Y.P. Li, *TNFalpha shedding in mechanically stressed cardiomyocytes is mediated by Src activation of TACE.* J Cell Biochem, 2015. **116**(4): p. 559-65.
315. Shi, W., et al., *TACE is required for fetal murine cardiac development and modeling.* Dev Biol, 2003. **261**(2): p. 371-80.
316. Scherer, P.E., et al., *Cell-type and tissue-specific expression of caveolin-2 caveolins 1 and 2 co-localize and form a stable hetero-oligomeric complex in vivo.* Journal of Biological Chemistry, 1997. **272**(46): p. 29337-29346.
317. Wakasaki, H., et al., *Targeted overexpression of protein kinase C β2 isoform in myocardium causes cardiomyopathy.* Proceedings of the National Academy of Sciences, 1997. **94**(17): p. 9320-9325.

318. Scherer, P.E., et al., *Identification, sequence, and expression of caveolin-2 defines a caveolin gene family.* Proceedings of the National Academy of Sciences, 1996. **93**(1): p. 131-135.
319. Scherer, P.E., et al., *Caveolin isoforms differ in their N-terminal protein sequence and subcellular distribution. Identification and epitope mapping of an isoform-specific monoclonal antibody probe.* Journal of Biological Chemistry, 1995. **270**(27): p. 16395-16401.
320. Cai, Q., et al., *Caveolar Fatty Acids and Acylation of Caveolin-1.* PLoS One, 2013. **8**(4).
321. Lisanti, M.P., et al., *Caveolae, caveolin and caveolin-rich membrane domains: a signalling hypothesis.* Trends Cell Biol, 1994. **4**(7): p. 231-5.
322. Shaul, P.W., et al., *Acylation targets emdothelial nitric-oxide synthase to plasmalemmal caveolae.* J Biol Chem, 1996. **271**(11): p. 6518-22.
323. Bucci, M., et al., *In vivo delivery of the caveolin-1 scaffolding domain inhibits nitric oxide synthesis and reduces inflammation.* Nat Med, 2000. **6**(12): p. 1362-7.
324. Michel, J.B., et al., *Reciprocal regulation of endothelial nitric-oxide synthase by Ca2+-calmodulin and caveolin.* J Biol Chem, 1997. **272**(25): p. 15583-6.
325. Cho, W.J., et al., *Caveolin-1 exists and may function in cardiomyocytes.* Can J Physiol Pharmacol, 2010. **88**(1): p. 73-6.
326. Garcia-Cardena, G., et al., *Targeting of nitric oxide synthase to endothelial cell caveolae via palmitoylation: implications for nitric oxide signaling.* Proc Natl Acad Sci U S A, 1996. **93**(13): p. 6448-53.
327. Frank, P.G., et al., *Genetic ablation of caveolin-1 confers protection against atherosclerosis.* Arterioscler Thromb Vasc Biol, 2004. **24**(1): p. 98-105.
328. Zhao, Y.Y., et al., *Defects in caveolin-1 cause dilated cardiomyopathy and pulmonary hypertension in knockout mice.* Proc Natl Acad Sci U S A, 2002. **99**(17): p. 11375-80.
329. Cohen, A.W., et al., *Caveolin-1 null mice develop cardiac hypertrophy with hyperactivation of p42/44 MAP kinase in cardiac fibroblasts.* Am J Physiol Cell Physiol, 2003. **284**(2): p. C457-74.
330. Augustus, A.S., et al., *Hearts lacking caveolin-1 develop hypertrophy with normal cardiac substrate metabolism.* Cell Cycle, 2008. **7**(16): p. 2509-18.
331. Dittrich, E., et al., *A di-leucine motif and an upstream serine in the interleukin-6 (IL-6) signal transducer gp130 mediate ligand-induced endocytosis and down-regulation of the IL-6 receptor.* J Biol Chem, 1996. **271**(10): p. 5487-94.
332. Trowbridge, I.S., J.F. Collawn, and C.R. Hopkins, *Signal-dependent membrane protein trafficking in the endocytic pathway.* Annu Rev Cell Biol, 1993. **9**: p. 129-61.
333. Wang, Y. and G.M. Fuller, *Phosphorylation and internalization of gp130 occur after IL-6 activation of Jak2 kinase in hepatocytes.* Mol Biol Cell, 1994. **5**(7): p. 819-28.
334. Thiel, S., et al., *Internalization of the interleukin 6 signal transducer gp130 does not require activation of the Jak/STAT pathway.* Biochem J, 1998. **330 (Pt 1)**: p. 47-54.

335. Ohno, H., et al., *Interaction of tyrosine-based sorting signals with clathrin-associated proteins.* Science, 1995. **269**(5232): p. 1872-5.
336. Hilton, D.J., N.A. Nicola, and D. Metcalf, *Distribution and binding properties of receptors for leukaemia inhibitory factor.* Ciba Found Symp, 1992. **167**: p. 227-39; discussion 239-44.
337. Balduini, C.L. and F. Melazzini, *Research at the heart of hematology: thrombocytopenias and platelet function disorders.* Haematologica, 2017. **102**(2): p. 203-205.
338. Weyrich, A.S., *Platelets: more than a sack of glue.* Hematology Am Soc Hematol Educ Program, 2014. **2014**(1): p. 400-3.
339. Clark, S.R., et al., *Platelet TLR4 activates neutrophil extracellular traps to ensnare bacteria in septic blood.* Nat Med, 2007. **13**(4): p. 463-9.
340. Tranum, B.L. and A. Haut, *Thrombocytosis: platelet kinetics in neoplasia.* J Lab Clin Med, 1974. **84**(5): p. 615-9.
341. Sharma, D. and G. Singh, *Thrombocytosis in gynecological cancers.* J Cancer Res Ther, 2017. **13**(2): p. 193-197.
342. Zeimet, A.G., et al., *Significance of thrombocytosis in patients with epithelial ovarian cancer.* Am J Obstet Gynecol, 1994. **170**(2): p. 549-54.
343. Shoda, K., et al., *[Thrombocytosis Associated with Poor Prognosis in Patients with Gastric Cancer].* Gan To Kagaku Ryoho, 2015. **42**(12): p. 1980-2.
344. Wang, F., et al., *The significance of platelet activation in rheumatoid arthritis.* Clin Rheumatol, 2007. **26**(5): p. 768-71.
345. Bunescu, A., et al., *Enhanced Fcgamma receptor I, alphaMbeta2 integrin receptor expression by monocytes and neutrophils in rheumatoid arthritis: interaction with platelets.* J Rheumatol, 2004. **31**(12): p. 2347-55.
346. Boilard, E., et al., *Platelets amplify inflammation in arthritis via collagen-dependent microparticle production.* Science, 2010. **327**(5965): p. 580-3.
347. Boilard, E., P. Blanco, and P.A. Nigrovic, *Platelets: active players in the pathogenesis of arthritis and SLE.* Nat Rev Rheumatol, 2012. **8**(9): p. 534-42.
348. Martin, J.F., et al., *The causal role of megakaryocyte-platelet hyperactivity in acute coronary syndromes.* Nat Rev Cardiol, 2012. **9**(11): p. 658-70.
349. Peters, A.M. and J.P. Lavender, *Platelet kinetics with indium-111 platelets: comparison with chromium-51 platelets.* Semin Thromb Hemost, 1983. **9**(2): p. 100-14.
350. Cohen, J.A. and C.H. Leeksma, *Determination of the life span of human blood platelets using labelled diisopropylfluorophosphonate.* J Clin Invest, 1956. **35**(9): p. 964-9.
351. Ghoshal, K. and M. Bhattacharyya, *Overview of platelet physiology: its hemostatic and nonhemostatic role in disease pathogenesis.* The Scientific World Journal, 2014. **2014**.
352. Freynhofer, M.K., et al., *Antiplatelet drugs in patients with enhanced platelet turnover: biomarkers versus platelet function testing.* Thrombosis and haemostasis, 2015. **114**(3): p. 459-468.

353. Garraud, O., H. Hamzeh-Cognasse, and F. Cognasse, *Platelets and cytokines: How and why?* Transfusion clinique et biologique, 2012. **19**(3): p. 104-108.
354. Owens, A.P., 3rd and N. Mackman, *Microparticles in hemostasis and thrombosis.* Circ Res, 2011. **108**(10): p. 1284-97.
355. Aatonen, M., M. Gronholm, and P.R. Siljander, *Platelet-derived microvesicles: multitalented participants in intercellular communication.* Semin Thromb Hemost, 2012. **38**(1): p. 102-13.
356. Bernal-Mizrachi, L., et al., *High levels of circulating endothelial microparticles in patients with acute coronary syndromes.* Am Heart J, 2003. **145**(6): p. 962-70.
357. Chen, Y., et al., *The Role of Circulating Platelets Microparticles and Platelet Parameters in Acute Ischemic Stroke Patients.* J Stroke Cerebrovasc Dis, 2015. **24**(10): p. 2313-20.
358. Hugel, B., et al., *Elevated levels of circulating procoagulant microparticles in patients with paroxysmal nocturnal hemoglobinuria and aplastic anemia.* Blood, 1999. **93**(10): p. 3451-6.
359. Jung, C., et al., *Circulating endothelial and platelet derived microparticles reflect the size of myocardium at risk in patients with ST-elevation myocardial infarction.* Atherosclerosis, 2012. **221**(1): p. 226-31.
360. Nomura, S., et al., *Platelet-derived microparticles may influence the development of atherosclerosis in diabetes mellitus.* Atherosclerosis, 1995. **116**(2): p. 235-40.
361. Preston, R.A., et al., *Effects of severe hypertension on endothelial and platelet microparticles.* Hypertension, 2003. **41**(2): p. 211-7.
362. Aatonen, M.T., et al., *Isolation and characterization of platelet-derived extracellular vesicles.* J Extracell Vesicles, 2014. **3**.
363. Frojmovic, M.M. and J.G. Milton, *Human platelet size, shape, and related functions in health and disease.* Physiol Rev, 1982. **62**(1): p. 185-261.
364. Isenberg, W.M., et al., *Topographic distribution of a granule membrane protein (GMP-140) that is expressed on the platelet surface after activation: an immunogold-surface replica study.* Blood Cells, 1986. **12**(1): p. 191-204.
365. Fukami, M.H., *Isolation of dense granules from human platelets.* Methods Enzymol, 1992. **215**: p. 36-42.
366. Holmsen, H. and H.J. Weiss, *Secretable storage pools in platelets.* Annu Rev Med, 1979. **30**: p. 119-34.
367. Rendu, F. and B. Brohard-Bohn, *The platelet release reaction: granules' constituents, secretion and functions.* Platelets, 2001. **12**(5): p. 261-73.
368. Vanhoutte, P.M., *Platelet-derived serotonin, the endothelium, and cardiovascular disease.* J Cardiovasc Pharmacol, 1991. **17 Suppl 5**: p. S6-12.
369. Sixma, J.J., et al., *Immuno-electron microscopical demonstration of lysosomes in human blood platelets and megakaryocytes using anti-cathepsin D.* Blood, 1985. **65**(5): p. 1287-91.
370. Chesney, C.M., E. Harper, and R.W. Colman, *Human platelet collagenase.* J Clin Invest, 1974. **53**(6): p. 1647-54.

371. Silverstein, R.L. and M. Febbraio, *Identification of lysosome-associated membrane protein-2 as an activation-dependent platelet surface glycoprotein.* Blood, 1992. **80**(6): p. 1470-5.
372. Heijnen, H.F., et al., *Multivesicular bodies are an intermediate stage in the formation of platelet α-granules.* Blood, 1998. **91**(7): p. 2313-2325.
373. Heijnen, H.F., et al., *Activated platelets release two types of membrane vesicles: microvesicles by surface shedding and exosomes derived from exocytosis of multivesicular bodies and alpha-granules.* Blood, 1999. **94**(11): p. 3791-9.
374. Hargett, L.A. and N.N. Bauer, *On the origin of microparticles: From "platelet dust" to mediators of intercellular communication.* Pulm Circ, 2013. **3**(2): p. 329-40.
375. Boilard, E., A.-C. Duchez, and A. Brisson, *The diversity of platelet microparticles.* Current opinion in hematology, 2015. **22**(5): p. 437-444.
376. Fox, J.E., et al., *Evidence that agonist-induced activation of calpain causes the shedding of procoagulant-containing microvesicles from the membrane of aggregating platelets.* J Biol Chem, 1991. **266**(20): p. 13289-95.
377. Perez-Pujol, S., P.H. Marker, and N.S. Key, *Platelet microparticles are heterogeneous and highly dependent on the activation mechanism: studies using a new digital flow cytometer.* Cytometry A, 2007. **71**(1): p. 38-45.
378. Connor, D.E., et al., *The majority of circulating platelet-derived microparticles fail to bind annexin V, lack phospholipid-dependent procoagulant activity and demonstrate greater expression of glycoprotein Ib.* Thromb Haemost, 2010. **103**(5): p. 1044-52.
379. Dean, W.L., et al., *Proteomic and functional characterisation of platelet microparticle size classes.* Thromb Haemost, 2009. **102**(4): p. 711-8.
380. Shai, E., et al., *Comparative analysis of platelet-derived microparticles reveals differences in their amount and proteome depending on the platelet stimulus.* J Proteomics, 2012. **76 Spec No.**: p. 287-96.
381. Garcia, B.A., et al., *The platelet microparticle proteome.* J Proteome Res, 2005. **4**(5): p. 1516-21.
382. Marcoux, G., et al., *Revealing the diversity of extracellular vesicles using high-dimensional flow cytometry analyses.* Sci Rep, 2016. **6**: p. 35928.
383. Gitz, E., et al., *CLEC-2 expression is maintained on activated platelets and on platelet microparticles.* Blood, 2014. **124**(14): p. 2262-70.
384. Duchez, A.C., et al., *Platelet microparticles are internalized in neutrophils via the concerted activity of 12-lipoxygenase and secreted phospholipase A(2)-IIA.* Proc Natl Acad Sci U S A, 2015. **112**(27): p. E3564-73.
385. Ray, D.M., et al., *Peroxisome Proliferator-Activated Receptor γ and Retinoid X Receptor transcription factors are released from activated human platelets and shed in microparticles.* Thromb Haemost, 2008. **99**(1): p. 86-95.
386. Cloutier, N., et al., *The exposure of autoantigens by microparticles underlies the formation of potent inflammatory components: the microparticle-associated immune complexes.* EMBO Mol Med, 2013. **5**(2): p. 235-49.

387. György, B., et al., *Improved Flow Cytometric Assessment Reveals Distinct Microvesicle (Cell-Derived Microparticle) Signatures in Joint Diseases.* PLoS One, 2012. **7**(11).
388. Pereira, J., et al., *Circulating platelet-derived microparticles in systemic lupus erythematosus. Association with increased thrombin generation and procoagulant state.* Thromb Haemost, 2006. **95**(1): p. 94-9.
389. Sellam, J., et al., *Increased levels of circulating microparticles in primary Sjögren's syndrome, systemic lupus erythematosus and rheumatoid arthritis and relation with disease activity.* Arthritis Res Ther, 2009. **11**(5): p. R156.
390. Mause, S.F., et al., *Platelet microparticles: a transcellular delivery system for RANTES promoting monocyte recruitment on endothelium.* Arterioscler Thromb Vasc Biol, 2005. **25**(7): p. 1512-8.
391. Forlow, S.B., R.P. McEver, and M.U. Nollert, *Leukocyte-leukocyte interactions mediated by platelet microparticles under flow.* Blood, 2000. **95**(4): p. 1317-23.
392. Dinkla, S., et al., *Platelet microparticles inhibit IL-17 production by regulatory T cells through P-selectin.* Blood, 2016. **127**(16): p. 1976-86.
393. Sprague, D.L., et al., *Platelet-mediated modulation of adaptive immunity: unique delivery of CD154 signal by platelet-derived membrane vesicles.* Blood, 2008. **111**(10): p. 5028-36.
394. Corrales-Medina, V.F., et al., *Increased levels of platelet microparticles in HIV-infected patients with good response to highly active antiretroviral therapy.* J Acquir Immune Defic Syndr, 2010. **54**(2): p. 217-8.
395. Rozmyslowicz, T., et al., *Platelet- and megakaryocyte-derived microparticles transfer CXCR4 receptor to CXCR4-null cells and make them susceptible to infection by X4-HIV.* Aids, 2003. **17**(1): p. 33-42.
396. Punyadee, N., et al., *Microparticles provide a novel biomarker to predict severe clinical outcomes of dengue virus infection.* J Virol, 2015. **89**(3): p. 1587-607.
397. Campos, F.M., et al., *Augmented plasma microparticles during acute Plasmodium vivax infection.* Malar J, 2010. **9**: p. 327.
398. Faille, D., et al., *Platelet microparticles: a new player in malaria parasite cytoadherence to human brain endothelium.* Faseb j, 2009. **23**(10): p. 3449-58.
399. Toth, B., et al., *Platelet-derived microparticles and coagulation activation in breast cancer patients.* Thromb Haemost, 2008. **100**(4): p. 663-9.
400. Ren, J.G., et al., *Elevated Level of Circulating Platelet-derived Microparticles in Oral Cancer.* J Dent Res, 2016. **95**(1): p. 87-93.
401. Zhao, L., et al., *Phosphatidylserine exposing-platelets and microparticles promote procoagulant activity in colon cancer patients.* J Exp Clin Cancer Res, 2016. **35**: p. 54.
402. Cazenave, J.P., et al., *[Platelet aggregation: a tool for clinical investigation and pharmacological study. Methodology].* Ann Biol Clin (Paris), 1983. **41**(3): p. 167-79.
403. Siljander, P., O. Carpen, and R. Lassila, *Platelet-derived microparticles associate with fibrin during thrombosis.* Blood, 1996. **87**(11): p. 4651-63.

404. Abid Hussein, M.N., et al., *Antigenic characterization of endothelial cell-derived microparticles and their detection ex vivo.* J Thromb Haemost, 2003. **1**(11): p. 2434-43.
405. Bustos, M., et al., *Protection against liver damage by cardiotrophin-1: a hepatocyte survival factor up-regulated in the regenerating liver in rats.* Gastroenterology, 2003. **125**(1): p. 192-201.
406. Jae-Ok Shin, E.-S.J., Hyun-Mi Song, Soo-Hyeon Yun, Byung-Kwan Lim, Jin-Ho Choi, Duk-Kyung Kim, Eun-Seok Jeon, *Effects of Cardiotrophin-1 on Adriamycin-Induced Apoptosis in H9c2 Cardiomyoblasts.* Korean Circulation Journal 2008. **38**(5): p. 264-269.
407. Araki, S., et al., *Apoptosis of vascular endothelial cells by fibroblast growth factor deprivation.* Biochem Biophys Res Commun, 1990. **168**(3): p. 1194-200.
408. Lindemann, S., et al., *Activated platelets mediate inflammatory signaling by regulated interleukin 1beta synthesis.* J Cell Biol, 2001. **154**(3): p. 485-90.
409. Coppinger, J.A., et al., *Characterization of the proteins released from activated platelets leads to localization of novel platelet proteins in human atherosclerotic lesions.* Blood, 2004. **103**(6): p. 2096-104.
410. Wijten, P., et al., *High precision platelet releasate definition by quantitative reversed protein profiling--brief report.* Arterioscler Thromb Vasc Biol, 2013. **33**(7): p. 1635-8.
411. Warshaw, A.L., L. Laster, and N.R. Shulman, *Protein synthesis by human platelets.* J Biol Chem, 1967. **242**(9): p. 2094-7.
412. Weyrich, A.S., et al., *Protein synthesis by platelets: historical and new perspectives.* J Thromb Haemost, 2009. **7**(2): p. 241-6.
413. Hottz, E.D., et al., *Platelets mediate increased endothelium permeability in dengue through NLRP3-inflammasome activation.* Blood, 2013. **122**(20): p. 3405-14.
414. Scheuerer, B., et al., *The CXC-chemokine platelet factor 4 promotes monocyte survival and induces monocyte differentiation into macrophages.* Blood, 2000. **95**(4): p. 1158-66.
415. Kasper, B., et al., *Platelet factor 4 (CXC chemokine ligand 4) differentially regulates respiratory burst, survival, and cytokine expression of human monocytes by using distinct signaling pathways.* J Immunol, 2007. **179**(4): p. 2584-91.
416. von Hundelshausen, P., et al., *Heterophilic interactions of platelet factor 4 and RANTES promote monocyte arrest on endothelium.* Blood, 2005. **105**(3): p. 924-30.
417. Holme, P.A., et al., *Stimulated Glanzmann's thrombasthenia platelets produced microvesicles. Microvesiculation correlates better to exposure of procoagulant surface than to activation of GPIIb-IIIa.* Thromb Haemost, 1995. **74**(6): p. 1533-40.
418. Thiagarajan, P. and J.F. Tait, *Collagen-induced exposure of anionic phospholipid in platelets and platelet-derived microparticles.* J Biol Chem, 1991. **266**(36): p. 24302-7.
419. Haslam, R.J., J.A. Lynham, and J.E. Fox, *Effects of collagen, ionophore A23187 and prostaglandin E1 on the phosphorylation of specific proteins in blood platelets.* Biochem J, 1979. **178**(2): p. 397-406.

420. Gerrard, J.M., J.G. White, and G.H.R. Rao, *Effects of the Ionophore A23187 on Blood Platelets: II. Influence on Ultrastructure.* Am J Pathol, 1974. **77**(2): p. 151-66.
421. Sims, P.J., et al., *Assembly of the platelet prothrombinase complex is linked to vesiculation of the platelet plasma membrane. Studies in Scott syndrome: an isolated defect in platelet procoagulant activity.* J Biol Chem, 1989. **264**(29): p. 17049-57.
422. Rubinstein, E., et al., *CD9, but not other tetraspans, associates with the beta1 integrin precursor.* Eur J Immunol, 1997. **27**(8): p. 1919-27.
423. Rubinstein, E., et al., *CD9, CD63, CD81, and CD82 are components of a surface tetraspan network connected to HLA-DR and VLA integrins.* Eur J Immunol, 1996. **26**(11): p. 2657-65.
424. Brisson, C., et al., *Co-localization of CD9 and GPIIb-IIIa (alpha IIb beta 3 integrin) on activated platelet pseudopods and alpha-granule membranes.* Histochem J, 1997. **29**(2): p. 153-65.
425. Indig, F.E., F. Diaz-Gonzalez, and M.H. Ginsberg, *Analysis of the tetraspanin CD9-integrin alphaIIbbeta3 (GPIIb-IIIa) complex in platelet membranes and transfected cells.* Biochem J, 1997. **327 (Pt 1)**: p. 291-8.
426. Margadant, C., et al., *Mechanisms of integrin activation and trafficking.* Curr Opin Cell Biol, 2011. **23**(5): p. 607-14.
427. Dong, Y., et al., *Cucurbitacin E, a tetracyclic triterpenes compound from Chinese medicine, inhibits tumor angiogenesis through VEGFR2-mediated Jak2-STAT3 signaling pathway.* Carcinogenesis, 2010. **31**(12): p. 2097-104.
428. Mavria, G., et al., *ERK-MAPK signaling opposes Rho-kinase to promote endothelial cell survival and sprouting during angiogenesis.* Cancer Cell, 2006. **9**(1): p. 33-44.
429. Carrithers, M., et al., *Enhanced susceptibility to endotoxic shock and impaired STAT3 signaling in CD31-deficient mice.* Am J Pathol, 2005. **166**(1): p. 185-96.
430. Kano, A., et al., *Endothelial cells require STAT3 for protection against endotoxin-induced inflammation.* J Exp Med, 2003. **198**(10): p. 1517-25.
431. Wang, M., et al., *Endothelial STAT3 plays a critical role in generalized myocardial proinflammatory and proapoptotic signaling.* Am J Physiol Heart Circ Physiol, 2007. **293**(4): p. H2101-8.
432. Kim, H.K., et al., *Platelet microparticles induce angiogenesis in vitro.* Br J Haematol, 2004. **124**(3): p. 376-84.
433. Berckmans, R.J., et al., *Cell-derived microparticles circulate in healthy humans and support low grade thrombin generation.* Thromb Haemost, 2001. **85**(4): p. 639-46.
434. Rank, A., et al., *Cellular origin of platelet-derived microparticles in vivo.* Thromb Res, 2010. **126**(4): p. e255-9.
435. Murakami, T., et al., *Impact of weight reduction on production of platelet-derived microparticles and fibrinolytic parameters in obesity.* Thromb Res, 2007. **119**(1): p. 45-53.
436. Michelsen, A.E., et al., *Increased level of platelet microparticles in survivors of myocardial infarction.* Scand J Clin Lab Invest, 2008. **68**(5): p. 386-92.

437. Biasucci, L.M., et al., *Differences in microparticle release in patients with acute coronary syndrome and stable angina.* Circ J, 2012. **76**(9): p. 2174-82.
438. Cui, Y., et al., *Circulating microparticles in patients with coronary heart disease and its correlation with interleukin-6 and C-reactive protein.* Mol Biol Rep, 2013. **40**(11): p. 6437-42.
439. Gamella-Pozuelo, L., et al., *Plasma Cardiotrophin-1 as a Marker of Hypertension and Diabetes-Induced Target Organ Damage and Cardiovascular Risk.* Medicine (Baltimore), 2015. **94**(30).
440. Gonzalez, A., et al., *Usefulness of plasma cardiotrophin-1 in assessment of left ventricular hypertrophy regression in hypertensive patients.* J Hypertens, 2005. **23**(12): p. 2297-304.
441. Gonzalez, A., et al., *Cardiotrophin-1 in hypertensive heart disease.* Endocrine, 2012. **42**(1): p. 9-17.
442. Lopez, B., et al., *Association of cardiotrophin-1 with myocardial fibrosis in hypertensive patients with heart failure.* Hypertension, 2014. **63**(3): p. 483-9.
443. Lopez-Andres, N., et al., *Cardiotrophin 1 is involved in cardiac, vascular, and renal fibrosis and dysfunction.* Hypertension, 2012. **60**(2): p. 563-73.
444. Malavazos, A.E., et al., *Association of increased plasma cardiotrophin-1 with left ventricular mass indexes in normotensive morbid obesity.* Hypertension, 2008. **51**(2): p. e8-9; author reply e10.
445. Talwar, S., et al., *Plasma cardiotrophin-1 following acute myocardial infarction: relationship with left ventricular systolic dysfunction.* Clin Sci (Lond), 2002. **102**(1): p. 9-14.
446. Tsutamoto, T., et al., *Plasma level of cardiotrophin-1 as a prognostic predictor in patients with chronic heart failure.* Eur J Heart Fail, 2007. **9**(10): p. 1032-7.
447. Yellon, D.M. and S.M. Davidson, *Exosomes: nanoparticles involved in cardioprotection?* Circ Res, 2014. **114**(2): p. 325-32.
448. Valadi, H., et al., *Exosome-mediated transfer of mRNAs and microRNAs is a novel mechanism of genetic exchange between cells.* Nat Cell Biol, 2007. **9**(6): p. 654-9.
449. Tian, T., et al., *Exosome uptake through clathrin-mediated endocytosis and macropinocytosis and mediating miR-21 delivery.* J Biol Chem, 2014. **289**(32): p. 22258-67.